THE EXPERIMENTAL INVESTIGATION

OF THE

INELASTIC BEHAVIOR OF GEOLOGIC MATERIALS

by

Henry Reginald Hardy Jr B.Sc., M.Sc.

Thesis Submitted to the Graduate Faculty of the
Virginia Polytechnic Institute
in candidacy for the degree of
DOCTOR OF PHILOSOPHY
in
Department of Engineering Mechanics

May 21, 1965

Blacksburg, Virginia.

TABLE OF CONTENTS

I INTRODUCTION 14

II REVIEW OF LITERATURE 19

1. General 19

2. Earlier Investigations of Time-Dependent Behavior of Geologic Materials 19

2.1 Creep Experiments 19

2.2 Other Experiments 24

3. Approaches to the Problem 26

3.1 The Empirical Approach 27

3.2 The Fundamental Approach 27

3.3 The Phenomenological Approach 28

4. The Mechanical Model Concept 29

4.1 General 29

4.2 The Burgers Model 31

III THE INVESTIGATION 35

1. Object of the Investigation 35

2. Test Material 35

2.1 Simple Geologic Materials 35

2.2 Wombeyan Marble 36

3. Incremental Creep Experiments 42

3.1 Mathematical Formulation 42

3.2 Description of Experimental Procedure ... 43

3.3 Analysis of Experimental Data 46

TABLE OF CONTENTS (Cont'd)

4. Experimental Results 65

4.1 General 65

4.2 Results of Incremental Creep Experiments 70

4.3 Unloading Experiments 88

IV DISCUSSION AND CONCLUSIONS 92

1. Experimental Facility and Technique..... 92

2. Mechanical Behavior of Wombeyan Marble.... 94

2.1 Suitability of the Burgers Model..... 94

2.2 Deformation Mechanisms 97

2.3 Proposed Future Work 99

3. Application to Mining Engineering Problems.. 100

V ACKNOWLEDGMENTS 102

VI BIBLIOGRAPHY 104

VII VITA 112

VIII APPENDIX 1 - Development of the Experimental Facilities and Experimental Techniques 113

1.1 Introduction..... 113
1.2 Test Area 113
1.3 Axial Loading System 137
1.4 Investigation of the Completed Axial Loading System 176
1.5 Stress, Strain and Confining Pressure Measurement System 195
1.6 Temperature Measurement System 240
1.7 Preparation and Strain Gaging of Test Specimens 255
1.8 Uniform Loading of Test Specimens 275

TABLE OF CONTENTS (Cont'd)

IX APPENDIX 2 - Analysis of the Burgers Mechanical Model 297

X APPENDIX 3 - Determination of Initial Parameters ... 308

XI APPENDIX 4 - Computer Program 312

XII APPENDIX 5 - Tabulated Data from Individual Incremental Creep Experiments 319

XIII APPENDIX 6 - Effect of Incremental Loading Rate 345

LIST OF FIGURES

FIGURE 1. The Burgers Mechanical Model 33

FIGURE 2. Series of Photomicrographs Showing Typical Structural Features of Wombeyan Marble Before Experimental Deformation 39

FIGURE 3. Stress—Strain Curves for Wombeyan Marble (after Paterson (1958)) 41

FIGURE 4. Typical Individual and Average Strain Versus Stress Data 48

FIGURE 5. Method Used to Determine the Instantaneous Elastic Strain 50

FIGURE 6. Method Used to Correct the Observed Strain Versus Time Data 54

FIGURE 7. Method Used to Determine the Initial Parameters 59

FIGURE 8. Typical Creep Curve for a Low Stress Level (Specimen WO-5)..... 63

FIGURE 9. Typical Creep Curve for a High Stress Level (Specimen WO-5) 64

FIGURE 10. Average Strain Versus Stress Curves, for Specimens WO-2 to WO-7..... 68

FIGURE 11. Variation of E_2 with Stress Level 69

FIGURE 12. Overall Strain Versus Time Curve for Specimen WO-5 71

FIGURE 13. Overall Strain Versus Time Curve for Specimen WO-6 72

FIGURE 14. Overall Strain Versus Time Curve for Specimen WO-7 73

FIGURE 15. Variation of Model Parameters (E_1, E_2, N_1, and N_2) with Stress Level for Specimen WO-5... 76

LIST OF FIGURES (Cont'd)

FIGURE 16. Variation of Model Parameters ($\mathcal{T}$ and C) with Stress Level for Specimen WO-5..... 77

FIGURE 17. Variation of Model Parameters (E_1, E_2, N_1, and N_2) with Stress Level for Specimen WO-6 .. 78

FIGURE 18. Variation of Model Parameters ($\mathcal{T}$ and C) with Stress Level for Specimen WO-6..... 79

FIGURE 19. Variation of Model Parameters (E_1, E_2, N_1, and N_2) with Stress Level for Specimen WO-7 .. 80

FIGURE 20. Variation of Model Parameters ($\mathcal{T}$ and C) with Stress Level for Specimen WO-7..... 81

FIGURE 21. Variation of Model Parameters (E_1, E_2, N_1, and N_2) with Stress Levels for Specimens WO-6/7 82

FIGURE 22. Variation of Model Parameters ($\mathcal{T}$ and C) with Stress Level for Specimens WO-6/7..... 83

FIGURE 23. Incremental Loading/Unloading Curves (Specimen WO-5)..... 89

FIGURE 24. Plan View of Test Enclosure 115

FIGURE 25. Construction Details of Test Enclosure..... 117

FIGURE 26. Outline of Test Enclosure Temperature Control System 120

FIGURE 27. Curves Showing the Variation of Ambient and Enclosure Temperature With Time..... 128

FIGURE 28. Construction Details of Antivibration Loading Frame Mounts 132

FIGURE 29. Block Diagram of Electrical Power Supply System..... 134

FIGURE 30. Circuit of Pneumatic Supply System..... 135

FIGURE 31. Two Axial Loading Frames Mounted on Anti-vibration Bases in Inner Room..... 139

LIST OF FIGURES (Cont'd)

FIGURE 32. Close-Up View of Loading Frame with Specimen Loading Jig in Position 140

FIGURE 33. Block Diagrams of a Basic Feedback Control System and a Control System for Rock Deformation Studies 141

FIGURE 34. Block Diagram of Type-A Loading System 145

FIGURE 35. Photograph Showing in the Foreground Two Racks Containing the Load Control System 148

FIGURE 36. Circuit of Pneumatic/Hydraulic Section of Control System 149

FIGURE 37. Two Views of Completed Pneumatic Controller Unit 151

FIGURE 38. Circuit Diagram for Pneumatic Control Unit 152

FIGURE 39. Photograph of Rapid Load/Rapid Unload Unit in Position above Loading Frame 156

FIGURE 40. Block Diagram of Electronic Control Unit 159

FIGURE 41. Circuit Diagram for Galvanometer Signal Conditioning Circuit 160

FIGURE 42. Circuit Diagram for Main Section of Electronic Controller 162

FIGURE 43. Photographs Showing a Number of Views of Completed Electronic Controller Unit 165

FIGURE 44. Circuit Diagram for Regulated Bridge Power Supply 168

FIGURE 45. Diagram Illustrating Details of Programming Arrangement 169

FIGURE 46. Circuit Diagram of IS-Mode Programming Module 171

LIST OF FIGURES (Cont'd)

FIGURE 47. Photographs Showing a Number of Views of Incremental Mode Programmer 173

FIGURE 48. Photographs of Load Program Plug-In Cards ... 174

FIGURE 49. Curves Illustrating Behavior of the Hydraulic Ram 178

FIGURE 50. Curves Illustrating Behavior of Control System Operating in the CS-Mode..... 184

FIGURE 51. Curves Illustrating Behavior of Control System Operating in the IS-Mode 190

FIGURE 52. Outline of a Simple System for CSR-Mode Operation..... 193

FIGURE 53. Block Diagram of Measurement System..... 201

FIGURE 54. Photograph Showing General View of Overall Measurement System..... 202

FIGURE 55. Block Diagram of Manual Readout System..... 205

FIGURE 56. Photographs Showing Two Views of Manual Readout System 206

FIGURE 57. Block Diagram of 12-Channel, "Slow", Y-T Recorder System 208

FIGURE 58. Photographs Showing Two Views of 12-Channel, "Slow", Y-T Recorder System 210

FIGURE 59. Circuit Diagram of Recorder Junction Unit..... 212

FIGURE 60. Circuit Diagram of 2-Arm and 4-Arm Zero Balance Units 214

FIGURE 61. Photographs Showing Two Views of 4-Arm Zero Balance Unit 216

FIGURE 62. Circuit Diagram of 2-Arm Junction Unit 217

FIGURE 63. Photographs Showing Two Views of 2-Arm Junction Unit Containing Six Junction Circuits.. 218

LIST OF FIGURES (Cont'd)

FIGURE 64. Circuit Diagram of 4-Arm Junction Unit 219

FIGURE 65. Photographs Showing Two Views of 4-Arm Junction Unit 220

FIGURE 66. Block Diagram of 2-Channel, "Fast", Y-T Recorder System 226

FIGURE 67. Photograph Showing Two-Channel, "Fast", Y-T Recorder System 227

FIGURE 68. Block Diagram of Single Channel Y-XT Recorder System 230

FIGURE 69. Photograph Showing Front View of Completed Y-XT Recorder System 231

FIGURE 70. Circuit Diagram of Dual Bridge Unit 233

FIGURE 71. Photographs Showing Various Views of Dual Bridge and Selecter/Marker Unit 235

FIGURE 72. Block Diagram of Marker System 237

FIGURE 73. Photographs Showing Master Marker Unit 238

FIGURE 74. Location of Temperature Monitoring Facilities in Test Enclosure 241

FIGURE 75. Block Diagram of Temperature Measurement System 243

FIGURE 76. Simplified Circuit of Temperature Measurement System 245

FIGURE 77. Construction Details of Reference Junction Unit 247

FIGURE 78. Circuit Diagram for Reference Junction Controller 248

FIGURE 79. Photograph Showing Top View of Reference Junction Unit 250

LIST OF FIGURES (Cont'd)

FIGURE 80. Photograph Showing Front View of Reference Junction Control Unit 250

FIGURE 81. Circuit Diagram for Thermocouple Signal Conditioning Unit 252

FIGURE 82. Photographs Showing a Number of Views of Signal Conditioning Unit 253

FIGURE 83. Wombeyan Marble as Received and after Preparation 264

FIGURE 84. Axial Strain Gage Pattern 265

FIGURE 85. Photographs Showing a Number of Views of Gaged Test Specimens 270

FIGURE 86. Orientation of Gage Axes to Specimen Axes 272

FIGURE 87. Details of Various Types of Specimen Loading Jigs 279

FIGURE 88. Stress-Strain Curves Obtained Using Various Types of Specimen Loading Jigs 280

FIGURE 89. Average Stress-Strain Curves Obtained Using Various Types of Specimen Loading Jigs 284

FIGURE 90. Details of Deformable Insert Type Loading Heads 288

FIGURE 91. Individual Stress-Strain Curves for Steel Specimen 289

FIGURE 92. Average Stress-Strain Curve for Steel Specimen 289

FIGURE 93. Individual Stress-Strain Curves for Wombeyan Marble Specimen (WO-3) 291

FIGURE 94. Average Stress-Strain Curve for Wombeyan Marble Specimen (WO-3) 291

LIST OF FIGURES (Cont'd)

FIGURE 95. Photographs Showing a Number of Views of Loading Jig 292

FIGURE 96. Curves Showing the Effect of Friction in the Specimen Loading Jig 294

LIST OF TABLES

TABLE 1.	General Data for Six Specimens of Wombeyan Marble	67
TABLE 2.	Summary of Details and Experimental Results from Incremental Creep Experiments on Wombeyan Marble Specimens	74
TABLE 3.	STUFF Analysis of Data - Specimen WO-5	84
TABLE 4.	STUFF Analysis of Data - Specimen WO-6	85
TABLE 5.	STUFF Analysis of Data - Specimen WO-7	86
TABLE 6.	STUFF Analysis of Data - Specimens WO-6/7	87
TABLE 7.	Controller Sensitivity.....	164
TABLE 8.	Details of Program (Calibration) Card 64/4 used for Initial Incremental Loading Studies on Wombeyan Marble	175
TABLE 9.	Load Cell Zero Drift Data.....	181
TABLE 10.	Variation of Load Fluctuation with Various Parameters (Control System in CS-Mode)	185
TABLE 11.	Optimum Control Conditions (CS-Mode).....	187
TABLE 12.	Values of Load Drift Obtained from a Number of Deformation Experiments	188
TABLE 13.	Optimum Control Conditions (IS-Mode).....	191
TABLE 14.	Behavior of a Simple System for Obtaining an Approximately Constant Rate of Loading...	194
TABLE 15.	Characteristics of 12-Channel "Slow" Y-T Recorder System	224
TABLE 16.	Characteristics of 2-Channel "Fast" Y-T Recorder System	228
TABLE 17.	Characteristics of Y-XT Recorder System	234

LIST OF TABLES (Cont'd)

TABLE 18.	Characteristics of Thermocouple Signal Conditioning Unit	254
TABLE 19.	Effect of Strain Gage Orientation.....	275
TABLE 20.	Fortran Program for Analysis of Creep Data Using the Burgers Model.....	313
TABLE 21.	Typical Computer Output Data: Section 1	317
TABLE 22.	Typical Computer Output Data: Section 2.....	318
TABLES (23-32).	Tabulated Data from Individual Creep Experiments (Specimen WO-5)	319-327
TABLES (33-40).	Tabulated Data from Individual Creep Experiments (Specimen WO-6)	328-336
TABLES (41-48).	Tabulated Data from Individual Creep Experiments (Specimen WO-7)	337-344

I

INTRODUCTION

A knowledge of the mechanical behavior of geologic materials (rocks and minerals) has become increasingly important in mining and civil engineering, geology, geophysics and more recently in a number of defence and aerospace fields. The majority of the basic research on the mechanical behavior of geologic materials has been carried out by the geologist and geophysicist. Studies by such workers as Griggs, Handin, Robertson and others* are classic, however their primary interest has been in the behavior of these materials under conditions which are normally associated with considerable depth in the earth's crust. As a result the majority of deformation experiments have been conducted under conditions of high confinement (30,000-150,000 psi) and have been concerned mainly with the observation of phenomena which occur at large strains (1-50%).

Until the early 1940's very few investigations were undertaken into the behavior of geologic materials under conditions which are compatible with such economically important operations as mining, comminution, drilling, construction etc. In these operations the material is usually under conditions of confinement and strain which are many

---

* A lengthy bibliography of research conducted on rock deformation with particular reference to geological applications has been published recently by Griggs and Handin (1960).

orders of magnitude lower than those normally of interest to the geologist. Most of the early research on the mechanical properties of geologic materials undertaken specifically in relation to mining and other engineering problems suffered from a number of defects, namely (a) the laboratory test conditions were not realistic in terms of field conditions, (b) non-standardized test procedures were employed and in many cases the test results were more dependent on the test procedure than on the properties of the test specimen, and (c) the materials studied were poorly defined and as a result it was impossible to develop any general concepts regarding the behavior of a specific rock type.

Early in the 1940's more realistic research on rock properties associated directly with mining engineering problems was initiated. Obert, Duval and Windes (1946) at the U.S. Bureau of Mines published the first comprehensive report outlining standardized tests for the determination of physical properties of mine rock under short-period uniaxial stress. Phillips (1948) soon after considered the physical properties of mine rock in relation to the general mining problem and, in particular, pointed up the importance of the "time effect" and the effect of confining pressure on the behavior of rock in the mine. In 1953 the U.S. Bureau of Reclamation published a report outlining their standardized laboratory procedures for studying rock under short-period triaxial stress (see Balmer (1953)). Since the 1940's there has been a

continually increasing interest in rock mechanics and in the associated study of the mechanical properties of rock. The U.S. Bureau of Mines and the U.S. Bureau of Reclamation have continued rather extensive programs initiated in the 1940's and similar research programs have been established by the British National Coal Board, the South African National Research Council, the Canadian Department of Mines and Technical Surveys and by numerous universities and research organizations throughout the world.

In spite of the increased research on the mechanical behavior of geologic materials being undertaken, many of their most important properties have not been investigated in detail. In particular the effect of time, although its importance has been suggested by many workers, has received very little attention from the experimental point of view. Many workers have reported that test results appeared to be influenced by the rate and duration of loading, although few have been willing to accept the fact that such behavior is indicative of an inelastic material.

The study of the mechanical properties of geologic materials was initiated in The Mining Research Section of the Fuels and Mining Practice Division, Mines Branch, Canadian Department of Mines and Technical Surveys, in 1951 as part of a fundamental study of ground stress in Canadian Coal Mines (see Brown (1958)). The

initial work was restricted to short-period tests on typical mine rock under uniaxial compressive stress, but as the importance of the "time factor" became more obvious, studies were undertaken to investigate time-dependent behavior. These studies, which were initiated in 1957, consisted mainly of a comprehensive literature search on the subject, and the initial development of experimental facilities (see Hardy (1959, 1962)). This research project was inactive during the period 1959-1961 due in part to the relocation of laboratory facilities.

In the fall of 1961 the project was reactivated with the proposed research program being broadly outlined (see Hardy (1961)) as follows:

"To study experimentally the mechanical behavior of selected geologic materials and to analyse these experimental data using the concept of mechanical models and the analytical methods of viscoelasticity. In particular to develop governing equations for these materials based on suitable laboratory experiments and valid at least within a range of stress, confining pressure, duration of loading, and temperature consistent with practical applications".

The first phase of this research program, namely the experimental investigation of the inelastic behavior of a "simple" geologic material (Wombeyan marble) using incremental creep experiments, and the associated development of the necessary experimental

facilities and analytical methods, is the topic of this dissertation. It was carried out as a co-operative research program between the Fuels and Mining Practice Division and the Engineering Mechanics Department of the Virginia Polytechnic Institute, with the associated research being conducted in the laboratories of the Physics Section, Fuels and Mining Practice Division, Ottawa, Canada.

II
REVIEW OF LITERATURE

1. General

Papers dealing with the behavior of geologic materials are found to be widely dispersed throughout the literature. However, extensive bibliographies dealing with the general mechanical properties of these materials have been published recently by Griggs and Handin (1960) and Mitra and Willson (1962). The former one is mainly concerned with studies conducted under conditions comparable with considerable depth in the earth's crust, whereas the latter one is basically concerned with studies associated with such operations as mining and drilling which occur at relatively shallow depth. In the more specific field of time-dependent behavior of geologic materials extensive bibliographies have been given in papers by Hardy (1959), Murrell and Misra (1962) and Robertson (1964).

2. Earlier Investigations of Time-Dependent Behavior of Geologic Materials

2.1 Creep Experiments

The majority of experiments conducted to investigate the time-dependent behavior of geologic materials have been creep* experiments carried out under conditions of constant applied load.

* The term creep will be defined, in a general sense, throughout this dissertation as the time-dependent strain observed in a material under a condition of constant applied load.

Compressive creep experiments under confinement conducted by Griggs (1936, 1939) and compressive and bending creep experiments at atmospheric pressure carried out by Phillips (1948) demonstrated that long-period time-dependent deformation of geologic materials, without producing immediate failure of the specimen, is possible. Griggs showed that the total strain (e) at a time (t) after the specimen is loaded can be represented by an empirical equation of the form:

$$e = A + B \log t + Ct, \qquad (1)$$

where A, B and C are coefficients that depend on the material. He classed this behavior as elastico-viscous and described it as being made up of two parts, namely: pseudoviscous flow - deformation at a constant rate, given by Ct, and elastic flow - deformation at a rate decreasing logarithmically with time, given by B log t. Equation 1 was found by Griggs (1939, 1954) to hold for Solenhofen limestone, halite and alabaster.

Other studies have indicated that a relation similar to equation 1 is applicable to the analysis of certain field observations. For example, Barron and Toews (1964) have shown recently that the time dependence of closure in an unlined vertical shaft in salt may be represented by a function of log t. Similarly, roof convergence studies by Parker and his associates (1963) in a salt mine unworked for some 14-20 years show deformations of the form Ct up to 0.5 inch over a period of some 300 days. Furthermore, Parker indicates that, when

renewed mining led to a rapid increase in the percentage extraction in the particular area, the convergence proceeded at an increased rate and could be represented by B log t.

The experiments of Griggs (1936) on Solenhofen limestone also indicate that there is a relationship between ultimate compressive strength and duration of loading, which would suggest that for long period loading the ultimate strength becomes asymptotic to a certain minimum value. Therefore, at applied stresses below this minimum value the rock will not fail during a finite time. Phillips (1948) describes similar results where failure of a beam-shaped rock specimen occurred after a period of sustained loading, at a stress well below the "normal" strength for that material. He suggests that for mining engineering purposes the "true" strength of rocks should be used. This he defines as "the smallest stress at which the material ultimately proceeds to failure".

It is suggested by this writer that the relationship between ultimate strength and the duration of loading must obviously be determined by the processes occurring during time-dependent deformation. A thorough study of time-dependent deformation may therefore be expected to throw much light on the phenomenon of time-dependent failure.

Matsushima (1956) has shown that the results of a series of short-period ($t < 1000$ seconds), incremental creep experiments* conducted under uniaxial compressive loading on Ajimura and Kitashirakawa granite could be described by the incremental creep form of the Burgers mechanical model**, namely:

$$e = \frac{\Delta\sigma}{K_1} + \frac{\Delta\sigma}{K_2}\left(1 - e^{-t/K_3}\right) + \frac{\sigma t}{K_4} \qquad (2)$$

where $\Delta\sigma$ is the stress increment, σ is the total stress, t is the time since the stress increment was applied, and K_1, K_2, K_3 and K_4 are parameters of the material. Matsushima has shown that for these materials K_2, K_3 and K_4 are functions of the stress level. Later creep experiments at a fixed compressive stress level on a number of granites including Kitashirakawa (Matsushima (1960)), which were conducted over longer periods of time (up to 10^6 seconds), were found to fit the expression

$$e = A_0 + A_1 e^{-\alpha_1 t} + A_2 e^{-\alpha_2 t} + A_3 e^{-\alpha_3 t} + B\log t + Ct \qquad (3)$$

where A_o, A_1, A_2, A_3, B, C, α_1, α_2 and α_3 are parameters.

---

*In an incremental creep experiment the applied load level is raised in a series of increments with the applied load being held constant for a period of time at each level and the associated strain versus time data being obtained.

**References to the theory of various mechanical models are given later in this section.

A series of long-period creep experiments conducted on various coal-measure rocks have recently been reported by Price (1964). In creep experiments on beam-shaped specimens of Wolstanton sandstone at a load level of approximately 50 per cent of the rupture strength of the material it was found that the creep data, for periods of time up to 6×10^5 seconds, could be fitted to an expression of the form

$$e = A + B \log t \qquad (4),$$

which consists of the first two terms of Griggs creep relation (equation 1). However for periods of time greater than 6×10^5 seconds a better fit was obtained using the creep expression obtained for the Zener mechanical model namely:

$$e = A + B (1 - e^{-t/C}) \qquad (5).$$

For higher applied loads the creep data from the bending experiments appears to fit a modified Burgers model (actually a series combination of a Bingham and a Kelvin-Voigt model) which contains an additional dry frictional element in order to introduce a characteristic yield stress (Y) into the model. The creep behavior of this model when $\sigma > Y$ may be written as

$$e = \frac{\sigma}{A_1} + \frac{\sigma}{A_2}\left(1 - e^{-t/A_3}\right) + (\sigma - Y) A_4 t \qquad (6),$$

where A_1, A_2, A_3, A_4 and Y are parameters of the material. However, after a series of creep experiments on Markham sandstone and Wolstanton

siltstone under uniaxial compressive loading Price rejects the modified Burgers model as it does not appear to fit the experimental data. It is felt by the writer that the quality of Price's uniaxial experiments are not adequate to allow these conclusions to be drawn.

2.2 Other Experiments

Although the use of creep experiments (where σ = constant) have been the most popular method of investigating time-dependent behavior in geologic materials, other types of experiments are equally useful. Wuerker (1959) for example discusses the influence of stress rate on the deformation and failure properties of rock. He states that, under uniaxial compressive stress, both the ultimate strength and the Young's modulus of such materials appear to increase with increasing stress rate.

Recent papers by Serdengecti and Boozer (1961) and by Heard (1963) are concerned with experiments conducted under conditions of constant strain rate ($\dot{e}$ = constant). Serdengecti and Boozer investigated the behavior of Solenhofen limestone, Berea sandstone and Pala gabbro under various confining pressures and at strain rates varying from 10 μs/sec* to 10^6 μs/sec. They concluded (a) that under sufficiently high confinement the mode of failure was strain rate

*For convenience and brevity the term "μs" is used to designate strain in microinches/inch.

dependent, brittle failure occurring at high strain rates and ductile failure being favoured at low strain rates, (b) the ultimate strength increased with increasing strain rate, and (c) the slope of the initial portion of the stress-strain curve (up to approximately 0.5 per cent) was independent of strain rate. The conclusion stated in section (c) would indicate that the Young's modulus (slope of the stress-strain curve) was independent of the strain rate. It is felt by the writer that such may be the case in the strain rate range investigated, however, at lower strain rates ($< 10\,\mu s/sec$) an increasing dependence on strain rate should be expected.

The studies described by Heard (1963), at strain rates from $0.3\,\mu s/sec$ to $4 \times 10^5\,\mu s/sec$ are basically of interest to the geologist since they have been mainly conducted under conditions of high confinement and high temperature. However, his experimental approach would be equally applicable to behavior of geologic materials at the lower confinements and temperatures associated with engineering problems. Heard's paper is notable in particular as it represents one of the first successful attempts to study time-dependent behavior of geologic materials by other than creep experiments. This writer would not agree however with Heard's statement that the apparatus and the method developed "is so simple and effective as to render obsolete all creep apparatus". First, even though such experimental methods

have been employed for some years for basic investigation of the mechanical behavior of metals, creep experiments are still considered necessary and in many cases more desirable. Secondly, there is no justification for assuming that creep experiments and constant rate experiments will yield the same results until such is demonstrated experimentally. Thirdly, using Heard's loading system (which uses an extensive gear train driven by an electric motor) at very slow strain rates ($< 1\ \mu s/sec$) it is felt that serious errors could be introduced by assuming that the actual strain rate is constant and dependent only on the motor speed and the reduction gear ratio of the loading system.

3. Approaches to the Problem

Time-dependent mechanical behavior is common to most materials. It has been found to be an important factor in the behavior of such materials as concrete, ice, plastics, coal and metals. The various approaches used to study this behavior in different materials has ranged from empirical to phenomenological to theoretical, depending on the material. Many of these studies have been carried out in the metals field because of their wide commercial use and the regularity of their structure, and an excellent review of this theoretical and experimental work is given by Cottrell (1953). Although it is difficult, if not impossible, to apply the theories developed for these other materials

directly to geologic materials, many of the general principles hold for all types of material provided their limitations are understood.

3.1 The Empirical Approach

Here the accent is on experimental evidence. Various parameters are measured experimentally (e.g. strain, strain rate etc.) as a function of time, stress, temperature, etc. and the experimental results are fitted to known empirical equations or to new equations developed to suit the particular case. This approach has been utilized extensively in the metals field for presentation of data obtained from creep experiments*. In the field of geologic materials this approach has been followed by Griggs (1939) and others. Although it provides a convenient method for presenting the data, it does not provide information on the actual mechanism of the deformation process or suggest how the same material would behave under different loading conditions.

3.2 The Fundamental Approach

For metals and to a limited extent for other materials, an attempt has been made to relate the mechanical behavior to processes on the atomic or molecular scale. The so-called dislocation theory of plastic flow (see Cottrell (1953)) has proved its usefulness in explaining and predicting many of the mechanical properties of metals. Basically, this theory considers that even the most perfect crystal structure

* Cottrell (1953) outlines many of the empirical relations developed for this purpose on pages 195-215.

contains lattice imperfections, called dislocations. These imperfections are mobile under an applied stress and produce glide in the individual crystals when their motion takes place in a glide surface. The strain observed in a specimen under load is considered to be associated with the sum of the individual microscopic slips. It is possible that such fundamental concepts as dislocation theory may be usefully applied to minerals which usually have well defined structure. However, their application to the deformation of rock which is normally heterogeneous and non-isotropic cannot be visualized at present.

3.3 The Phenomenological Approach

As it appears that there is little hope at present of utilizing a fundamental approach to the investigation of the mechanical behavior of geological materials, and as the empirical approach adds little to the overall understanding of the mechanical behavior, it was considered necessary to take the intermediate, phenomenological approach. This consists of expressing the behavior of the material in terms of a combination of a number of simple mechanical models. This approach has been applied extensively in the field of rheology* and in such fields as mechanical engineering and acoustics in order to describe the behavior of the so-called inelastic materials.

* Rheology is the study of deformation and flow in materials. Much of the research in this field has been in rubber, plastics and viscous liquids, with a little work in the field of geologic materials. A comprehensive discussion on many aspects of this subject is given by Eirich (1956, 1958 and 1960).

4. The Mechanical Model Concept

4.1 General

According to Freudenthal (1950): "The theory of mechanical models considers combinations of elements which are supposed to behave mechanically like the constituent phases of the materials but which, apart from the mechanical behavior, have nothing in common with the real material". A number of mechanical models have been postulated to explain the time-dependent deformation of various materials. Where relatively slow variations of stress are involved, these models consist of combinations of elastic and viscous elements. The stress (σ) and the strain (e) in the elastic element are related by Hooke's law, namely, $\sigma = eE$ where E is the elastic modulus. In the viscous element, the stress (σ) and the strain rate ($\dot{e}$) are related by Newton's Law of Viscosity, namely $\sigma = \dot{e}N$ where N is the coefficient of viscosity. The E's and N's are collectively known as the model parameters or the viscoelastic coefficients. It should be noted that the mechanical model approach is really a specific application of the theory of linear viscoelasticity. In the former case, the model is thought of visually in terms of a combination of elastic and viscous elements. In the latter case, the model is developed on a purely mathematical basis.

The general development and analysis of various

mechanical models have been considered in detail by a number of workers including Freudenthal (1950), Jastrzebski (1959), Lubahn and Felgar (1961) and Sperry (1964). The more general theories of visco-elasticity have been discussed by such workers as Bland (1960), Bergen (1960) and Boley and Weiner (1960).

In general for one dimension, all mechanical models may be represented by the general equation between stress (σ) and strain (e)

$$a_0\sigma + a_1\frac{\partial\sigma}{\partial t} + \cdots + a_m\frac{\partial^m\sigma}{\partial t^m} = b_0 e + b_1\frac{\partial e}{\partial t} + \cdots + b_n\frac{\partial^n e}{\partial t^n} \quad (7),$$

where a different set of coefficients will have non-zero values for each model configuration. The particular form of equation 7 which is associated with each model is called the governing equation for that model. The solutions of this differential equation for various states of loading or deformation yield a set of specific equations. This set of equations describes the behavior of the particular model under various conditions of loading or deformation, (e.g. constant stress, constant strain, constant stress rate etc.). The governing equations and the associated specific equations for a number of two-, three- and four-element models were recently compiled at the Mines Branch by Steppel (1964).

The real usefulness of the mechanical model approach lies in the fact that once the correct model has been determined for a particular material and its associated parameters evaluated (for example from a creep experiment where the specimen stress was held constant) it is possible then to write down equations that express the behavior of the material under other conditions of deformation and load. These equations provide answers to a number of important questions with regard to the behavior of the material such as whether the material can be considered to be basically elastic, whether the material will exhibit creep under sustained loads, whether the material will exhibit "elastic rebound" etc.

The use of mechanical models to describe the deformation behavior of geologic material has been discussed by a number of writers, including Hardy (1965, 1959), Price (1964), Iman (1964), Ito and Terada (1962), Hunt (1962), Attewell (1962, 1961), Salustowicz (1958), Iida and Kumazawa (1957), Terry (1957), Matsushima (1956) and Litwiniszyn (1955). A review of the general application of visco-elasticity to the behavior of geologic materials has been published recently by Robertson (1964).

4.2 The Burgers Model

Studies by Hardy (1965), Matsushima (1956) and others on rock, by Terry (1957) on coal and by Ross (1958) on concrete, a

material very similar in many respects to rock, indicate that deformation behavior of these materials under sustained loading may be analyzed satisfactorily in terms of the Burgers model. This model consists of the series combination of two simpler units, the Maxwell model consisting of an elastic and a viscous element in series and the Kelvin-Voigt model consisting of an elastic and a viscous element in parallel. Figure 1A illustrates the Burgers model.

The theoretical behavior of this model has been investigated in detail by Frederick and Garcia (1953), and more recently by Steppel (1964). The governing equation (see Appendix 2) is found to be

$$\left(\frac{N_1}{E_2}\right)\ddot{\sigma} + 1 + \frac{E_1}{E_2} + \frac{N_1}{N_2}\ \dot{\sigma} + \left(\frac{E_1}{N_2}\right)\sigma = N_1\ddot{e} + E_1\dot{e} \qquad (8),$$

where σ and e are respectively the stress and strain, and E_1, E_2, N_1 and N_2 are the model parameters.

The data from experiments conducted under various loading conditions are fitted to the respective specific equations, namely solutions of equation 8 (see Appendix 2). For example if we are concerned with creep experiments, the following specific equation would apply

$$e(t) = \frac{\sigma_c}{E_2} + \frac{\sigma_c}{E_1}\left(1 - \exp(-E_1 t/N_1)\right) + \frac{\sigma_c t}{N_2} \qquad (9),$$

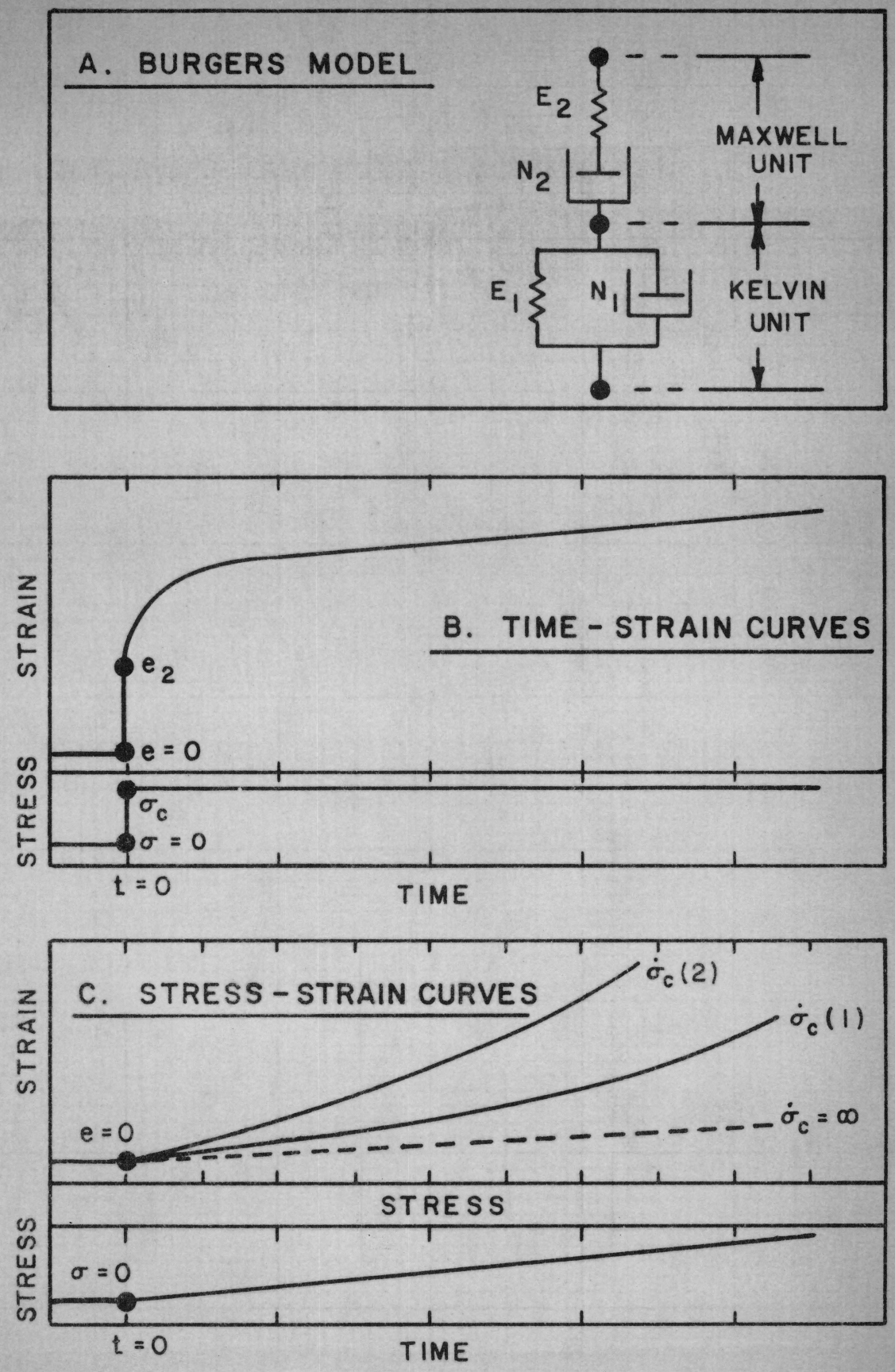


FIGURE 1 - The Burgers Mechanical Model.

where σ_c is the magnitude of the constant stress, t is the time, and all other factors have been defined previously. Figure 1B illustrates the time-strain behavior defined by equation 9.

Under some circumstances it is convenient to consider the so-called retardation time ($\mathcal{T}$) of the model. In the Burgers model this retardation time is defined as the time necessary for the strain associated with the Kelvin element to go to within 1/e of its maximum value. From this definition it is easily shown that

$$\mathcal{T} = N_1/E_1 \qquad (10).$$

If however we wished to analyse the results of a loading experiment where the stress rate was constant ($\dot{\sigma}_c$), then we would use the following specific equation

$$\epsilon(\sigma) = \sigma\left(\frac{E_1+E_2}{E_1E_2}\right) + \frac{\sigma^2}{2N_2\dot{\sigma}_c} - \frac{N_1\dot{\sigma}_c}{E_1^2}\left[1-\exp(-E_1\sigma/N_1\dot{\sigma}_c)\right] \qquad (11),$$

where $\dot{\sigma}_c$ is the constant stress rate and all other factors have been defined previously. Figure 1C illustrates the stress-strain behavior defined by equation 11. The shape of the stress-strain curve is dependent on the stress rate ($\dot{\sigma}_c$), however for large values of $\dot{\sigma}_c$ the curve will be approximately linear and independent of $\dot{\sigma}_c$ (see Appendix 2).

III
THE INVESTIGATION

1. The Object of the Investigation

The object of the investigation was to study experimentally the inelastic behavior of a "simple" geologic material (Wombeyan marble) using incremental creep experiments, and to investigate the suitability of analyzing the experimental results in terms of the Burgers mechanical model.

2. Test Material

2.1 Simple Geologic Materials

Until recently engineers and in particular mining engineers have been mainly concerned with the behavior and properties of the specific local geologic materials with which they were working. The detailed experimental investigation of such materials may be merited for certain applied studies, however, such investigations do not appreciably assist in developing our understanding of basic rock behavior. The writer favours the selection of a few "simple" materials, approximately equivalent to those encountered in practice and upon which a concentrated effort would be made to understand the behavior of these materials. When this is accomplished, the results could be extended to the geologic materials encountered in specific problems.

Experience by many workers has shown that it would be unwise, at least initially, to study "complex" geologic materials

such as typical mine rocks as these are in general anisotropic, heterogeneous, and in many cases completely unrelated in composition and structure. Similarly, although fabricated synthetic geologic materials (such as special plaster mixes, mineral grain-epoxy combinations, etc.) and similar non-geologic materials (such as cement, plastics, ceramics, etc.) may provide a more homogeneous, isotropic, and controllable group of experimental materials, it is felt that these do not resemble true geologic materials in sufficient detail for this type of study.

It was therefore decided that studies should be carried out initially on "simple" geologic materials", namely those naturally occurring geologic materials that are basically monomineralic, and macroscopically isotropic and homogeneous. Such "simple" rocks as Solenhofen and Indiana limestone, Wombeyan marble, and Berea sandstone are typical examples. Once the behavior of these "simple" materials is understood, increasingly more complex materials can be investigated until a sufficient background of experience is developed to make it practical to study typical mine rocks.

2.2 Wombeyan Marble

Wombeyan marble was selected as the test material for our initial investigation of inelastic behavior of geologic materials, as earlier experiments by Paterson (1958) had indicated that its

deformation behavior was reasonably reproducible, that it was approximately isotropic both in its fabric* and in its measured mechanical properties, and that it exhibited inelastic behavior within a range of stress compatible with the writers experimental facilities. A supply of this material in the form of 7/8 inch diameter core was kindly made available by Dr. M. S. Paterson of the Department of Geophysics, The Australian National University, Canberra, Australia.

The location and constitution of Wombeyan marble are described by Paterson (1958) as follows:- "Samples of marble were obtained from a quarry near Wombeyan in New South Wales (Australia). This rock is Silurian and has probably been affected by several orogenies. A chemical analysis of the marble showed it contains 96.0 per cent $CaCO_3$, 2.5 per cent $MgCO_3$, and 0.2 per cent SiO_2. It is fairly coarse grained (average grain size about 1 mm), and most grains show notable twinning parallel to at least one and usually two or three sets of planes. Fabric analysis shows that the marble has no pronounced anisotropy.--Chi-square tests showed no significant

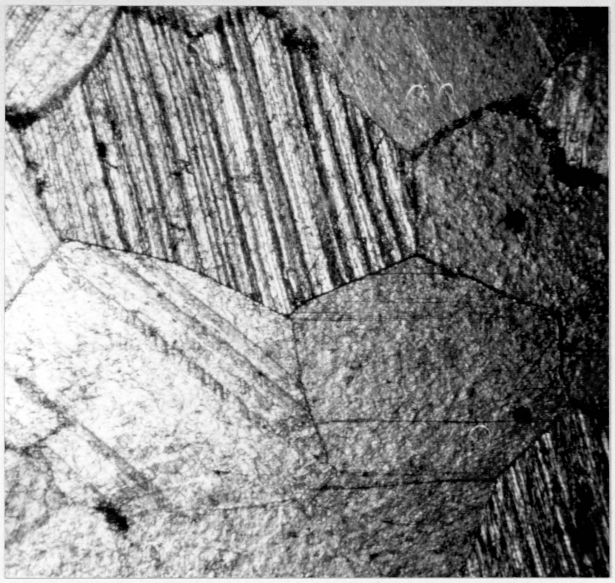
* The fabric of a material refers to the orientation of shape or crystallographic elements in the structure of the material. If the orientation of the various elements are statistically random, then the material is termed isotropic; otherwise the material is said to have a preferred orientation, or to be anisotropic.

departure from randomness in measured orientations. This was born out by mechanical tests in which specimens were cut from several unoriented blocks but gave similar results".

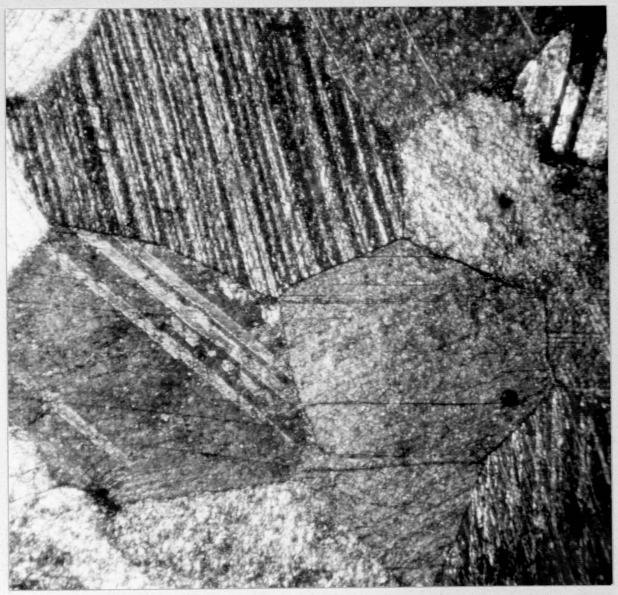
A number of thin sections were prepared by the writer, from the virgin and the experimentally deformed material, in order to investigate its general microscopic appearance and to ascertain if any obvious changes in structure were induced by the experiments. Figure 2 shows a number of photomicrographs taken of thin sections of the virgin material. They show the normal grain structure, and the presence of twinning and cleavage on at least one set of planes. An initial study of thin sections of the experimentally deformed material showed no obvious deviations from those of the virgin material. This was somewhat expected since the maximum inelastic strain developed during experimental deformation did not exceed 500 μs*. It is possible that a more refined study of such factors as twin frequency, degree of microfracturing etc, based on a statistical study of a number of sections of deformed and undeformed material, may provide some indication of the deformation mechanism. Such a study was not included in the present investigation but will be part of a future program presently under consideration.

---

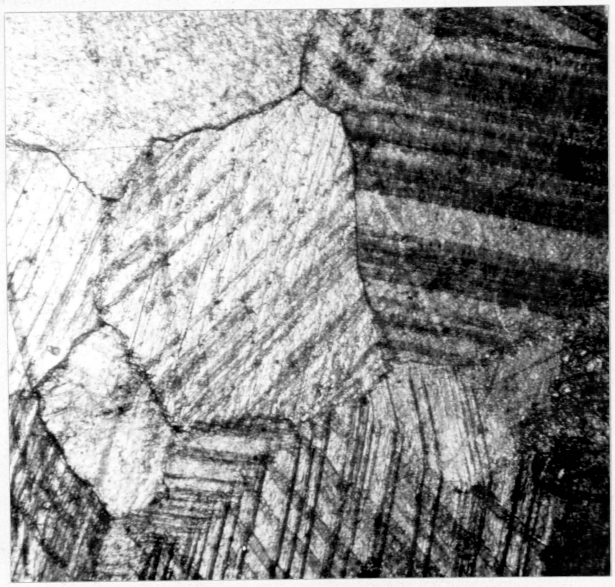
*It is possible that some of this strain was recovered during the period of some five months which elapsed between the experimental deformation of the material and the preparation of the thin sections, and/or during the actual preparation of the thin sections themselves.



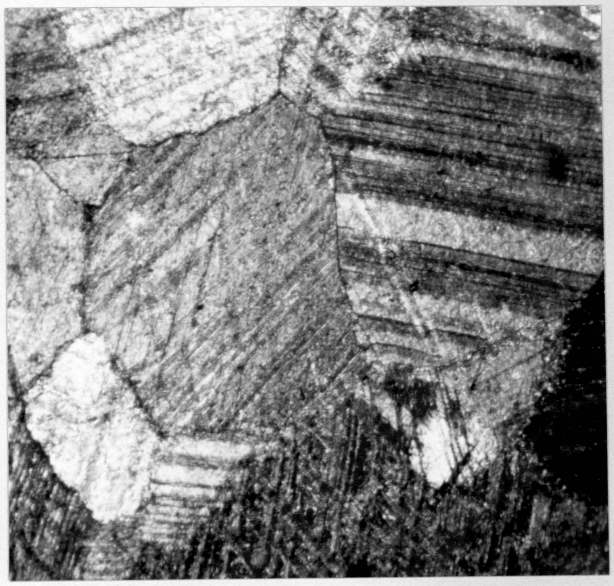
A. Typical Section Perpendicular to Axis of Core, Plane-Polarized Light, X70.



B. Typical Section Perpendicular to Axis of Core, Crossed Nicols, X70.



C. Typical Section Parallel to Axis of Core, Plane-Polarized Light, X70.



D. Typical Section Parallel to Axis of Core, Crossed Nicols, X70.

FIGURE 2 - Series of Photomicrographs Showing Typical Structural Features of Wombeyan Marble Before Experimental Deformation.

The apparent density (ρ_A) of a number of cylindrical specimens of Wombeyan marble* was determined from an accurate measurement of their weight (W), length (ℓ) and diameter (d) using the relation:

$$\rho_A = \frac{4W}{\pi d^2 \ell} \qquad (12).$$

The values of ρ_A before deformation ranged from 2.69-2.703 g/cm^3 with an average of 2.699 g/cm^3. Based on Patersons chemical analysis of the material and a density for calcite of 2.712 g/cm^3 (Peselnick and Robie (1963)) and for magnesite of 2.95-3.2 g/cm^3 (Hodgman (1949)), it appears that the porosity of the material ranges from 0.7-1.2%. No determination of ρ_A was made on specimens of the deformed material.

Figure 3 illustrates a set of typical stress - strain curves for Wombeyan marble (after Paterson (1958)). From the data presented by Paterson the compressive strength+ of the material at a confining pressure of 1-1000 Kg/cm^{2}++ (15-15,000 psi) ranged from 750-1700 Kg/cm^2 (10,600-24,000 psi).

---

* Specimens WO-11 to -18 were prepared from the same group of cores samples as specimens WO-2 to -7.

+ Strength is defined here as the maximum differential stress which the material will sustain. The differential stress is defined as ($\sigma_{zz} - \sigma_{vv}$) where σ_{zz} is the applied axial stress and σ_{vv} is the applied radial stress or confining pressure.

++ 1 Kg/cm^2 is equivalent to 14.223 psi.

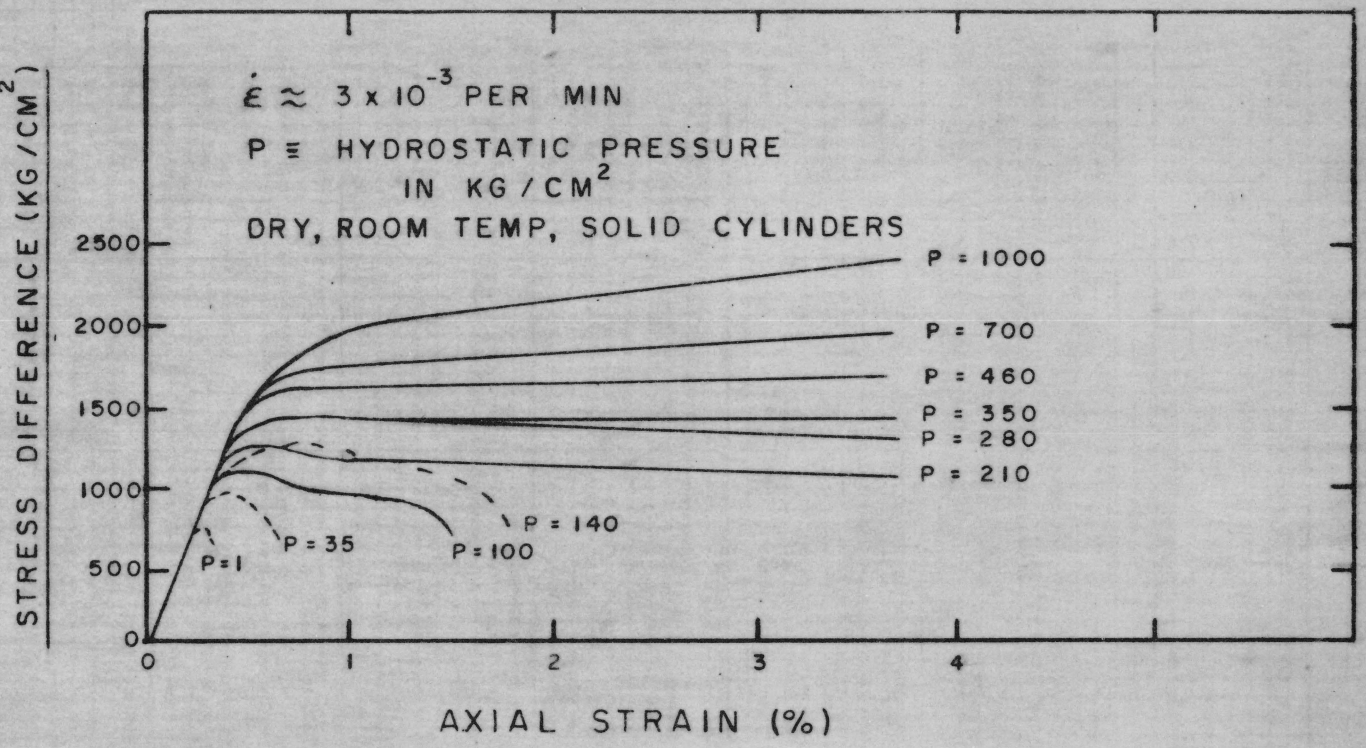


FIGURE 3 - Stress-Strain Curves for Wombeyan Marble (after Paterson (1958)).

3. Incremental Creep Experiments

3.1 Mathematical Formulation

It has been shown earlier (equation 9) that for a constant stress σ_c the Burgers model predicts a strain versus time curve of the form

$$e(t) = \frac{\sigma_c}{E_2} + \frac{\sigma_c}{E_1}\left[1 - \exp(-t/\tau)\right] + \frac{\sigma_c t}{N_2} \qquad (13).$$

In order to investigate the behavior of the test material at various compressive stress levels it was found convenient to use incremental loading. In this case the specimen stress was increased in a number of small increments ($\Delta\sigma_n$). After each increment the resulting stress (σ_n) was maintained constant at that level for a period of time (t_n), such that $t_n \gg \tau$ in which case the factor $\exp(-t/\tau) \to 0$. Under these conditions the strain e_I developed during the incremental loading and the period (t_n) of constant stress following it will be of the form

$$e_I = \frac{\Delta\sigma_n}{E_2} + \frac{\Delta\sigma_n}{E_1}\left[1 - \exp(-t/\tau)\right] + \frac{\sigma_n t}{N_2} \qquad (14),$$

where all factors have been defined previously. This may be written as

$$e_I = \Delta e_E + e_n(t) \qquad (15),$$

where $\Delta e_E = \Delta\sigma_n/E_2$ is the instantaneous elastic strain produced by the stress increment $\Delta\sigma_n$, and $e_n(t)$ is the time-dependent (creep)

strain which occurs at the constant stress σ_n. Therefore

$$e_m(t) = \frac{\Delta\sigma_n}{E_1}\left[1 - \exp(-t/\tau)\right] + \frac{\sigma_n t}{N_2} \qquad (16).$$

3.2 Description of Experimental Procedure*

Cylindrical test specimens of Wombeyan marble with attached resistance-type strain gages were deformed under uniaxial compressive load, following a prescribed loading program. The experimental procedure was as follows:

(a) The test specimen was mounted in the loading jig and leads from the three attached strain gages (1/2, 2/2 and 3/2) soldered to the mounting strip on the jig. The jig was inserted in position in the loading frame and the extension leads from the strain gage terminals on the jig were soldered to the input terminals of the strain gage measurement system (which are mounted on the lower platten of the loading frame).

(b) The overall facility was activated, and a general check-out of all systems was carried out. A "warm-up" period of 12 hours was normally allowed, after which the general check-out was repeated. Zero adjustments and sensitivity checks were made on the various sections of the load control and measurement system.

---

* Details of specimen preparation, strain gage mounting and the loading and measurement systems used are described in detail in Appendix 1.

(c) The selector switches on the measurement system were set so that signals from the three gages, the associated load cell and the inner room thermocouple were fed to the 12-channel "slow" Y-T recorder. The zero position on the recorder of each of these signals was adjusted, and the time marker system activated. The recorder scan system was turned on (chart speed of 300 mm/hr) and kept operating continuously throughout the complete experiment in order to provide a master time base for the overall experiment.

(d) The no-load condition of the strain and load channels were recorded for approximately 15 minutes, before specimen loading was initiated, in order to obtain reliable zero load values for these parameters, and to check on the noise level and stability of the recorder system.

(e) At this time the incremental loading module, in the load control system, was set at its lowest position and the hydraulic loading ram manually pumped down till the loading button on the attached load cell made contact with the loading jig. The alignment of the load cell and the loading jig was checked.

(f) The load controller was set to its auto-mode. The compressive stress on the specimen was then increased to the first level (approximately 1200 psi) and held at that point. The alignment cylinder on the loading jig was unclamped, raised, and locked in its "free"-position.

(g) The specimen stress was increased through a number of increments, as determined by the program plug-in card in the incremental loading module, up to a stress of approximately 7000 psi*. The stress was maintained constant at each of these levels for approximately 15 minutes before it was raised to the next level. During this phase of the experiment the recorder channels monitoring the output of the three specimen strain gages were constantly checked to verify that the specimen was being loaded uniformly.

(h) At the 7000 psi level the load cell signal was shifted to the 2-channel "fast" Y-T recorder system and the signal from strain gage 1/2 was shifted to the Y-axis input of the Y-XT recorder. The timing marker systems in these recorders, which were interlocked to the master marker system, were activated insuring that the data on all three recorders was correlated in time.

(i) A series of incremental creep experiments were then initiated. These consisted of rapidly raising the specimen stress level by approximately 625 psi and recording the resulting transient time-strain data for a period of approximately 40 minutes. After this time the stress was again rapidly increased by approximately the same

*Initial experiments conducted on specimens WO-2, WO-3 and WO-4 indicated that below a stress of approximately 7000 psi this material exhibited negligible inelastic behavior.

amount to the next level and the next transient time-strain curve recorded. During the incremental loading period and the period of approximately constant load which followed it, the load was accurately recorded on the 2-channel "fast" recorder. This data allowed an accurate determination of E_2 to be made and the time-strain data to be corrected for small load fluctuations.

(j) This incremental loading procedure was repeated eight to ten times, at increasing stress levels, until the specimen failed or it was felt desirable to terminate the experiment. In the latter case the signal from the load cell and from strain gage 1/2 were shifted back to the 12-channel recorder, the specimen was rapidly unloaded, and the strain and load cell behavior at zero load observed for a period of approximately 30 minutes.

3.3 Analysis of Experimental Data

The experimental data was contained on the master data sheet (from the 12-channel recorder) and the set of eight to ten strain versus time, and load versus time charts (from the Y-XT recorder and the 2-channel "fast" Y-T recorder). The various stages in the analysis of this data will be briefly outlined.

(i) Stress-Strain Curves

Utilizing the time-strain and time-stress data from the recorder charts, the individual stress-strain data for the three strain gages (1/2, 2/2 and 3/2) were obtained. From this data the

average stress-strain data and the per cent strain deviation ($\Delta_e\%$), which indicates the degree of non-uniform loading was computed (see Appendix 1). Figure 4 shows this data (obtained from specimen WO-7) displayed graphically. The individual stress-strain curves shown in Figure 4A include the time-dependent strains experienced during sustained loading at the various levels. In most experiments the stress-strain curves for the three gages were found to be in good agreement. Figure 4B shows the variation of $\Delta_e\%$ with stress level. The deviation* is initially high, falling rapidly to a low value and remaining there until the material starts exhibiting appreciable time-dependent strain. At this point the deviation begins to increase rapidly with increasing stress level. Figure 4C illustrates the average stress-strain curve. Here the contribution of the elastic and the time-dependent strains are shown separately. The vertical sections of the curve indicating the total time-dependent strain observed during each sustained loading period, and the dashed section indicating the total strain curve, including the time-dependent strains.

---

*Initially the contact between the end-surfaces of the test specimen and the teflon inserts in the loading jig heads are incomplete and as a result the specimen is loaded non-uniformly. As the applied load increases the teflon deforms; the contact between it and the specimen becomes complete and the load becomes uniform. Finally at high stresses, where the specimen exhibits considerable inelastic behavior, the specimen itself may strain non-uniformly even though the applied load remains uniform.

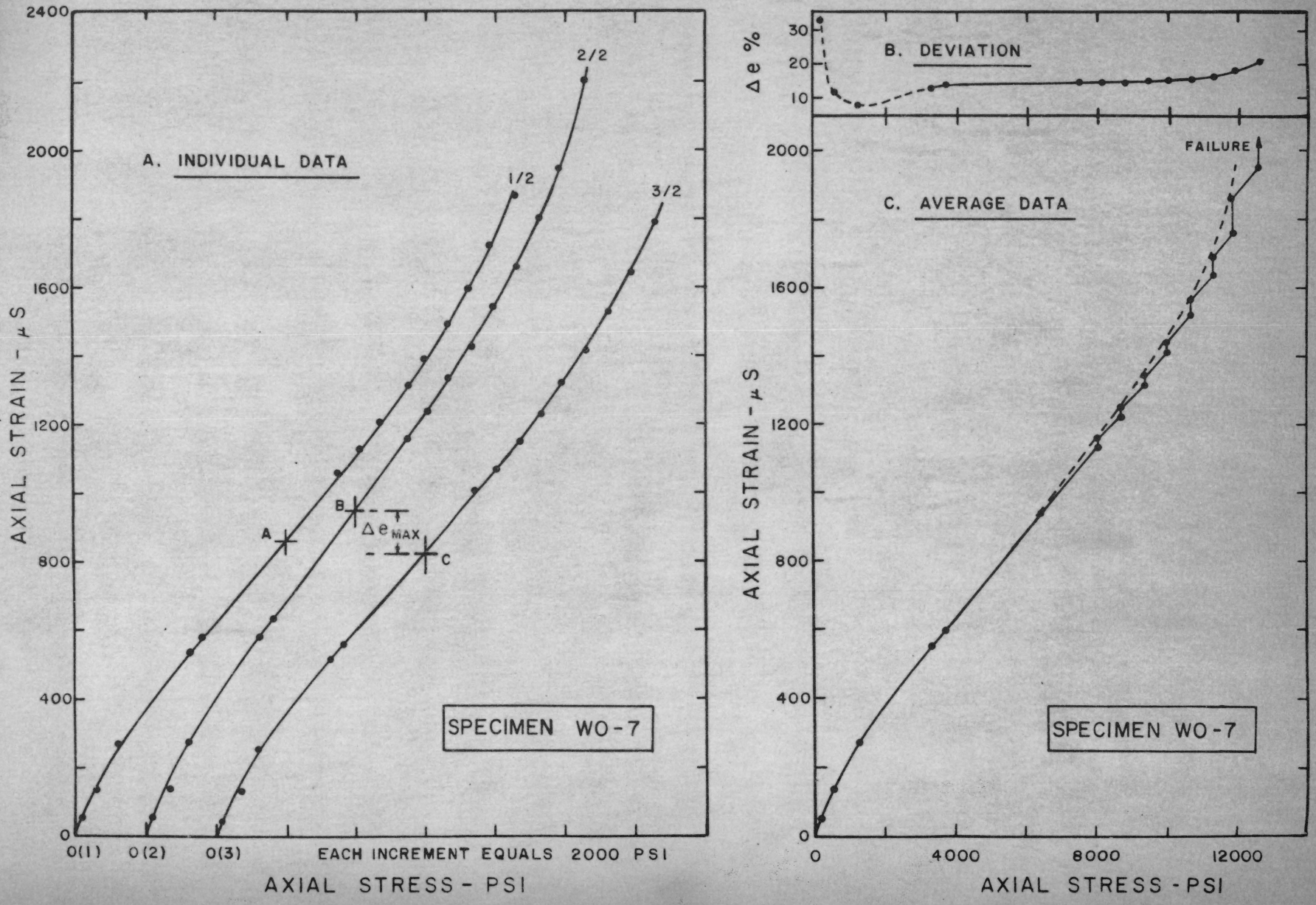


FIGURE 4 - Typical Individual and Average Strain Versus Stress Data.

(ii) Instantaneous Elastic Strain

In order to compute the value of the parameter E_2 in the Burgers model it is necessary to determine the magnitude of the instantaneous elastic strain (Δe_E) resulting from a rapidly applied incremental load. In initial experiments (WO-2, -3, -4), an attempt was made to estimate the value of Δe_E directly from the strain versus time curves. This method was found satisfactory for stress levels below 7000 psi where the material was effectively elastic in behavior. Above this level however, the strain versus time curves were complicated by superimposed inelastic effects and by small fluctuations in the applied load. It was therefore found necessary to develop a more refined method of analysis for use in the inelastic region.

This analysis involved the use of both the strain versus time (Y-XT recorder) and load versus time (2-channel "fast" Y-T recorder) recordings and necessitated the development of a time marker system (see Appendix 1). Figure 5 illustrates diagrammatically sections of the time-strain and time-load recordings. Section AB (similarly A'B') represent the end of the previous experiment conducted at a sustained load of $L_c(1)$. At time t = 0 the load is rapidly increased and eventually becomes stable at a new level $L_c(2)$. However, due to the typical load fluctuations (B'D'E'F'G), which normally accompany an

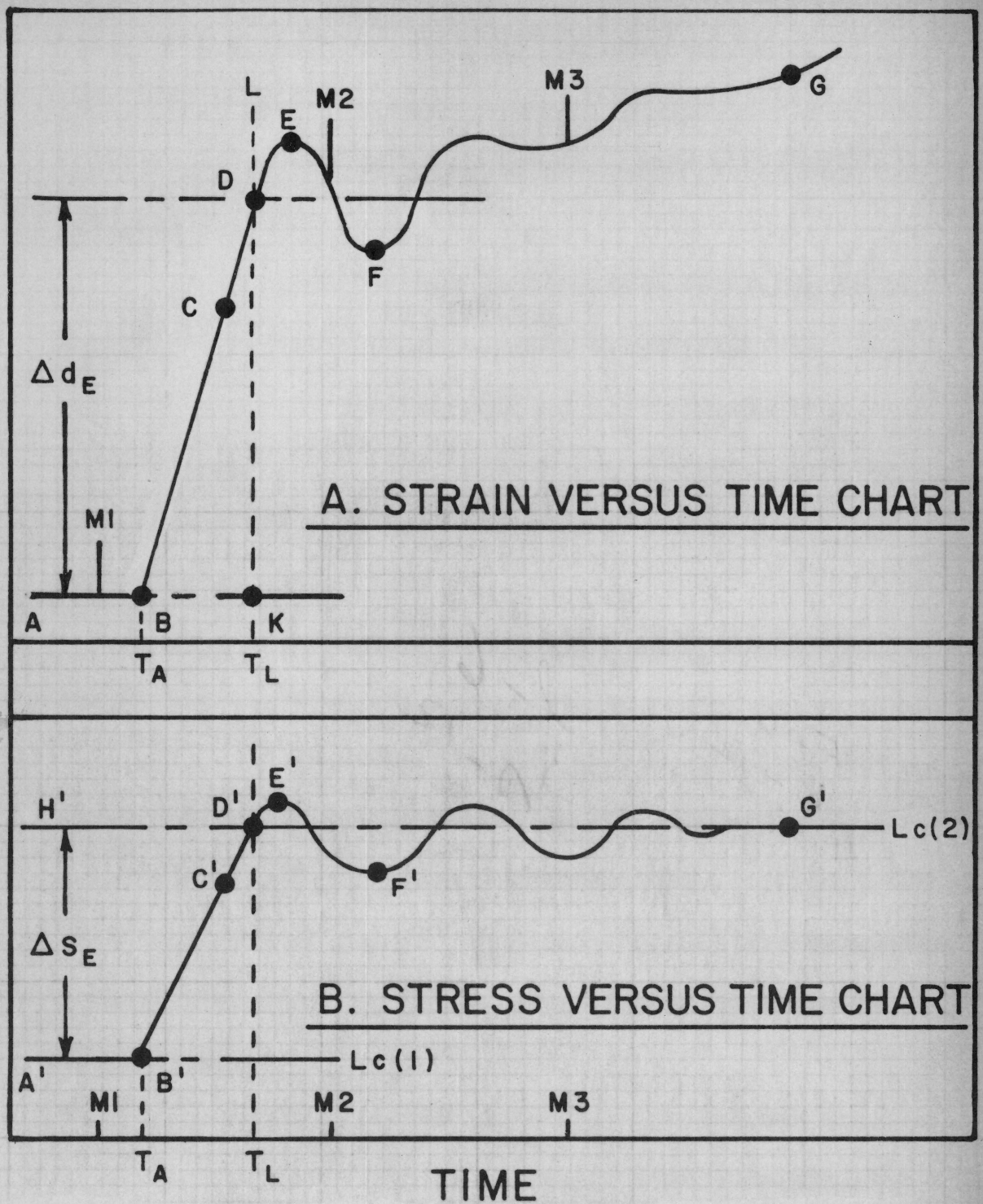


FIGURE 5 -Method Used to Determine the Instantaneous Elastic Strain.

incremental load change and which are reflected in the time-strain curve, it is not possible to estimate the instantaneous elastic strain Δe_E associated with the load increment $(L_c(2)-L_c(1))$ by a simple inspection of the time-strain curve. Instead the following procedure was used:

(a) The final equilibrium level of $L_c(2)$, at point G', was determined by inspection of the overall time-load curve.

(b) The line G'H' was drawn through G' parallel to the time axis, cutting the load-time curve at point D'; the chart displacement Δd_E corresponding to the incremental load $(L_c(1)-L_c(2))$.

(c) The corresponding time T_L was determined, in relation to the timing markers M_1 and M_2.

(d) At the corresponding time on the time-strain curve a vertical line KL was drawn which cut the time-strain curve at the Point D.

(e) The chart displacement (Δd_E) corresponding to the instantaneous elastic strain (Δe_E) is represented by the distance KD as shown.

(f) The elastic modulus (E_2) associated with the instantaneous elastic strain was determined from the expression

$$E_2 = \Delta\sigma_m / \Delta e_\varepsilon \qquad (17),$$

where

$$\Delta e_E = k_3 \Delta d_E \qquad (18),$$

and

$$\Delta \sigma_n = k_1 \Delta s_E \qquad (19),$$

and k_1 and k_3 are the stress and strain sensitivities of the two recording systems.

The incremental loads were applied rapidly ($\Delta T < 4$ seconds), and the position of T_L on the recorder charts could be determined to within one second. It may be shown (see Appendix 6) that under these conditions the maximum error in Δe_E introduced by neglecting the inelastic contribution to the instantaneous strain will be less than 1.5%.

(iii) Time-Dependent Strain

Two difficulties were encountered initially in analyzing the time-dependent strain data. First it was not possible to determine by inspection the time (t_o) at which this strain was initiated. Secondly the time-dependent strains observed were relatively small, ranging from 5-200 μs in 40 minutes, and it was therefore necessary to correct the original experimental strain-time curves for the small fluctuations in the applied load. The procedure developed to overcome these difficulties will be outlined briefly.

The difficulty of accurately determining the point $e(t) = 0$, $t = 0$ on the strain versus time curve was overcome once the

procedure described in the last section for accurately determining Δe_E was developed. On the strain versus time curve shown in Figure 5 the Point D represents both the limit of the instantaneous elastic strain and the point e(t) = 0, t = 0 on the time-dependent strain versus time curve.

The procedure developed for correcting the strain versus time data for fluctuations in the applied load is briefly as follows:

(a) Figures 6A and 6B show diagrammatically an enlarged view of the inelastic section of the strain versus time curve and the load versus time curve, shown earlier in Figure 5. A vertical grid* is first superimposed on both curves using the time markers for reference.

(b) The chart displacements (d_1, d_2, ---, d_n) corresponding to the observed strain at times t_1, t_2, etc. are tabulated along with the chart displacements (Δd_1, Δd_2, ---, Δd_n) corresponding to the deviation of the applied load from the control point $L_c(2)$ for the same time.

---

* Experience has shown that the following grid spacing is satisfactory for most cases: 6-5 sec intervals, 10-30 sec intervals, 5-60 sec intervals, and the remainder 120 sec intervals.

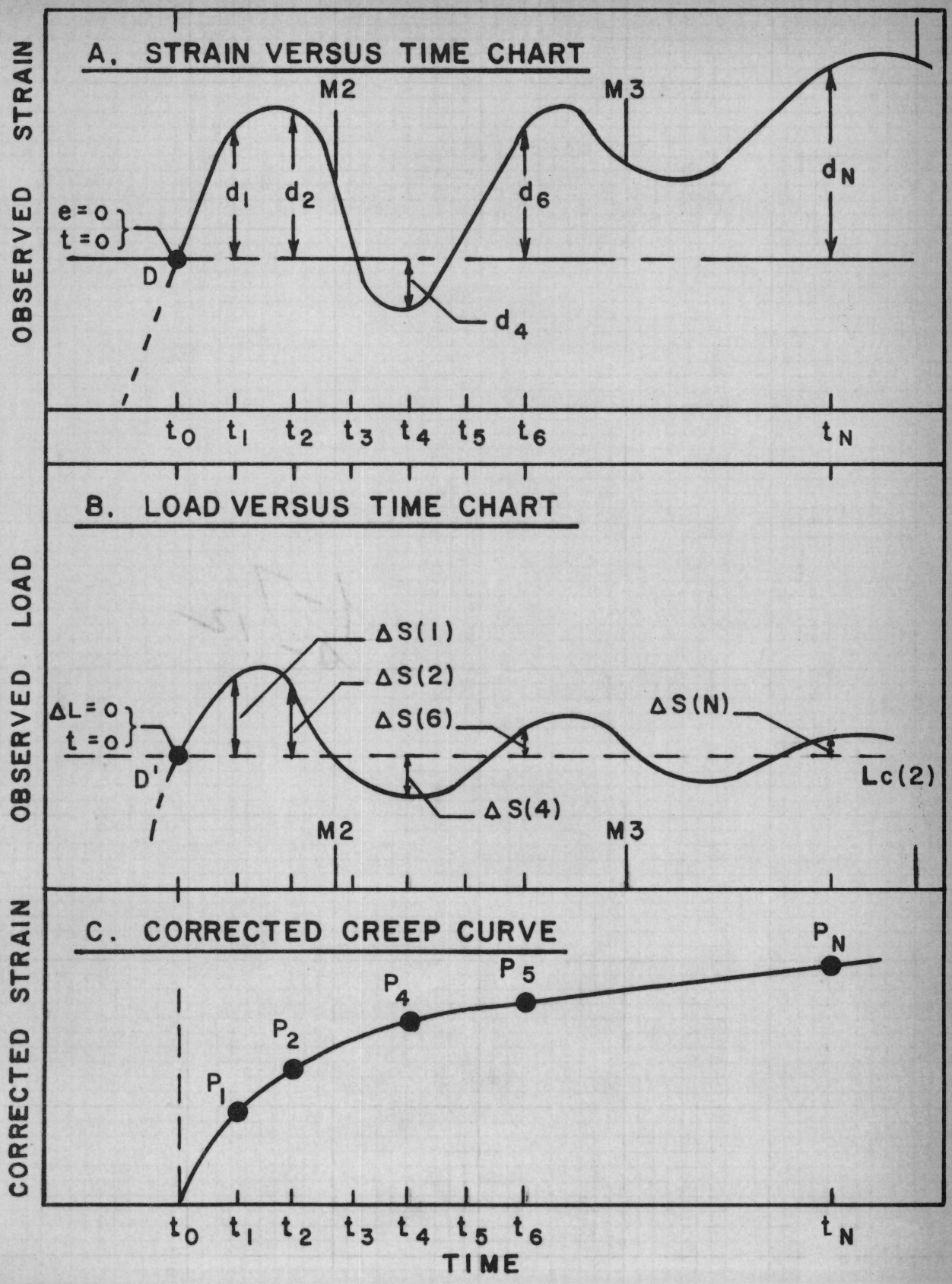


FIGURE 6 - Method Used to Correct the Observed Strain Versus Time Data.

(c) The observed strain (e_{ob}) at t_1, t_2 --- t_n are calculated from the relation

$$e_{ob} = k_3 d \qquad (20),$$

and the load deviation at t_1, t_2 --- t_n are calculated from the relationship

$$\Delta \sigma_c = k_1 \Delta d \qquad (21),$$

where $\Delta \sigma_c$ will be positive for loads greater than the control load, and all other factors have been defined previously.

(d) The strain deviations (Δe_c) caused by the stress fluctuations $\Delta \sigma_c$ will be associated almost entirely with the series elastic element in material. This is the same element responsible for the instantaneous elastic strain discussed earlier. The strain deviation may therefore be simply calculated from

$$\Delta e_c = \Delta \sigma_c / E_2 \qquad (22),$$

where E_2 is the modulus of the elastic element determined earlier from equation 17.

(e) The corrected strain (e_c) at t_1, t_2, --- t_n is then obtained from the relationship

$$e_c = e_{ob} - \Delta e_c \qquad (23).$$

(f) Finally the values of e_c are plotted against the corresponding times t_1, t_2, ---, t_n, as shown in Figure 6C, to obtain the corrected creep curve.

(iv) Determination of Model Parameters from Creep Data

Once the corrected creep data was obtained the next step was to analyze this data in terms of the Burgers model. In earlier studies by the writer and others this analysis was normally carried out by graphical construction. When this form of analysis was investigated in more detail, however, it was found that it was too subjective and that the results obtained for the model parameters were not consistent. To overcome this the writer established a program, in the summer of 1964, to investigate various means for analyzing the data (see Steppel 1965).

The procedure finally developed (see Hardy, Steppel and Toews (1965)) consisted of determining a set of initial (rough) parameters from the corrected creep curve, and then using these parameters and the Gauss-Newton method the least squares values of the model parameters were obtained. Initially the Gauss-Newton procedure was applied manually, but as this was found to be too time consuming, a program for this analysis was written for the Mines and Technical Surveys IBM-1620 computer. The overall analysis procedure will be briefly outlined here, but no attempt will be made to discuss in detail

either the Gauss-Newton method or the computer program.

Equation 16 may be written in the form

$$e_m(t) = A\left[1 - \exp(-t/B)\right] + Ct \qquad (24),$$

where

$$A = \Delta\sigma_m / E_1 \qquad (25),$$

$$B = \tau = N_1/E_1 \qquad (26),$$

$$C = \sigma_m / N_2 \qquad (27).$$

The purpose of the analysis is to find the values of A, B and C which make the theoretical expression (equation 24) fits the experimental data as closely as possible. Once these values are determined the model parameters E_1, N_1 and N_2 may be calculated from equations 25, 26 and 27.

Since equation 24 is non-linear the least squares values of A, B and C can not be found directly. Instead initial approximations A_o, B_o and C_o must first be determined and these corrected by an iterative procedure to give the "best values".

(v) Determination of Initial Parameters

A number of methods were investigated for determining the initial parameters (see Steppel (1965)). However the most practical method involved the use of data from three specific points on the

corrected creep curve. Complete details of this method are given in Appendix 3. Briefly the method is as follows:

(a) Figure 7 shows a typical corrected creep curve OPA. A point P is selected on the curve, at a location just outside where the line AB becomes tangent to the curve. The corresponding time T associated with this point is noted.

(b) Three other points P_1, P_2 and P_3 are located on the curve with time coordinates T/8, 7T/8 and T/2 respectively. The strain coordinates (e_1, e_2 and e_3) of these points are determined.

(c) The slope (tan α) of the line AB, which is tangent to the linear portion of the curve, is determined. This slope is equal to C_o one of the required parameters.

(d) The parameter A_o is calculated from the relationship

$$A_o = \frac{f_3^2 - f_1 f_2}{2f_3 - f_1 - f_2} \qquad (28),$$

and

$$f_m = e_m - C_o t_m \qquad (29),$$

where e_m and t_m are the coordinates of the points P_1, P_2 and P_3, and C_o is the parameter determined in step (c).

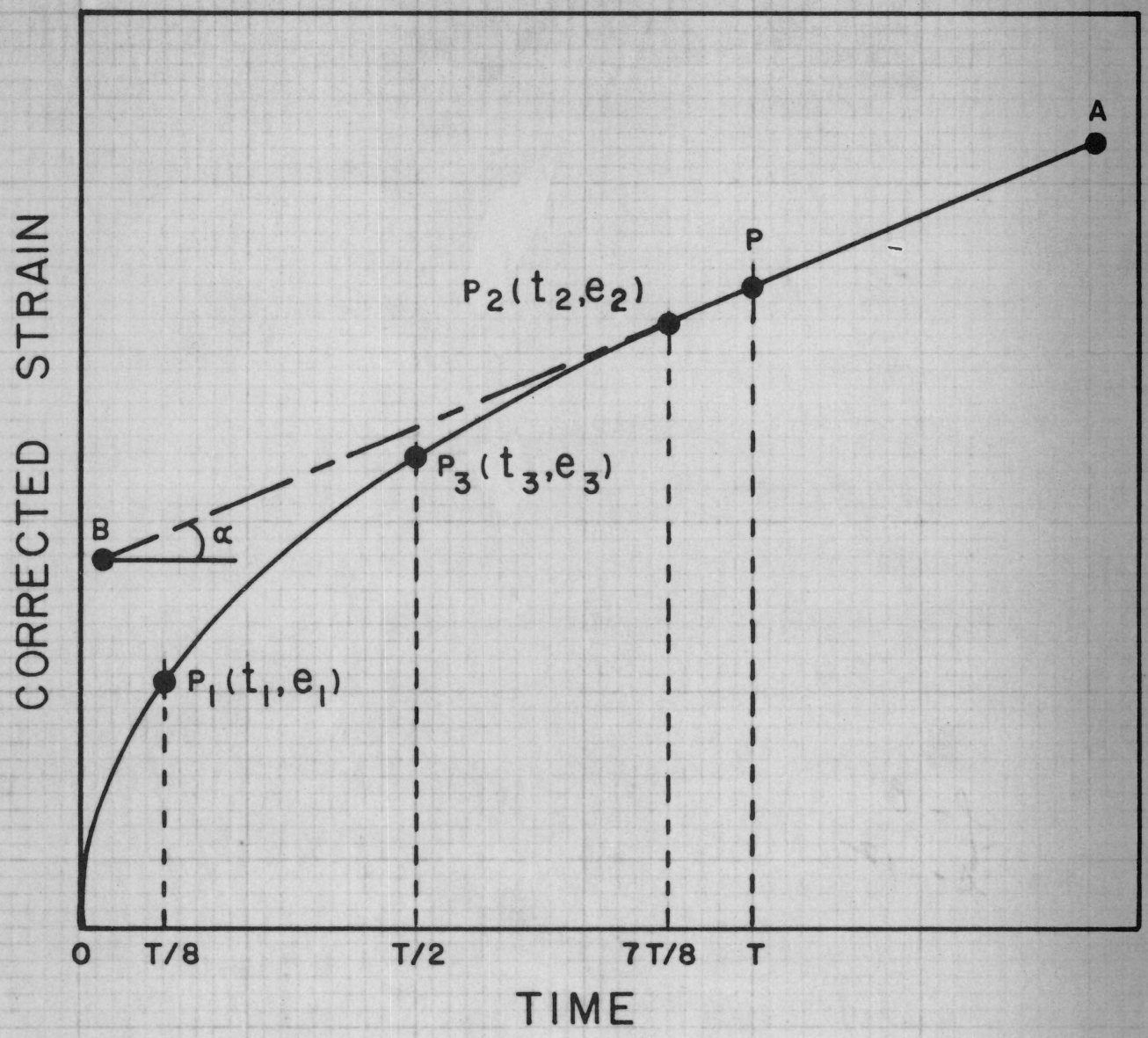


FIGURE 7 - Method Used to Determine the Initial Parameters.

(e) The parameter B_o is calculated from the relationship

$$B_o = \sum_{o}^{3} B_m / 3 \qquad (30),$$

where

$$B_m = \frac{t_m}{\ln\left(\frac{A_o}{A_o - f_m}\right)} \qquad (31),$$

and all other factors have been defined previously.

(vi) Least Squares Analysis

The standard method of function fitting by the technique of least squares (see Deming (1943)) can not be applied when the function contains non-linear terms (e.g. $e^{-t/B}$). Instead the Gauss-Newton method of least squares analysis (see Hartley (1961)) was used. In this method an iterative procedure is employed in which parameters A_o, B_o and C_o are used as initial estimates of A, B, and C and the analysis carried out to give values A_1, B_1 and C_1 which are better estimates of A, B, and C. The values A_1, B_1 and C_1 themselves are then used as the new initial estimates of the parameters and the analysis carried out again. This procedure is repeated k times until the values of the parameters A_k, B_k and C_k obtained provide a satisfactory fit to the experimental data.

(vii) Computer Program

A Fortran program using the Gauss-Newton method was written for the IBM-1620 computer. This allowed efficient handling of the large volume of data and permitted as many iterations as necessary to be carried out. A copy of the Fortran program is given in Appendix 4 along with a set of typical output data.

One of the main aspects of the program which was investigated was that of the relationship between the quality of the initial parameters (A_o, B_o and C_o) and the probability of convergence. From a number of tests it appears that the parameters converge to their true values even with widely different values of the initial parameters. For example in one case the analysis of a specific set of creep data was carried out using two different sets of initial parameters namely,

I. $A_o = 38.0$
$B_o = 150.0$
$C_o = 0.217$

II. $A_o = 125.0$
$B_o = 440.0$
$C_o = 0.127$

After three iterations set I produced the results,

$A = 66.17$
$B = 278.55$
$C = 0.185$

and after five iterations set II produced the results,

$$A = 66.19$$

$$B = 279.33$$

$$C = 0.185$$

The close agreement of the two sets of results indicate the relative insensitivity of the analysis to the values of the initial parameters. It is planned to investigate this aspect of the analysis further with the aim of developing a less refined method for estimating suitably accurate initial parameters.

Figures 8 and 9 illustrate how well the theoretical expression (equation 24) may be fitted to the experimental data. Figure 8 shows the creep data for specimen WO-5 at a stress level where the inelastic behavior is relatively small. The total creep strain after sustained loading for approximately 40 minutes being of the order of 10 μs. Figure 9 illustrates the behavior of the same specimen at a stress level near the failure stress. Here the total creep strain was of the order of 120 μs during a sustained loading period of approximately 70 minutes. In both cases the analysis provided a theoretical curve which fitted the data extremely well, the standard deviation being 0.37 and 1.8 μs respectively.

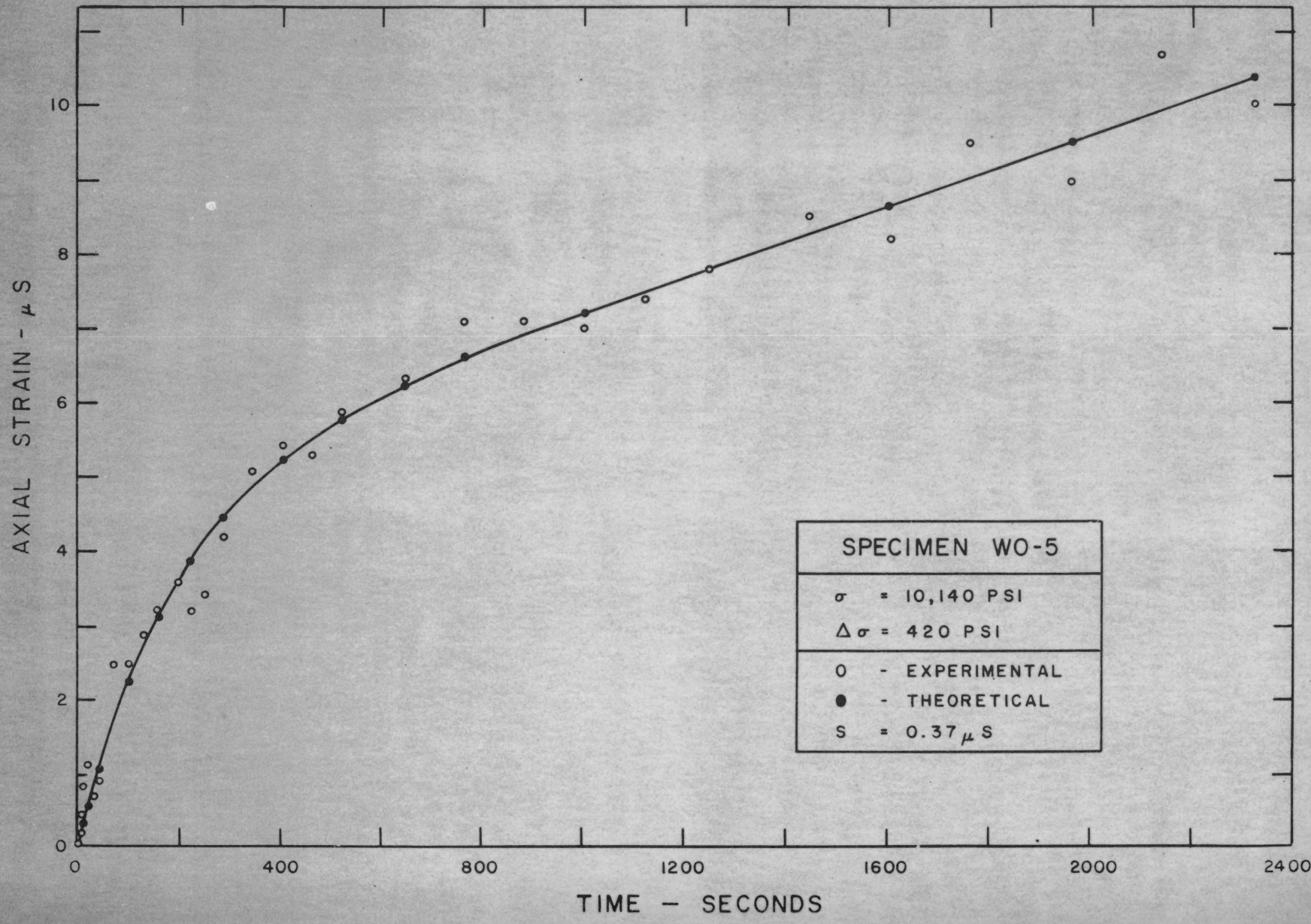


FIGURE 8 - Typical Creep Curve for a Low Stress Level (Specimen WO-5).

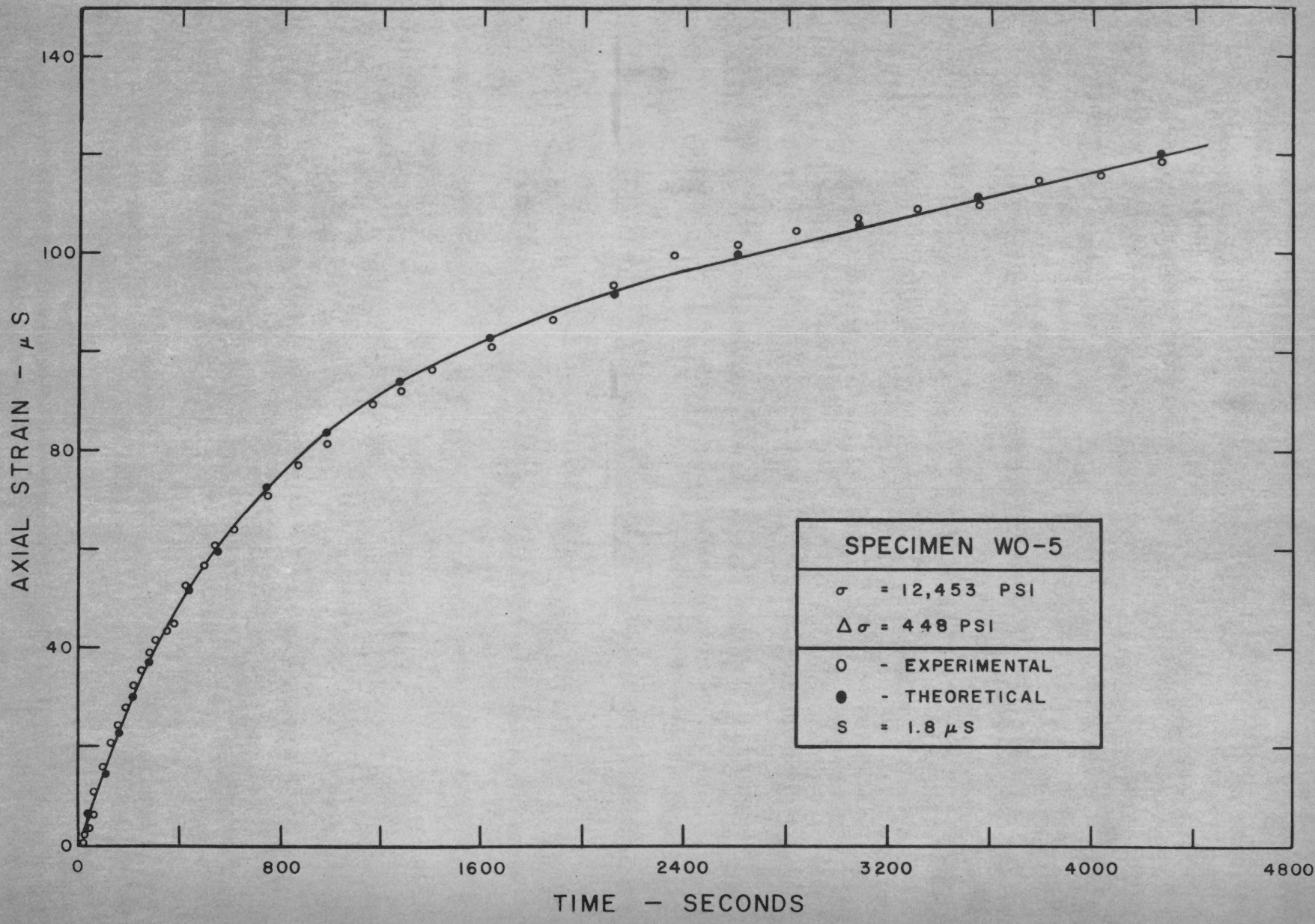


FIGURE 9 - Typical Creep Curve for a High Stress Level (Specimen WO-5).

4. Experimental Results

4.1 General

The deformation behavior of six specimens of Wombeyan marble was investigated using incremental creep experiments. The experiments conducted on specimens WO-2, -3, and -4 served to provide approximate data on a number of the mechanical properties of the material (e.g. ultimate strength*, critical stress**, model parameters, etc.), and to allow further development and modification of the apparatus and the experimental technique. As a result of these initial experiments, it was found that corrections for very small load fluctuations were necessary in order to obtain meaningful creep curves at low stress levels. This requirement also necessitated the development of the time marker system in order to accurately correlate data from the strain versus time and the load versus time recorder charts. Since creep data from tests on these three specimens were badly in error, due to lack of suitable corrections for load fluctuation, they will not be presented here.

The experiments conducted on specimen WO-5 included the necessary data for correction of small load fluctuations. These

---

* The ultimate strength (σ_u) is defined here as the maximum stress reached during an experiment. At this stress the specimen either failed immediately or strained at an accelerating rate.

** The critical stress (σ_A) is defined here as the stress at which time-dependent strain was first observed.

experiments indicated however that the model parameters appeared to be dependent on the magnitude of the stress increment ($\Delta\sigma$) and the duration (T) of the individual incremental creep experiments. To eliminate the effect of these two factors experiments were carried out on specimens WO-6 and WO-7 using nearly constant values of $\Delta\sigma$ and T for each incremental creep experiment. In these latter experiments it was found that extremely consistent results were obtained.

Figure 10 shows the average stress-strain curves for each of the six specimens. On the dashed section of the curves the total strain consists of an elastic and a time-dependent component. Table 1 lists a number of the important parameters associated with each test specimen. There is a remarkable similarity between the stress-strain curves for all six specimens. All curves exhibit the same initial curvature followed by a linear region from about 4000 to 8000 psi. This is followed by a region of increasing curvature which appears to be associated with the initiation of time-dependent behavior. The stress-strain curves for specimens WO-6 and WO-7, which were deformed following exactly the same loading program, were found to be very nearly identical. The elastic modulus E_2, associated with the instantaneous elastic response of the material, was found to vary with stress level for these two specimens as shown in Figure 11. At a stress level of 200-300 psi the modulus is of the order of 3×10^6 psi. With increasing

TABLE 1

General Data for Six Specimens of Wombeyan Marble

Specimen Number	Nominal Specimen Length	Nominal Specimen Diameter	Storage Time (1)	σ_A (2)	σ_u (3)	e_u (4)	Comments
	inches	inches	months	psi	psi	μs	
WO-2	1.50	0.75	12	7461	13,698*	1574	Immediate failure
WO-3	1.50	0.75	12	7170	13,990	2185	Failure after considerable creep
WO-4	1.50	0.75	12	7092	13,931	2575	Failure after considerable creep
WO-5	1.75	0.75	1	7026	12,539	1735	Specimen unloaded before failure
WO-6	1.75	0.75	1	7487	12,544	1872	Specimen unloaded before failure
WO-7	1.75	0.75	1	7468	12,562	>1950	Failure after considerable creep

(1) Time between preparation and testing of specimens.

(2) Critical compressive stress at which time-dependent strain first observed, values only approximate.

(3) Maximum compressive stress reached during specific experiment.

(4) Maximum average strain reached during specific experiment.

* Specimen stable at 12,979 psi but failed immediately at next level, 14,417 psi. σ_u quoted is average of these two levels.

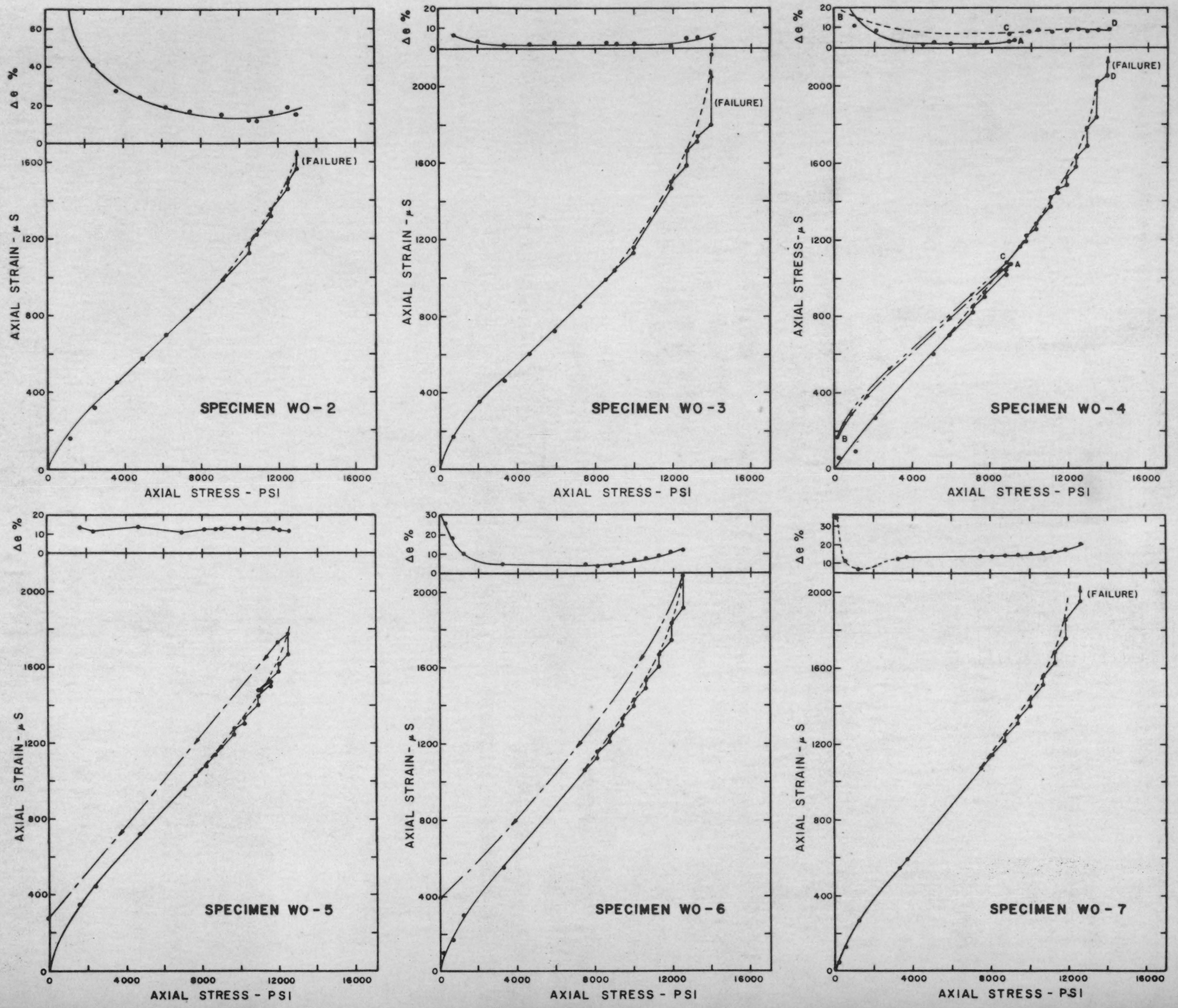


FIGURE 10 - Average Strain Versus Stress Curves for Specimens WO-2 to WO-7.

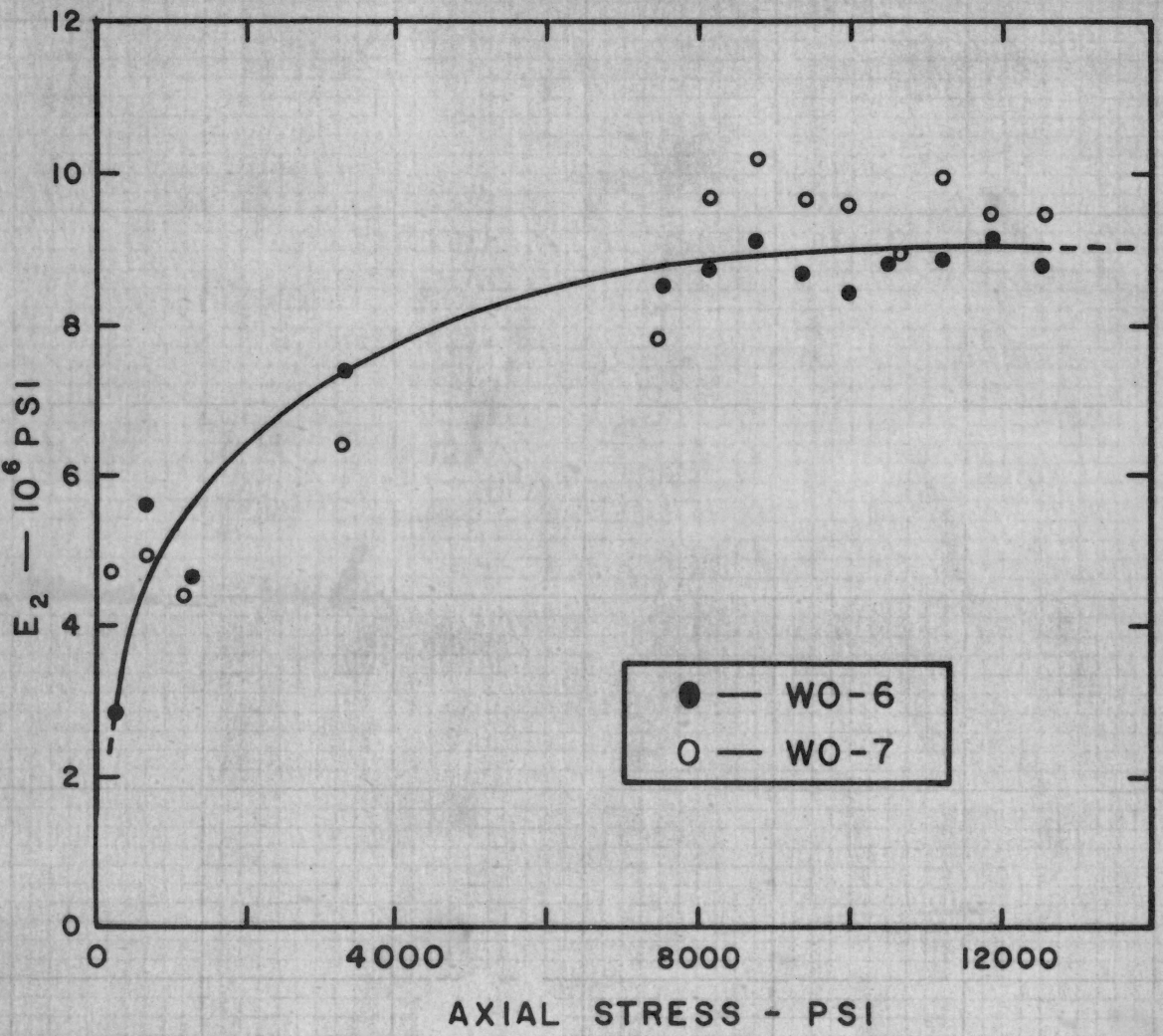


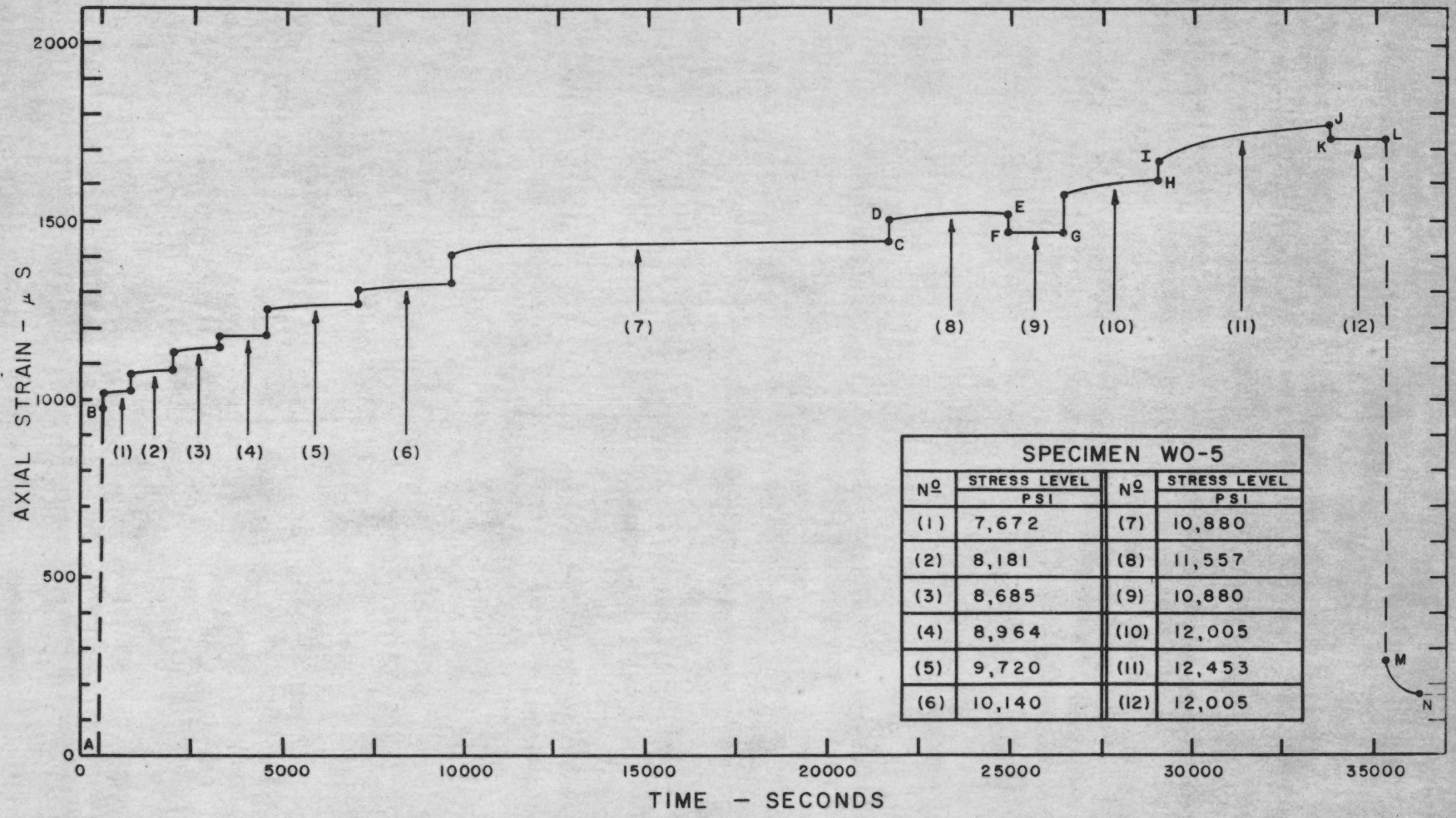
FIGURE 11 - Variation of E_2 with Stress Level.

stress the value rises to approximately 9 x 10^6 psi (at a stress of 8000 psi) remaining nearly constant at this value up to failure.

4.2 Results of Incremental Creep Experiments

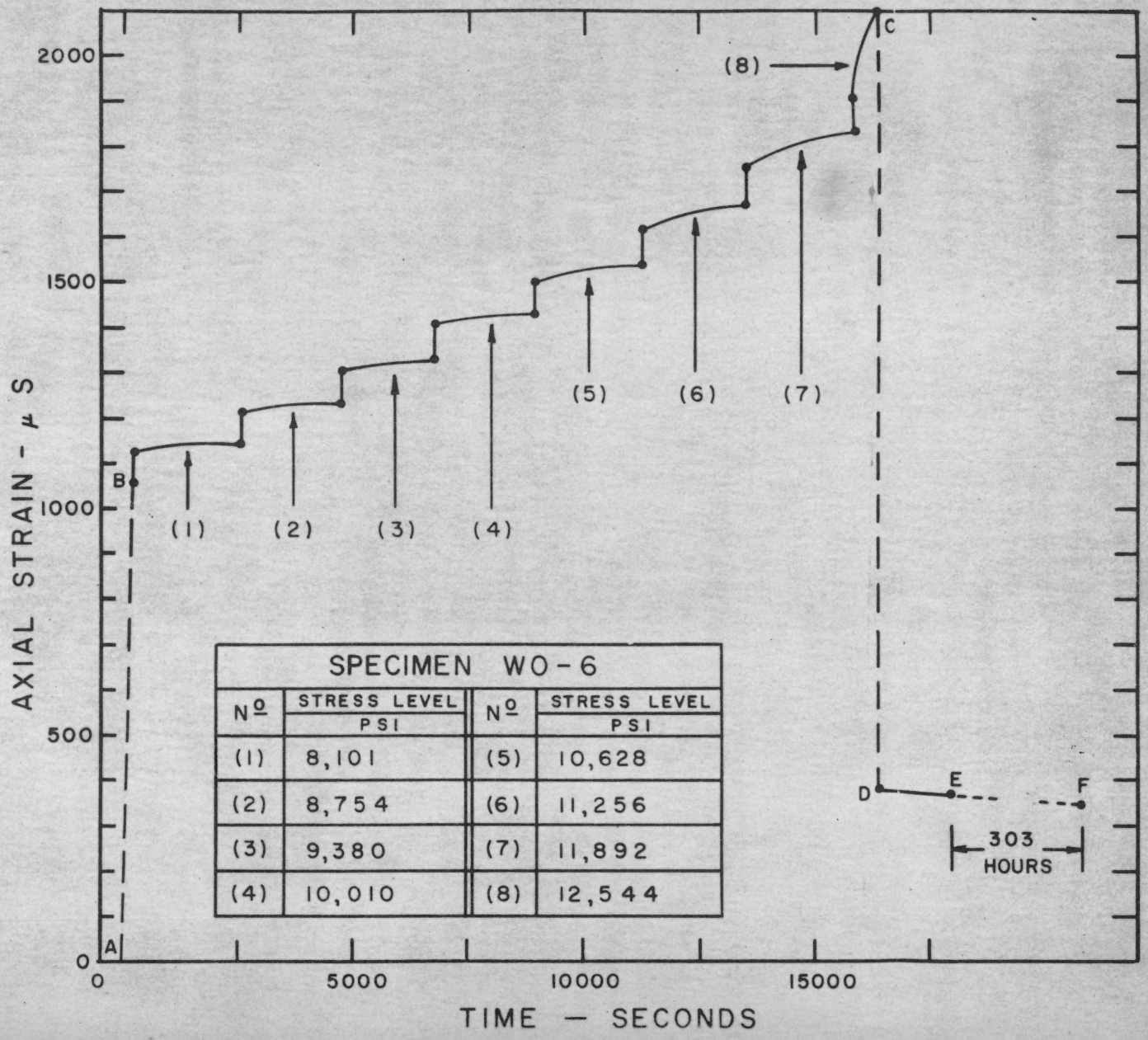
A total of 26 incremental creep experiments were carried out on specimens WO-5, -6 and -7. Figures 12, 13 and 14 show diagrammatically the sequence of the individual experiments and the overall time-strain data for each specimen. Tables 23 to 48 in Appendix 5 give the detailed experimental and theoretical* creep data for each experiment. Table 2 summarizes the experimental details and the results for each test.

* The theoretical creep strains listed in these tables are based on a least squares fit of the experimental data to the Burgers mechanical model.



SPECIMEN WO-5			
Nº	STRESS LEVEL PSI	Nº	STRESS LEVEL PSI
(1)	7,672	(7)	10,880
(2)	8,181	(8)	11,557
(3)	8,685	(9)	10,880
(4)	8,964	(10)	12,005
(5)	9,720	(11)	12,453
(6)	10,140	(12)	12,005

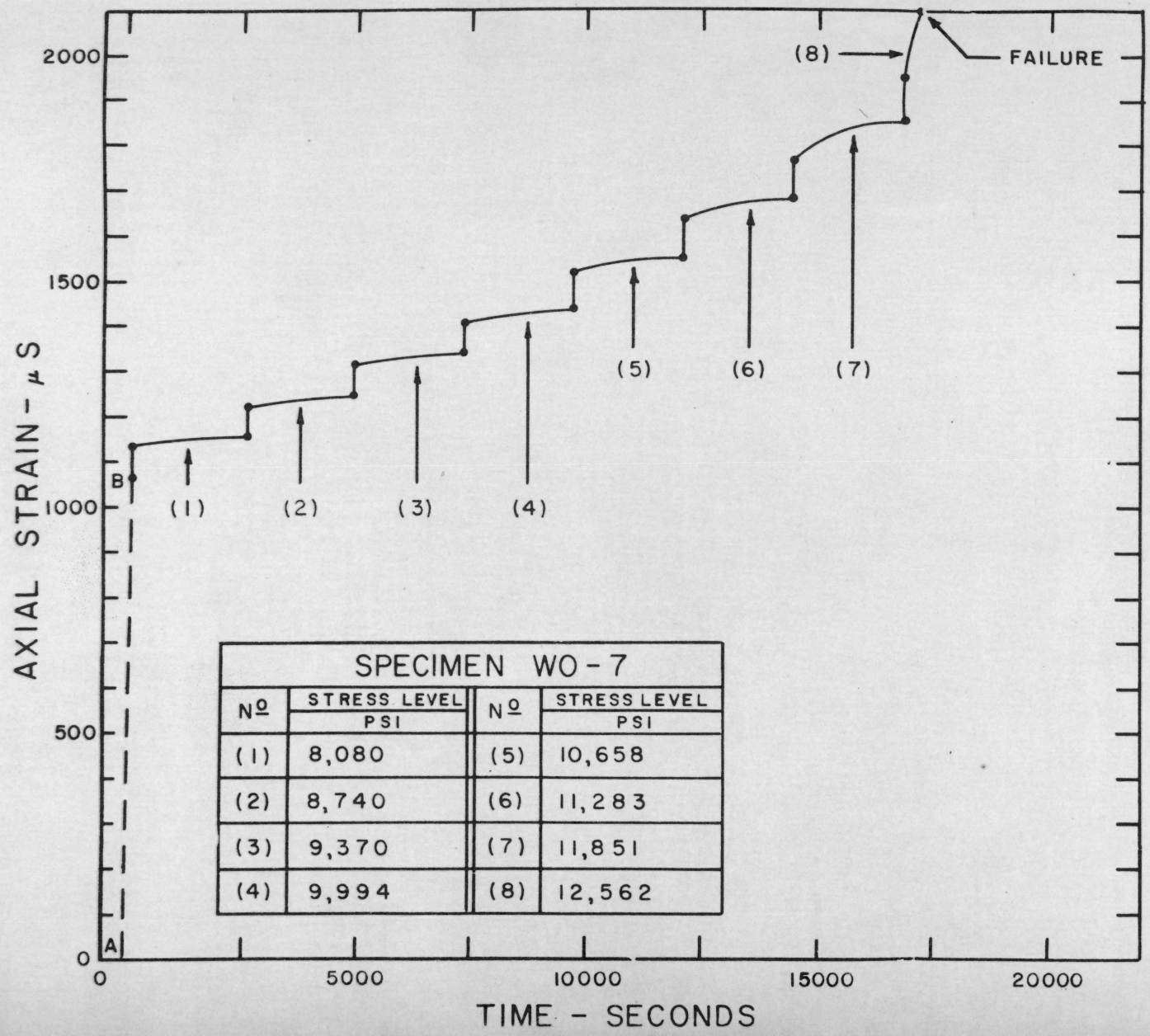
FIGURE 12 - Overall Strain Versus Time Curve for Specimen WO-5.



SPECIMEN WO-6

No.	STRESS LEVEL PSI	No.	STRESS LEVEL PSI
(1)	8,101	(5)	10,628
(2)	8,754	(6)	11,256
(3)	9,380	(7)	11,892
(4)	10,010	(8)	12,544

FIGURE 13 - Overall Strain Versus Time Curve for Specimen WO-6.



SPECIMEN WO-7

Nº	STRESS LEVEL PSI	Nº	STRESS LEVEL PSI
(1)	8,080	(5)	10,658
(2)	8,740	(6)	11,283
(3)	9,370	(7)	11,851
(4)	9,994	(8)	12,562

FIGURE 14 - Overall Strain Versus Time Curve for Specimen WO-7.

TABLE 2

Summary of Details and Experimental Results from Incremental Creep Experiments on Wombeyan Marble Specimens

Specimen Number	Experiment Number (1)	σ_i(2)	σ_f	$\Delta\sigma$	T	A(3)	B	C	S(4)	E_1(5)	N_1	E_2	N_2
		psi	psi	psi	seconds	μs	seconds	μs/sec	μs	10^6 psi	10^9 psi-sec	10^6 psi	10^9 psi-sec
WO-5	5 - (1)	7026	7672	646	543	2.5	72.8	.0003	0.35	253.9	18.5	11.0	23,080
"	5 - (2)	7672	8181	509	1095	3.3	81.6	.0014	0.70	154.7	12.6	11.2	5708
"	5 - (3)	8181	8685	504	1223	4.0	22.1	.0033	0.43	125.1	2.8	10.8	2622
"	5 - (4)	8685	8964	279	1320	1.3	290.7	.0011	0.37	223.0	64.8	11.5	8068
"	5 - (5)	8964	9720	756	2400	9.4	39.9	.0044	0.86	80.6	3.2	11.2	2218
"	5 - (6)	9720	10,140	420	2700	4.9	190.2	.0024	0.39	86.1	16.4	10.6	4272
"	5 - (7)	10,140	10,880	740	12,000	25.4	121.6	.0055	1.54	29.2	3.6	10.7	1993
"	5 - (8)	10,880	11,557	677	2200	4.9	16.9	.0058	0.88	137.3	2.3	11.9	1978
"	5 - (10)	10,880	12,005	1125	2610	27.7	905.9	.0032	0.80	40.6	36.8	11.3	3677
"	5 - (11)	12,005	12,453	448	4680	88.7	583.9	.0121	1.79	5.1	3.0	9.9	1027
WO-6	6 - (1)	7487	8101	614	2386	11.4	81.2	.0047	0.74	53.9	4.4	8.6	1719
"	6 - (2)	8101	8754	653	2190	15.6	45.3	.0057	1.42	41.8	1.9	9.1	1540
"	6 - (3)	8754	9380	626	2064	19.6	108.2	.0074	1.19	31.9	3.5	8.6	1263
"	6 - (4)	9380	10,010	630	2184	21.5	84.3	.0067	1.97	29.3	2.5	8.4	1505
"	6 - (5)	10,010	10,628	618	2300	35.4	117.4	.0125	1.70	17.5	2.1	8.9	854
"	6 - (6)	10,628	11,256	628	2294	56.4	118.2	.0136	4.11	11.1	1.3	8.9	830
"	6 - (7)	11,256	11,892	636	2303	78.2	180.9	.0234	3.20	8.1	1.5	9.2	509
"	6 - (8)	11,892	12,544	652	440	170.9	158.3	.1796	4.86	3.8	0.6	8.8	70
WO-7	7 - (1)	7468	8080	612	2440	13.8	42.9	.0030	1.08	44.5	1.9	9.7	2700
"	7 - (2)	8095	8740	645	2320	15.2	23.7	.0049	1.28	42.4	1.0	10.2	1772
"	7 - (3)	8759	9370	611	2449	15.9	117.2	.0049	0.97	38.3	4.5	9.7	1898
"	7 - (4)	9386	9994	608	2313	19.9	63.3	.0066	1.44	30.6	1.9	9.6	1505
"	7 - (5)	10,031	10,658	627	2391	24.0	122.1	.0070	2.12	26.2	3.2	8.9	1516
"	7 - (6)	10,640	11,283	643	2394	37.4	105.1	.0124	2.89	17.2	1.8	10.0	909
"	7 - (7)	11,212	11,851	639	2382	48.9	237.8	.0138	2.14	13.1	3.1	9.5	861
"	7 - (8)	11,912	12,562	650	333	20.9	27.9	.3182	2.07	31.0	0.9	9.5	40

(1) Experiment Numbers correspond to those given in Figures 12, 13 and 14, and in Tables in Appendix 5.

(2) σ_i is the initial stress, σ_f is the final stress, $\Delta\sigma$ is the incremental stress, and T is total duration of experiment.

(3) A, B and C are parameters obtained by least squares fit to equation 24.

(4) S is standard deviation associated with least squares fit.

(5) E_1, N_1, E_2 and N_2 are model parameters calculated from A, B, C and Δe_a.

The experimental data was found to fit the incremental creep form of the Burgers model (equation 14) extremely well (as illustrated earlier in Figures 8 and 9). Initial experiments, however, had indicated that the model parameters (E_1, N_1, E_2, N_2 and $\mathcal{T}$) as well as the final steady state strain rate (C) were functions of the axial stress. The more refined experiments conducted on specimens WO-5 to WO-7 verified this fact. Figures 15-20 show the variation of these factors as a function of axial stress (σ_{zz}). To further emphasize the close agreement of results for specimens WO-6 and WO-7 Figures 21 and 22 show the combined results for both specimens.

In order to investigate the stress dependency of the Burger model parameters in more detail, the experimental results were analyzed using the IBM-STUFF Program* and fitted by least squares to a straight line relationship** ($X = A_o + A_1\sigma$, where X is the particular factor, σ is the axial compressive stress, and A_o and A_1 are the intercept and the slope of the theoretical curve). These theoretical curves are shown on the respective figures, and Tables 3 to 6 list the coefficients A_o and A_1 associated with the stress dependency of the various factors. Where an isolated inconsistent data point appeared, it was rejected from the STUFF analysis.

---

*IBM-1620 Universal Function Fitting program.

**Attempts were made to fit the experimental data to higher order polynominals but in most cases the improvement in the quality of the fit was relatively small. Until further creep studies are conducted, at stresses in the neighbourhood of σ_A where inelastic behavior appears to commence, it is felt that a straight line fit is adequate.

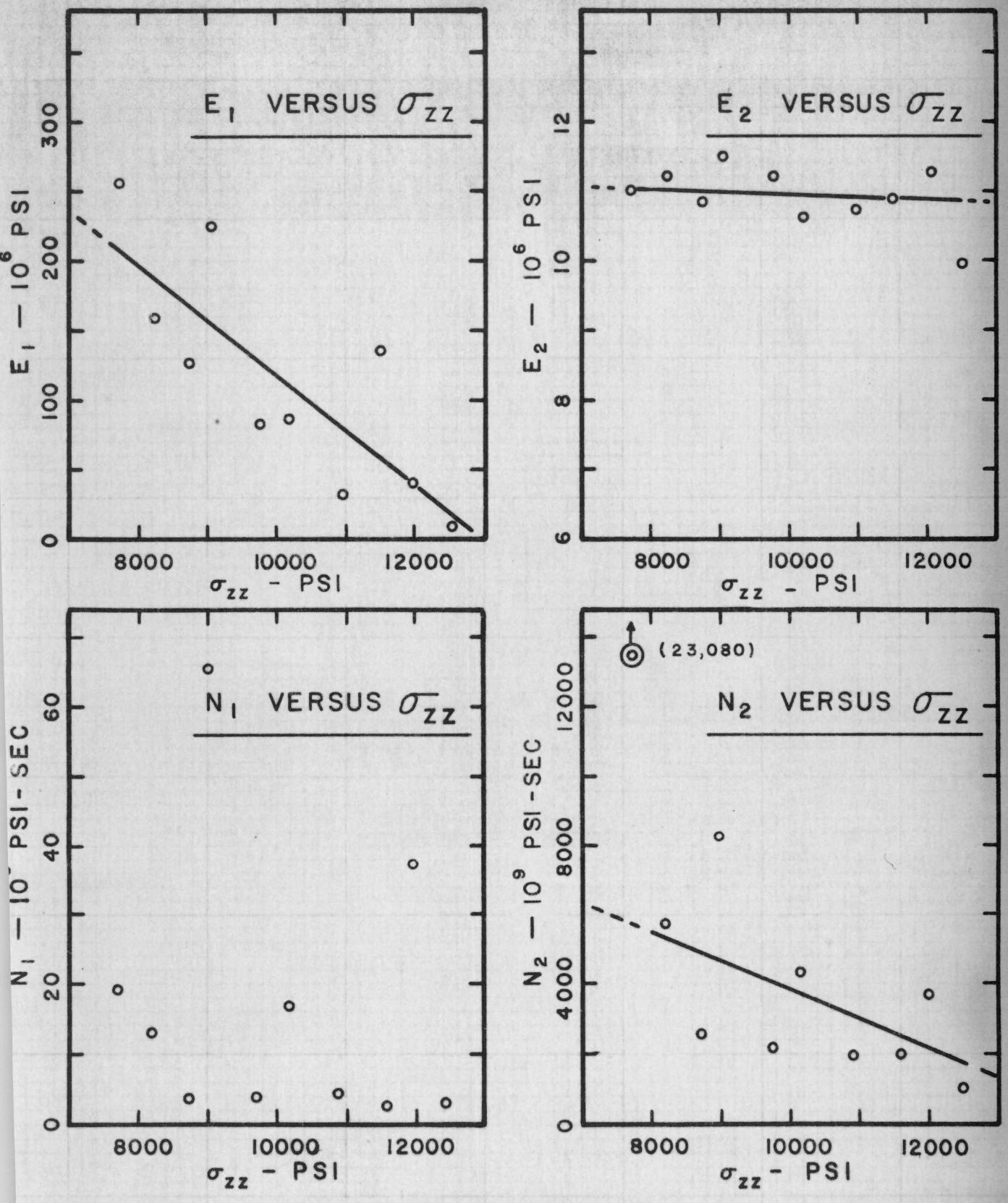


FIGURE 15 - Variation of Model Parameters (E's and N's) with Stress Level for Specimen WO-5.

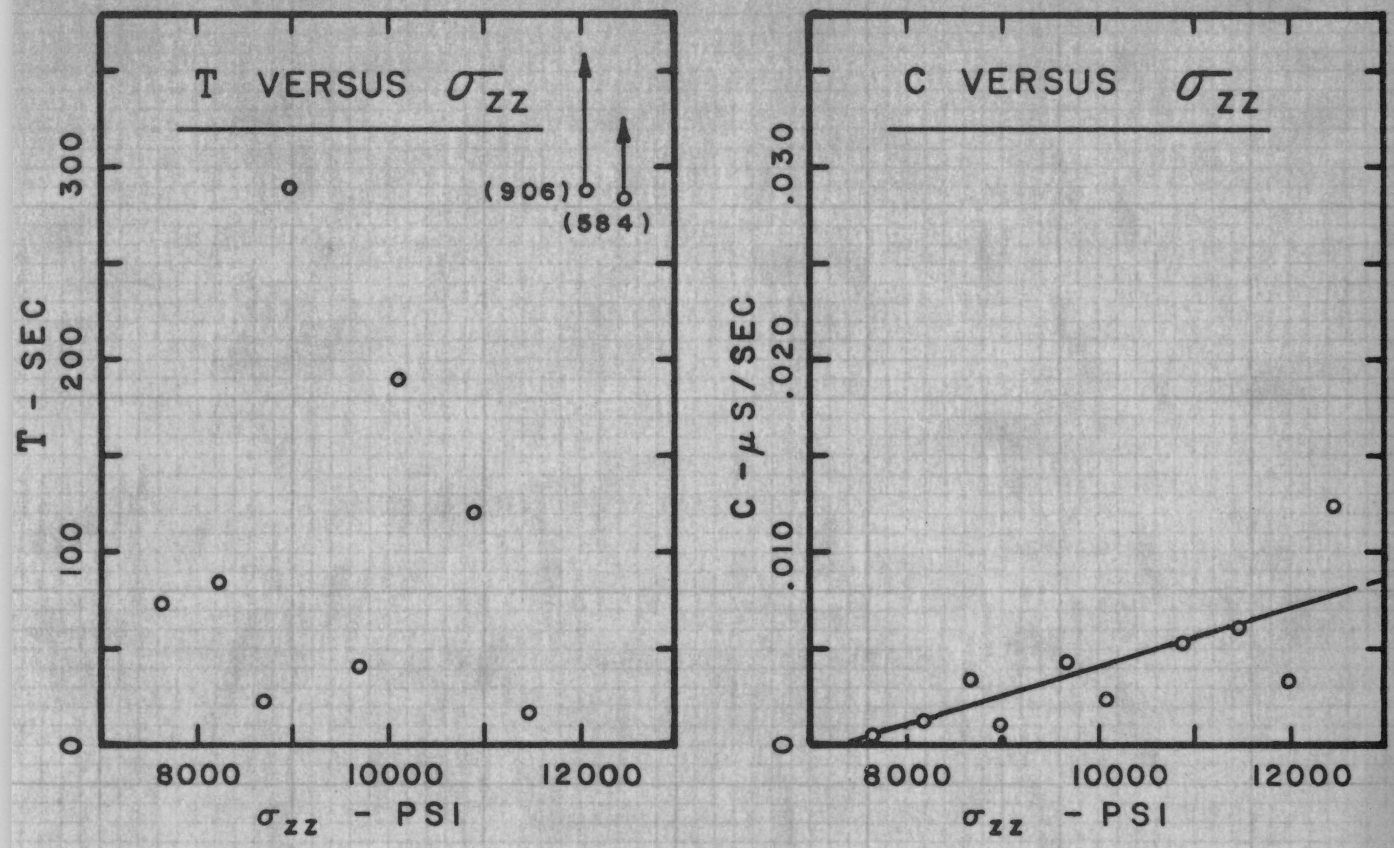


FIGURE 16 - Variation of Model Parameters (T and C) with Stress Level for Specimen WO-5.

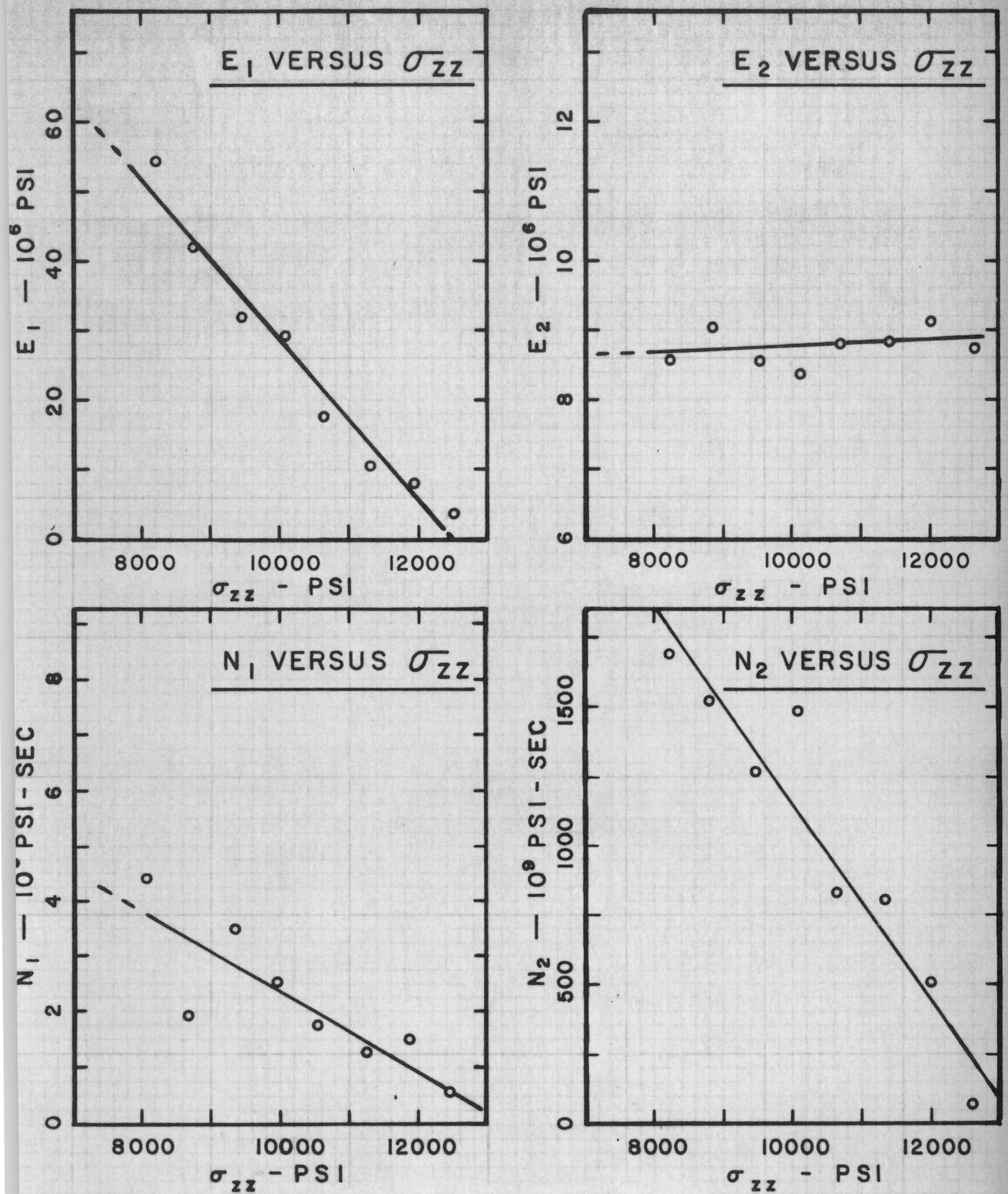


FIGURE 17 - Variation of Model Parameters (E's and N's) with Stress Level for Specimen WO-6.

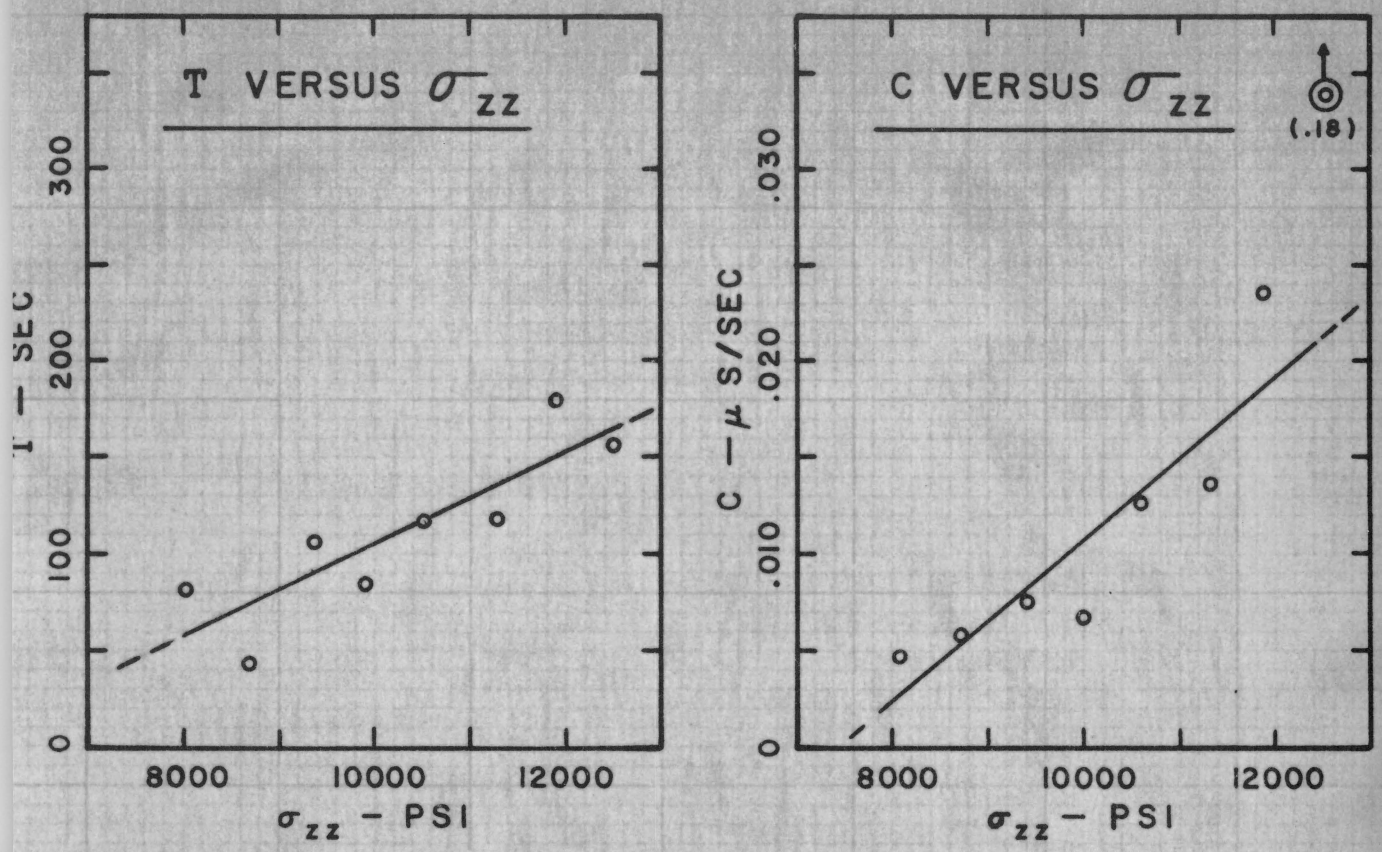


FIGURE 18 - Variation of Model Parameters (T and C) with Stress Level for Specimen WO-6.

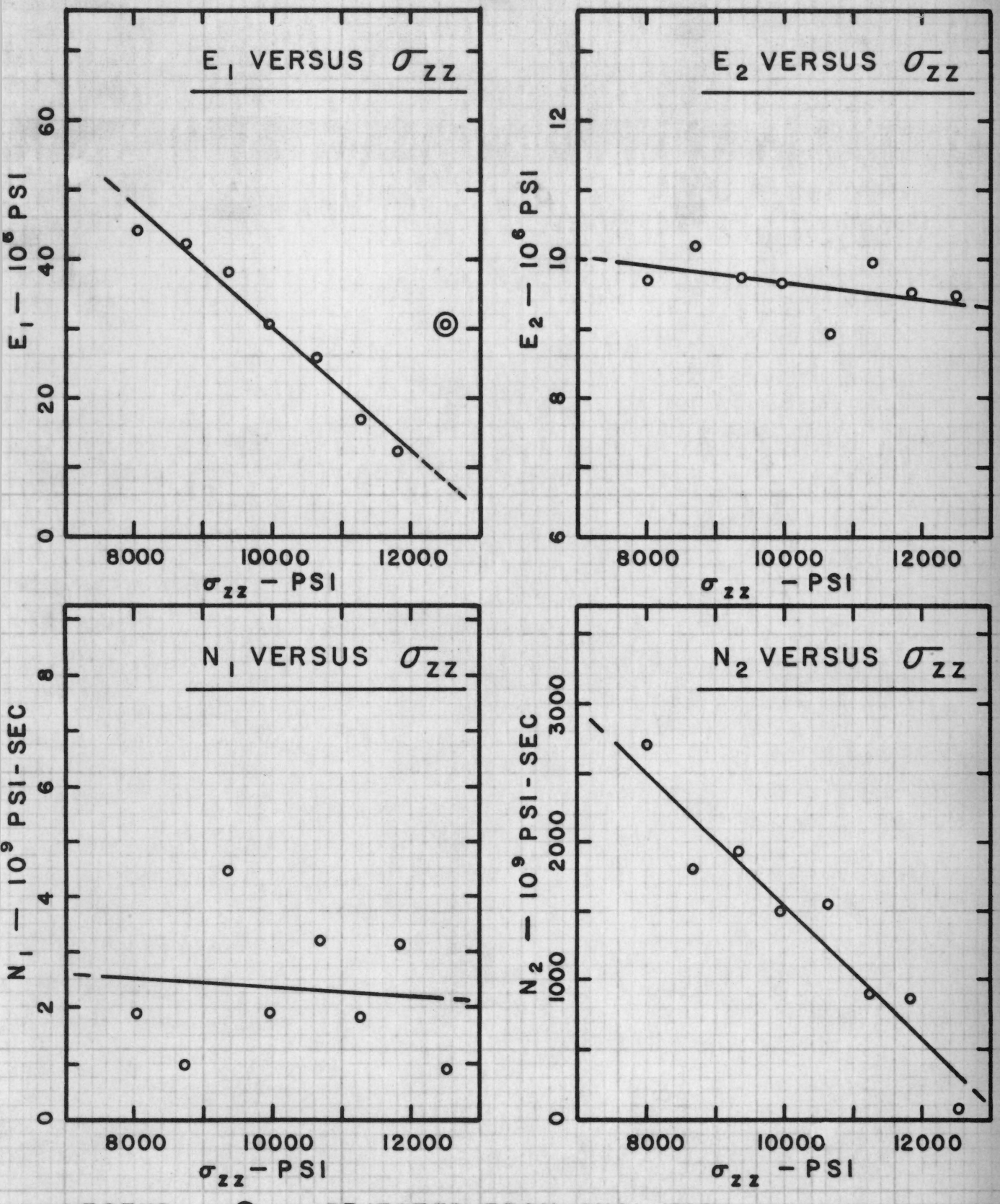


FIGURE 19 - Variation of Model Parameters (E's and N's) with Stress Level for Specimen WO-7.

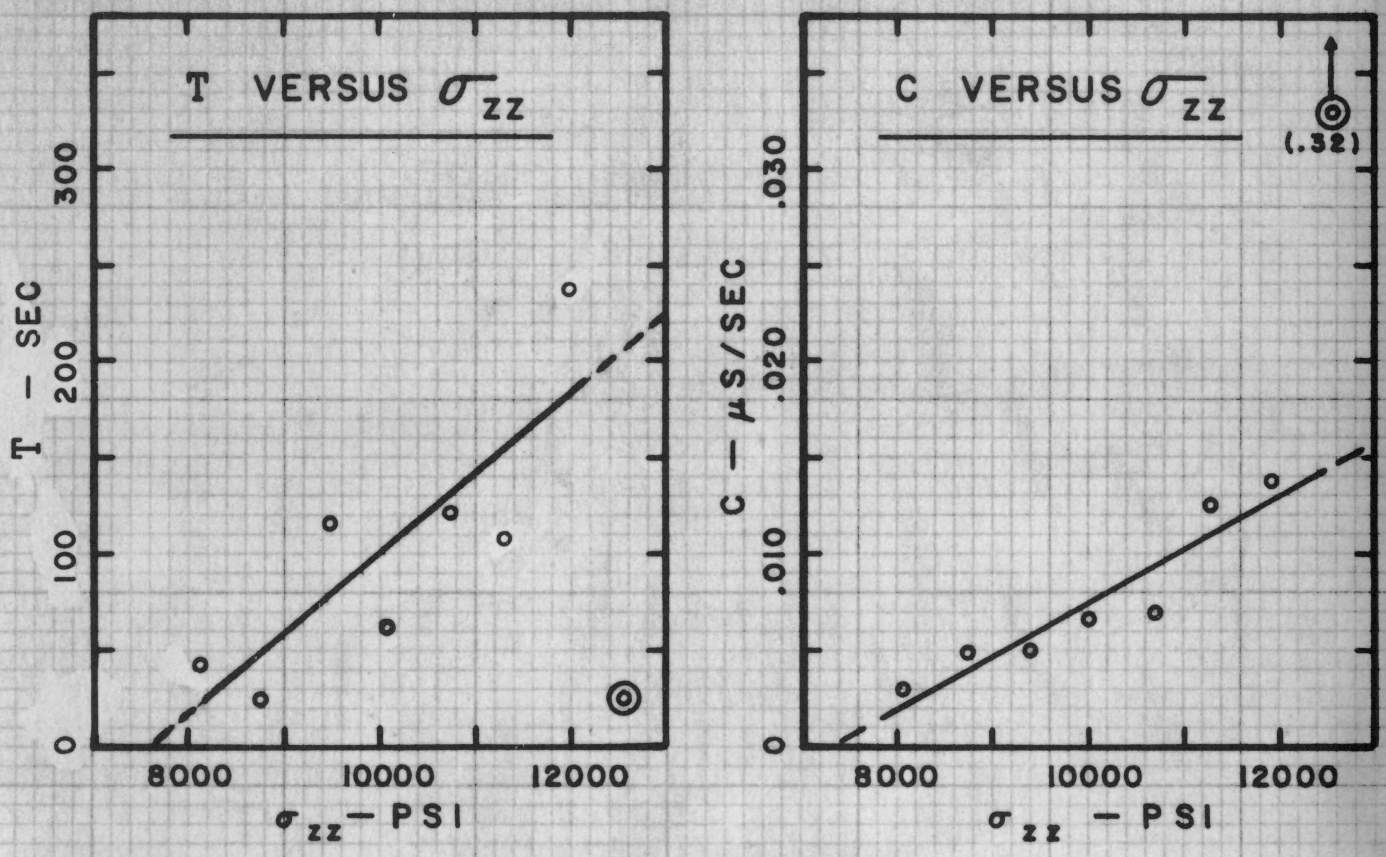


FIGURE 20 - Variation of Model Parameters (T and C) with Stress Level for Specimen WO-7.

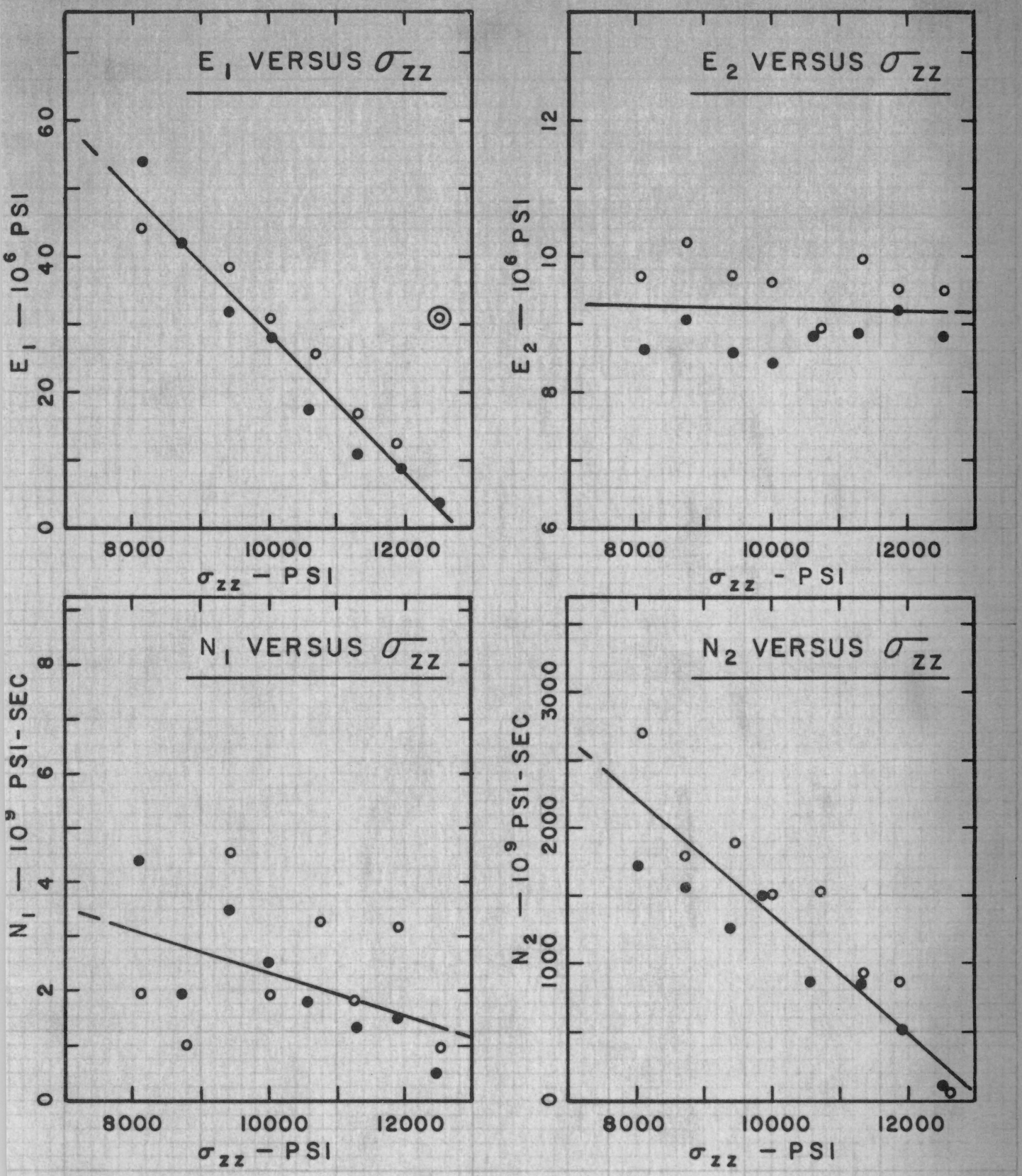


FIGURE 21 - Variation of Model Parameters (E's and N's) with Stress Level for Specimens WO-6/7.

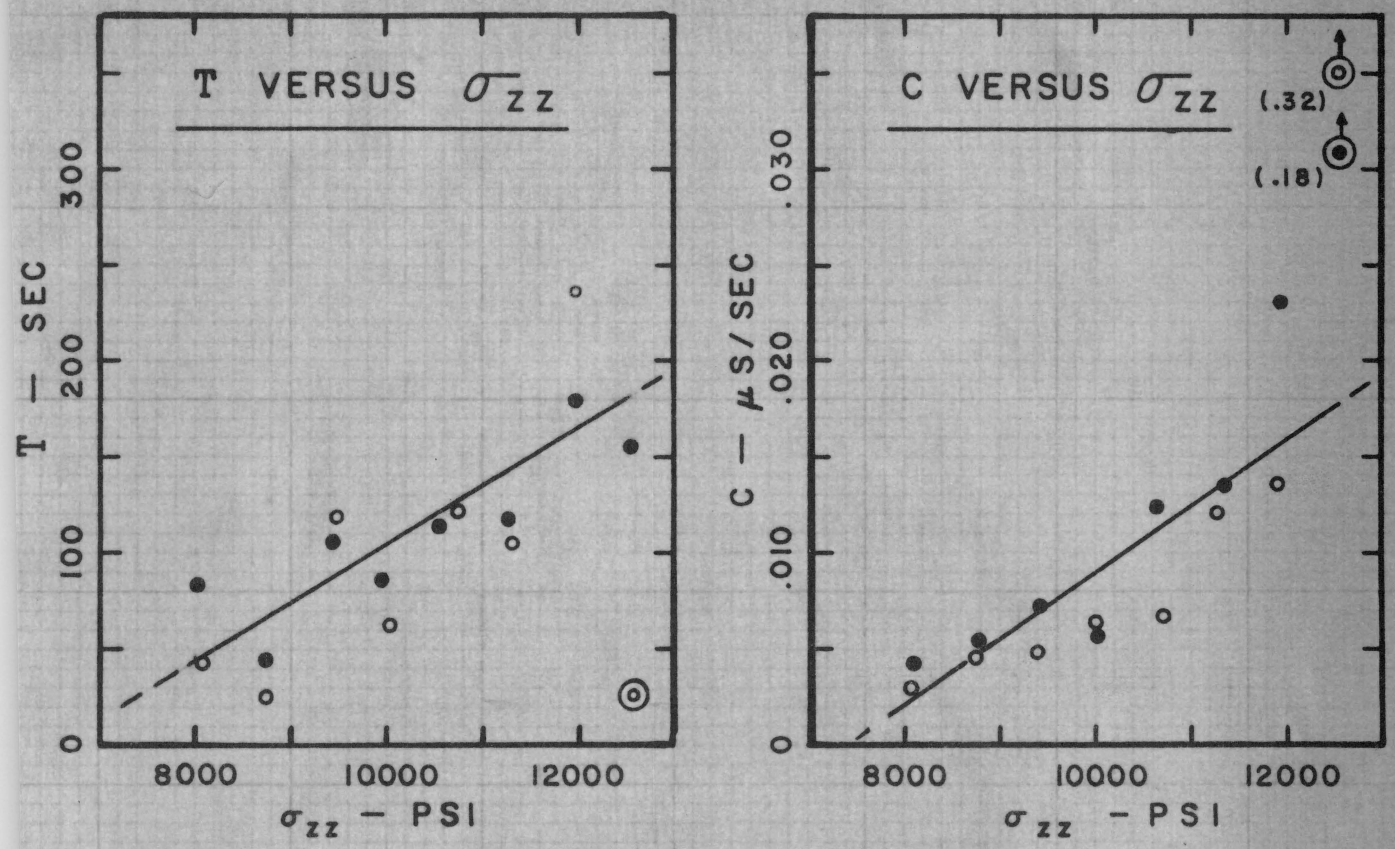


FIGURE 22 - Variation of Model Parameters (T and C) with Stress Level for Specimen WO-6/7.

TABLE 3

STUFF Analysis of Data - Specimen WO-5

Fitting Function $X = A_o + A_1 \sigma$ Stress Range --- 7672 - 12,453 psi					
Parameter X	Units (1)	X_m (2)	A_o	A_1 (3)	Variance of Estimate (4)
E_1	10^6 psi	113.5	506.5	-3.920×10^{-2}	2.74×10^3
N_1	10^9 psi-sec	16.38	37.33	-2.089×10^{-3}	4.47×10^2
E_2	10^6 psi	10.99	11.77	-7.767×10^{-5}	0.324
N_2	10^9 psi-sec	3507	12,612	-0.885	3.55×10^6
C	μs/sec	3.956×10^{-3}	-1.189×10^{-2}	1.580×10^{-6}	5.23×10^{-6}
$\mathcal{T}$	seconds	232.5	-852.2	.108	6.00×10^4

(1) These units apply to all factors except A_1 and the variance.

(2) This represents the mean value of the particular parameter over the stress range quoted.

(3) A_1 is dimensionless but has the same multiplier as the other factors.

(4) The units of the variance are the square of those quoted for X.

TABLE 4

STUFF Analysis of Data - Specimen WO-6

Fitting Function $X = A_o + A_1\sigma$ Stress Range --- 8101 - 12,544 psi					
Parameter X	Units (1)	X_m (2)	A_o	A_1 (3)	Variance of Estimate (4)
E_1	10^6 psi	24.6	140.0	-1.117×10^{-2}	12.04
N_1	10^9 psi-sec	2.21	9.11	-6.686×10^{-4}	0.485
E_2	10^6 psi	8.80	8.14	6.41×10^{-5}	7.54×10^{-2}
N_2	10^9 psi-sec	1036	4666	-0.3517	3.45×10^4
C	μs/sec	1.05×10^{-2}	-3.31×10^{-2}	4.37×10^{-6}	9.9×10^{-6}
$\mathcal{T}$	seconds	111.8	-137.1	2.41×10^{-2}	567.4

(1) These units apply to all factors except A_1 and the variance.

(2) This represents the mean value of the particular parameter over the stress range quoted.

(3) A_1 is dimensionless but has the same multiplier as the other factors.

(4) The units of the variance are the square of those quoted for X.

TABLE 5

STUFF Analysis of Data - Specimen WO-7

Fitting Function $X = A_o + A_1\sigma$ Stress Range --- 8080 - 12,562 psi					
Parameter X	Units (1)	X_m(2)	A_o	A_1(3)	Variance of Estimate (4)
E_1	10^6 psi	30.31	118.87	-8.859×10^{-3}	4.29
N_1	10^9 psi-sec	2.29	3.02	-7.018×10^{-5}	1.73
E_2	10^6 psi	9.64	10.65	-9.789×10^{-5}	0.143
N_2	10^9 psi-sec	1400	6466	-0.4910	6.66×10^4
C	μs/sec	7.53×10^{-3}	-2.03×10^{-2}	2.78×10^{-6}	2.25×10^{-6}
$\mathcal{T}$	seconds	101.7	-319.9	4.22×10^{-2}	2064

(1) These units apply to all factors except A_1 and the variance.

(2) This represents the mean value of the particular parameter over the stress range quoted.

(3) A_1 is dimensionless but has the same multiplier as the other factors.

(4) The units of the variance are the square of those quoted for X.

TABLE 6

STUFF Analysis of Data - Specimens WO-6/7

Fitting Function $X = A_o + A_1\sigma$ Stress Range --- 8080 - 12,562 psi					
Parameter X	Units (1)	X_m (2)	A_o	A_1 (3)	Variance of Estimate (4)
E_1	10^6 psi	27.31	132.5	-1.035×10^{-2}	11.50
N_1	10^9 psi-sec	2.25	6.04	-3.678×10^{-4}	1.168
E_2	10^6 psi	9.22	9.41	-1.770×10^{-5}	0.310
N_2	10^9 psi-sec	1218	5572	-0.4219	9.25×10^4
C	μs/sec	9.05×10^{-3}	-2.67×10^{-2}	3.57×10^{-6}	8.86×10^{-6}
τ	seconds	107.1	-211.6	3.13×10^{-2}	1224

(1) These units apply to all factors except A_1 and the variance.

(2) This represents the mean value of the particular parameter over the stress range quoted.

(3) A_1 is dimensionless but has the same multiplier as the other factors.

(4) The units of the variance are the square of those quoted for X.

4.3 Unloading Experiments

No detailed unloading experiments have been carried out to date. However, during the deformation of specimen WO-5 it was found necessary to lower the specimen load on two occasions by a small increment (see sections EF and JK in Figure 12). The detailed time-strain data associated with these unloadings are shown graphically in Figure 23. Here the upper section of the figure illustrates the stress variation and the lower section the resulting strain variation both as a function of time. A number of features were noted, as follows:

(a) The instantaneous elastic strain during incremental loading and unloading appear to be consistent (in the first sequence CD and EF are equal, in the second sequence HI is approximately 20% larger than JK).

(b) There appears to be no recovery of inelastic strain as a result of a small incremental unloading. In the first sequence the total time-dependent strain is of the order of 16 μs of which approximately 12 μs may be accounted for by the steady state component (Maxwell component). However, the transient portion in this case (Kelvin component) would only be of the order of 5-10 μs at most and the recovery of this which might be difficult to detect. In the second sequence the total time-dependent strain is of the order of

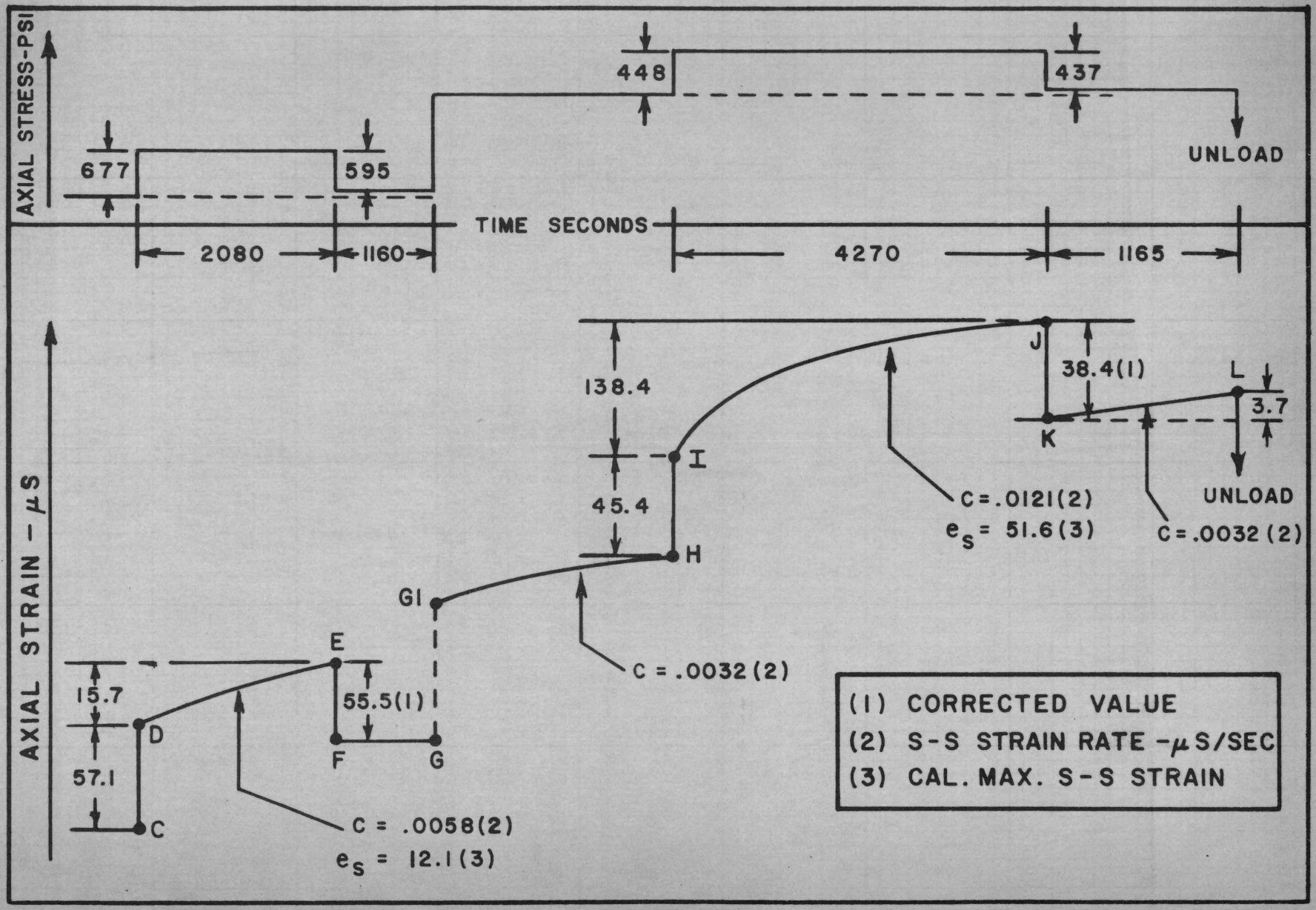


FIGURE 23 - Incremental Loading/Unloading Curves for Specimen WO-5.

140 μs of which approximately 50 μs may be accounted for by the steady state component. In this case the transient portion would be of the order of 90 μs and should be easily detected. In both cases, however, no recovery of this transient strain was observed.

(c) In the first sequence the section of the curve (F-G) after the incremental unloading was flat indicating that the strain rate was zero; in the second sequence the section of the curve (K-L) after an incremental unloading was found to increase linearly with time at a strain rate C = .0032 μs/sec. It is interesting to note that this corresponds to the steady state strain rate observed (section G_1 - H) when the specimen stress was previously at this level.

When specimen WO-5 was completely unloaded, at the end of the experiment, (see section LMN, Figure 12) its behavior was found to be considerably different. At zero load, immediately after rapidly unloading the specimen, the average strain was found to be approximately 270 μs*. This value decreased with time reaching a minimum value of approximately 180 μs after about 1200 seconds. The sum of the transient strains and the sum of the steady state strain observed during the complete loading program were determined to be

* Unfortunately the complete strain versus time curve during the unloading was not obtained and hence the initial strain value at zero load quoted would be somewhat less than the actual value.

approximately e_{tr} = 170 μs and e_{ss} = 160 μs respectively. It is interesting to note that the total time-dependent strain ($e_T = e_{tr} + e_{ss}$) is of the order of 330 μs which is compatible with the zero load strain of 270 μs observed a short period of time after the unloading was completed. The calculated value of e_{ss} = 160 μs compares closely with the observed permanent strain of 180 μs. It would appear then that when the specimen is completely unloaded, the total transient creep strain (Kelvin component) is recovered. This is in contrast to the situation where no recovery was observed when small changes were made in the applied load.

IV

DISCUSSION AND CONCLUSIONS

1. Experimental Facility and Technique

The various tests conducted on the experimental facility and the results of the actual experiments conducted on specimens of Wombeyan marble indicate that the facility and the experimental techniques developed have proved to be most satisfactory. Throughout the experiments it has been possible to maintain the laboratory temperature to within $\pm$ 1/10°C, to control the axial compressive load on the specimen to within $\pm$ 1/10 per cent and to measure the resulting specimen strains to within $\pm$ 0.5 μs. Using a special loading jig it has been possible to load the test specimen uniformly to such a degree that the maximum deviation of the three axial strain gages, mounted at 120° around the specimen, rarely exceeded eight per cent. The experimental method developed for rapid incremental loading and unloading was found to be satisfactory. It was found possible to make incremental stress changes of up to 1000 psi in less than three seconds, which corresponds to a stress rate of approximately 300 psi/sec. The method developed for obtaining accurate values of the instantaneous elastic strain, and for correcting the initial section of the creep curve after incremental loading, was found to be very satisfactory. Consistent results were obtained from corrected creep curves whose maximum

strain was less than 5 μs. The reproducibility of the experiments are verified by the excellent agreement in the results from the experiments on specimen WO-6 and WO-7.

A number of modifications are suggested which would improve the quality of the experimental data and reduce the time required for data analysis. These are as follows:

(a) Strain measurement facilities should be modified to allow the recording of average strain (rather than the strain observed by only one of the three axial gages) on the Y-XT recorder during incremental creep experiments. This would provide more representative data particularly at the higher stress levels where inelastic effects appear to cause non-uniformities to develop in the axial strain distribution.

(b) A method should be developed to enable incremental loading to be carried out more rapidly. A stress rate of 3000 psi/sec (approximately 10 times the maximum present rate) would be useful to insure positive separation of the instantaneous elastic and the inelastic strains. This is particularly important at stress levels near failure, where the inelastic effects become more prominent.

(c) An automatic method for obtaining corrected creep curves should be developed as the graphical method presently employed is tedious and time consuming (requiring from one to two

hours for each incremental creep curve). A technique utilizing a relatively simple analog computer circuit has been considered for this purpose.

Future experiments are planned to investigate the inelastic behavior of geologic material under confinement. To date most of the facilities for these experiments have been completed. These include a triaxial test vessel and confining pressure supply which will allow experiments to be conducted at confining pressures up to 10,000 psi. A convenient method of specimen jacketing has been developed for sealing the test specimen from the confining pressure fluid. It is hoped that these experiments will commence later this year.

2. Mechanical Behavior of Wombeyan Marble

2.1 Suitability of the Burgers Model

With few exceptions the creep data was found to fit the incremental creep form of the Burgers model extremely well. The typical quality of the fit is exemplified by the results shown in Figures 8 and 9. A comparison of the experimental and the theoretical values quoted in the tables of Appendix 5, and the standard deviation between the experimental and theoretical curves quoted in Table 2 provide further evidence of this fact.

The model parameters E_1, N_1, and N_2 were found to be functions of the applied stress in the region above approximately

7700 psi. The functional relationship appeared to be approximately linear, with the magnitude of the parameters decreasing with increasing stress level. In this same region the parameter E_2 was found to be relatively independent of stress. Below 7700 psi no data was available for the parameters E_1, N_1, and N_2 as the inelastic strains associated with stresses below this point were too small to be detected, however, E_2 (results for specimens WO-6 and WO-7 are shown in Figure 11) was found to decrease with decreasing stress. This initial region of low modulus is often associated with the closure of cracks and pores in the material, however the validity of this concept will not be discussed here.

The factor C which represents the final steady state strain rate is found to be a linear increasing function of the applied stress. If the line representing the least squares fit to the data is projected to lower stresses it is found to intercept the stress axis (C = O) at a stress (σ_B)* greater than zero, rather than passing through the origin. In the case of Wombeyan marble $\sigma_B \approx$ 7500 psi. A similar condition has been reported by Price (1964) for bending tests on Pennant sandstone and Wolstanton sandstone and by Matsushima (1956)

*It is important to note the distinction between σ_B, and σ_A (discussed earlier, see Table 1). σ_B is defined as the intercept of the C versus σ curve and σ_A is the lowest stress level at which inelastic behavior was noted.

for Kitashirakawa granite. In all cases the value of C appears to be zero up to some stress level (σ_B) after which C becomes non-zero and increases in an approximately linear manner with increasing stress. For Wombeyan marble the values of E_1 and N_1 are found to be highest in the region of 7500 psi, decreasing with increasing stress. This would indicate that the Kelvin-Voigt section of the model was relatively inactive up to this level. These observations would suggest that the stress level σ_B was associated with some basic yield phenomenon in the material.

Since a critical stress (σ_B) appears to exist at about 7500 psi for Wombeyan marble, it is suggested that with decreasing stress the parameters E_1, N_1, and N_2 should go to infinity at σ_B rather than increasing linearly as shown. Experimental verification of this fact will require a number of additional incremental creep experiments in the neighbourhood of σ_B.

Tentatively it is suggested that on the basis of incremental creep experiments the material appears to behave as a Burgers model with stress dependent parameters as follows:

$\sigma < \sigma_B$	$\sigma > \sigma_B$
$E_1 = \infty$ $N_1 = \infty$ $N_2 = \infty$	$E_1 = f_1(\sigma)$ $N_1 = f_2(\sigma)$ $N_2 = f_3(\sigma)$
$E_2 = f_4(\sigma)$	E_2 = constant

where f_1, f_2 and f_3 are approximately linear functions of the axial compressive stress for $\sigma > \sigma_B$. The numerical values of the coefficients associated with these function have been given previously in Tables 3-6. The analysis, by the writer, of creep data for Kitashirakawa and Ajimura granite by Matsushima (1956) and for slate by Evans and Wood (1936) indicate the applicability of a similar model. It is interesting to note that creep experiments, on austenitic stainless steel at 1300°F, conducted by Garofalo (1960) also appear to be conveniently described by this model.

2.2 Deformation Mechanisms

The main purpose of this research has been to investigate the inelastic behavior of Wombeyan marble and to analyze the results in terms of the Burgers mechanical model. Future studies are planned in which the basic mechanisms responsible for the observed deformation behavior will be investigated, however tentatively the following qualitative explanation of this behavior is suggested.

Macroscopically the material may be considered to be an isotropic polycrystalline aggregate which consists of a large number of calcite grains oriented randomly. Each grain has associated with it a number of critical shear stresses, associated with twin and translational glide mechanisms, which are characteristic of calcite. Similarly there are other critical shear stresses associated with grain boundary glide. However, because of the orientation distribution of the various grains to the axis of the applied stress, not all grains will experience the same resolved shear stress for a given applied load. At low levels of applied stress the inter- and intra-crystalline resolved shear stresses will be below the critical level and the material will behave elastically. As the stress level increases, a point (σ_B) will be reached where the resolved shear stress in the most favourably oriented grains or on the most favourably oriented grain boundaries is sufficient to activate one or more of the possible glide mechanisms. The extent of this glide is limited by the surrounding matrix, which still being elastic will develop a back-stress on the deforming grain. As the grain deformation continues the back-stress rises, eventually inhibiting further glide at that stress level. Under these conditions the material will exhibit an inelastic as well as an elastic component. As the applied stress is increased the critical resolved shear stresses in more and more of the constituent grains are exceeded and the

magnitude of the inelastic component thus increases with stress level. The observed behavior for Wombeyan marble agrees with this qualitative description.

2.3 Proposed Future Work

The results obtained for Wombeyan marble to date, using incremental creep experiments, suggest that the material may be described by a Burgers model with stress dependent parameters. A number of factors should be investigated further before this model is fully accepted. These include the following:

(a) The investigation of the apparent effect on the parameters E_1, N_1 and N_2 of the magnitude of the stress incremental ($\Delta\sigma_n$) and the duration of the experiment (t_n) which were noted in the experiments on specimen WO-5. In particular the investigation of the behavior for values of $t_n \geq 10^5$ seconds ($\approx$ 24 hours).

(b) The anomalous effect noted in the incremental unloading experiments conducted on specimen WO-5. Here no recovery of transient strain was observed for small unloading increments but the total accumulated transient strain appeared to be recovered when the specimen was completely unloaded. Such an affect would suggest the presence of a critical "locking" or frictional force associated with stress reversal.

(c) The determination of the critical stress σ_B and the values of the parameters (E_1, N_1 and N_2) in the vicinity of σ_B.

(d) The investigation of the material under other loading conditions (e.g. $\dot{\sigma}_c$ = constant) to verify that the model obtained is the unique model for the material.

3. Application to Mining Engineering Problems

The results of the present studies themselves provide no immediate solution to any of the numerous mining engineering problems. They do provide, however, further basic information on the mechanical behavior of the material itself. Geological materials, until recently, have usually been considered to be elastic for the purposes of mathematical analysis. This simplification has not been possible or desirable in the analysis of many recent problems and instead the material has been considered to be inelastic.

Examples of the type of problems and the approach being used in their solution are given in two papers published recently by the Polish Academy of Science (Salustowicz (1958) and Litwinis:yn (1955)). These are concerned with the solution of mining stress problems when the associated rock is represented by various mechanical models. An extension of this work has recently been carried out by Iman (1964) at the University of Minnesota. He has been concerned with

the analysis of subsidence based on the assumption that rock behaves as an inelastic material.

At present considerable difficulty is experienced in analyzing mining problems due to the fact that little is known of the mechanical behavior of the rock itself. It is only through a large number of experimental investigations, such as the present one, that this behavior will be understood and the parameters necessary for the successful analysis of the various problems obtained.

V

ACKNOWLEDGMENTS

The author wishes to express his gratitude to the members of his graduate committee; Professors R. Chicurel, D. Frederick, W.D. Lowry, and C.W. Smith for their constant interest and suggestions during this project. The frequent discussion with Professor Frederick, the authors director, and with Professor C.T. Holland (formerly Head of the Mining Department at V.P.I.) have assisted greatly in a successful completion of this work. The author is particularly indebted to Professor D. H. Pletta, Head of the Engineering Mechanics Department for his encouragement both academic and personal during this project.

The author would like to thank Mr. A. Ignatieff, Chief of the Fuels and Mining Practice Division of the Mines Branch for his faith and assistance in establishing this research program. It was through his suggestion in 1956, while the author was a member of the Mining Research Section, that the author originally became interested in the study of time-dependent behavior. Dr. W.M. Gray, the author's Section Head, has formed the link between the Mines Branch and V.P.I. during this research and his constant assistance and encouragement are greatly appreciated.

A number of persons in the Mines Branch have provided valuable assistance throughout the project. In particular Dr. J. Soles of the Mineral Sciences Division, Mr. P. Hudson and Mr. L. Nadon of the Fuels and Mining Practice Division and Miss A. Kosowan of the

Physical Metallurgy Division. The assistance of Mr. B. Feldstead, M. Tienhaara and S. Steppel, Physics Section, Summer Student Assistants during the last three summers is gratefully acknowledged. Mr. P. Okulich of this section was responsible for the preparation of the majority of the test specimens and the preparation of the final drawings and graphs.

The assistance of a number of members of the Mining Research Section of the Fuels and Mining Practice Division, including Mr. S. Cook, H. Cross, F. Kapeller and J. Sullivan in preparation and strain gaging of test specimens has been appreciated.

The author would also like to express his thanks to Dr. M.S. Paterson of the Australian National University, Canberra, Australia, for supplying the samples of Wombeyan marble used in the experiments.

VI

BIBLIOGRAPHY

Ahrendt, W.R., and Savant, C.J., Jr., (1960), Servomechanism Practice: McGraw-Hill Book Company, Inc., New York.

Attwell, P.B., (1961), Response of Rocks to High Velocity Impact: Trans. Inst. Min. Metall., 71, 697.

Attwell, P.B., (1962), Composite Model to Simulate Porous Rock: Engineering, 193, 574.

Balmer, G.G., (1953), Physical Properties of Some Typical Foundation Rocks: Concrete Laboratory Report SP-39, Bureau of Reclamation, U.S. Department of the Interior, Denver.

Barron, K., and Toews, N.A., (1964), Deformation Around a Mine Shaft in Salt: Proceedings of Second Canadian Rock Mechanics Symposium, Queen's University, December, 1963 (page 115), (Published by The Mines Branch, Canadian Department of Mines and Technical Surveys, 1964).

Bergen, J.T., (1960), Viscoelasticity-Phenomenological Aspects: Academic Press, New York.

Bland, D.R., (1960), The Theory of Linear Viscoelasticity: Pergamon Press, New York.

Boley, B.A., and Weiner, J.H., (1960), The Theory of Thermal Stresses: John Wiley and Sons, Inc., New York, 1960.

Brace, W.F., (1962), Private Communication, Dunbar Geophysics Laboratory, Havard University (October 1962).

Brace, W.F., (1963), Brittle Fracture of Rock: International Conference on State of Stress in the Earth's Crust, Santa Monica, California, May 1963.

Brown, A., (1958), Ground Stress Investigations in Canadian Coal Mines: AIME Trans. 211, 879.

Cermi, R.H., and Foster, L.E., (1962), Instrumentation for Engineering Measurement: John Wiley and Sons, Inc., New York (Pages 136-142).

Cottrell, A.H., (1953), Dislocations and Plastic Flow in Crystals: Clarendon Press, Oxford.

Cross, H., (1964), Private Communication, Mining Research Laboratories, Mines Branch, Canadian Department of Mines and Technical Surveys, Ottawa (June 1964).

Deming, W.E., (1943), Statistical Adjustment of Data: John Wiley and Sons, New York.

Donath, F.A., (1962), Private Communication, Geology Department, Columbia University (May 1962).

Eirich, F.R., (1956), Rheology-Theory and Application, Volume 1: Academic Press Inc., New York.

Eirich, F.R., (1958), Rheology-Theory and Application, Volume 2: Academic Press Inc., New York.

Eirich, F.R., (1960), Rheology-Theory and Application, Volume 3: Academic Press Inc., New York.

Evans, R.H., (1936), The Elasticity and Plasticity of Rocks and Artificial Stone: Proc. Leeds Phil. Lit. Soc., 3 (3), 145.

Evans, R.H., and Wood, R.H., (1937), Transverse Elasticity of Natural Stones: Proc. Leeds Phil. Lit. Soc., 3(5), 340.

Fairhurst, C., (1961), Laboratory Measurement of Some Physical Properties of Rock: Proceedings of the Fourth Symposium on Rock Mechanics, Bull. Mineral Industries Experiment Station, No. 76, Page 105, Pennsylvania State University.

Frederick, D., and Garcia, M.A., (1953), The Theoretical Behaviour of an Inelastic Material Model: Bull. Virginia Polytechnic Institute, Eng. Exp. Station Series, No. 85, Blacksburg, Virginia.

Freudenthal, A.M., (1950), The Inelastic Behaviour of Engineering Materials and Structures: John Wiley and Sons, Inc., New York.

Garofalo, F., (1960), Resistance to Creep Deformation and Fracture in Metals and Alloys: Properties of crystalline Solids, ASTM Special Technical Publication No. 283, page 82.

Gill, D., (1963), Private Communication, Mining and Geophysics Department, McGill University (December 1963).

Gill, D., and Paquin, J.A., (1964), Private Communication, Mining and Geophysics Department, McGill University (February 1964).

Griggs, D.T., (1936), Deformation of Rocks Under High Confining Pressures: Jour. Geol. 44, 541.

Griggs, D.T., (1939), Creep of Rocks: Jour. Geol. 47, 225.

Griggs, D.T., (1954), Handbook of Physical Constants: Geol. Soc. Amer. Special Papers No. 6, page 129.

Griggs, D.T., and Handin, J., (1960), Rock Deformation (Symposium): Geol. Soc. Amer., Memoir 79.

Grosvenor, N.E., (1963), Specimen Proportion-Key to Better Compressive Strength Tests: Mining Engineering, 15, 31.

Handin, J., (1953), An Application of High Pressure in Geophysics - Experimental Rock Mechanics: Trans. ASME, 75, 315.

Handin, J., (1960), Private Communication, Shell Development Company, Houston, Texas (February 1960).

Harboe, E.M., (1962), A Loading System for Compressive Creep Studies on Concrete Cylinders: Report C-1033, Concrete and Structural Branch, U.S. Bureau of Reclamation, Denver, Colorado.

Hardy, H.R., Jr., (1956), The Design and Testing of Apparatus for the Experimental Determination of the Time-Strain Characteristics of Mine Rock: FRL-234, Fuels and Mining Practice Division, Mines Branch, Canadian Department of Mines and Technical Surveys, Ottawa.

Hardy, H.R., Jr., (1959A), Standardized Procedures for the Determination of the Physical Properties of Mine Rock Under Short-Period Uniaxial Compression: TB-8, Mines Branch, Canadian Department of Mines and Technical Surveys, Ottawa.

Hardy, H.R., Jr., (1959B), Time-Dependent Deformation and Failure of Geologic Materials: Quarterly Colorado School of Mines, 54, 134.

Hardy, H.R., Jr., (1961), Proposed Research Project to Develop the Governing Equations for the Mechanical Behaviour of Geologic Materials Under Various States and Durations of Stress and Various Temperatures Using the Phenomenological Approach: Internal Report FMP-61/241-P, Fuels and Mining Practice Division, Mines Branch, Canadian Department of Mines and Technical Surveys, Ottawa.

Hardy, H.R., Jr., (1962A), Design of Instrumentation for the Measurement of Time-Dependent Strain in Stressed Rock Specimens: ISA Transactions, 1, 147.

Hardy, H.R., Jr., (1962B), Development of Apparatus to Study the Strain Rate Sensitivity Factor in Copper Single Crystals by Incremental Transient Creep Experiments: M.Sc. Thesis, Physics Department, University of Ottawa.

Hardy, H.R., Jr., (1965), New Rock Mechanics Program Underway by Canadian Government: Mining Engineering, 17, 62.

Hardy, H.R., Jr., and Larocque, G.E., (1965), An Electronic - Pneumatic Load Maintaining System: (Report in preparation).

Hardy, H.R., Jr., and MacLean, M.J., (1965), Measurement of the Coefficient of Linear Thermal Expansion of Mine Rock: (Report in preparation).

Hardy, H.R., Jr., Steppel, W. and Toews, N.A., (1965), The Analysis of Incremental Creep Data Using the Burgers Mechanical Model: (Report in Preparation).

Hartley, H.O., (1961), The Modified Gauss-Newton Method for Fitting of Non-Linear Regression Functions by Least Squares: Technometrics, 3 (2), 269.

Heard, H.C., (1963), Effect of Large Changes in Strain Rate in the Experimental Deformation of Yule Marble: Jour. Geol. 71 (2), 162.

Hetenyi, M., (1957), Handbook of Experimental Stress Analysis: John Wiley and Sons, Inc., New York (Pages 160-238).

Hodgman, C.D., (1949), Handbook of Chemistry and Physics, 31st Edition, Chemical Rubber Publishing Co., Cleveland (Page 1284).

Hunt, C.A., (1962), The Development of Apparatus to Determine the Time-Dependent Properties of Rock Salt and Their Measurement on Several Specimens: IR.FMP-62/60-MIN, Fuels and Mining Practice Division, Mines Branch, Canadian Department of Mines and Technical Surveys.

Iida, K., and Kumazawa, M., (1957), Visco-elastic Properties of Rocks: J. Earth Sci., Nagoya University, 5, 68 (In English).

Iman, H.F., (1964), A Viscoelastic Analysis of Mine Subsidence in Horizontally Laminated Strata: Ph.D Thesis, School of Mineral and Metallurgical Engineering, University of Minnesota.

Ito, I., and Terada, M., (1962), A Rheological Study on the Dynamical Behaviour of Rocks: J. Min. Metall. Inst. Japan, 78, 723 (In Japanese)

Jastrzebski, Z.D., (1959), Nature and Properties of Engineering Materials: John Wiley and Sons, Inc., New York, (pages 184-190).

Kerper, M.J., Mong. L.E., Stiefel, M.B., and Holley, S.F., (1958), Evaluation of Tensile, Compressive, Torsional, Transverse, and Impact Tests and Correlation of Results for Brittle Cermets: Jour. Res. Nat. Bur. Standards, 61 (3), 149.

Larocque, G.E., (1960), Measurement of the Mechanical Properties of Eight Rock Types as part of the Jet Piercing Project: IR FMP-60/37-MIN, Fuels and Mining Practice Division, Mines Branch, Canadian Department of Mines and Technical Surveys.

Leeman, E.R., and Grobbelaar, C., (1957A),A Compressometer for Obtaining Stress-Strain Curves of Rock Specimens Up to Fracture: J. Sci. Instrum., 34, 279.

Leeman, E.R., and Grobbelaar, C., (1957B), A Lateral Extensometer for the Determination of Poisson's Ratio of Rock: J. Sci. Instrum., 34, 503.

Lion, K.S., (1959), Instrumentation in Scientific Research: McGraw Hill Book Co. Inc., New York, (Pages 167-176).

Litwiniszym, J., (1955), The Effect of Time on Deformation and Stress on Rock Bodies: Polish Academy of Science, Archivium Gornictwa-Hutnictwa, 3, 479 (In Polish).

Loizou, N., and Sims, R.B., (1953), The Yield Stress of Pure Lead in Compression: Jour. Mech. Phys. Solids, 1, 234.

Lubahn, J.D., and Felgar, R.P., (1961), Plasticity and Creep of Metals: John Wiley and Sons, Inc., New York, (Pages 363-404).

Matsushima, S., (1956), On the Deformation and Fracture of Granites: Zisin (II), 8 (4), 174 (In Japanese).

Matsushima, S., (1960), On the Flow and Fracture of Igneous Rocks: Bulletin No. 36, Disaster Prevention Research Institute, Kyoto University, Kyoto, Japan (In English).

Mitra, D., and Willson, J.E., (1962), A. Bibliography of Geo-mechanics, Bulletin 119, Utah Eng. Exp. Station, University of Utah, Salt Lake, Utah.

Murrell, S.A.F., and Misra, A.K., (1962), Time-Dependent Strain or "Creep" in Rocks and Similar Non-Metallic Materials: Bull. Inst. Mining Met., 71 (7), 353.

Obert, L., Windes, S.L. and Duvall, W.I., (1946), Standardized Tests for Determining the Physical Properties of Mine Rock: RI 3891, Bureau of Mines, U.S. Department of the Interior, College Park, Maryland.

Papirno, R., (1960), Elevated Temperature Extensometer using a Differential Capacitor Sensor: Tech. Report SM-60-2, Eng. Res. Division, New York University.

Paquin, J.A., (1964), Some Aspects of Uniaxial Compression in Rocks: Proceedings of Second Canadian Rock Mechanics Symposium, Queen's University, December, 1963 (Page 73) (published by Mines Branch, Canadian Department of Mines and Technical Surveys, 1964).

Parker, F.L., (1963), Private Communication, Oak Ridge National Laboratories, Oak Ridge Tennessee (May 1963).

Paterson, M.S., (1958), Experimental Deformation and Faulting in Wombeyan Marble: Bull. Geol. Soc. Amer., 69, 465.

Peselnick, L., and Robie, R.A., (1963), Elastic Constants of Calcite: Jour. Appl. Phys. 34, 2494.

Peterson, R.E., (1953), Stress Concentration Design Factors: John Wiley and Sons, Inc., New York.

Phillips, D.W., (1948), Tectonics of Mining: Colliery Engineering, 25, 312.

Price, N.J., (1964), A Study of the Time-Strain Behaviour of Coal-Measure Rocks: Int. J. Rock Mech. Mining Sci., 1, 277.

Robertson, E.C., (1955), Experimental Study of the Strength of Rocks: Bull. Geol. Soc. Amer., 66, 1275.

Robertson, E.C., (1959), Private Communication, U.S. Geological Survey, Silver Spring, Maryland (February 1959).

Robertson, E.C., (1964), Viscoelasticity of Rocks: State of Stress in the Earth's Crust, American Elsivier Publishing Co., Inc., (Page 181).

Ross, A.D., (1958), Elasticity, Creep and Shrinkage of Concrete: Mechanical Properties of Non-Metallic Brittle Materials, Butterworths Scientific Publications, London, (Page 1).

Salustowicz, A., (1958), Rocks as a Viscoelastic Medium: Polish Academy of Science, Archivum Gornictwa, 3, 141 (In Polish).

Serdengecti, S., and Boozer, G.D., (1961), The Effects of Strain Rate and Temperature on the Behaviour of Rocks Subjected to Triaxial Compression: Proceedings of the Fourth Symposium on Rock Mechanics, Bull. Mineral Industries Experiment Station, No. 76, Page 83, Pennsylvania State University.

Shih, T., (1964), Investigation of the Physical Properties of a Gaspé Skarn: Proceedings of Second Canadian Rock Mechanics Symposium, Queen's University, December, 1963 (Page 75), (Published by Mines Branch, Canadian Department of Mines and Technical Surveys, 1964).

Sokolnikoff, I.S., Mathematical Theory of Elasticity: McGraw Hill Co., New York.

Solvason, K.R., (1961), Private Communication, Building Research Division, National Research Council, Ottawa.

Sperry, W.C., (1964), Rheological - Model Concept: Jour. Acoustical Soc., 36, 376.

Steppel, S., (1964), The Differential Equations Representing Several Simple Rheological Models and Their Solutions for Various Conditions: FMP-64/87-P, Fuels and Mining Practice Division, Mines Branch, Canadian Department of Mines and Technical Surveys, Ottawa.

Steppel, S. (1965), Mathematical Procedures for Fitting the Burgers Rheological Model to Experimental Data: (Report in Preparation).

Terry, N.B., (1957), The Elastic Properties of Coal; Part 6, Some Measurements of Internal Damping and Some Considerations of Visco-Elastic Behaviour: MRE Report No. 2080, British National Coal Board.

Thaler, G.J., and Brown, R.G., (1960), Analysis and Design of Feedback Control Systems (2nd Edition): McGraw-Hill Book Co. Inc., New York.

Truxal, J.G., (1958), Control Engineers Handbook: McGraw-Hill Book Company, Inc., New York.

Udd, J.E., (1964), Private Communication, Mining and Geophysics Department, McGill University (February 1964).

Wuerker, R.G., (1959), Influence of Stress Rate and Other Factors on the Strength and Elastic Properties of Rocks: Quarterly Colorado School of Mines, 54, 3.

The vita has been removed from the scanned document

VIII
APPENDIX 1

Development of the Experimental Facilities and Experimental Techniques

1.1 Introduction

To date relatively few workers have undertaken detailed investigations into the inelastic behavior of geologic materials. This has been due in part to the many experimental difficulties which must be overcome if meaningfull data is to be obtained. In this appendix the various difficulties will be outlined along with the methods developed by the writer to overcome them. In all, the development of the final experimental facilities have taken approximately three years, and represent a total of approximately five man-years labour.

1.2 Test Area

1.2.1 Introduction

Early experiments by the writer, Hardy (1956) had indicated the necessity of conducting any fundamental static and quasi-static deformation experiments on geologic materials, particularly those under uniaxial stress, in a controlled environment. Such conditions are necessary due to the fact that the control and measuring systems, as well as the test materials themselves, are sensitive to temperature and humidity variations. For example, the temperature

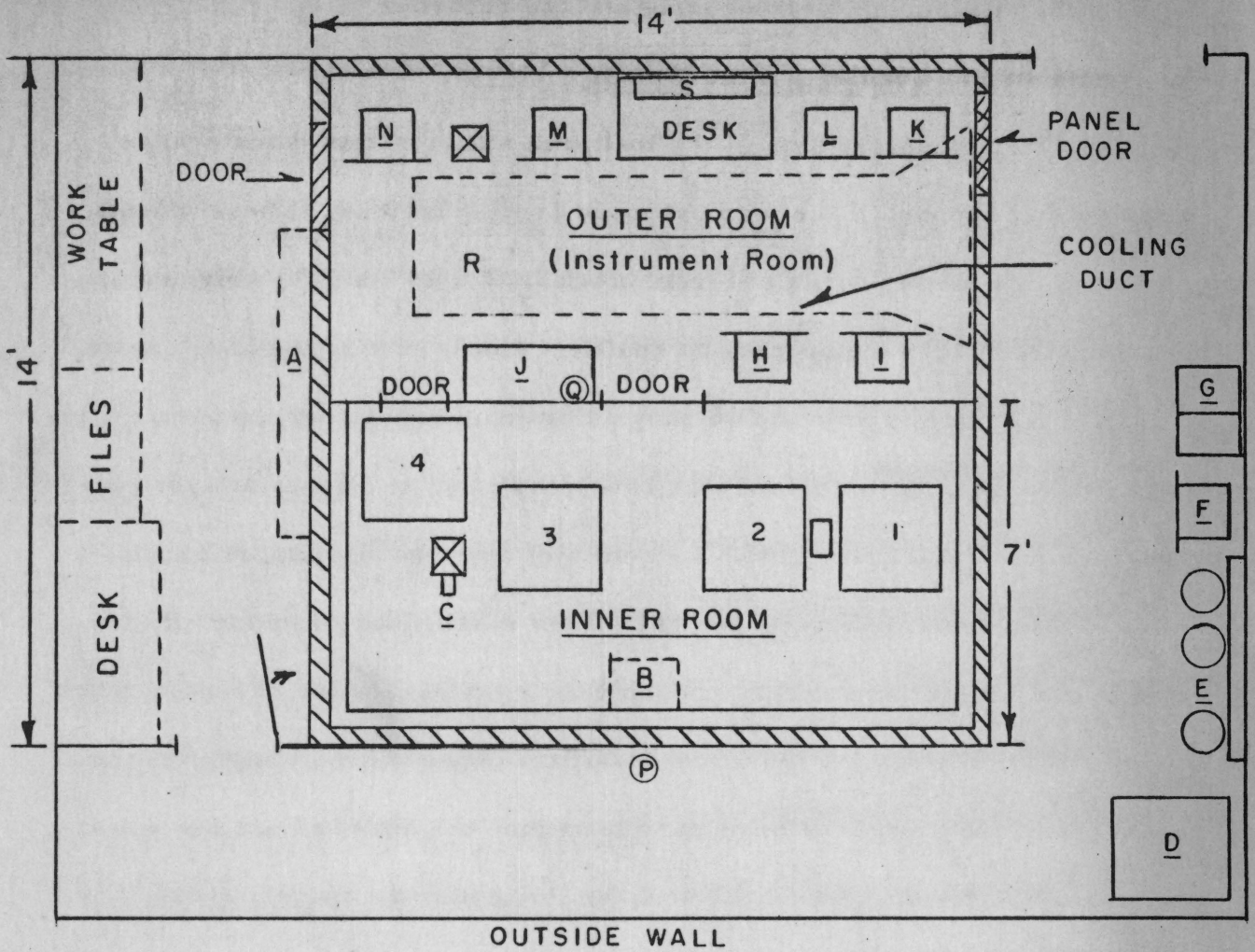
coefficients of a number of typical Canadian shales and sandstones (Hardy and MacLean (1965) have been found to be in the range of 10-15μs/°C. Thus a change in room temperature of 10°C would result in an error of 100-150μs in the observed strain, which could be equivalent to the total time-dependent strain observed in a 10 day creep test. Many geologic materials are similarly sensitive to moisture. The design of a suitable test enclosure and a temperature and humidity control system was begun early in 1961.*

A number of other features were considered necessary for a satisfactory test area. These included the use of antivibration mounting bases for the loading frames to reduce as much as possible the effects of local vibration+; the development and installation of suitable electrical and pneumatic supplies to allow uninterrupted long period operation of the control and measurement systems independent of local power; and the installation of an extensive network of highly stable and well shielded electrical circuits for the control and monitoring systems. Figure 24 shows a general floor plan of the test enclosure and the surrounding area.

---

* The initial design of the enclosure, and the temperature and humidity control system was carried out by Dr. W.M. Gray of the Fuels and Mining Practice Division, Mines Branch, during the spring and summer of 1961 while the writer was in attendance at V.P.I.

+ The building housing the test facility was located adjacent to a heavily travelled main street and was subject to vibrations from explosive studies and heavy machinery in adjacent buildings.



A - Temp. and Humidity Control Panel
B - Humidifier
C - Humidity Transducer
D - Compressor
E - Nitrogen Gas Supply
F - Standby Power and Battery Charger
G - Storage Batteries
H, I - Load and Pressure Control Racks (Type A Loading Machines)
J - 2-Channel "Fast" X-T Recorder
K - Operations Control Rack
L - Manual Readout Rack
M - 12-Channel "Slow" X-T Recorder
N - Y-XT Recording System
P - External Thermostat
Q - Room Thermostat
R - Duct Thermostat
1, 2, 3, 4 - Antivibration Bases

FIGURE 24 - Plan View of Test Enclosure.

1.2.2 The Enclosure

The location selected for the test area was a second storey laboratory area with a poured concrete subfloor which had originally supported heavy machinery. The base of the enclosure itself was constructed on the existing wooden floor but concrete bases, to support the heavy loading frames, were poured directly onto the concrete subfloor. The test enclosure measures 14' x 14' x 10' high overall with a six foot hall on three sides and a three foot space between its roof and the existing ceiling. The structure consists of an outer insulated shell and a smaller inner shell as shown in Figure 25. Effectively the inner shell is a room within a room, since the air in the outer shell circulates freely around it on all sides. The construction hence defines two area, an inner room which houses the loading frames, and an outer room containing the control and monitoring systems.

The outer shell is approximately 14' x 14' x 10' high O.D. and was framed using wooden two-by-fours. A layer of foil vapour barrier was first placed on the existing floor and the base constructed with the two-by-fours on edge lying east-west. The space between the framing was filled with rock wool insulating batts and a dust barrier consisting of a layer of heavy paper tacked over the framing to prevent loose rock wool fibres being picked up by the circulating air. A second set of two-by-fours on edge, running north-south were then erected.

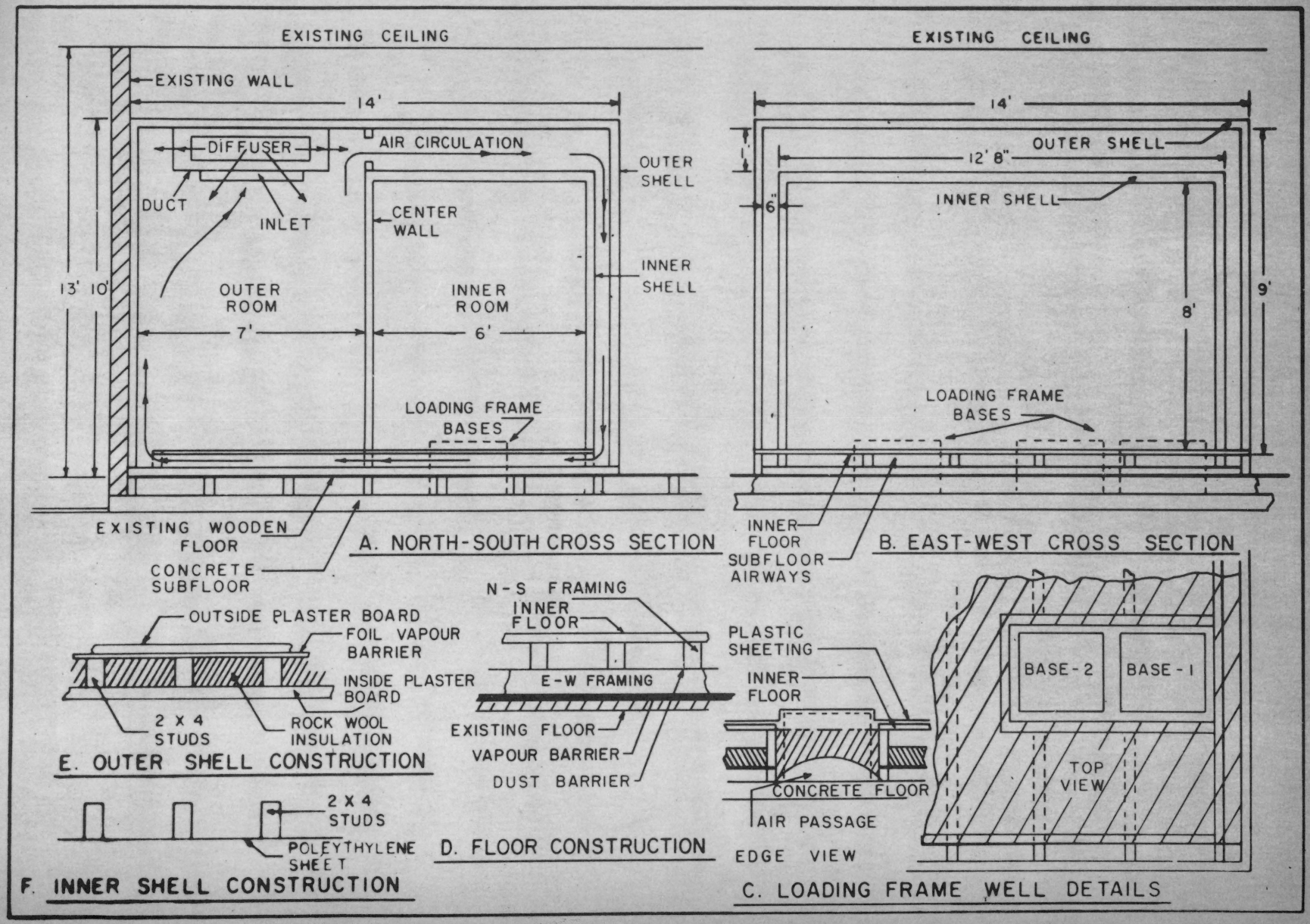


FIGURE 25 - Construction Details of Test Enclosure.

The inner floor of 3/4 inch plywood was then nailed to this set of two-by-fours leaving an open space seven inches wide across both ends. This allowed air to circulate through the airways formed by the top set of two-by-fours. Figure 25D illustrates some details of this construction. The wall framing was then erected followed by the roof and the center wall. The rough 110 VAC wiring for lights and power outlets were installed at this stage. The roof and outer shell walls were then insulated with four inch thick batts of rock wool, foil vapour barrier was applied to the outer side of the walls and roof and these surfaces were sheeted inside and outside with 1/2 inch thick plaster board. Both sides of the center wall were sheeted with similar material. Figure 25E illustrates the construction used on the outer shell.

The main function of the inner shell was to form a vapour tight seal around the inner room to provide an area where deformation experiments on materials subjected to various humidity conditions could be carried out. First the framework of the inner shell were erected. Holes were cut in the floor, and wells constructed to take the loading frame bases. Details of these wells are shown in Figure 25C. Where the construction of a well caused a serious blockage of the airways, an arched opening was made in the well panel (see Figure 25D, edge view) to allow the air to circulate around the

bases once they were installed. At this stage of construction the joints on the inside walls and ceiling of the outer shell and the center wall were plastered. The inside walls and ceiling were then painted along with the inner shell framework. The loading frame bases were cast in position and the concrete allowed to cure for about two weeks. The walls, ceiling and floor of the inner shell were then covered with No. 6 gauge clear polyethylene sheet* which was supplied in rolls six feet wide. This was attached to the inside of the inner shell frame using small flat-headed tacks after first applying a 3/4 inch strip of cloth masking tape+ over the sheet along each tacking line in order to prevent tearing.

The construction of the enclosure was completed by the installation of a heavy insulated door and removable door panel (see Figure 24 for location), the installation of corrugated rubber matting on the floors of the inner and outer rooms and the installation of lighting fixtures and 110 VAC outlets.

1.2.3 Temperature Control System

The system used to control the temperature of the test enclosure is based on a design suggested by Solvason (1961). Figure 26 illustrates the main features of the system. Basically it consists of a

*Coverall No. 6CG polyethylene sheet manufactured by Warp. Bros., Chicago, U.S.A.

+Tuck Tape, adhesive cloth tape, manufactured in Canada by Canadian Technical Tape Ltd., Montreal.

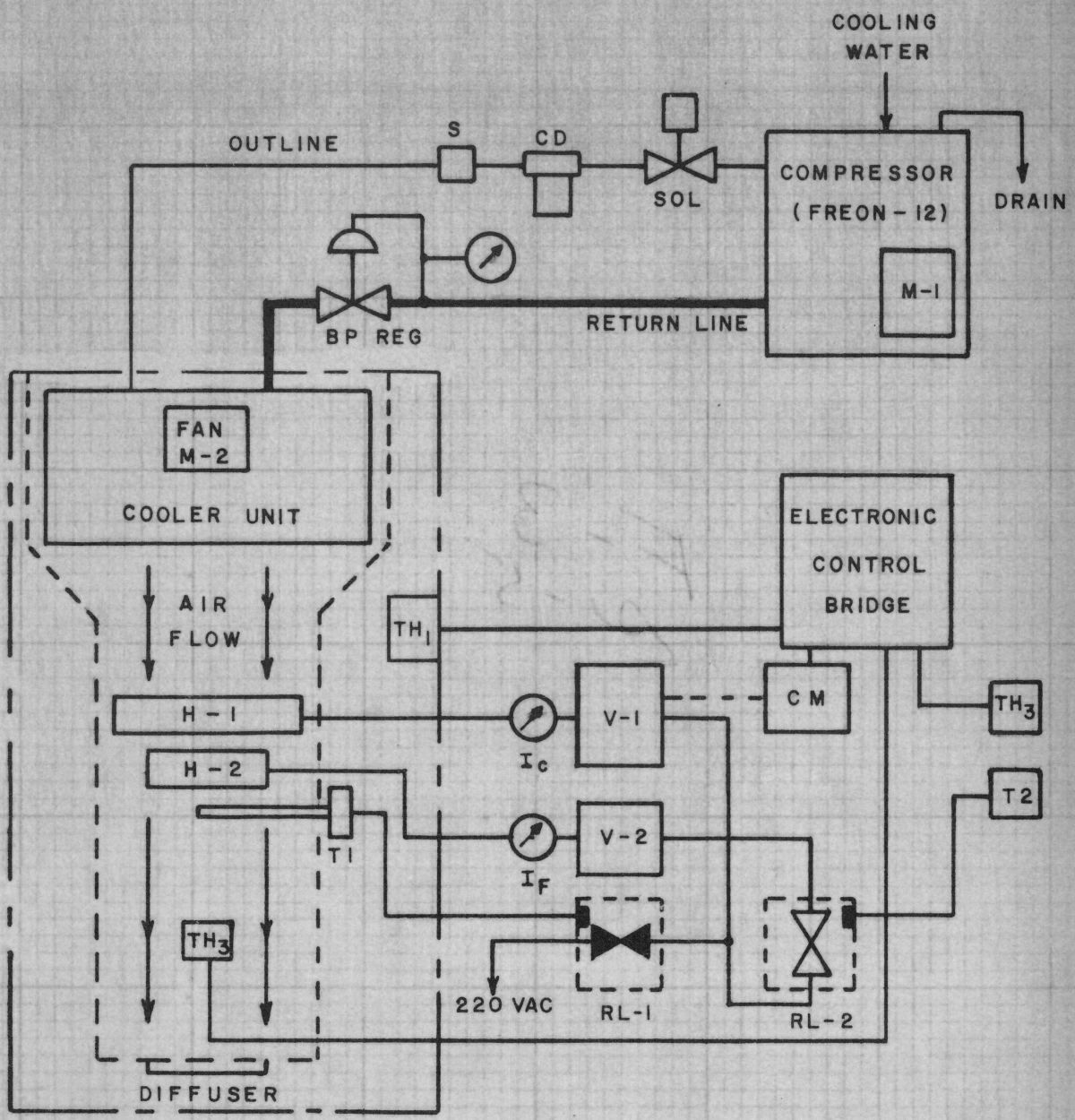


FIGURE 26 - Outline of Test Enclosure Temperature Control System.

cooling section, a reheating section and an electrical control section. In operation, air from the outer room is drawn up into a duct (in the ceiling of this room) and passed through a set of cooling coils which lowers its temperature below that of the outer room. This cooled air is then forced over a set of heating coils and its temperature raised to some higher value. The reheated air is passed out a diffuser at the far end of the duct where a fan mixes it with the existing room air. A series of five blower type fans* located around the perimeter of the center wall forces this mixed air over the roof and around the walls of the inner room. It finally returns to the outer room via the airways below the inner floor and the ducts along the north wall of the outer room. A ten inch fan located in the inner room circulates the inside air to reduce thermal gradients to a minimum. Figure 25A illustrates the approximate air paths.

The degree of reheating of the cooled air is controlled by a motor driven variac. The control motor is modulated by an electronic control bridge unit which coordinates signals from three temperature sensing transducers.

After a period of time the temperature of the air circulating around the outside of the inner room reaches an equilibrium temperature. Due to the relatively low insulation provided by the

*Electrohome junior blower, Model 197-44-05-15B, capacity 100 cfm.

polyethylene covering on the inner shell and the fact that very little heat is generated within it, the temperature of the inner room approaches that of the outer room, remaining however always slightly higher. The constancy of the inner room temperature however is always much greater than that of the outer room since it is a completely closed system.

The cooling system (see Figure 26) consists essentially of a water cooled compressor* (mounted on antivibration blocks and located about six feet from the test enclosure) which supplies Freon-12 to a cooler unit+ mounted at one end of a large ceiling duct running the width of the outer room. The Freon liquid leaves the compressor through a normally closed solenoid valve (which opens when the compressor is operating), passes through a filter-drier unitx and an in-line** sight glass and is carried (via copper tubing, 1/4" O.D. x .030" wall) to the cooler unit in the inner room. There it passes through an expansion valve++ and hence through the cooling coils. The Freon gas leaves the cooling coils via a back-pressure regulator+++ and returns

---

*Kelvinator compressor, one ton capacity, Type No. 1151178, F-12 Charge 6 lbs, driven by a 1 HP, 1760 rpm, Delco motor which requires 220 VAC at 7 amps.

+Keeprite Roundell unit cooler, model R 375, rated at 373 Btu per degree, and 770 cfm.

xSporlan filter-drier type c-162

**Imperial sight glass type 270C

++Detroit high temperature thermostatic expansion valve, 1/2 ton capacity, No. 71800.

+++Aminco back-pressure regulator No. 1205, Type JV-FM-5/8, with attached 0-100 psi pressure gauge.

to the compressor (via 3/8" O.D. x .030" wall copper tubing). The liquid and the return lines are taped together and insulated in a common jacket over most of their length to increase efficiency and to prevent the condensation of water vapour.

The compressor operates continuously when the temperature control system is in use. The unit is cooled by tap water which circulates through the compressor and leaves via a drain line to the sewer. The compressor motor is electrically interlocked with transducers which sense the compressor output pressure and temperature and the compressor is automatically shut-off if preset limits are exceeded. The compressor motor is electrically protected for overload and is interlocked with the fan motor in the cooler unit so that a failure of the fan motor will automatically shut-off the compressor preventing icing-up of the cooling coils.

The reheating section of the system is illustrated in Figure 26 and consists of two sheathed heaters* which span the air duct about two feet down-line from the cooler unit and a set of variacs and relays which supply power to these heaters. The largest heater (H-1) is termed the control heater and is rated at 2000 watts. The smaller heater (H-2) is termed the fixed heater and has a rating of 1000 watts. The power supplied to H-1 and H-2 is controlled by two

* Both heaters are Chromalux brand, Finstrip iron sheathed heaters, H-1 -- 2000 watts, 230 volts, No. SEF-38, H-2 -- 1000 watts, 230 volts, No. SEF-19.

variacs V-1 and V-2 (230 volts, 10 amp and 5 amp capacity respectfully) and monitored by two ammeters (I_c and I_f) in series with the heaters. The setting of V-1 is determined by the electronic control system and is automatically varied by the associated control motor (CM) so as to keep the room at a constant temperature.

The purpose of H-2 is to provide a certain fixed amount of heat to the duct air in order that H-1 will be capable of maintaining control over the full range of ambient temperature with the required accuracy. Under normal ambient conditions $65°F < T_o < 110°F$, H-2 is not utilized. However in the late spring and early fall, and when trouble occasionally developes in the building heating system the ambient temperature may drop below 65°F, heat losses through the walls of the enclosure increase, and additional heating capacity is required in the system. Relay RL-2*, and thermostat T2** located outside the enclosure control the power to H-2. When the ambient temperature falls below 65°F, T2 closes RL-2 (which is normally open) supplying power to H-2 at a preset level determined by V-2. At an ambient temperature $T_o > 65°F$ RL-2 remains open.

To prevent overheating of the air duct in the event of a control system failure a normally closed relay (RL-1)* was placed

*Honeywell mercury switch-type relay, type R879B.
**Honeywell thermostat, type T42B.

in series with the primary of V-1 and V-2 and an associated thermostat (T1)[+] was located approximately two feet down-stream of the heaters. In operation this thermostat senses the temperature of the reheated air in the duct and if it exceeds a preset limit both heaters are shut-off. Since the room temperature was to be controlled at 22°C (approximately 72°F) and the thermostat used had a fixed differential[x] of 12.5°C, a set point of approximately 38°C was selected. In this case if the duct temperature rises above 30°C the heaters are shut-off and remain off until the temperature drops to below 25.5°C.

The electronic control section is illustrated briefly in Figure 26. It utilizes a Honeywell electronic controller[*], a modulating motor (CM)[xx] which operates variac V-1 and which in turn controls the amount of power to the control heater (H-1), and a set of three resistance type thermostats[++]. The room thermostat (TH_1) is located on the wall of the inner room, the duct discharge thermostat

---

+Honeywell Airstat controller type LA219A, incorporating a bimetallic-operated mercury switch.

x The differential rating of a bimetallic strip-type thermostat is the number of degrees the temperature must fall below the set point before the switch contacts of the thermostat will reopen.

*Honeywell MD-791A electronic temperature control panel, Model W626A.

xx Honeywell Modutrol motor, Model M905J.

++ TH_1 - Honeywell Thermostat, Model T7018C.
TH_2 - Honeywell Thermostat, Model L7033A-5".
TH_3 - Honeywell Thermostat, Model T7001A.

(TH_2) is located in the air duct near the outlet diffuser, and the external space thermostat (TH_3) is located in the hall outside the test enclosure. Each of the thermostats are assigned a certain control authority*.

The system operates as follows: on a call for heat from the room thermostat (TH_1) the control bridge becomes unbalanced and the modulating motor adjusts the variac to provide more power to the duct heater. Since TH_1 has 100% authority, the motor could turn the attached variac fully on, which would cause the room temperature to overshoot. However TH_2 (authority 0-40%) senses the increased discharge temperature and tries to rebalance the control bridge and in so doing it starts shutting the variac off. In other words TH_2 tends to snub the action of TH_1 to prevent overshooting. A decrease in hall temperature is sensed by TH_3 (authority 0-40%) which is able to operate the control motor and increase the variac output even if the room temperature is at the control point. Thus the system will compensate for the increased heat loss through the walls which will eventually result from the lower hall temperature. With this arrangement the actual room temperature and the temperature at TH_1 are

* The percentage authority is defined as the percentage of the total possible rotation of the control motor which is produced by an unbalance in the individual thermostats. For example assuming the motor is capable of a total rotation of 160 degrees, an unbalanced thermostat with a 20 per cent authority could produce a maximum angular rotation of 32 degrees.

precisely in phase and as a result offset in the system is eliminated. This type of correction is frequently referred to as anticipation compensation.

A complete description of the system, wiring details, and the computation and check-out procedure used in the adjustment and calibration of the system will not be presented here since they are available in detailed form elsewhere*.

During 1963 a number of studies were conducted on the constant temperature system in order to obtain optimum performance. A control temperature of 22°C was selected along with TH_2 and TH_3 authorities of 10% and 30% respectively. Full time operation of the system commenced on May 30, 1964. Figure 27 illustrates the variation of ambient (hall) temperature (T_o) and the temperature of the outer room[x] (T_c) with time over a period of 22 days. In both cases temperature was measured with regular glass stemmed thermometers which provided an accuracy of $\pm$ 0.5°C and $\pm$ 0.1°C in the observed value of T_o and T_c respectively. On June 18, after approximately

---

* See the following engineering data available from Minneapolis-Honeywell Regulator Company, Minneapolis 8, Minn., U.S.A.
Form 77-7316 - Engineering data for electronic control system W626A.
Form 77-7301 - Computations for electronic control system adjustments.
Form 77-7507 - Check-out and testing data for electronic control system W626A.

x The majority of temperature stability experiments to date have been conducted with the door open between the inner and outer rooms. Since no effort is being made to control humidity in the inner room at present this does not introduce any difficulties and simplifies experimental procedure.

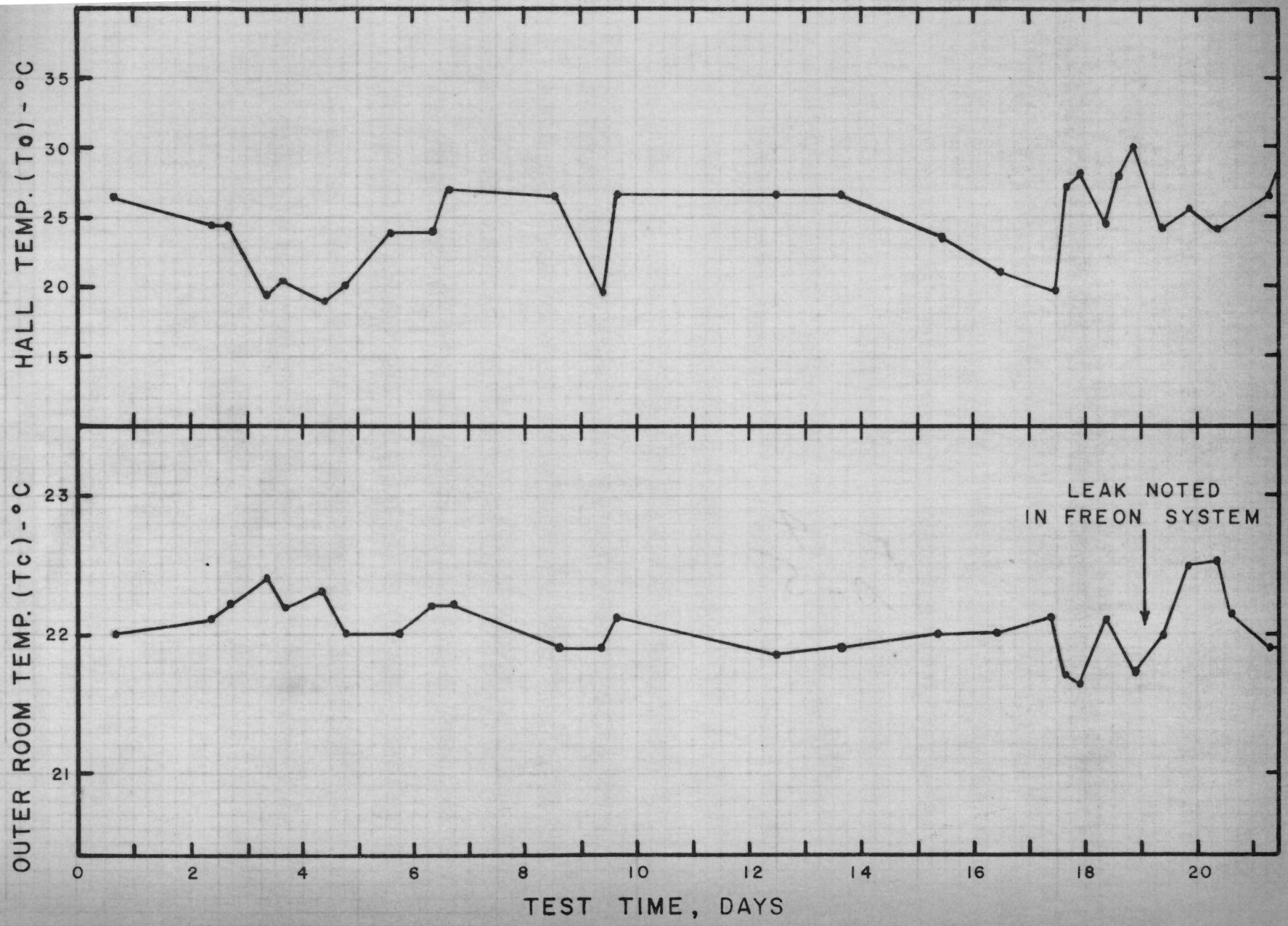


FIGURE 27 - Curves Showing the Variation of Ambient and Enclosure Temperature with Time.

18 days operation, a series of leaks developed in the cooling system necessitating a shut down. After repairs were made and the Freon circuits refilled the system was started up again and ran continuously for some 36 days, at which time trouble developed in the compressor motor forcing another shut down. The system was started up again on July 24 and has been running continuously since (approximately 150 days). During this later period the ambient temperature range was found to be 18.9 to 33.3°C, whereas the outer room temperature varied only over the range 21.3 to 22.5°C. The mean and standard deviation of T_c and T_o over this period were found to be $T_c = 22.0 \pm 0.29$°C and $T_o = 24.8 \pm 2.34$°C. It should be noted that much greater stabilities were often observed over periods of up to 48 hours. The main stability problem remaining appears to be associated with the authority setting for TH_3. Originally an authority of 30% was used, this was subsequently reduced to 15% when short period outside temperature fluctuations were found to be affecting T_c. However, even with the 15% setting it is found that a large increase in ambient temperature causes the control system to drop T_c too low. This situation is probably due in part to the very good thermal insulation of the outer shell. The behavior of the system with lower values of TH_3 authority are to be investigated.

1.2.4 Humidity Control

As it was anticipated that in the future deformation experiments would be conducted on a number of evaporite minerals (NaCl, KCl etc.), which are particularly sensitive to moisture, the inner room was equipped so that its humidity could be accurately controlled. Humid air was generated by a simple humidifier unit* consisting of a large water-soaked wick, a water reservoir, and an associated air circulating fan. Dry room air is drawn in by the fan and passed out over the wick, where it picks up moisture. The water level in the reservoir is maintained automatically by a float operated microswitch which operates a solenoid valve in series with the water supply line to the unit. A humidity sensitive element** located in the inner room and an associated hygrometer controller+ unit located outside the test enclosure control the operation of the humidifier fan. With this relatively simple arrangement it is possible to control the relative humidity of the inner room to ± 2%.

1.2.5 Antivibration Loading Frame Mounts

During construction of the test area antivibration mounts were installed for support of the four proposed loading frames. These

---

*Electrohome Humidette, Model A26.

**Hygrodynamics Inc. narrow range sensing element, class A, type 4-4820.

+Hygrodynamics Inc. Hygrometer Controller, Model 15-3110.

mounts consisted of a large poured concrete block (18" x 24" x 24" high) weighing approximately 800 lbs supported on resilient pads, consisting of alternate layers of isomode rubber[x] and 16 gauge aluminum, at the four corners. These pads rested on a multiple sandwich base consisting of alternate layers of 1/2-inch thick steel plate and 1/2-inch thick ten-test insulation board. Figure 28 illustrates the arrangement. This system has been used in the past by the writer (Hardy (1962) and has proven very satisfactory for removing much of the vibration resulting from local traffic and general building vibration.

1.2.6 Electrical Power Supply System

Since the axial load and confining pressure control system and sections of the axial load, confining pressure and strain measurement system must operate 24 hours a day over extended periods of time it was necessary to provide a high capacity storage battery system and a 110 VAC standby system for operation of this equipment. Four six-volt, 220 ampere-hour storage batteries, arranged in two sets, provide a series of 2 and 6 volt DC lines for operation of control and measurement circuits and a 12 volt DC line for operation of a 110 VAC, 300 watt standby system. A separate 6V bias supply utilizing No. 6 dry cells is also included. An auto-

x Available in Canada from Upton, Braden and James Co. Ltd., Montreal.

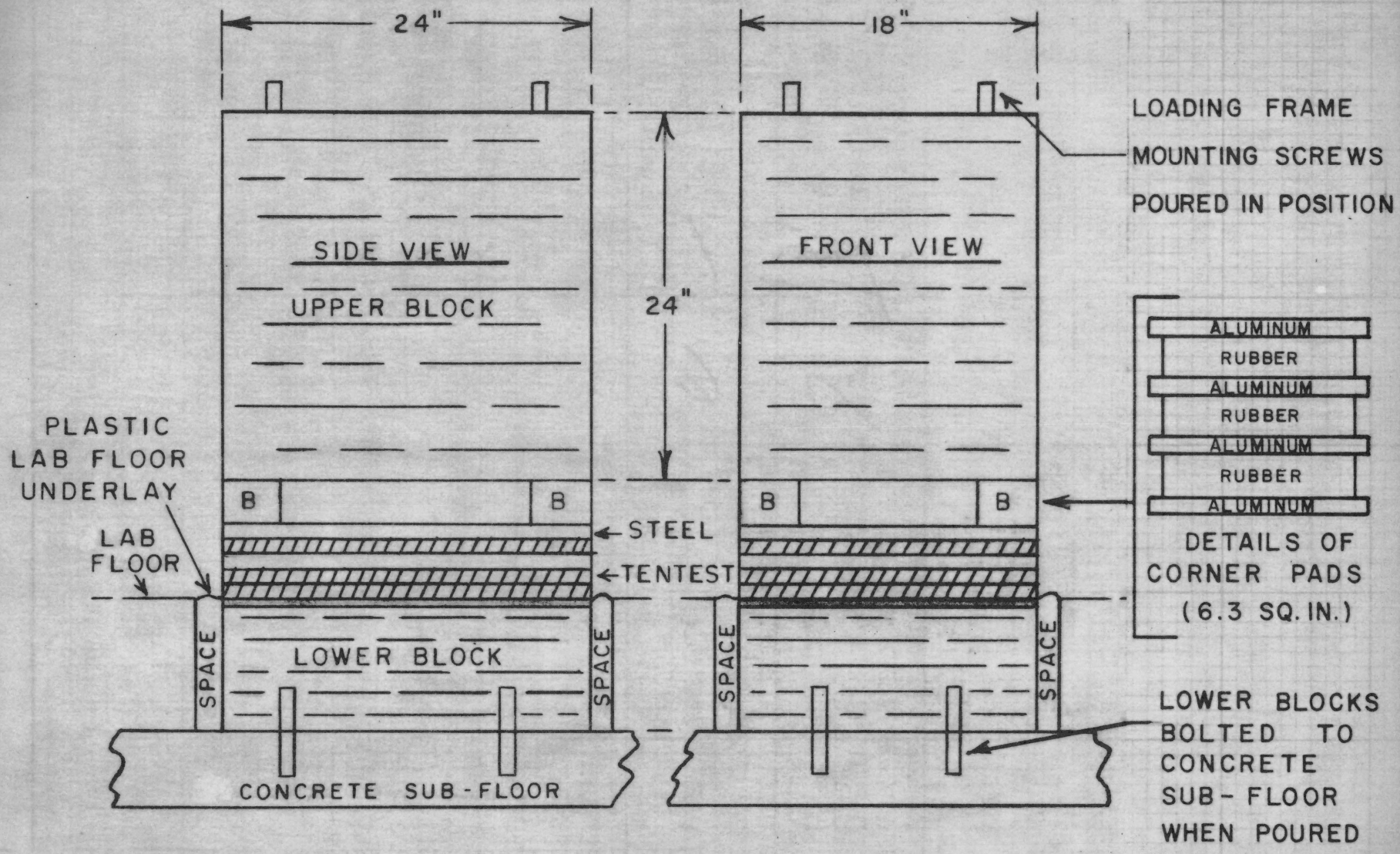


FIGURE 28 - Construction Details of Antivibration Loading Frame Mounts.

matic battery charger and associated cycler unit insures that both sets of storage batteries are kept at full charge when the facility is not in use. During operation of the facility the automatic charger is connected only to battery set-B and a high current power supply is connected across battery set-A to maintain it at full charge.

The standby unit, batteries and associated charging units are located in the hall outside the constant temperature enclosure. DC and AC distribution panels located in the outer room of the test enclosure monitor the active circuits and provide facilities for metering the voltage in each circuit. Figure 29 illustrates the arrangement of these power supplies and the monitoring facilities.

1.2.7 Pneumatic Supply System

A 2000 psi nitrogen gas supply system for operation of the Type-A axial loading and confining pressure systems in shown in Figure 30. The gas supply consists of eight standard nitrogen cylinders in two separate circuits of four each. One cylinder (primary supply) in each circuit is located in the outer room near the load and pressure control systems, and the other cylinders (secondary supply) are located in the hall outside the constant temperature room. The primary supply in the inner room eliminates the possibility of a high pressure drop between the secondary supply and the pressure control systems when a large volume gas flow is

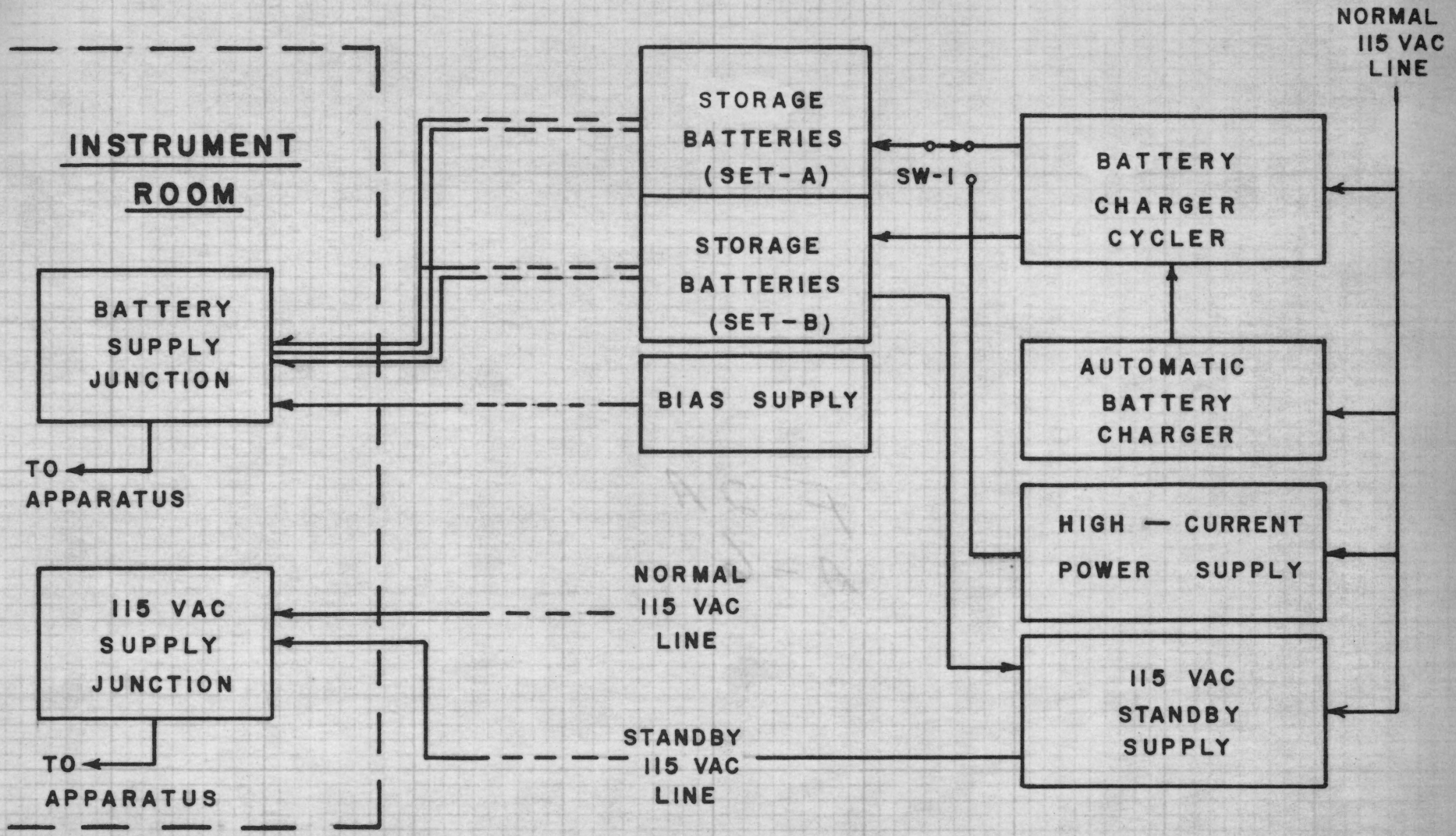


FIGURE 29 - Block Diagram of Electrical Power Supply System.

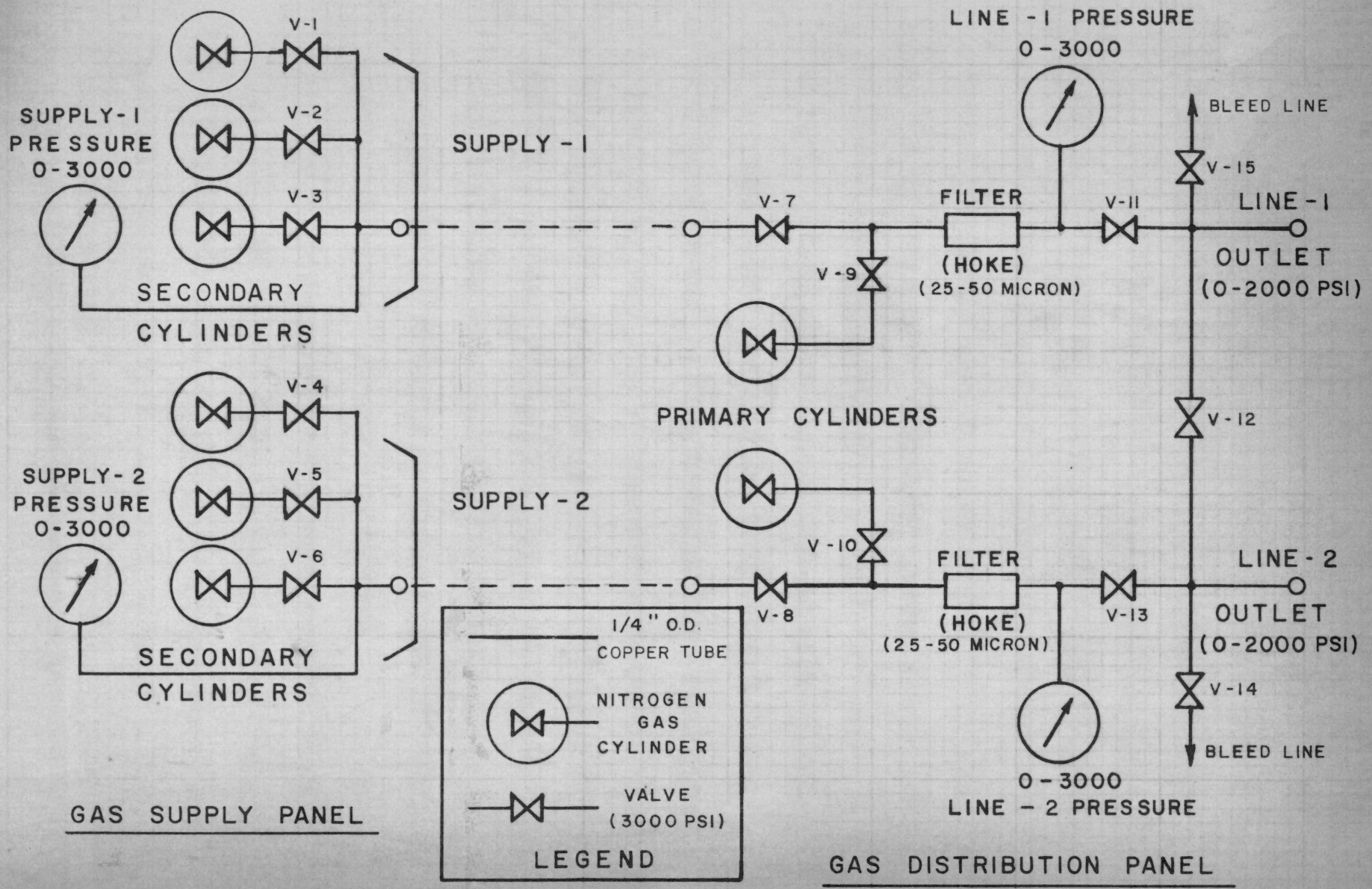


FIGURE 30 - Circuit of Pneumatic Supply System.

required. A system of valves allows individual nitrogen cylinders to be removed and replaced, and allows the primary and/or secondary gas supplies to be connected into or disconnected from the circuit. The pressure in the two circuits is monitored by dial type pressure gauges located both at the secondary supply (outside the constant temperature room), and on the gas distribution panel in the outer room. Inline filters with 25-50 micron sintered bronze elements are located at the input to the distribution panel.

1.2.8 Electrical Wiring

Since many of the control and monitor signals were in the 5-20μv level it was necessary to take very special care with all electrical wiring. All 110-220 VAC power wiring was shielded where possible, and kept as far from control and monitor as practical. All 110 VAC power cables from wall outlets to various instruments utilized shielded cables and polarized connectors. In most cases cables carrying DC power from the battery supplies were also shielded. All relay racks were grounded, via their individual 110 VAC power cables, to the electrical ground of the building.

Shielded cables were used for all control and monitor signals. In most cases the longer cables were terminated at both ends on terminal strips located in steel junction boxes, shorter cables connected these lines to the various pieces of apparatus. The cable

shields themselves were connected to the electrical ground of the building and the junction boxes were grounded via the cable shields. Most low level signals (up to 10 MV) were carried in individual cables to prevent interference. All cables were permanently tied or clamped in place.

1.3 Axial Loading System

1.3.1 Loading Frames

In the past many workers studying time-dependent properties of geologic materials have utilized lever type loading systems to axially load cylindrical test specimens, (e.g. Fairhurst (1961), Hardy (1956), Phillips (1948), Price (1964) etc.). Such systems may have an apparent advantage due to their basic simplicity but they do not provide the highly stable loading conditions required to determine meaningful deformation parameters. The loading system finally developed by the writer is based on the design of a load maintaining system described by Hardy and Larocque (1965). It consists of a loading frame incorporating a single acting hydraulic ram with an attached load cell and an associated control system which monitors the ram thrust or the specimen strain and adjusts the input pressure to the ram so that the ram thrust or specimen strain varies in accordance with an established loading program. Such a system is generally referred to as a feedback control system.

Figure 31 shows a photograph of two of the axial loading frames mounted on antivibration bases in the inner room of the test enclosure. The loading frame consists of an upper and a lower steel platten (15-1/2" x 15-1/2" x 1-1/2" thick) which are tied together by four heavy steel rods (1-1/2" diameter). These rods are threaded at both ends to provide adjustment of the working space between the plattens and to allow the plattens to be adjusted perfectly parallel. A modified Blackhawk 50 ton hydraulic ram* is threaded into the upper platten and locked into position by an upper and a lower locking ring. A strain gage type load cell is attached to the lower end of the ram piston to monitor the thrust. Figure 32 shows a close-up view of one of the loading frames with a specimen loading jig in position between the load cell and the lower press platten.

1.3.2 Feedback Control Systems

The description and analysis of feedback control systems is presented in detail in many recent texts (e.g. Ahrendt and Savant (1960), Truxal (1958), and Thaler and Brown (1960). Figure 33A shows the arrangement of the basic feedback control system. It consists

* The Blackhawk hydraulic ram type RC-210 has an effective piston area of 11.045 sq in., an outside diameter of 5 in. and a 6 in. stroke. Modification involved the removal of an attached handle, and the cutting of a 5"-12 UN thread on the outside diameter of the ram body over a length of approximately 7 in.

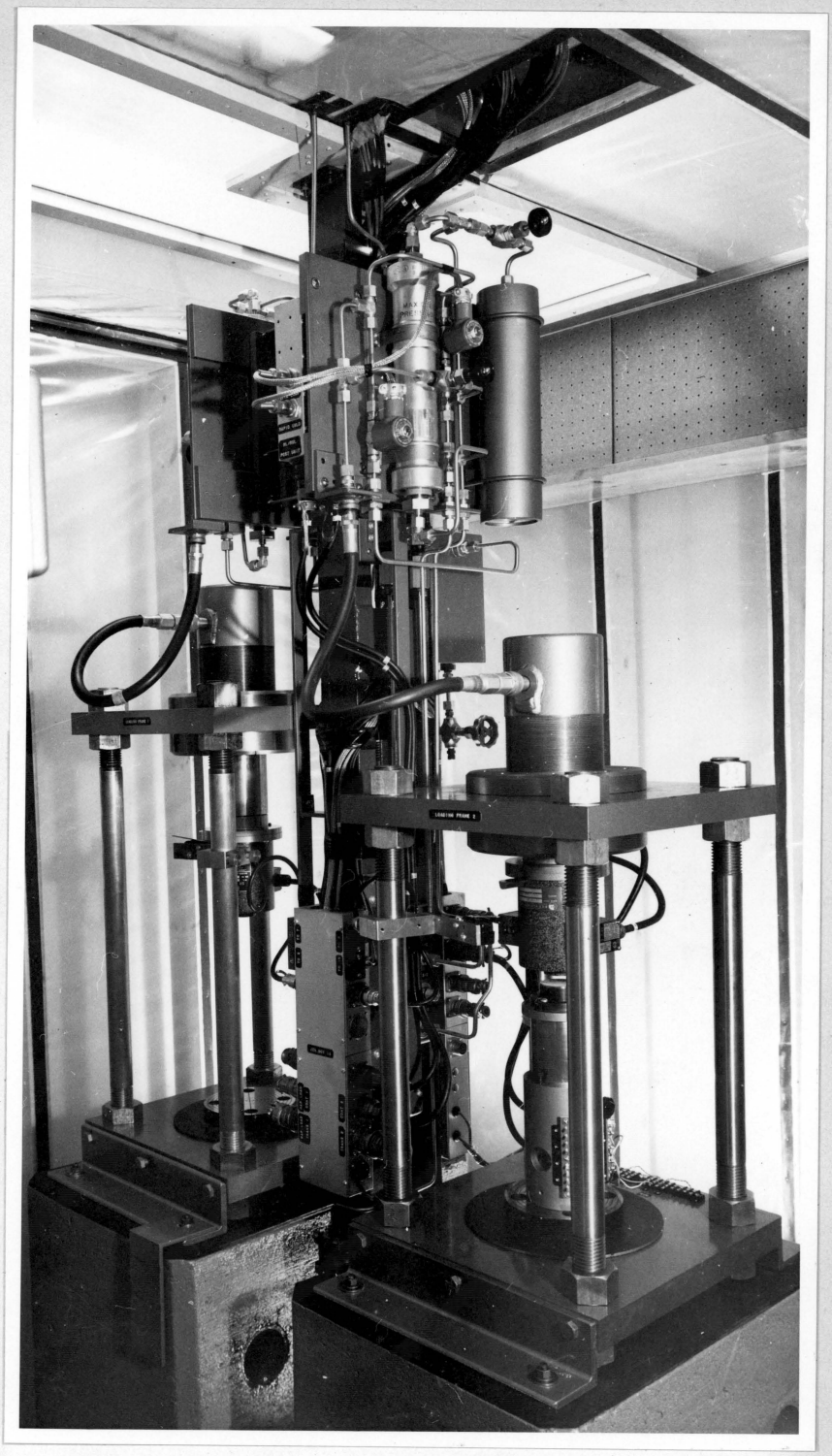
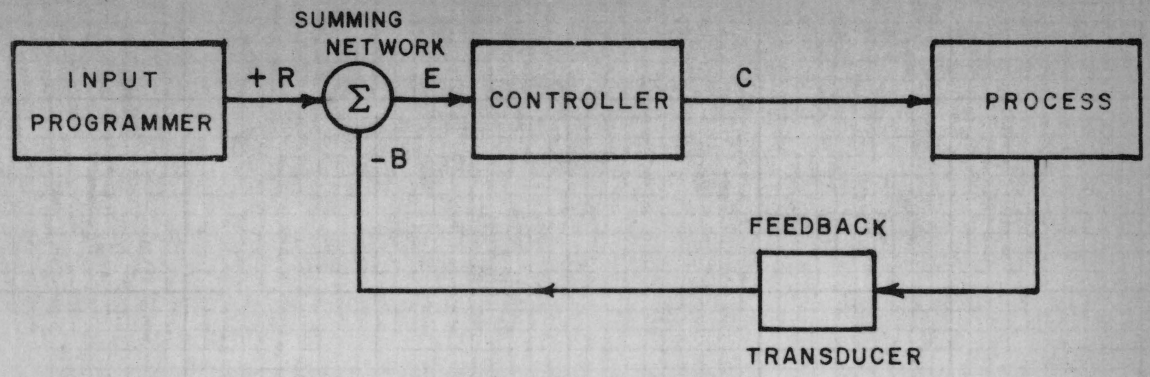


FIGURE 31 - Two Axial Loading Frames Mounted on Antivibration Bases in Inner Room.

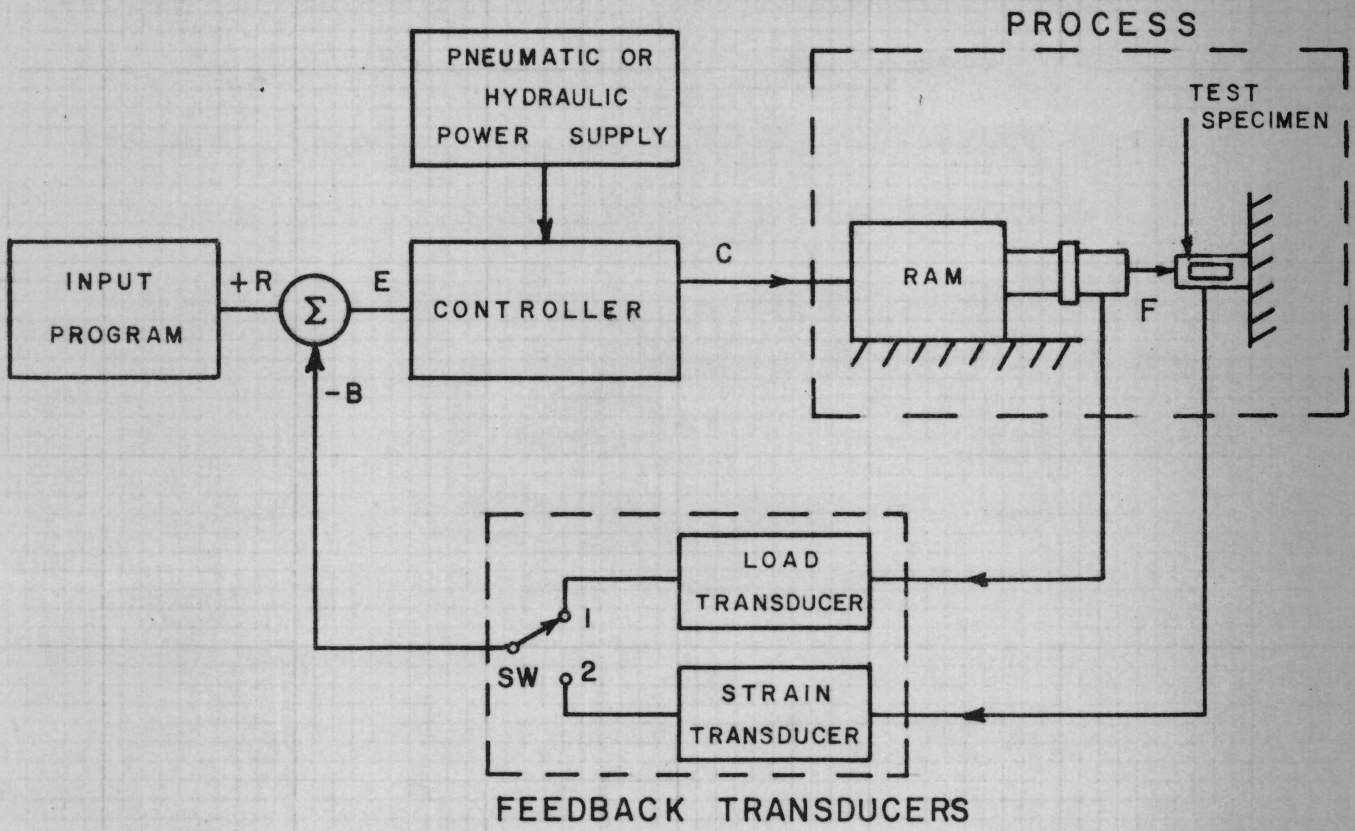


FIGURE 32 - Close-Up View of Loading Frame with Specimen Loading Jig in Position.



R - INPUT PROGRAM SIGNAL
B - FEEDBACK SIGNAL
E - ERROR SIGNAL (R - B)

A. BASIC FEEDBACK CONTROL SYSTEM



B. SIMPLIFIED BLOCK DIAGRAM OF CONTROL SYSTEM FOR ROCK DEFORMATION EXPERIMENTS

FIGURE 33 - Block Diagrams of a Basic Feedback Control System And a Control System for Rock Deformation Studies.

of a process to be controlled, a controller, a programmer, a feedback transducer, and a summing network. The input programmer puts out a signal (R) which is designed to be an analog of the desired process state and the feedback transducer puts out a signal (B) proportional to the actual process state. These two signals are applied to the summing network and the error signal E = (R - B) applied to the input of the controller. In operation the controller adjusts the process state so that the error signal (E) to the controller is a minimum. Under optimum conditions the process state will accurately follow the input program. Feedback control systems have been developed which utilize pneumatic, hydraulic, mechanical and electrical signals. Using appropriate transducers mixed systems which incorporate a number of types of signals may be designed.

Figure 33B shows a block diagram illustrating the form of the feedback system developed for carrying out rock deformation experiments. Here the "process" consists of the loading of a test specimen under various test modes, the controlled variables being specimen stress (σ) and strain (e). By selection of the appropriate input program and feedback transducer the following test modes may

be obtained:

(i) Controlled strain rate ----------(CER)

(ii) Controlled stress rate ----------(CSR)

(iii) Constant strain (stress relaxation experiment) ----(CE)

(iv) Constant stress (creep experiment) ----------(CS)

(v) Incremental ----------(I)

(vi) Cyclic ----------(CY)

Depending on the time scale and the desired control quality two types of controllers may be utilized. These are classed as "continuous" and "on-off" types. In the "continuous-type" controller the rate of correction of the controlled variable is proportional to the error signal (i.e. the difference between the actual value and the required value of the controlled variable). However in the case of the "on-off" type controller only two states are possible. The controller is normally in the "off" state and can only be switched into the "on" state if the error signal exceeds some definite level. Hence the rate of correction of the controlled variable is independent of the magnitude of the error in the controlled variable. Under this condition the actual value of the controlled variable will tend to oscillate about the required value. If rapid changes in the controlled variables (σ and e) are required a "continuous"-type controller must be utilized, whereas if only slow changes are involved a simpler "on-off" type may be used.

Since it was decided that initial deformation experiments would be conducted over relatively long periods of time which would involve either fixed or slowly varying controlled variables it was decided that the "on-off" type control system would be the most practical. The loading system utilizing this control system and the loading frame discussed earlier will be referred to for convenience as the Type-A loading system. It should be noted that some time was spent in designing and in initial development of a loading system incorporating a "continuous" type controller to be used in experiments at higher loading rates. This system is referred to as the Type-B loading system and is still under development.

1.3.3 Type-A Loading System

Figure 34 shows a simplified block diagram of the Type-A loading system. Since the system has both stress and strain feedback available it is capable of operating in any of the test modes described earlier. To illustrate the operation of the system let us consider that it is connected in the constant stress (CS) mode*, and that the axial specimen stress (σ_{zz}), as measured by the load cell, is below the control point ($\sigma_{zz}(c)$). Since σ_{zz} is below the control

*Note that in the CS-mode the programmer output remains constant for a particular value of stress, and the control mode selector will be set for stress feedback. The unit marked ZB-1 in the stress feedback line is a zero balancing unit to enable the output voltage of the load cell to be set to zero when the applied load is zero.

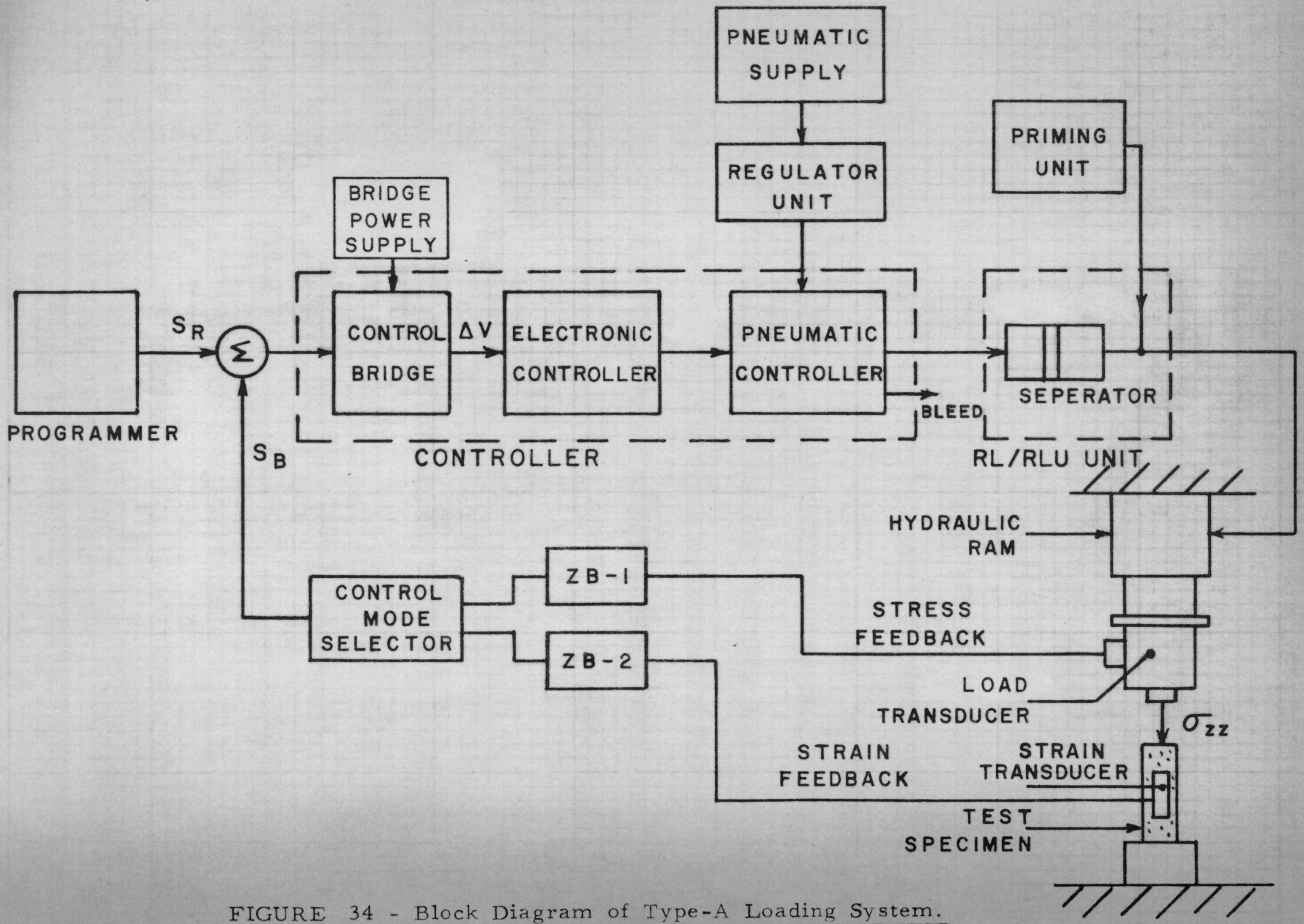


FIGURE 34 - Block Diagram of Type-A Loading System.

point the pneumatic controller will be in the "load-on" state which will allow gas to flow from the regulator unit to the primary side of the separator. As a result the oil pressure on the secondary side of the separator will rise, increasing the pressure in the hydraulic ram, and raising σ_{zz}. The load cell, placed between the ram and the test specimen, senses the magnitude of the applied load and provides a feedback signal (S_B) to the control bridge which is proportional to $\sigma_{zz}(c) - \sigma_{zz}$. The resulting output voltage from the control bridge (ΔV), which is proportional to S_B, is fed to the electronic controller which in turn operates the pneumatic controller. Now as σ_{zz} approaches $\sigma_{zz}(c)$, ΔV tends to zero and the electronic controller switches the pneumatic controller into the "off" state, shutting off the flow of gas to the separator. If $\sigma_{zz}(c)$ is exceeded the resulting feedback voltage triggers the pneumatic controller into the "unload-on" state which allows gas to bleed out of the separator reducing σ_{zz}.

Operation in the other various test modes will be similar. For example if a controlled rate of straining is required strain feedback will be employed and the programmer will provide a signal corresponding to the required strain vs time function.

Basically the system may be divided into two sections namely a pneumatic/hydraulic section and an electronic section. The former consisting of the pneumatic controller and its associated

regulator unit, the RL/RUL unit, containing the separator and its associated priming unit, and the hydraulic ram. The latter consists of the electronic controller, the control bridge, the programmer, and the feedback transducers and associated circuitry. Figure 35 is a photograph which shows in the foreground two racks containing the load control system.

1.3.4 Pneumatic/Hydraulic Section

Figure 36 gives details of the pneumatic/hydraulic (p/h) section of the system. The regulator, pneumatic controller and priming unit are located in the outer room (see Figure 35). The RL/RUL unit is located near the hydraulic ram in the inner room, as shown in Figure 39. In most cases standard hydraulic fittings*, valves** and tubing+ rated for at least 2000 psi were used in the construction of this equipment.

---

* Weatherhead, Ermeto-type steel fittings rated at 15,000 psi were used in most applications.

** Manual valves used throughout the system were Hoke, Type 270N equipped with nylon stem tips.

+ 1/4" O.D. steel tubing rated at 10,000 psi was used in most applications. Where long distances or difficult bends were involved standard 1/4" O.D. soft copper tubing was employed (e.g. between the pneumatic controller and the RL/RUL unit). No failures have been observed with such installations even in cases where pressures of up to 2000 psi have been maintained over periods of at least two years.

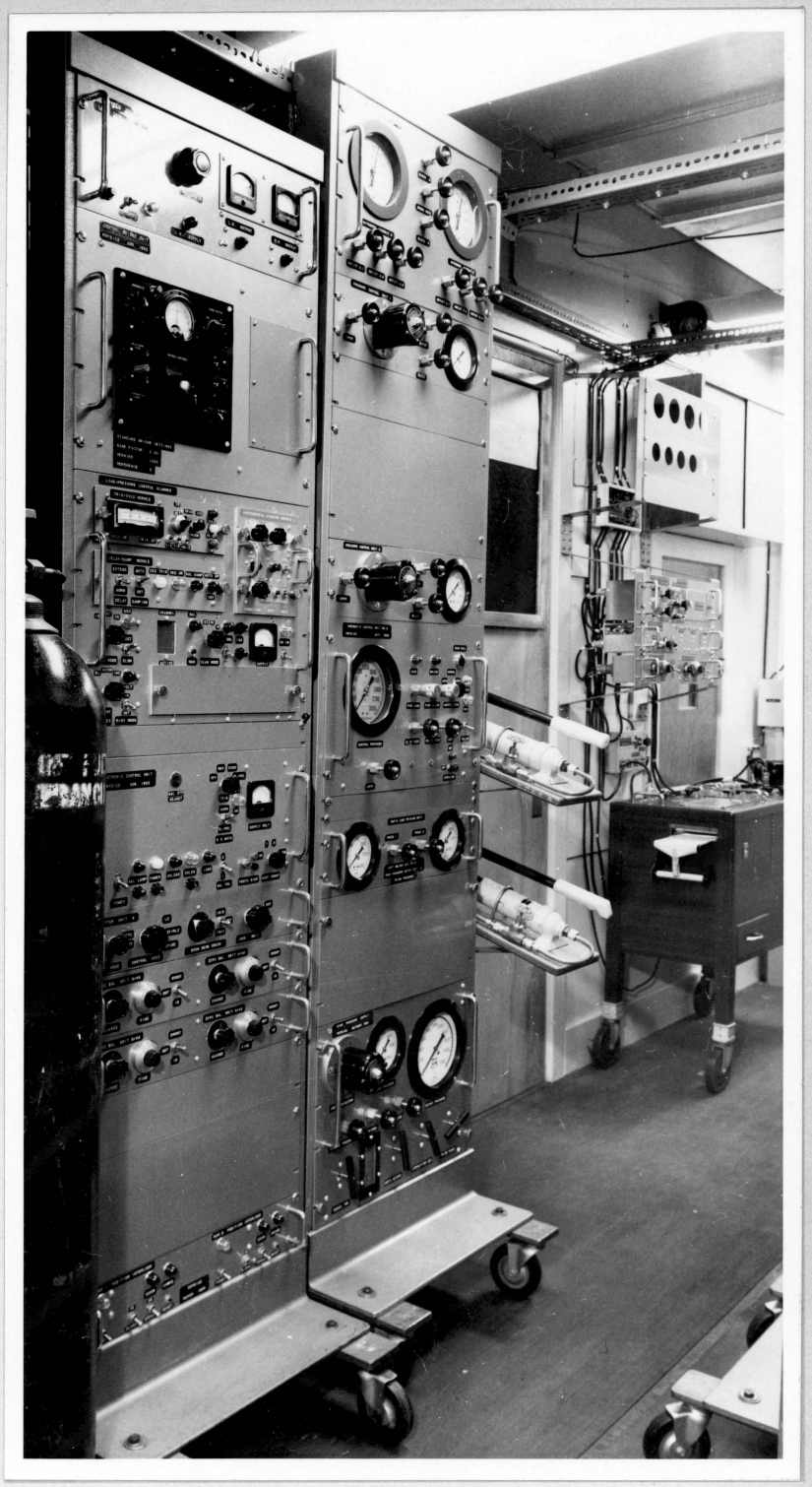


FIGURE 35 - Photograph Showing in the Foreground Two Racks Containing the Load Control System.

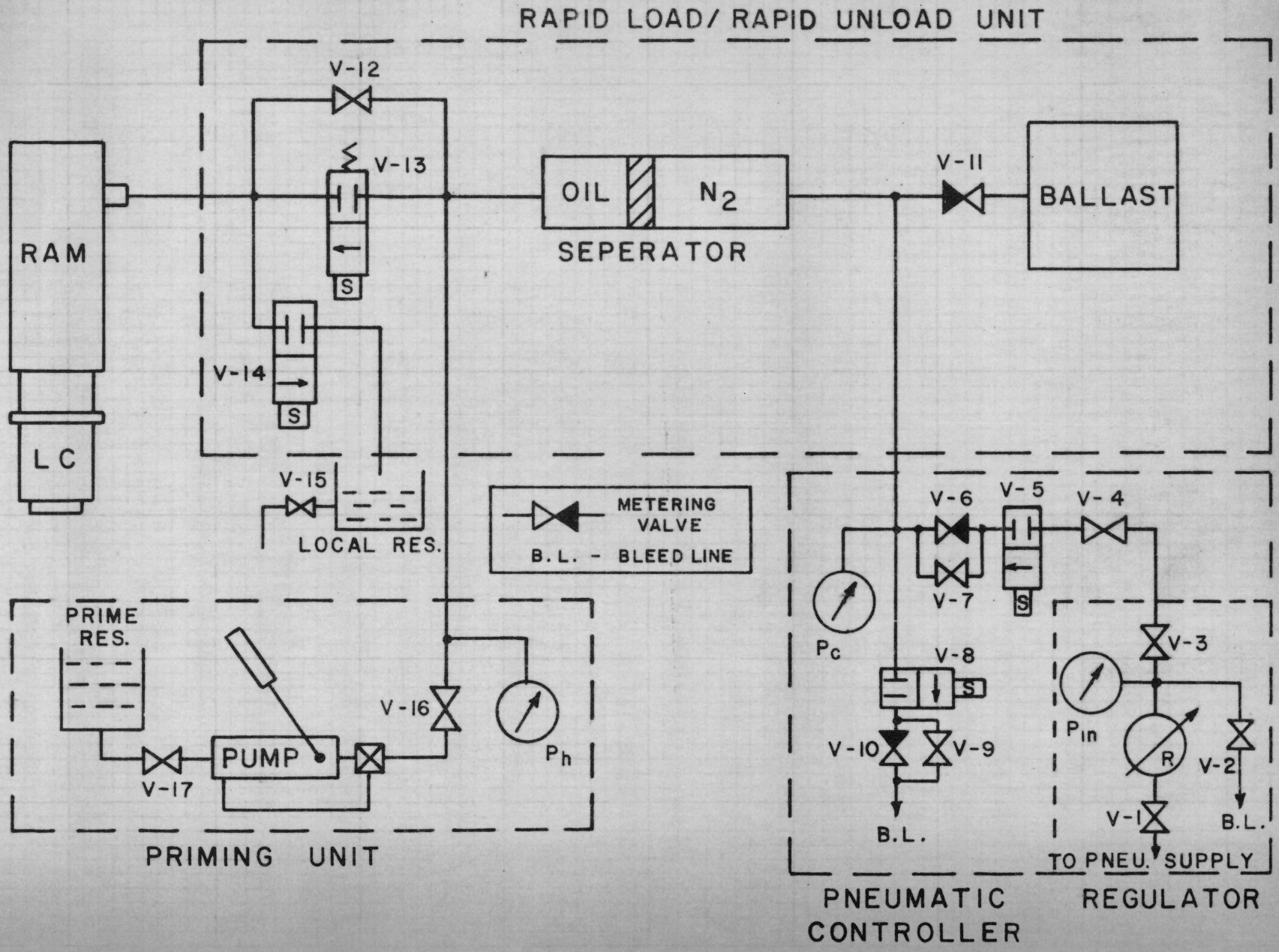


FIGURE 36 - Circuit of Pneumatic/Hydraulic Section of Control System.

(i) Pneumatic Controller

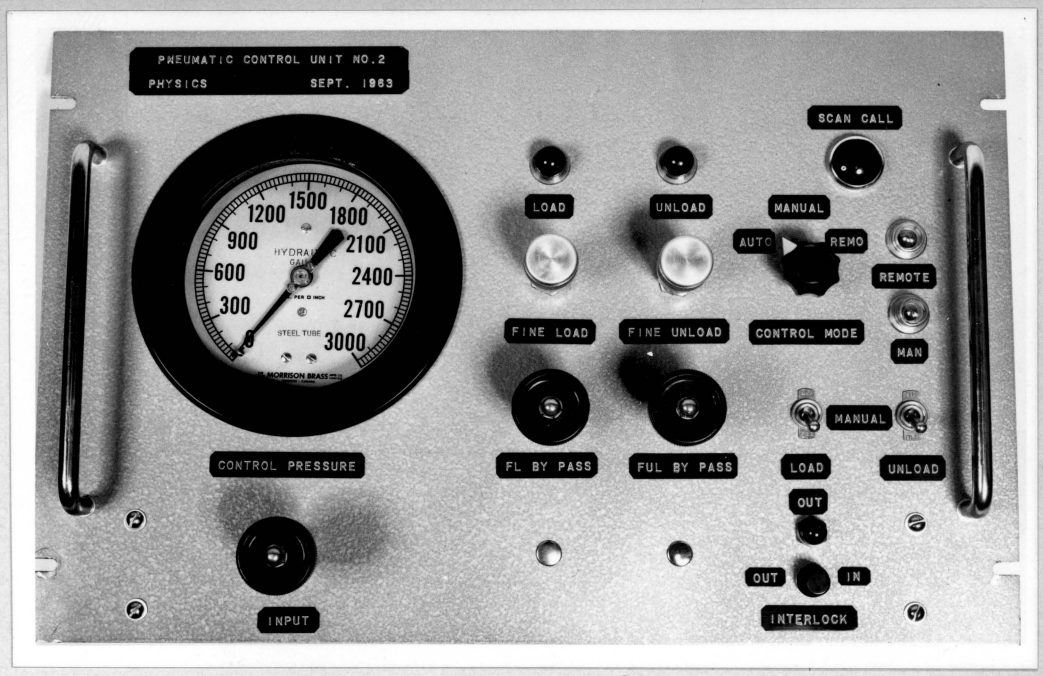
Figure 36 shows the pneumatic circuit of this unit. It contains two solenoid valves* the loading valve (V-5) and the unloading valve (V-8) which control the gas pressure on the primary side of the separator. These valves are activated by electrical signals from the electronic controller. Micrometer-type metering valves** (V-6 and V-10) in series with the solenoid valves allow the gas flow during loading and unloading to be finely adjusted to obtain optimum control. For some operations it is desirable to have full gas flow and for these cases by-pass valves (V-7 and V-9) are included. The pneumatic control pressure (P_c), which corresponds to the gas pressure on the primary side of the separator, is monitored by a large 0-3000 psi gauge included in the controller. Figure 37 shows two views of the completed controller.

The electrical wiring diagram of the controller is shown in Figure 38. The controller has a number of control modes as selected by switch SW-1, namely: auto, manual and remote. Normal operation is in the auto-mode in which case the loading and unloading

---

*ASCO, type 8262-99 solenoid valves, rated at 3000 psi, and fitted with 6V d-c solenoid coils.

**Hoke, type 2RB280 metering valves with attached vernier handwheels.



A. Front View of Pneumatic Controller Unit.



B. Rear View of Pneumatic Controller Unit.

FIGURE 37 - Two Views of Completed Pneumatic Controller Unit.

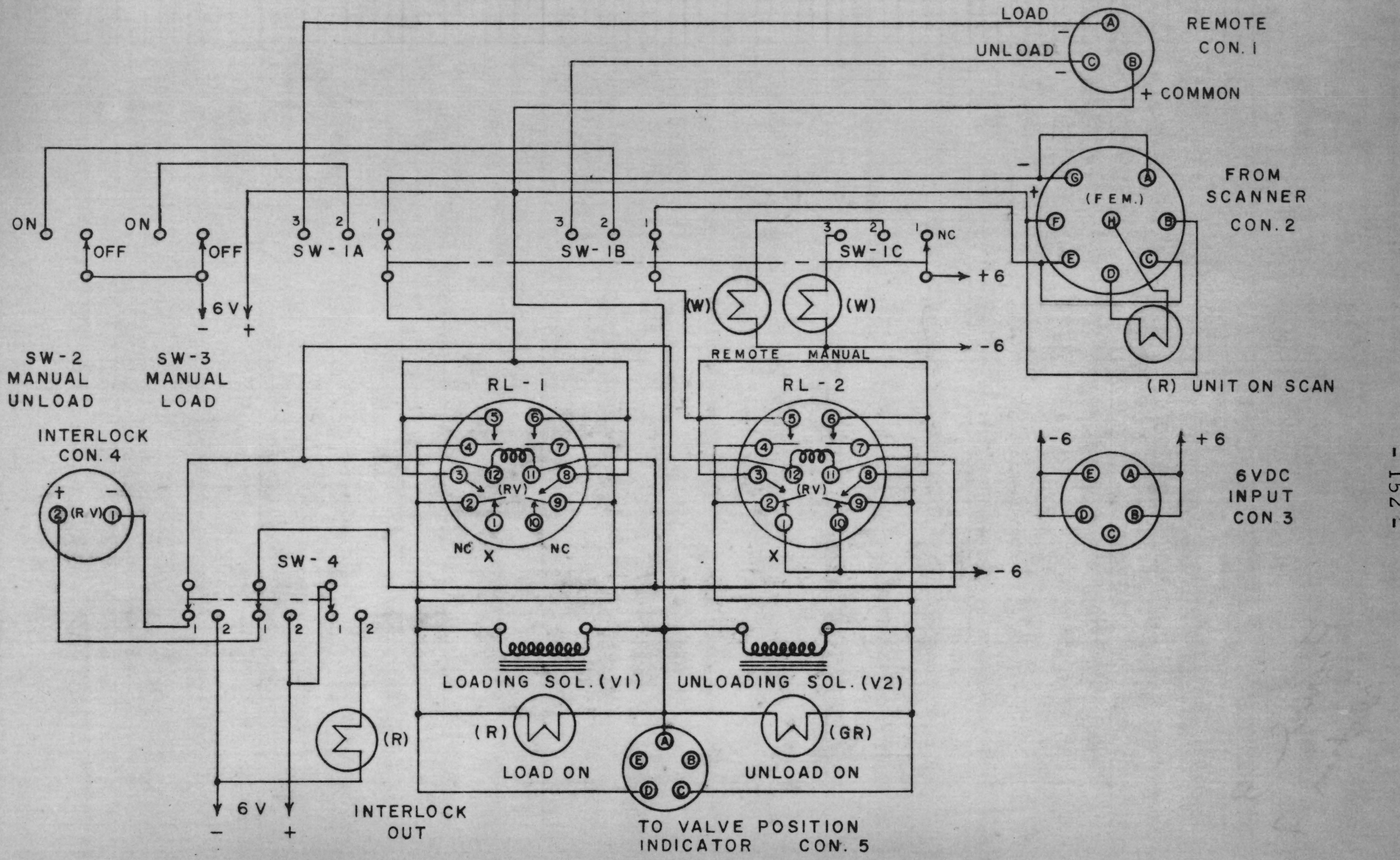


FIGURE 38 - Circuit Diagram for Pneumatic Control Unit.

solenoid valves are energized by the electronic controller via connector CON-2*. During certain experimental operations it is necessary to operate the load or the unload valves manually. This is accomplished by putting the controller in the manual-mode and activating the loading or unloading valves using switches SW-3 or SW-2 respectively. In this mode power to operate the solenoids is obtained from the external storage battery supply via connector CON-3.

The operation of the solenoid valves is interlocked with other parts of the control system so that in the advent of certain system failures the controller will "fail-safe". Relays RL-1 and RL-2 are connected in such a way that an interlock signal must be applied to connector CON-4 before they will operate normally. In the advent of certain system failures this interlock signal is lost and in this case the unload solenoid valve will automatically be energized and the loading solenoid valve will be prevented from operating. Switch SW-4 (pos 2) provides a temporary override of the interlock to allow various adjustments to be made to the system. Other parts of the circuit do not pertain to the present description and will not be discussed further here.

---

*Note that connector CON-2 is labeled "From Scanner". This refers to a special arrangement which is utilized when more than one loading frame is being operated from a single electronic controller. When only one loading frame is being used this connection would go directly to the output of the electronic controller.

Associated with the pneumatic controller is a regulator unit which is illustrated in Figure 36. It consists of a highly stable spring-type regulator+, a gauge to indicate outlet pressure and a number of valves. This regulator supplies nitrogen gas at a fixed pressure (P_{in}) to the input of the pneumatic controller. It serves two purposes; first, it provides a means for adjusting the differential pressure $\Delta P = (P_{in} - P_c)$ across valves V-5 and V-6 to a minimum, which is a requirement for optimum operation of the control system. Secondly, if due to some system malfunction the loading valve became jammed in the on-position the maximum ram pressure would be limited to the regulator setting (P_{in}).

(ii) Rapid Load/Rapid Unload Unit

The pneumatic circuit of this unit is presented in Figure 36. The unit was incorporated in the control system to serve three purposes. First to provide a separation between the hydraulic fluid in the ram and the nitrogen control gas, secondly to facilitate slow, positive motion of the ram during alignment and preloading of the test specimen, and thirdly to provide an arrangement whereby rapid loading and unloading of the test specimen could be carried out. The unit consists of a separator*, a ballast tank, two solenoid

+ Grove, small volume, high pressure, combination reducing and relief regulator, model 15LH.

* Sprague, model 60010 accumulator with a volume of approximately 25 cu in. and rated at 4000 psi.

valves* (one for rapid loading (V-13) and one for rapid unloading (V-14)), a by-pass valve (V-12) and a metering valve (V-11). Figure 39 shows a photograph of the RL/RUL unit in position above the loading frame in the inner room.

The hydraulic circuit of the priming unit, which is associated with the RL/RUL unit, is also shown in Figure 36. It consists of a small hydraulic hand pump+, a reservoir for hydraulic fluid++, a series of valves, and a pressure gauge (P_h) which indicates the pressure of the hydraulic oil on the secondary side of the separator. The priming unit is located on one of the racks in the outer room.

For normal operation the solenoid valves remain in the normally closed state and the by-pass valve (V-12) is opened. Any increase in gas pressure on the primary side of the separator results in an increase in the oil pressure on the secondary side and a resulting increase in ram thrust. During the initial stages of a typical deformation experiment the gas pressure in the separator is set to some low value (approximately 50 psi) and the ram piston slowly lowered into contact with the specimen loading jig using the hand pump in the priming unit. Once in position, valve V-16 is closed isolating the RL/RUL

---

*Hoke solenoid valves, type - B90D-120C rated at 2000 psi and fitted with 6V d-c solenoid coils.

+Blackhawk hand pump, model P-39.

++Blackhawk hand pump oil, type HF-47.



FIGURE 39 - Photograph of Rapid Load/Rapid Unload Unit in Position above Loading Frame.

unit from the priming unit. A ballast cylinder, having an internal volume of approximately 35 cu in. is included in the circuit to improve the load stability of the system when it is operating in the constant stress or constant strain mode. Its effect on the system may be increased or decreased by adjustment of the metering valve (V-11).

When rapid loading experiments[x] are to be carried out valve V-12 is shut off. Valve V-13 is remotely opened and the system preloaded as just described for normal operation. Once the specimen has been preloaded V-13 is shut-off. The gas pressure on the primary side of the separator is increased to a specific level after which V-5 in the pneumatic controller is shut-off and the control system clamped in an inactive mode. To initiate rapid loading V-13 is remotely opened causing the ram pressure to suddenly rise and come to equilibrium with the pressure on the secondary of the separator. When the specimen stress just reaches the control point the control system is unclamped and normal operation of the system is reestablished.

1.3.5 Electronic Section

(i) Electronic Controller

The electronic controller performs a number of important functions. First it accepts the low level, unbalance signals (ΔV) from the control bridge and converts these to high level signals

---

x A number of additional electronic units are involved in the operation of the rapid loading system. Since this system has not yet been employed in actual deformation experiments further details of these electronic units will not be presented here.

for operation of the loading and unloading solenoids in the pneumatic controller. In this respect it performs the function of an amplifier. Secondly it contains a number of logic circuits which insure that correct sequencing of the loading and unloading valves is maintained (e.g. the loading valve must be closed before the unloading valve can be opened). Thirdly, additional logic circuits are included so that the controller will "fail-safe" (e.g. failure of a critical section of the controller will automatically put the controller into the neutral position, where both loading and unloading valves will be closed).

Figure 40 shows a block diagram of the controller. The low level output signal from the control bridge enters the controller via the galvanometer signal conditioning circuit (GSC), shown in Figure 41. The output of this circuit is connected to the coil of a light-spot-type galvanometer in the galvanometer-photocell unit (GPU). This circuit allows the polarity of the galvanometer input signal to be selected (SW-4), provides a manual galvanometer sensitivity control (SW-1) and includes circuitry for manually or automatically shunting the galvanometer system. Switch SW-3 selects the various shunting (or damping) modes. In position-1 the galvanometer is connected directly to the output of the control bridge via connector CON-1. In position-2 relay RL-1 is activated, this removes the input signal, and shunts the galvanometer with R_s. The other

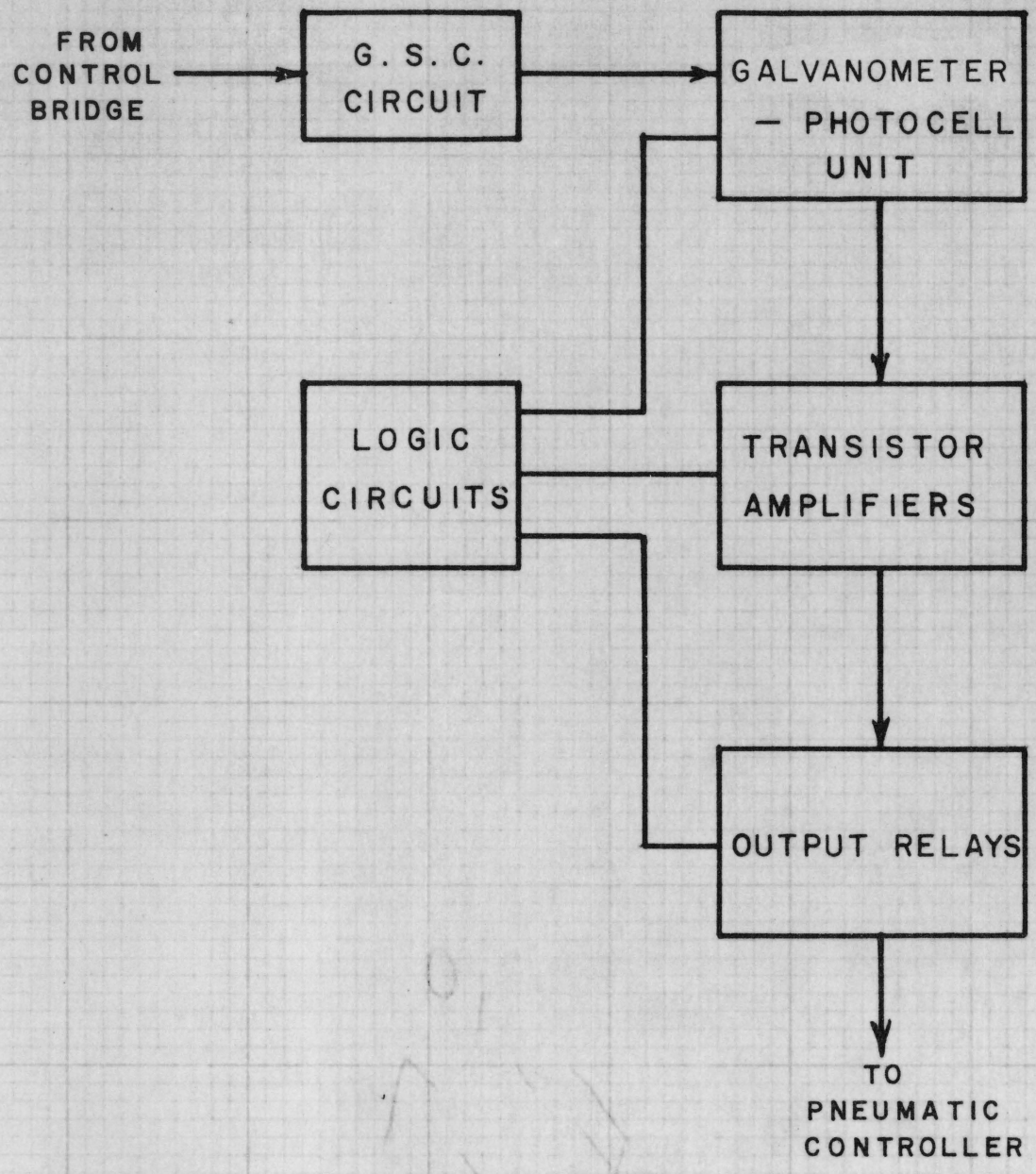


FIGURE 40 - Block Diagram of Electronic Control Unit.

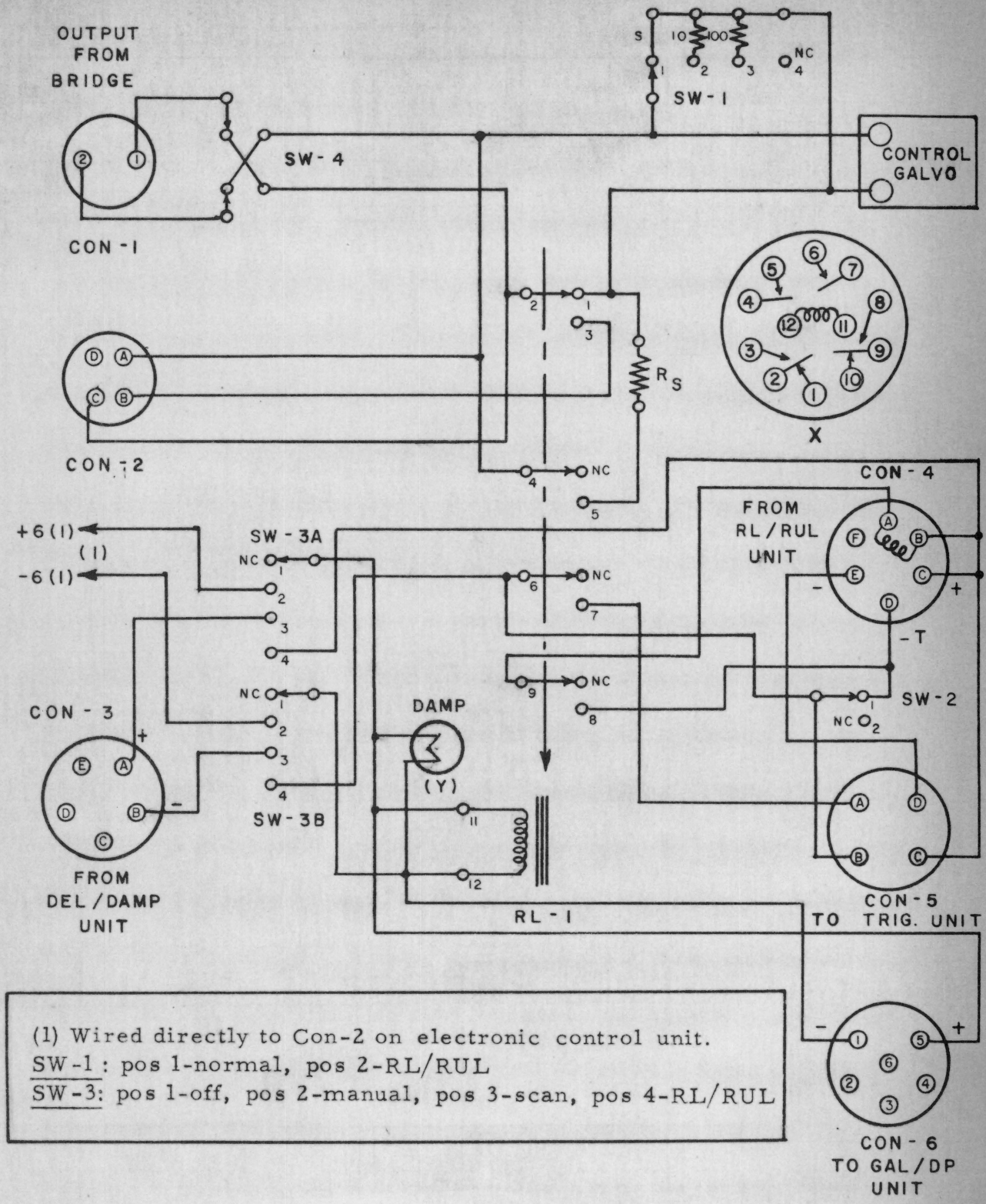


FIGURE 41 - Circuit Diagram for Galvanometer Signal Conditioning Circuit.

shunting modes are activated by signals from various external systems such as the RL/RUL system. These are connected to the GSC circuit via connectors CON-3, -4, -5 and -6.

A circuit diagram of the main section of the controller is given in Figure 42. Details of this section are discussed by Hardy and Larocque (1965) in a recent paper, hence its operation will be outlined only briefly here. The bridge unbalance signal (ΔV) causes the light spot galvanometer in the GPU to deflect an angle α which is proportional to the magnitude and the sign of the unbalance. For example if the load were above the control point, the unbalance signal would be positive in sign and the galvanometer would deflect in a counter clockwise direction. A series of three photocells are located as shown in Figure 42. If the control bridge unbalance continues to increase to $+ \Delta V_{\beta}$, where the angle of deflection becomes $\alpha = +\beta$, then photocell C-1 will be illuminated generating an output signal (E_1). This signal is amplified and in turn closes relay R-1 which energizes the unloading solenoid valve in the pneumatic controller. As the load begins to decrease ΔV decreases and when $\alpha < \beta$ the loading valve is turned off. If, however, the load increases too rapidly it may overshoot the control point, ΔV will become negative in sign, and the galvanometer will deflect clockwise. If it reaches a level of $-V_{\beta}$, where $\alpha = -\beta$, photocell C-3 will be illuminated, which will result in

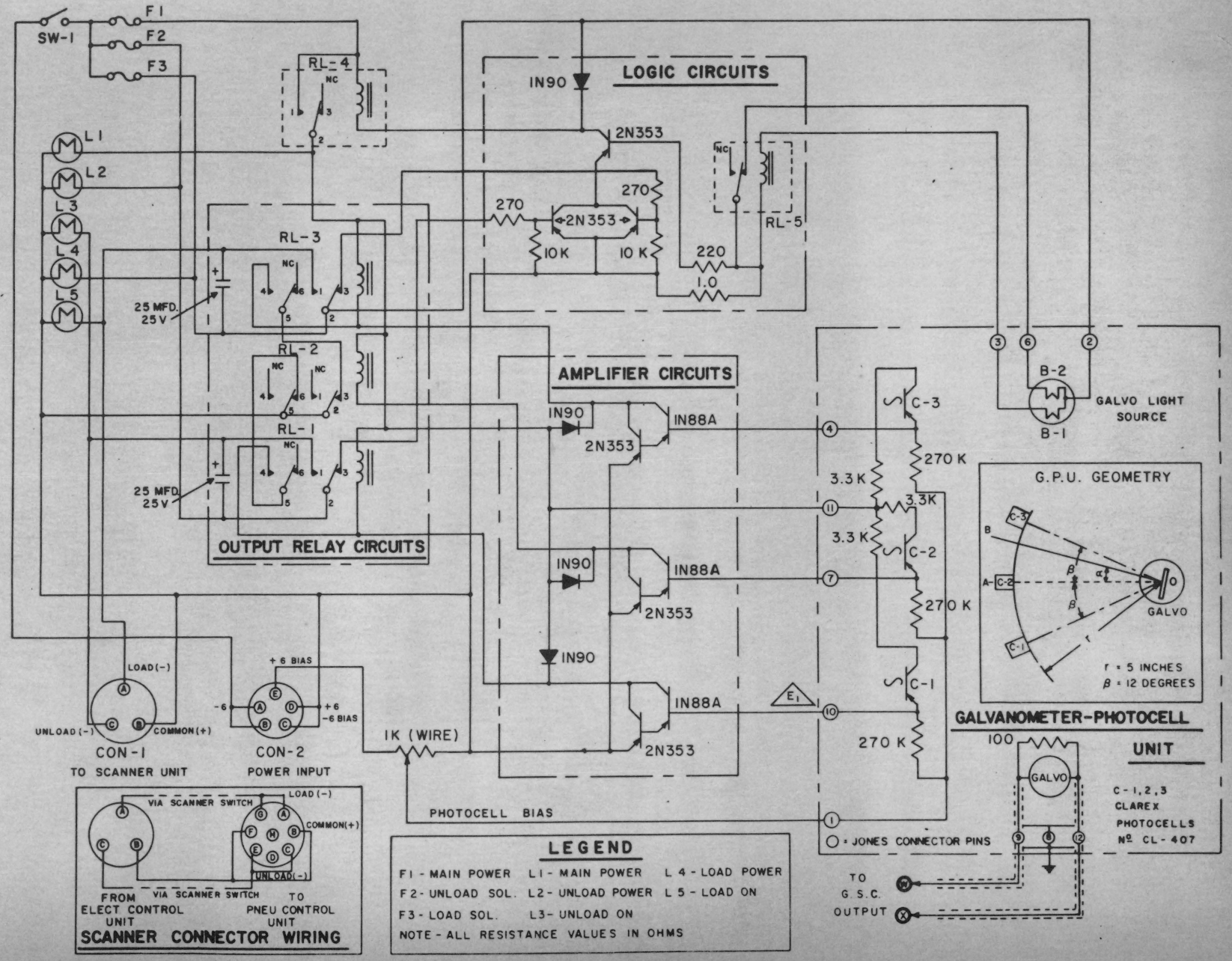


FIGURE 42 - Circuit Diagram for Main Section of Electronic Controller.

relay R-3 closing and the loading solenoid valve in the pneumatic controller being opened. In effect the electronic controller is a highly sensitive relay circuit. For $\Delta V \geq |V_\beta|$ either the loading or unloading solenoid valve will be open depending on the sign of ΔV. For $\Delta V < |V_\beta|$ both valves will be closed. The controller therefore has a dead-band of $2\Delta V_\beta$, which places a limit on the control precision of the overall system. The relative importance of the magnitude of the dead-band depends on the gain in the feedback loop and the control bridge. For example consider that the system is operating in the constant stress (CS) mode, and that a change in specimen stress $\Delta\sigma_A$ results in an unbalance signal ΔV_A at the input of the electronic controller. If it is desired to control the stress to within a value $\Delta\sigma_A$ then it is necessary that $\Delta V_A \geq \Delta V_\beta$. Since $\Delta V_A = GK\Delta\sigma$, where G is the gain of the control bridge, and K is the sensitivity of the feedback transducer in volts/psi stress, the importance of the dead-band may be reduced by having large values of G and K.

The central photocell in the GPU is associated with one of the logic circuits. This circuit prevents either solenoid valves being energized until the other is de-energized. The light spot galvanometer is illuminated by a bulb (B-1), containing two separate

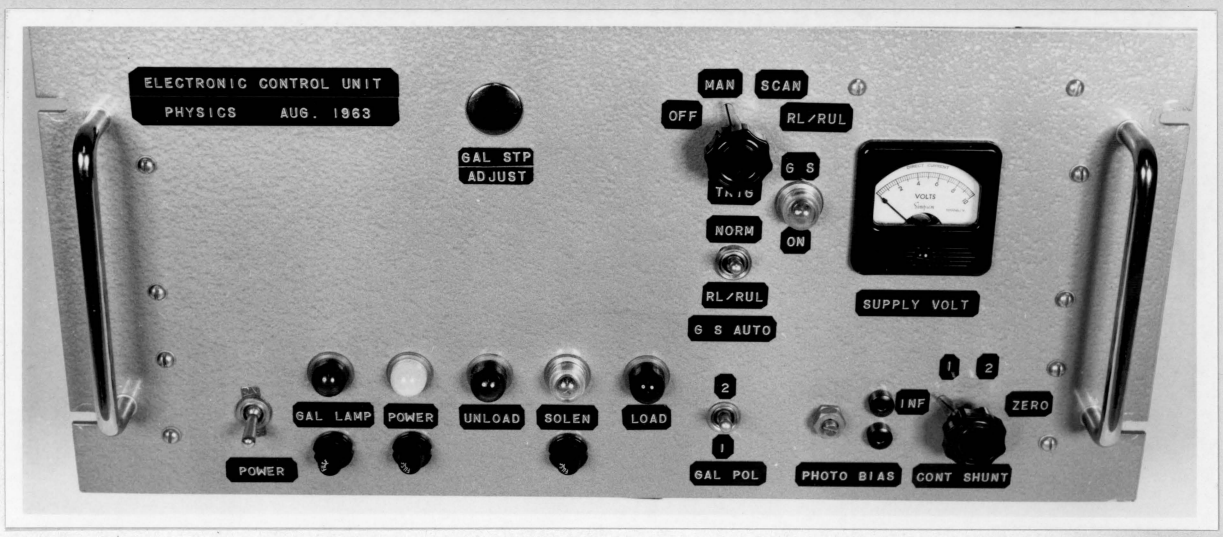
filaments. In the advent of a failure of the active filament an associated logic circuit switches the second filament into operation.

A series of tests were conducted to check on the sensitivity of the electronic controller. In particular the critical input current (I_c) which would just deflect the galvanometer through the angle $\pm \beta$ (and hence trigger the solenoid valves) was measured for different settings of the galvanometer sensitivity control (SW-1, see Figure 41). The results are shown in Table 7. Figure 43 shows a number of views of the completed controller. Figure 43 B shows a top view of the unit including the inside of the galvanometer-photocell unit.

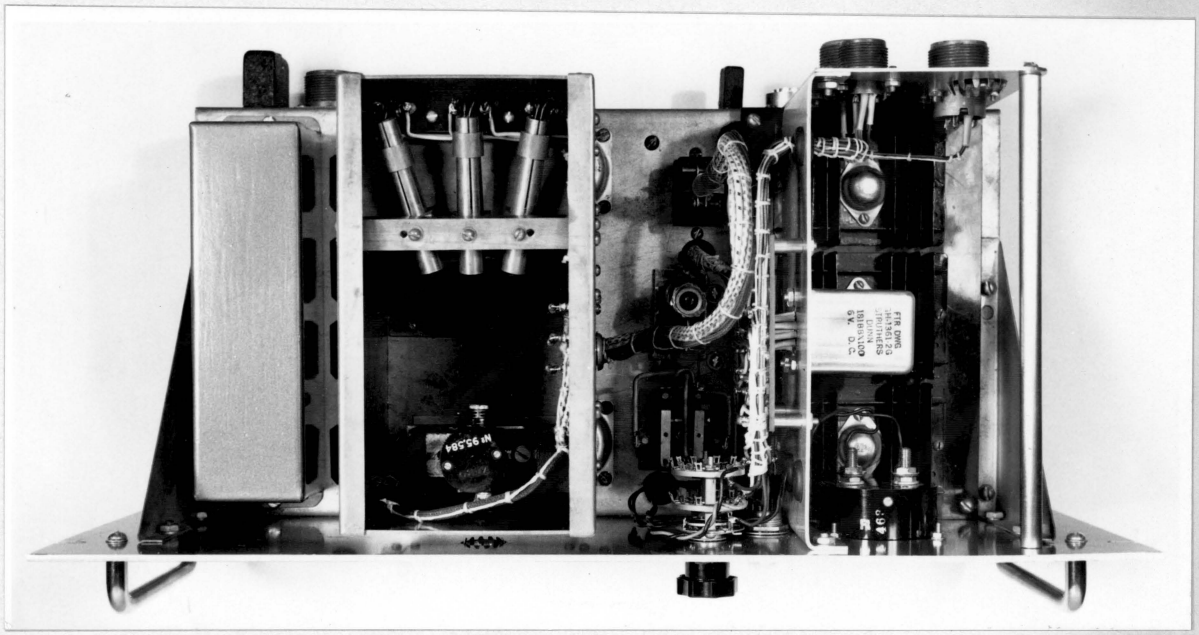
TABLE 7

Controller Sensitivity

Switch Position	Shunt Resistance	I_c
	Ohms	μ amps
1	≈ 0	28,000
2	10	27
3	100	5
4	infinity	2.4



A. Front View of Electronic Controller.



B. Top View of Electronic Controller(section at left contains the galvanometer-photocell unit)

FIGURE 43 - Photographs Showing a Number of Views of Completed Electronic Controller Unit.

(ii) Control Bridge

The control bridge serves two purposes, first it supplies an excitation voltage to the bridge circuits in the feedback transducers, and second it amplifies the low level unbalance signals from these transducers to a higher level for activation of the electronic controller. The design and merits of various types of control bridges are described in detail by Hetenyi (1957). The control bridge used was a Baldwin type-K strain indicator modified for use with external four-arm bridge transducers. This was mounted in a standard relay rack panel. The rear of the unit was enclosed in a thick walled (1/4 in.) aluminum box which was insulated by a one inch layer of glass wool, and enclosed by an outer steel case attached to the rack panel. This arrangement was utilized in an attempt to stablize the system from short term temperature variations. Some sections of the indicator were rewired to enable all electrical connections to be made at the rear of the unit. A signal (ΔV) denoted as the control bridge unbalance, was obtained by a parallel connection across the existing panel galvanometer in the indicator. This was brought by shielded cable to a connector at the rear of the unit.

In its original form the type-K indicator operated from a set of self contained A and B batteries. Since it was necessary that the bridge operate continuously for long periods of time these batteries

were replaced by a regulated A and B power supply operated from the 110 VAC lines. Figure 44 shows the circuit of this supply.

(iii) Programmer and Feedback Section

The relationship between the controller, programmer and feedback sections is somewhat unconventional in this system. Rather than summing a feedback voltage with a program voltage to give an error signal, the programmer, which is basically a variable resistance, is connected directly to the feedback transducer bridge as illustrated in Figure 45A. The program resistance R_v is connected across one of the arms of the transducer bridge and hence variations in R_v will cause the balance condition of the bridge to shift. The error signal (Δe) will thus be proportional to the difference in the effect on the transducer bridge due to measured variable, and the unbalancing effect due to the programming resistor. This type of system is simple and relatively convenient for some type of programming (e.g. constant stress, constant strain etc. where R_v will be either constant or will vary in definite increments). Since, however Δe will be a nonlinear function of R_v* programming of continuous variations in the controlled variable (e.g. constant rate of stressing) requires the use of special non-linear potentiometers.

---

* See standard equations for balance conditions in a four-arm Wheatstone bridge, e.g. Hetenyi (1957).

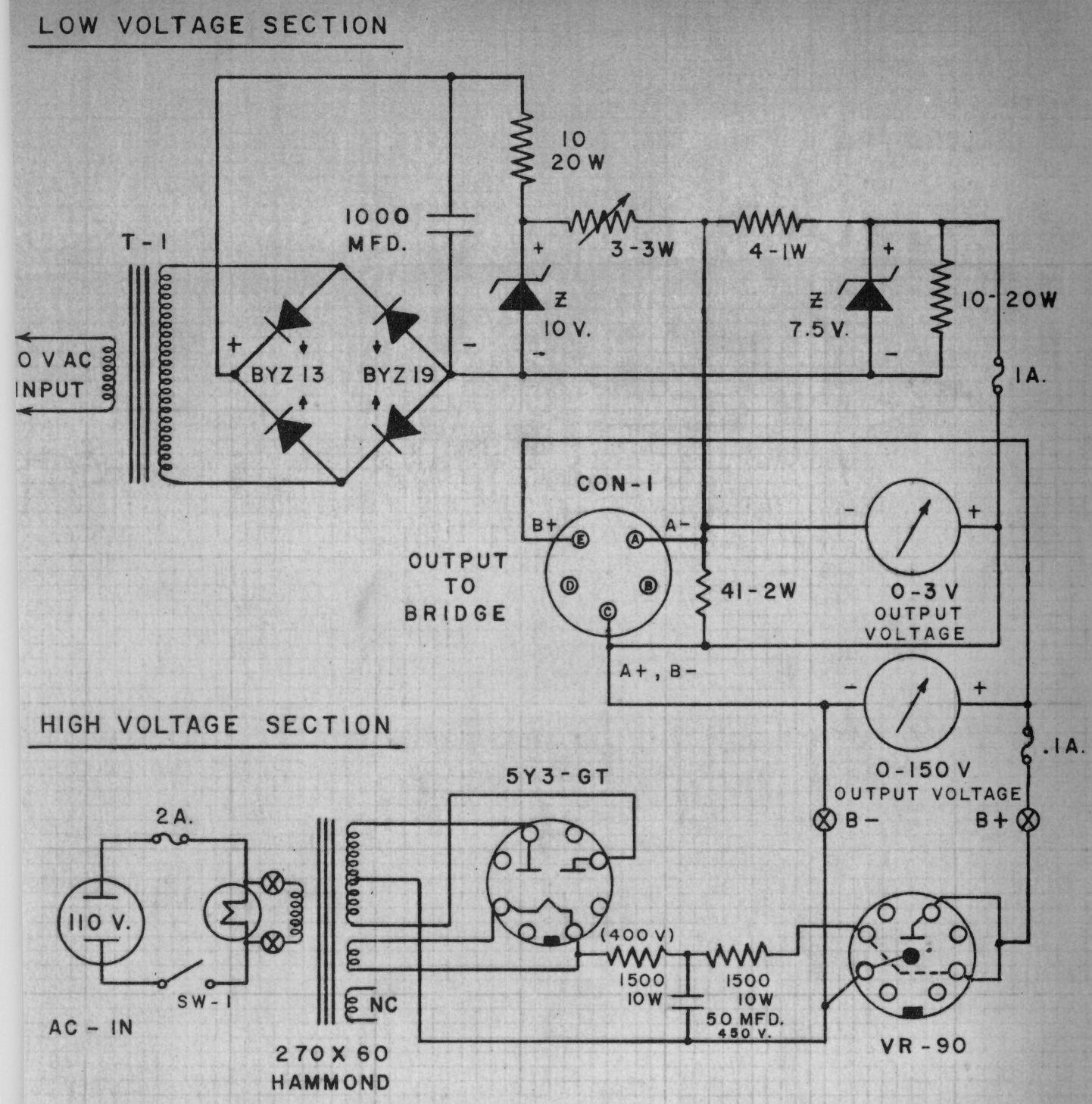
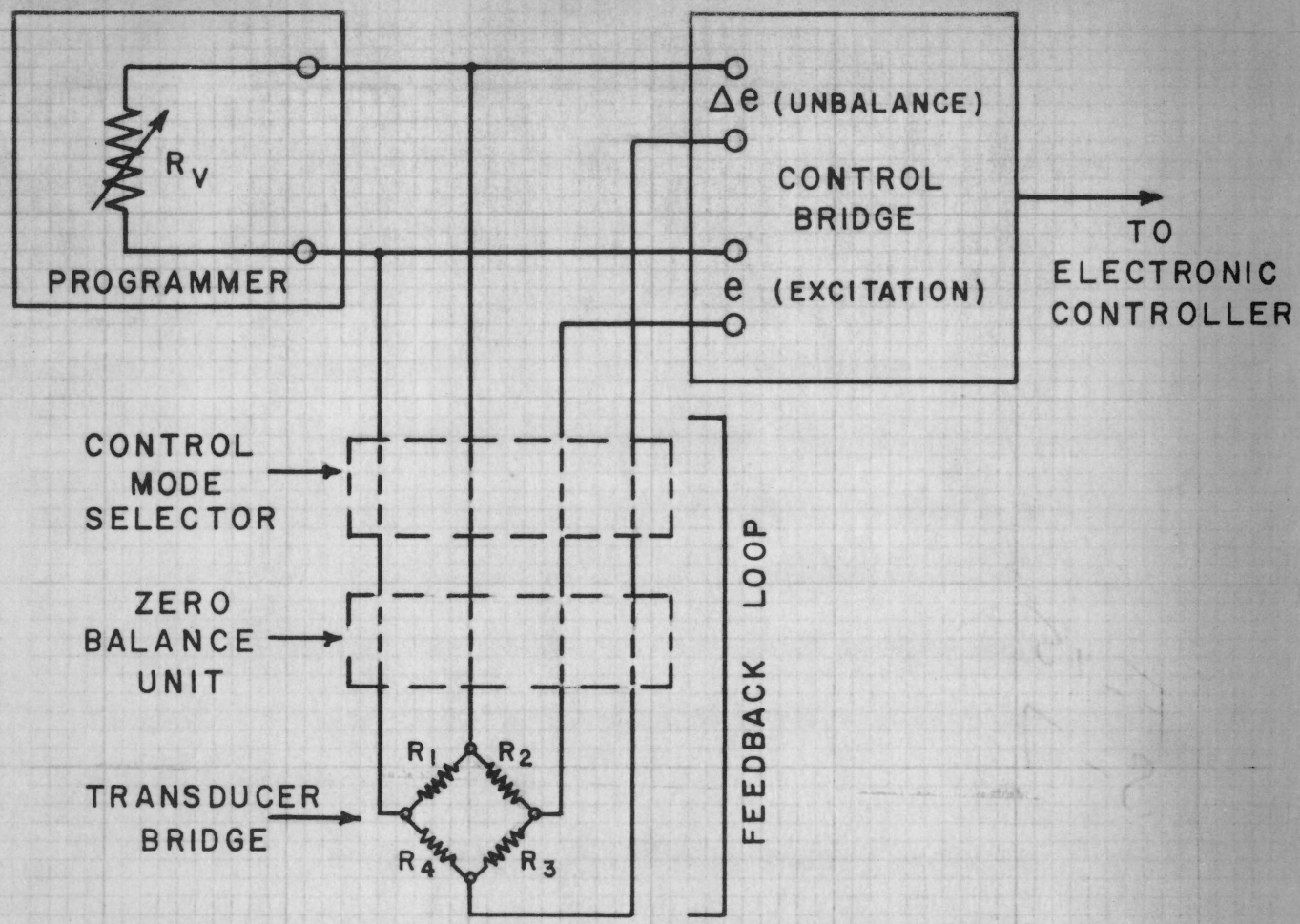
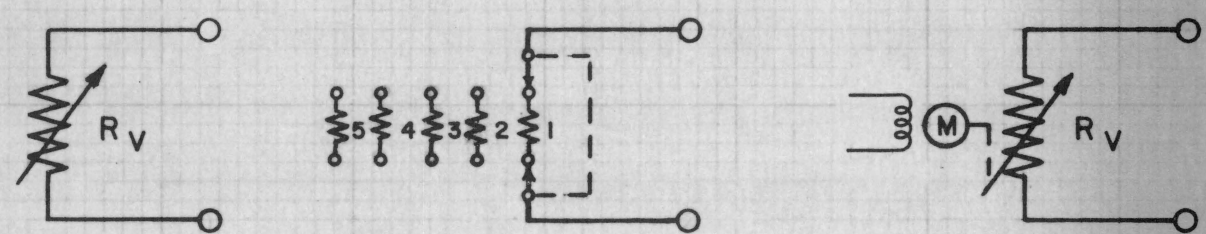


FIGURE 44 - Circuit Diagram for Regulated Bridge Power Supply.



A. RELATIONSHIP OF PROGRAMMER TO FEEDBACK LOOP



a) CS/CE b) I c) CSR/CER/CY

B. TYPES OF PROGRAMMING MODES

FIGURE 45 - Diagram Illustrating Details of Programming Arrangement.

(iv) Programmer

Figure 45B shows some of the programming arrangements that have been investigated. In the constant stress (CS) or constant strain (CE) mode the stress or strain level may be set manually using a ten-turn potentiometer for R_V. If it is desired to operate in the incremental (I) mode, (i.e. to vary the stress or strain over a set of fixed levels) the simple switching circuit shown may be used. The values of the resistors being selected to give the desired levels. Finally operation in the controlled stress rate (CSR), the controlled strain rate (CER) or the cyclic (CY) mode may be accomplished by using a suitable non-linear potentiometer driven by a small constant speed motor.

Since the majority of experiments carried out to date have used incremental loading, the programmer developed for IS-mode programming will be briefly described. Figure 46 shows the circuit of the IS-mode programmer. It consists of the galvo damping circuit, the valve control circuit and the program circuit. A function switch (SW-1) co-ordinates the operation of the unit. In position-1 the system is inactive; in position-2 the system is active (or set) with one of the programming resistors connected across one of the arms of the feedback transducer bridge. Under these conditions the control system will maintain the stress constant at a value determined by the

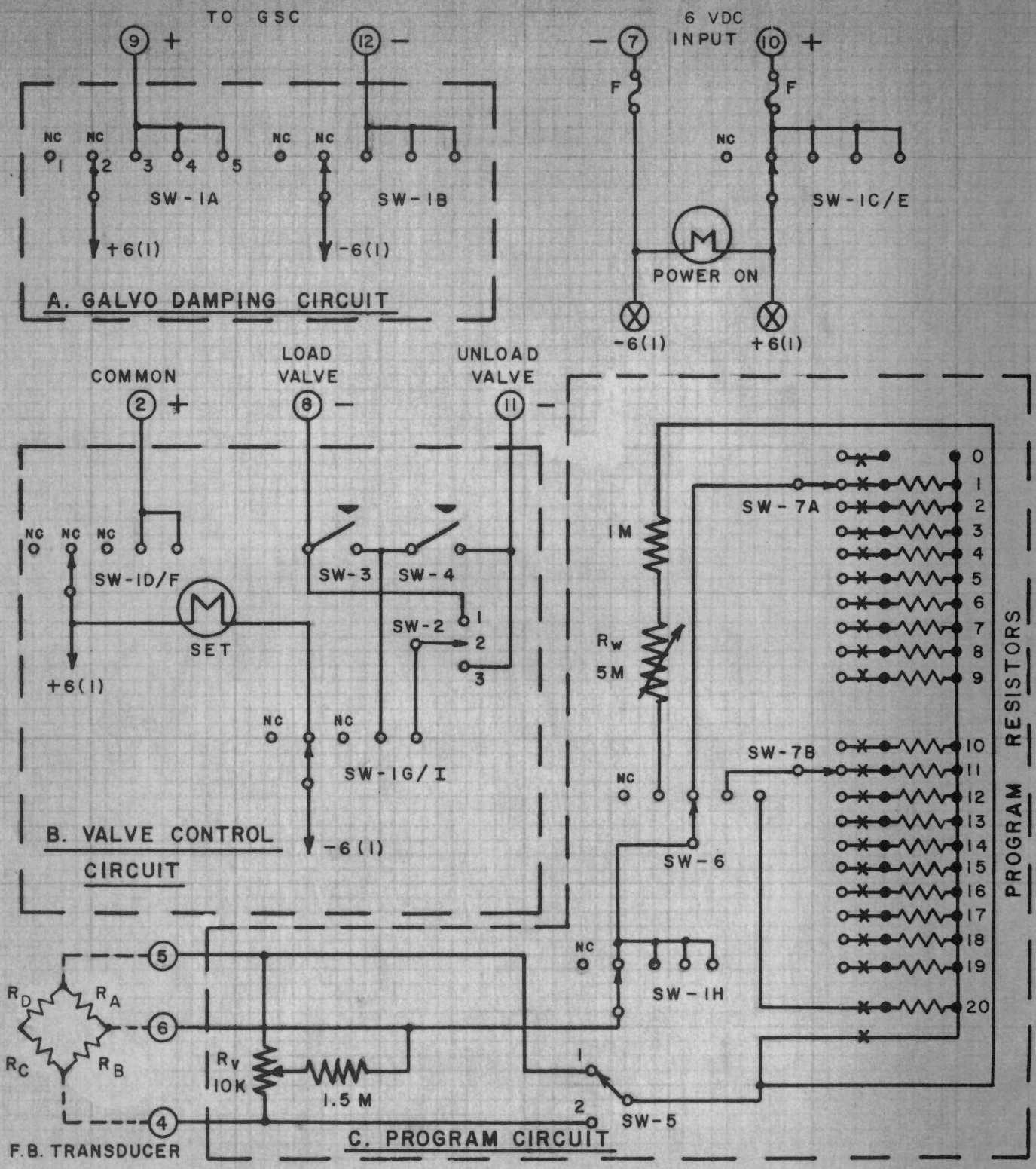
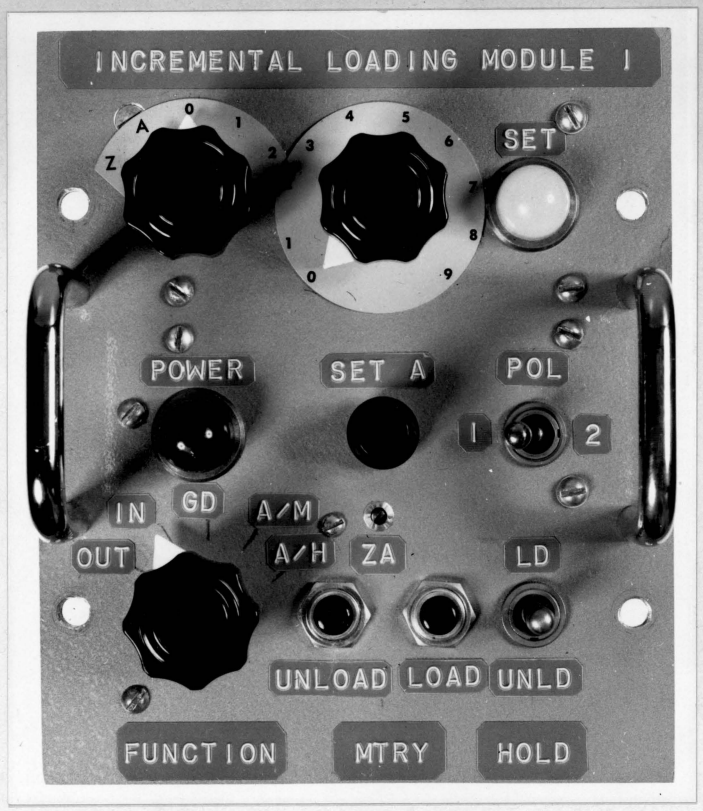


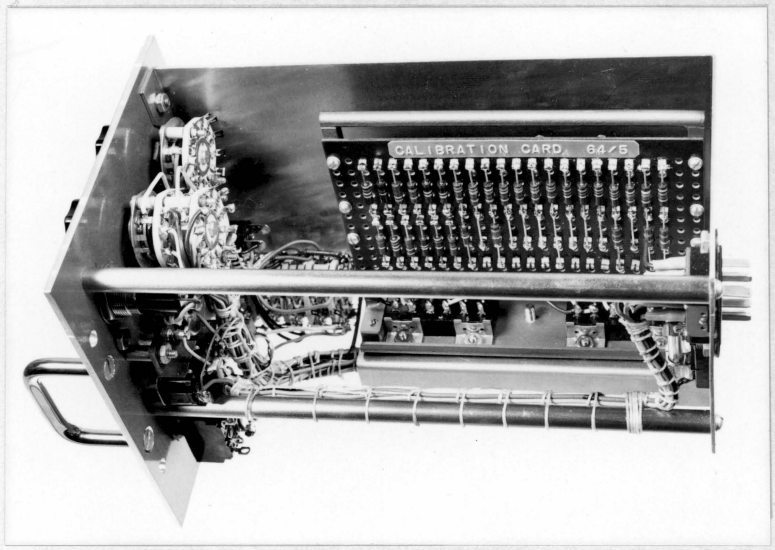
FIGURE 46 - Circuit Diagram of IS-Mode Programming Module.

particular programming resistor (selected by SW-5, SW-6 and SW-7). For example the circuit diagram shows the programming resistor R_1 shunted across the arm R_A of the feedback transducer bridge. To increase the control stress to the next higher level switch SW-1 is first placed in position-3, which damps the control galvanometer, SW-7 is shifted to position-2, SW-1 is then placed in position-4, and switch SW-4 may now be used to open the loading solenoid valve in the pneumatic controller and allow the stress to rise. Observation of the panel galvanometer on the control bridge indicates when the system is approaching balance at the new level and at that time switch SW-1 is placed back in position-2. The unloading sequence follows the same order. Figure 47 shows two views of the completed IS-mode programmer module.

The program (or calibration) resistors each consist of an approximate resistance in series with a trimming potentiometer. Final adjustment of the particular values are made using a calibration chart with the controller connected into the actual control system. For convenience each set of resistors and their associated trimming potentiometers are mounted on a plug-in card, as shown in Figure 48. Various loading programs, covering different ranges and with different increments, may be designed, each being constructed on its own plug-in card. Table 8 gives the calculated values of the program (calibration)

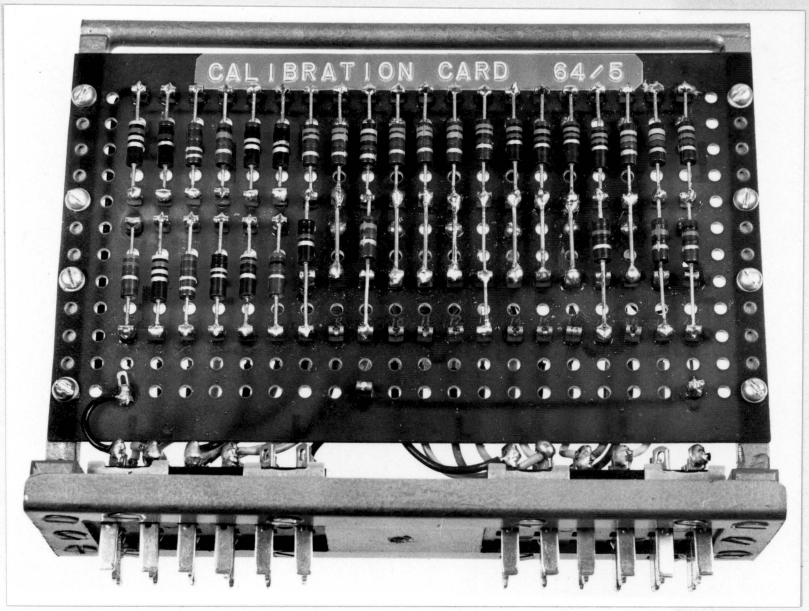


A. Front View of Program Module.

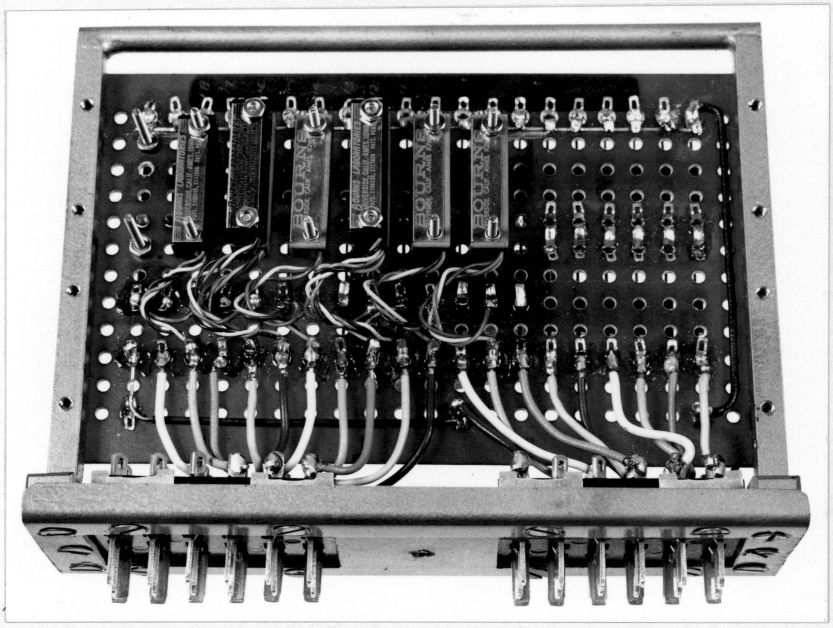


B. Side View of Program Module.

FIGURE 47 - Photographs Showing a Number of Views of Incremental Mode Programmer.



A. View of Plug-In Card Showing Fixed Resistors.



B. View of Plug-In Card Showing Trimming Potentiometers.

FIGURE 48 - Photographs of Load Program Plug-In Cards.

resistors in program 64/4 which was utilized for initial incremental studies on Wombeyan marble. It should be noted that since this material does not show appreciable inelastic behavior until a stress level of approximately 6500 psi the initial stress increments in the program are large up to this level.

TABLE 8

Details of Program (Calibration) card 64/4 used for Initial Incremental Loading Studies on Wombeyan Marble

Switch Pos (1)	Load lbs	Specimen Stress (2) psi	Program Resistor Ohms	Switch Pos (1)	Load lbs	Specimen Stress (2) psi	Program Resistor Ohms
0	0	0	-	11	4400	9,944	71.8K
1	500	1130	625K	12	4600	10,396	68.7K
2	1000	2260	320K	13	4800	10,848	65.8K
3	2000	4520	158.8K	14	5000	11,300	63.3K
4	3000	6780	106.9K	15	5200	11,752	60.8K
5	3200	7232	98.6K	16	5400	12,204	58.1K
6	3400	7684	92.8K	17	5600	12,656	55.9K
7	3600	8136	87.8K	18	5800	13,108	54.1K
8	3800	8588	83.0K	19	6000	13,560	52.2K
9	4000	9040	79.1K	20	6200	14,012	50.6K
10	4200	9492	75.1K	--	--	--	--

(1) Refers to setting of switches SW-6 and SW-7.

(2) Based on test specimen with a diameter of 0.750 in.

(v) Feedback Section

The feedback section consists of a stress (load) transducer, a strain transducer, two zero balance units to allow adjustment of the two transducers, and a control mode selector which allows either stress or strain feedback to be selected.

Stress feedback is obtained by a Baldwin type-C strain gage type load cell with a capacity of 20,000 lbs, attached to the piston of the hydraulic ram. The load cell employed is a double bridge type which provides two separate outputs. One is used to provide the feedback signal in the control system, the other is fed to the measurement system to enable the specimen stress to be accurately monitored. These cells are calibrated to give an output of 2 MV per volt excitation at an applied load equivalent to their capacity. The 20,000 lb cell employed has a sensitivity (K) of 0.6 μV/lb (or 1.36 μV/psi on a specimen with a diameter of 0.750 in.) with an excitation voltage of 6 volts.

Strain feedback is obtained from a single resistance type strain gage attached to the test specimen. This gage and a similar dummy gage form two arms of a four-arm bridge arrangement, the output of which provides the strain feedback signal. It is planned to modify this bridge arrangement so that two arms of the bridge are strain sensitive. In this configuration the strain sensitivity of the transducer will be increased by a factor of approximately two.

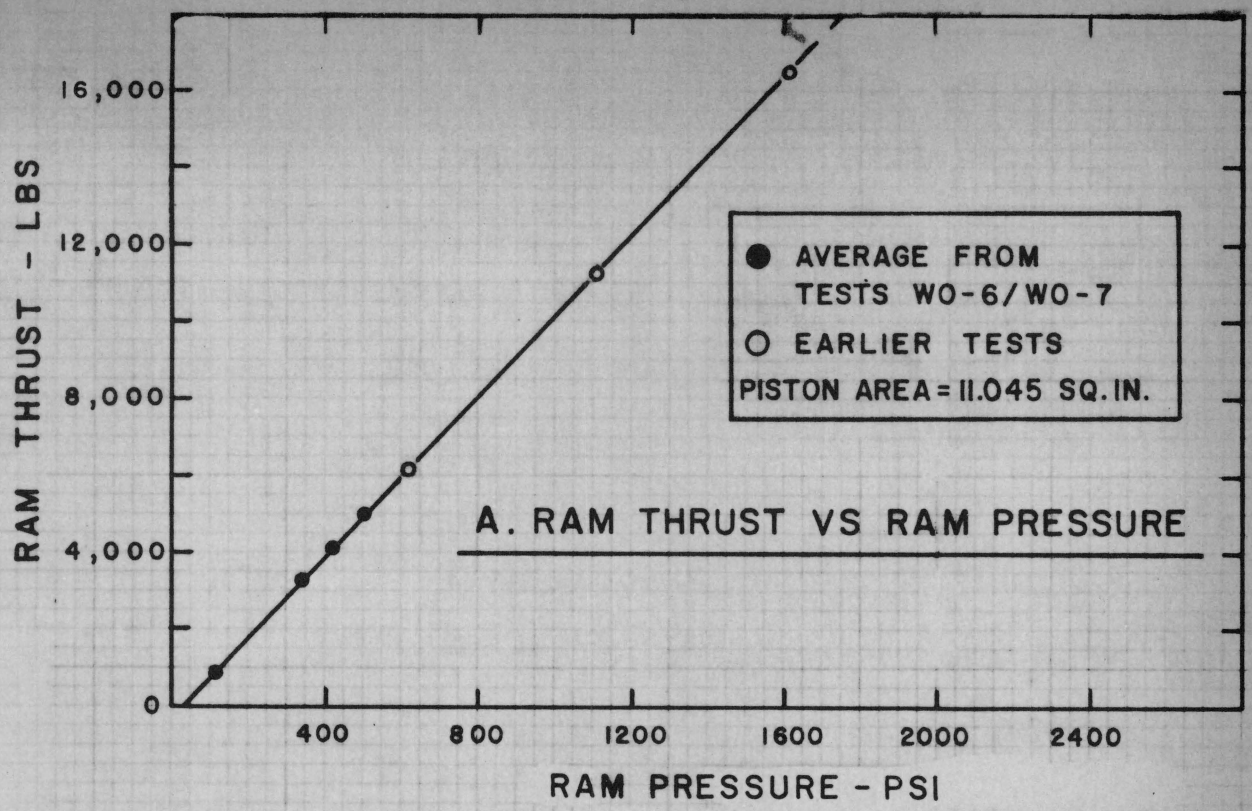
1.4 Investigation of the Completed Axial Loading System in Various Operating Modes

During the development of the system and after its completion a series of studies were made on its operation. These included an investigation of the behavior of the hydraulic ram,

investigation of zero drift effects in the load feedback transducer (load cell), investigation of the effect of various parameters in the pneumatic control unit (in order to obtain optimum stability in the constant stress (CS) mode), studies of stability in the CS-mode, investigation of the behavior of the system in the incremental stress (IS) mode, and finally the investigation of a simple method of loading at a constant rate of stress.

1.4.1 Behavior of the Hydraulic Ram

The hydraulic ram used in the axial loading system had an effective piston area of 11.045 sq. in. Thus a ram pressure of 1000 psi would be expected to produce a ram thrust of 11,045 lbs if the ram piston was friction-free. Since however, some friction must necessarily be present as a result of the piston packing, a series of experiments were carried out to study the relationship of ram thrust to ram pressure. In these experiments the ram thrust was measured by a 20,000 lb load cell and ram pressure by a 0-3000 psi pressure gauge which could be read to $\pm$ 7 lbs. Figure 49A shows graphically the results of a number of experiments. The relationship appears to be linear for ram pressures greater than 100 psi. However, the curve does not appear to pass through zero, indicating the presence initially of an internal restoring force of approximately 600 lbs. The slope of the curve, which should be equal to the area of the ram piston,



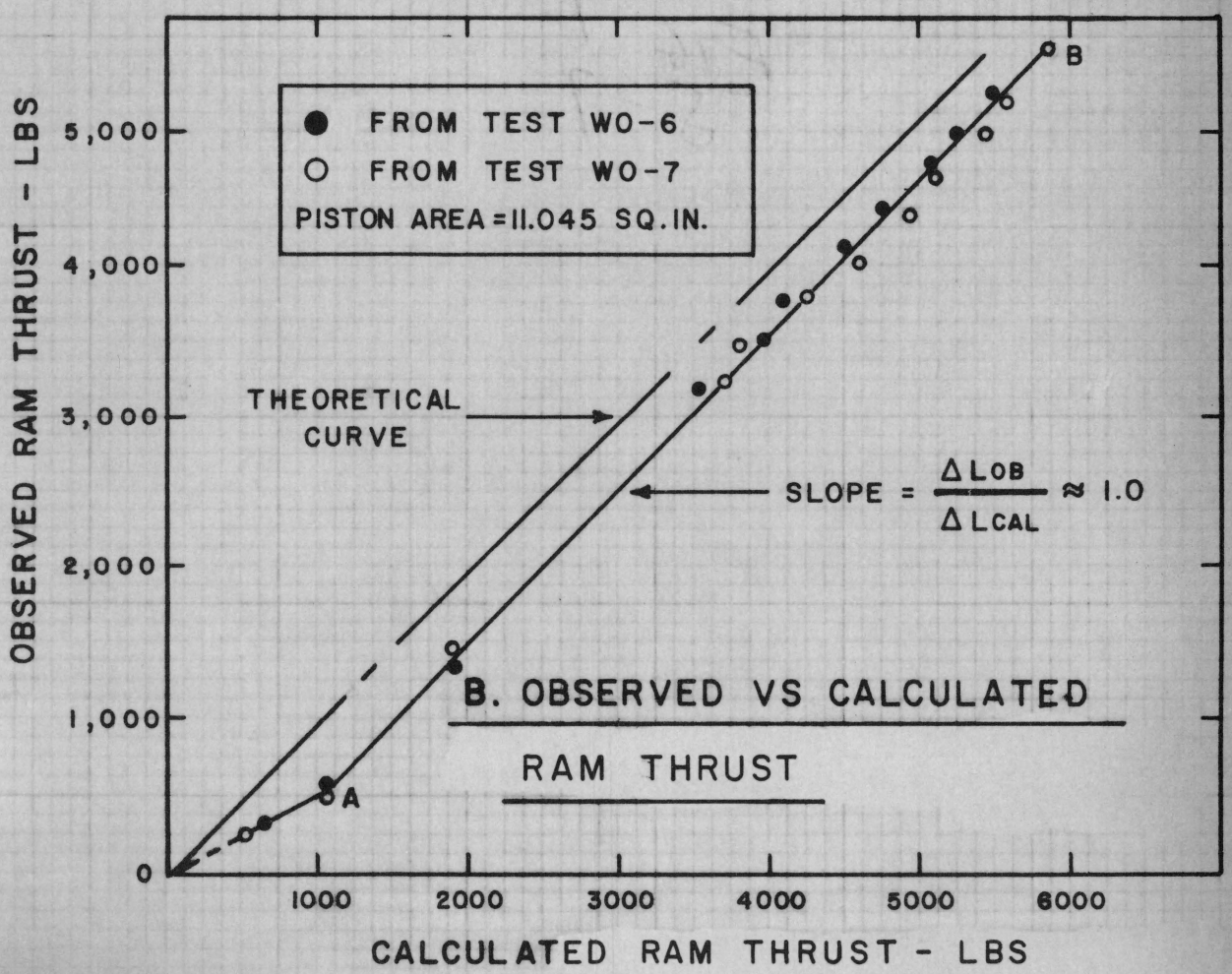


FIGURE 49 - Curves Illustrating Behavior of Hydraulic Ram.

was found to be approximately 10.7 sq. in. This value differs from the quoted effective piston area (11.045 sq. in.) by approximately 3 per cent which is within the experimental error. The maximum ram thrust obtainable from this system is approximately 20 800 lbs which is developed at a ram pressure of 2000 psi (the maximum available nitrogen supply pressure).

Since the majority of the initial deformation experiments were to be conducted at relatively low axial loads (0-6000 lbs), the behavior of the ram at these lower levels was further investigated. Figure 49B illustrates the variation of observed versus calculated ram thrust for two different experiments. The calculated ram thrust was determined from the measured ram pressure and the quoted effective ram area. The curve appears linear (region A-B) for ram thrusts above 550 lbs, having a slope of approximately 1.0. Below this level (region O-A) the slope of the curve decreases to a lower value and the projected curve appears to pass through zero. It is suggested that the behavior in the region O-A is associated with packing friction and possibly with the extension of an internal spring which serves to return the ram piston to its initial position when the piston pressure is reduced.

The behavior of the hydraulic ram, in the region of interest (600-5000 lbs) was found to be linear and reproducible. In

this region the measured ram thrust was found to be approximately 450 lbs lower than that calculated from the applied ram pressure. The anomalous behavior at ram thrusts below 600 lbs is not considered important in the present application.

1.4.2 Constant Stress Mode

(i) Load Cell Zero Drift

The stability of the control system in both the CS- and IS-mode depends on the stability of the load cell. Since no experimental method could be conceived to determine this stability during actual loading conditions indirect means were adopted to estimate its magnitude. These consisted of studying the zero drift of the load cell over a period of time under no-load conditions, and investigating the zero drift produced after a period of sustained loading. It should be noted that all studies presented refer to a 20,000 lb, Baldwin, Type-C load cell. Table 9 lists the data from a number of these experiments.

All measurements of equivalent load variation quoted in Table 9 were made using a 12-channel printing recorder with no external amplification. From past experience it was determined that the charts from this recorder could be read to $\pm$ 1/10 of a small division, which corresponds to an experimental error of $\pm$ 8.5 lbs.

TABLE 9

Load Cell Zero Drift Data

Test	Reference	Temperature	Average Load(1)	Test Period	ΔL(2)	$\Delta\sigma$(3)
		°C	lbs	Hours	lbs	psi
A	(WO-4)	22 ± 0.2	ZERO	20	± 8.5	± 19.3
B	(64-7)	22 ± 0.2	ZERO	48	± 8.5	± 19.3
C	(WO-4)	22 ± 0.2	2600	1-1/2	- 8.8	- 20
D	(WO-6)	22 ± 0.2	3500	5	- 9.2	- 21
E	(WO-7)	22 ± 0.2	3500	5	- 25.2	- 55
F	(WO-2)	22 ± 0.2	4700	2	+ 26.0	+ 59

(1) In some experiments the load was maintained at various levels for a period of time. The value quoted is an average of these levels.

(2) Value quoted is load equivalent to observed maximum deviations from initial zero value.

(3) Value quoted is stress due to ΔL acting on a specimen with a diameter of 0.750 in.

The zero drift under no-load conditions (Tests A and B) was found to be very randomly about a relatively constant mean. The maximum limits of this variation being of the order of ± 8.5 lbs. These variations are within the limits of the experimental error of the measurement system. The values of zero drift observed after the application of various sustained loads (Tests C-F) represent the difference between the initial and the final zero load levels. These measurements represent displacements, hence if $-17 \leq \Delta L \leq +17$ lbs the variations will be within

the experimental error. This is certainly the case for Tests C and D. Tests E and F lie slightly outside the range of experimental error which may indicate that there has been a small zero drift, but the fact that the drift is positive for one test and negative for the other would suggest that the estimated value of experimental error was too low.

For the experiments carried out to date it appears that the load cell zero is stable to within approximately $\pm$ 13 lbs which compares closely with the calculated experimental error of $\pm$ 8.5 lbs.

(ii) Optimization of the Pneumatic Controller

The pneumatic controller contains a number of parameters which must be adjusted to provide optimum control. These are (see Figure 36) the settings of the loading and unloading micrometer valves*(V-6 and V-10), the differential pressure ($\Delta P = P_{in} - P_c$) across the loading valve (V-6), and the ballast volume. The effect of these various parameters were investigated in considerable detail** but on a brief review of these studies and the conclusions will be presented here.

---

* The settings of the loading and unloading micrometer valves are abbreviated as LV and ULV. For example the statement LV = 11 means that the loading valve is set at 11.

** During the period December 1963-September 1964 a number of experiments were carried out. These include Tests Series 63-6 and 64-13. The detailed data and results of these tests are held by the writer.

In the CS-mode the optimum control conditions are defined as "those conditions which results in the axial applied load remaining as nearly constant as possible with time". The typical variation of applied load with time is shown diagrammatically in Figure 50A. It consists of a cyclic variation about the control point (L_c). The control point (L_c) for convenience is defined as the average load level based on the peak values, namely $L_c = (L_{max} + L_{min})/2$. The load fluctuation ($\Delta L(F)$) is defined as the peak to peak value of the fluctuation, namely, $\Delta L(F) = (L_{max} - L_{min})$. Table 10 illustrates the results of a number of typical tests conducted over short periods of time for various settings of the parameters. Figure 50B illustrates a section of a typical load versus time curve. The short period disturbance on this recording are due to background noise in the measurement system.

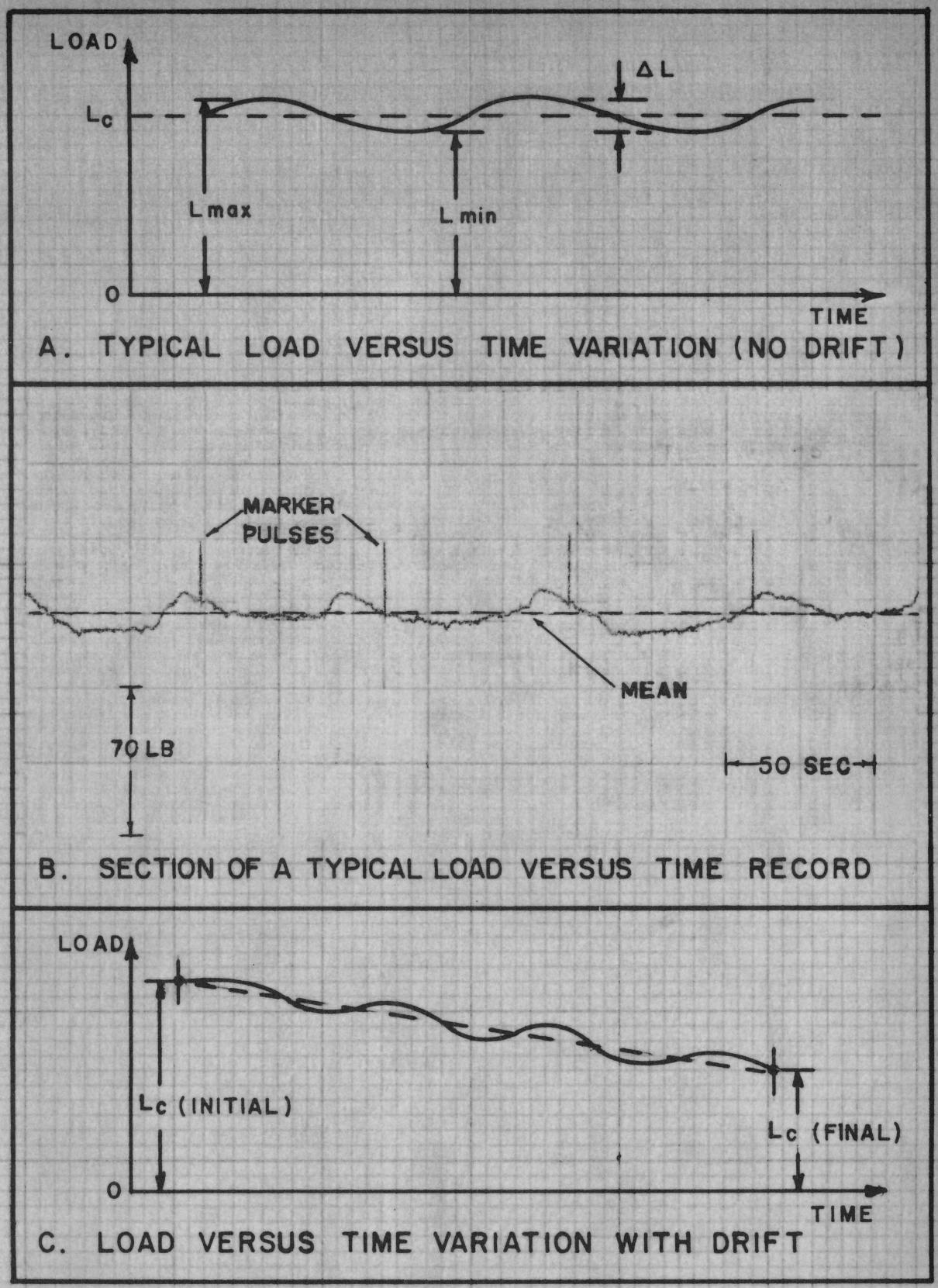


FIGURE 50 - Curves Illustrating Behavior of Control System Operating in CS-Mode.

TABLE 10

Variation of Load Fluctuation with Various Parameters

(Control System in CS-Mode)

Test	P_c(1)	Control Parameters			Ballast	L_c	$\Delta L(F)$	$\frac{\Delta L(F)}{L_c} \times 100\%$
		ΔP(1)	LV(2)	ULV(2)				
	psi	psi	Valve - Setting			lbs	lbs	
A	700	100	11	4	out	7830	222	2.8
B	700	100	9	4	out	7830	156	2.0
C	700	100	7	4	out	7830	102	1.3
D	700	100	5	4	out	7830	22	0.3
E	700	100	7	4	in	7830	31.2	0.4
F	700	100	5	4	in	7830	13.2	0.17
G	700	100	5	3	in	7830	22.8	0.29
H	700	100	4	3	in	7830	4.5	0.06
I	480	100	4	4	in	5297	8.2	0.16

(1) P_c and ΔP values are approximate.

(2) LV and ULV settings quoted are in terms of the smallest calibrated divisions on the valve micrometer. Each division corresponds to a rotation of 36 degrees.

The results of these tests have indicated the following:

(1) The smaller the value of ΔP the less sensitive the control system is to the LV setting. The lowest possible ΔP is therefore desirable. However when using low values of ΔP care must be taken to ensure that the regulator controlling ΔP is sufficiently stable to maintain the desired value.

(2) The lowest load fluctuations are attained with the ballast cylinder in the system.

(3) In general the lowest load fluctuations are obtained with the lowest values of LV and ULV settings. The lower limit of the LV setting is determined by the natural leakage of the system. The response time of the system is also a function of the LV and ULV settings. If these are too low the system will require an undesirably long time to come back into a stable condition if unbalanced significantly from the control point by a disturbance*. In general a LV and ULV setting of 4.0 has been found to be the most satisfactory.

(4) It has been generally found that the percentage load fluctuation ($\Delta L/L_c$) x 100% decreases with increasing load level. It is felt that this is due in part to the fact that frictional effects in the hydraulic ram and the separator become less important at higher load

* This condition is undesirable when incremental loading is being carried out and will be discussed later in this section.

levels, and that the overall control system is only sensitive to load fluctuations greater than $\pm \Delta L(a)$. The value of $\Delta L(a)$ depends on the design of the galvanometer-photocell unit in the electronic controller, the sensitivity of the load cell and the overall gain of the system. It is, therefore, a constant independent of load level, thus its effect on the percentage fluctuation will be of less importance at the higher load levels.

Based on these studies the optimum conditions given in Table 11 are employed when operating in the CS-mode:

TABLE 11

Optimum Control Conditions
(CS-Mode)

Ballast	-	IN
ΔP	=	100 psi
LV	=	4.0
ULV	=	4.0

For these settings the load fluctuation ($\Delta L(F)$) appears to be less than $\pm$ 15 lbs for experiments conducted over periods of time up to 10 hours.

(iii) Load Drift

The load drift ($\Delta L(D)$) of the control system is defined as the variation of the average load level (L_c) with time,

namely $\Delta L(D) = L_c$ (final) - L_c (initial). Figure 50C illustrates a case where there appears to be a linear load drift. Table 12 presents load drift data from a number of deformation experiments conducted at different load levels and for various periods of time. The magnitude and direction of the load drift does not appear to be dependent on the load level or on the duration of the test, although it may be significant that the largest load drift (+ 35 lbs) observed in Test G was associated with the longest test duration (1481 minutes). The other observed load drifts are within the limits of load cell drift ($\pm$ 13 lbs) determined experimentally and quoted earlier in this section.

TABLE 12

Values of Load Drift Obtained from a Number of Deformation Experiments

Test	References	Time	L_c	$\Delta L(D)$	$\frac{\Delta L(D)}{L_c} \times 100\%$
		Minutes	lbs	lbs	
A	(WO-3)	165	4420	0	0
B	"	113	5270	0	0
C	"	606	5620	0	0
D	(WO-4)	51	4850	+8.9	+.18
E	"	170	5700	-26	-.46
F	"	128	5930	0	0
G	"	1481	5930	+35	+.59
H	(WO-5)	22	3960	-9.3	-.23
I	"	37	5100	+2.2	-.04
J	"	44	5340	+24.3	-.46
K	(WO-6)	34	4150	+2.7	+.07
L	"	38	4970	-3.5	+.07
M	"	38	5270	-15.5	-.29

1.4.3 Incremental Stress Mode

The IS-mode of operation makes it possible to rapidly raise or lower the load control level between two preselected values. To date its main purpose has been in incremental creep experiments. Here it is necessary to carry out creep experiments on the same specimen over a preselected range of load levels. To obtain significant data from such experiments it is necessary that the shift from one load level ($L_c(1)$) to the next ($L_c(2)$) be carried out as rapidly as possible. This is accomplished by first shunting the control galvanometer in the electronic controller, setting the load level selector switch in the IS-mode unit to the new required level, manually raising the control pressure (P_c) to the correct value, and finally removing the control galvanometer shunt and allowing the load control system to settle at the new level ($L_c(2)$).

Figure 51A illustrates the form of the load versus time disturbance produced during such an incremental load change. Three important parameters (see Figure 51A) are associated with this type of operation, namely: the loading time (T_L), the setting time (T_s), and the load overshoot ($\Delta L(O)$). Optimum operation in this mode requires that T_L be as small as possible while still maintaining T_s and $\Delta L(O)$ within certain limits. If an attempt is made to obtain very low values of T_L (which requires the control pressure to be

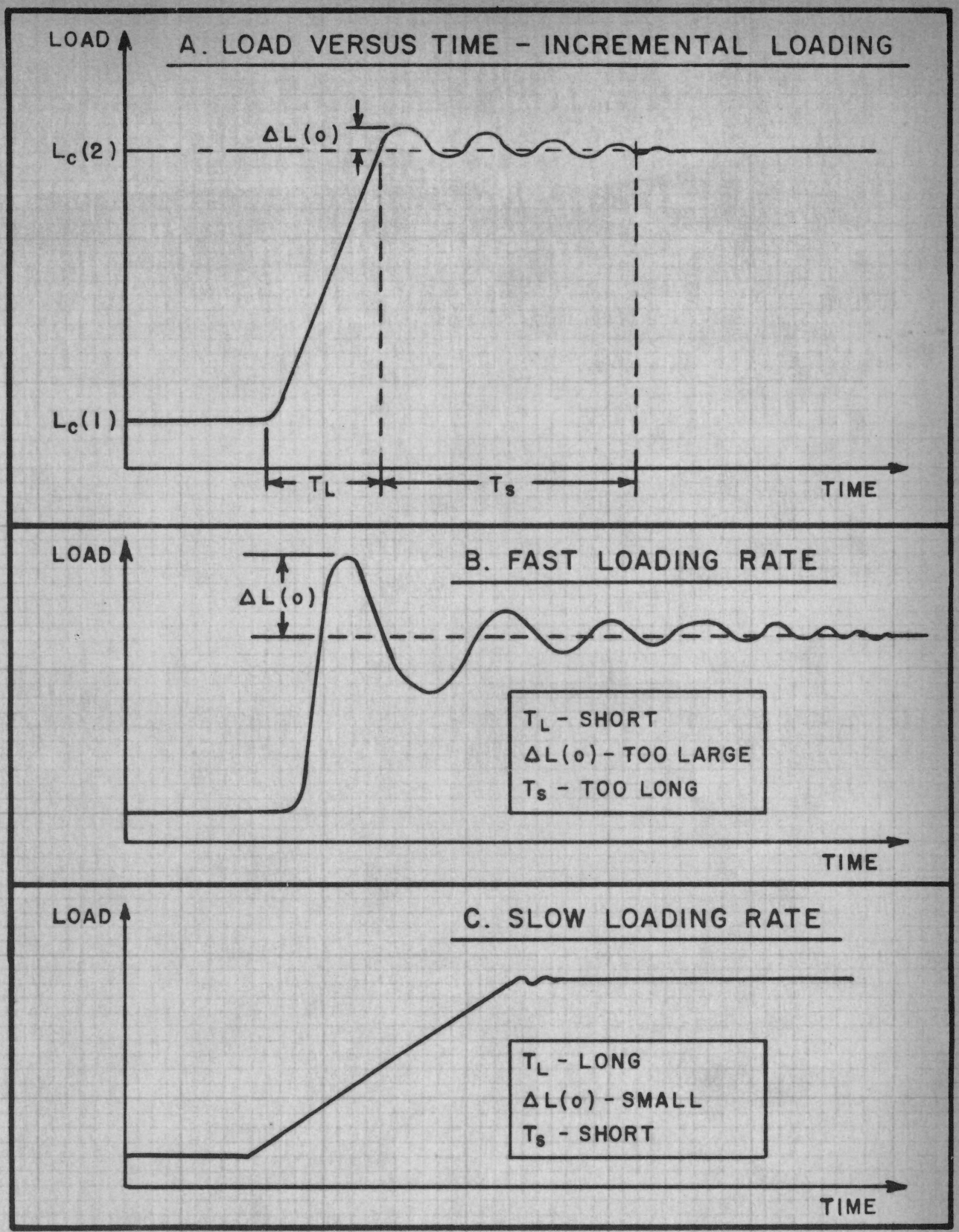


FIGURE 51 - Curves Illustrating Behavior of Control System Operating in the IS-Mode.

raised very rapidly) it is found that both $\Delta L(O)$ and T_s become excessive (see Figure 51B). If an attempt is made to maintain $\Delta L(O)$ and T_s at too low a value T_L will necessarily be excessively large (see Figure 51C).

The results of a large number of experiments has indicated that with care it is possible to carry out incremental loading experiments within the range of conditions listed in Table 13.

TABLE 13

Optimum Operating Conditions
(IS-Mode)

Factor	Range
ΔL	100 - 500 lbs
L_c	2000 - 6000 lbs
T_L	4 - 6 sec
$\Delta L(O)$	4 - 20 lbs
T_s	100 - 300 lbs

The reproducibility of the various load levels was also investigated, using the load data obtained from two separate experiments (WO-6 and WO-7). It was found that the average error was only $\pm$ 10 lbs, which was well within the possible error ($\pm$ 13 lbs) due to load cell drift.

1.4.4 Constant Stress Rate Mode

A simple method for carrying out deformation experiments at an approximately constant stress rate (constant loading rate) was investigated. In this method only the pneumatic control unit was used, the remainder of the feedback control system was not employed. A nearly constant rate of loading was obtained by manually opening the loading solenoid valve (V-8) (see Figure 36) and allowing gas at the supply pressure to flow via the micrometer metering valve (V-10) to the separator, thus increasing the hydraulic pressure and the ram thrust. Figure 52A shows a simplified drawing of the pneumatic circuit.

A short series of experiments were carried out to check on the range of loading rates ($\dot{L}$) obtainable and their linearity. In all cases a supply pressure of 1000 psi was used, and load versus time curves were obtained for various settings of the micrometer loading valve. Figure 52B illustrates diagrammatically a typical load versus time curve. The data for these experiments is presented in Table 14.

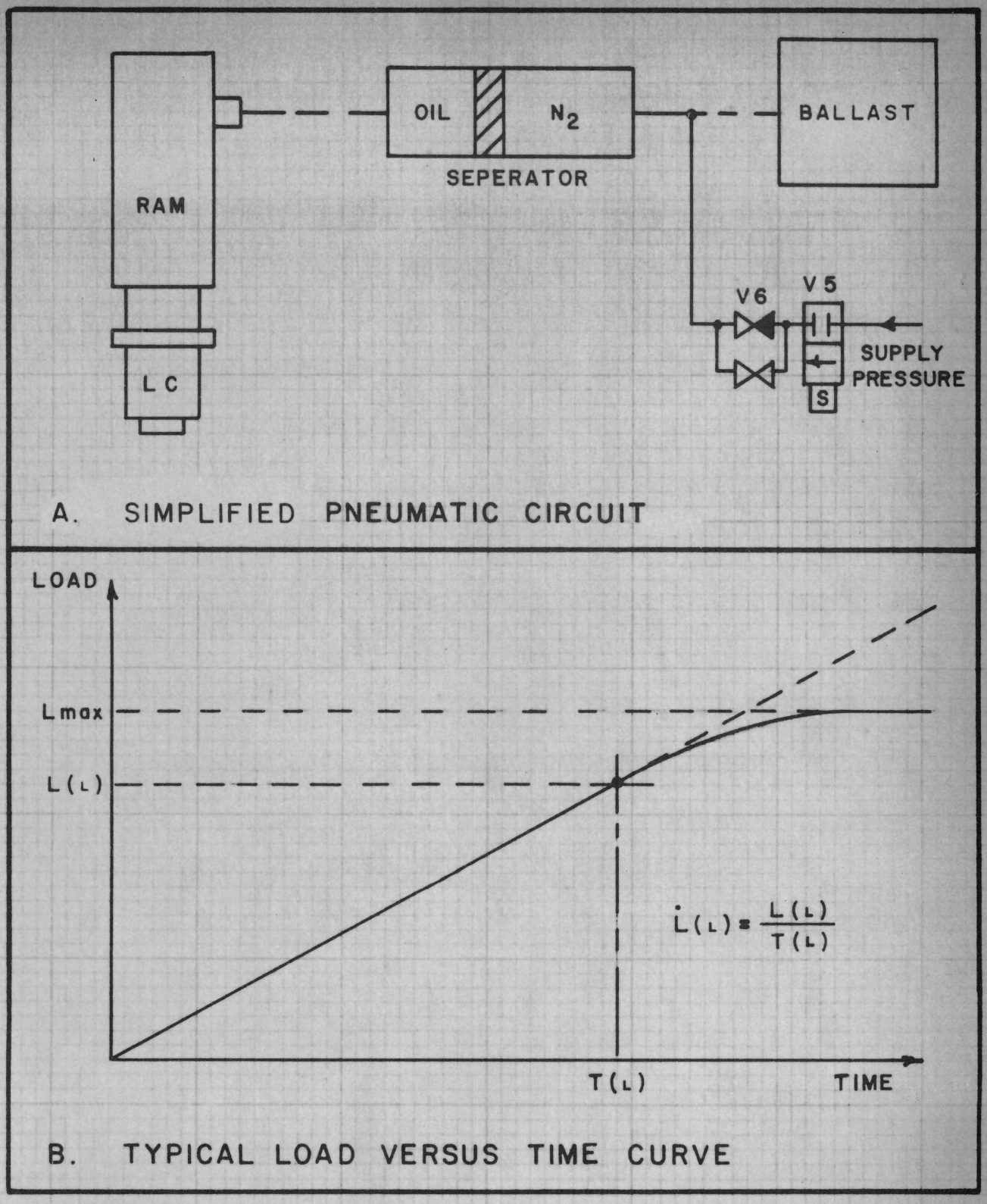


FIGURE 52 - Outline of a Simple System for CSR-Mode Operation.

TABLE 14

Behavior of a Simple System for Obtaining an Approximately Constant Rate of Loading

Test	Reference	Supply Pressure	LV (1) Setting	L_{max} (2)	$L(\ell)$ (3)	$\frac{L(\ell)}{L_{max}} \times 100\%$	$L(\ell)$ (4)
		psi		lbs	lbs		lbs/sec
A	(64-15A)	1000	3.5	11,600	9,650	83	5.4
B	(64-15C)	1000	4.0	11,600	8,700	75	15.0
C	(64-15D)	1000	6.0	11,600	7,000	60	62.0

(1) LV settings quoted are in terms of the smallest calibrated divisions on the valve micrometer. Each division corresponds to a rotation of 36 degrees.

(2) L_{max} is the maximum load obtained in the test.

(3) $L(\ell)$ is the load at which the load versus time curve starts deviating from linearity.

(4) $\dot{L}(\ell)$ is the loading rate determined from the linear region of the load versus time curve.

From the results it appears that the method is satisfactory. A wider range of loading rates and an extended linear region should be possible if the ballast cylinder is disconnected from the circuit and if higher supply pressures (up to 2000 psi being available) are employed. It should also be noted that a number of unloading experiments were also carried out. Here the gas pressure in the system was bled-off at a rate which was also determined by a micrometer metering valve. It was found however that under these conditions the load versus time curves were very non-linear over most of their range.

I.5 Stress, Strain and Confining Pressure Measurement System

1.5.1 Strain Transducers

The strain transducer itself, presents a problem to which the final solution may be at best a compromise. In metals testing, strain gages directly attached to the test specimen and clip-on type gages using differential transformers have been widely used for uniaxial testing. Transducers using capacitance type elements, vibrating wire elements, as well as a number utilizing various sonic and optical principles have also been employed. The majority of these methods are difficult and inconvenient to apply to testing of basically brittle geologic materials due to difficulties in specimen preparation and in attachment of the transducer to the test specimen. Furthermore

it is desirable that the method used for the present uniaxial studies be equally applicable to future triaxial experiments.

Geophysicists and engineers involved in the study of the mechanical properties of geologic materials have utilized a number of methods of strain measurement both for uniaxial and triaxial tests. In uniaxial tests at the Mines Branch early experiments (see Hardy (1959)) utilized an optical-mechanical system known as the Martens Mirrors apparatus. This system was time consuming and did not lend itself to recording. Later experiments utilized wire-type strain gages bonded directly to the specimen, and more recently foil-type strain gages have been employed. However, at present the majority of routine short period uniaxial tests on geologic materials at the Mines Branch utilize an axial strain gage type compressometer and a transverse differential transformer type extensometer which are clamped to the test specimen. These were modified from the original design of Leeman and Grobbelaar (1957A, 1957B), and have proven very successful for short period test work. Recently Hunt (1962) utilized this type of compressometer in a series of creep experiments on salt. The compressometer appeared to function in a well behaved manner over a 24 hour period to a maximum strain level of approximately 500 μs, however it was not possible to assess the actual stability of the transducer by such indirect means.

A number of methods have been utilized by various workers in which specimen strain was determined by measurements of loading piston displacement. Griggs (1936), Handin (1953) and Robertson (1955) have measured loading piston displacement by means of dial gages. Griggs (1960) and Handin (1953) have also used dial gages with attached precision potentiometers to give displacement data in a convenient form for recording. Handin (1960) and Donath (1962) have used differential transformers to measure piston travel. A recent paper by Serdenzecti and Boozer (1961) illustrates their use of linear potentiometers for the same purpose. The capacitance-type strain transducer developed by Papirno (1960) or some modified form of unbonded strain gage might also be applied. The latter concept has been under consideration by the United States Bureau of Reclamation for some time.

Although methods involving the measurement of piston displacement have proven more or less satisfactory for experiments where large strains (up to 10%) were involved, their use in experiments where small strains (maximum 0.5%) and small strain increments (.001%) are of interest would probably be unsatisfactory in most cases. First there is the problem of the interface between the specimen and the loading piston, secondly the stability and accuracy of the necessary mechanical arrangement, and finally the degree of resolution of the transducer itself.

Even with extremely fine polishing of specimen end-surfaces the actual surface will contain a large number of asperities, and under a compressive load such a surface will compress rapidly upon initial loading due to failure or the development of plastic deformation in the individual asperities. It is obvious that strain measurements based on deformation measurements made across such a surface (as would be the case if relative motion of the loading piston were being considered) would be seriously in error, particularly at low loads.

Secondly the mechanical stability and accuracy of an external strain measuring system, although not too difficult to achieve in large strain experiments becomes a major difficulty when small strains are being considered. It is also important to remember that transducers such as potentiometers have an upper limit in their resolution based on the size and spacing of their resistive elements, and this limits their use to displacement increments of 100 μs or greater. Although such elements as capacitance- and differential transformer-type strain gages are capable of higher resolutions, there would be considerable difficulty in obtaining suitable mechanical stability in the overall deformation measuring device.

It is felt at the moment that the use of electric resistance strain gages attached directly to the test specimen offer

the most convenient and reliable method of strain measurement. Their geometry and small size make it possible to mount a number on each specimen to provide data on possible specimen bending and on strain uniformity during the experiments. Considering future triaxial studies this type of strain transducer offers no difficulty with regard to specimen jacketing, mechanical stability, or end-effects. However, this type of transducer does introduce another factor, namely the effect of confining pressure on the strain gage element itself. Brace (1963) has investigated this effect in detail for confining pressures up to 150,000 psi. In his experiments Brace utilized three axial strain gages mounted at 120° apart around the circumference of the test specimen. This enabled him to determine the average axial strain and the maximum axial strain due to bending. Following discussions with Brace (1962) it was decided to apply the same strain measurement procedure in the writer's experiments.

1.5.2 General Description of Measurement System

After considerable consideration it was decided to utilize measurement transducers* based exclusively on electric resistance strain gages. As a result load (stress) measurements are

*Most strain gage transducers are classed as either four-arm (4A) or two-arm (2A) transducers. This refers to the fact that transducer itself contains either a full four-arm bridge circuit, or a two-arm bridge circuit with the remaining two arms of the bridge being either remote from the transducer or in the measuring instrument itself.

made using Baldwin Load Cells, specimen strains are measured by foil-type strain gages attached directly to the test specimen, and in future triaxial experiments confining pressures will be monitored by Baldwin Pressure Cells. The choice of this form of instrumentation has been influenced by the convenience in size and operation of the equipment, by the fact that the theory and application of strain gage measurement is well developed, and by the commercial availability of the equipment.

Figure 53 shows a block diagram of the overall measurement system. A general view of the system is shown in Figure 54. A system for very accurate monitoring of room and specimen temperatures, using thermocouples, is also included in the "Slow" Y-T recorder system. This system will be discussed in more detail in a later section. Load, confining pressure, strain, and temperature are converted to electrical signals by the appropriate transducers at the test area. These signals are carried by cable from the test area in the inner room to junction boxes and switching units in the outer room. Readout facilities here consist of,

(1) A manual readout system,
(2) A 12-channel "Slow" Y-T recorder system,
(3) A 2-channel "Fast" Y-T recorder system, and
(4) A single channel Y-XT recorder system.

The first three systems are mainly utilized for constant stress (CS) and constant strain (CE) experiments with the Type-A loading system.

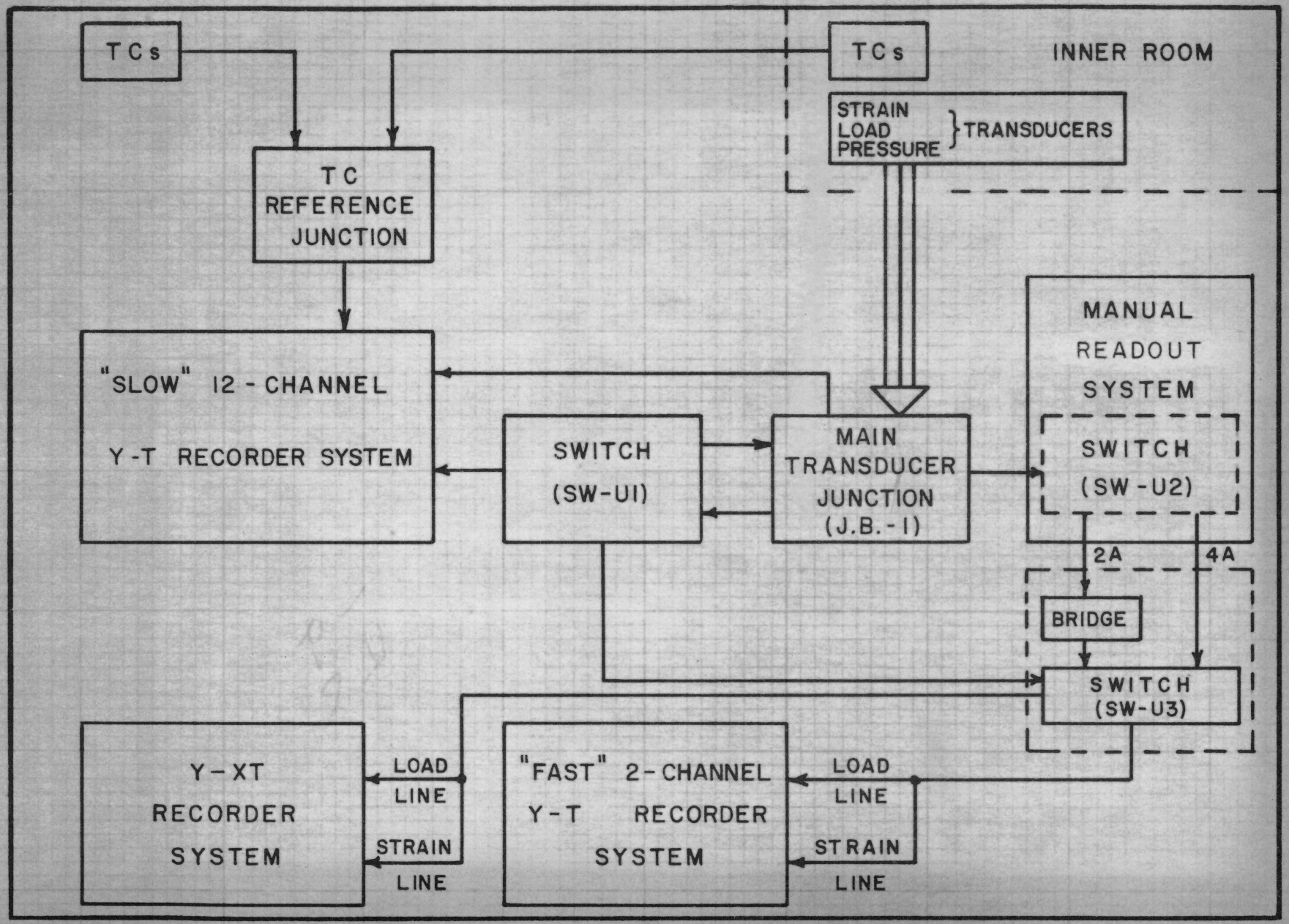


FIGURE 53 - Block Diagram of Measurement System.

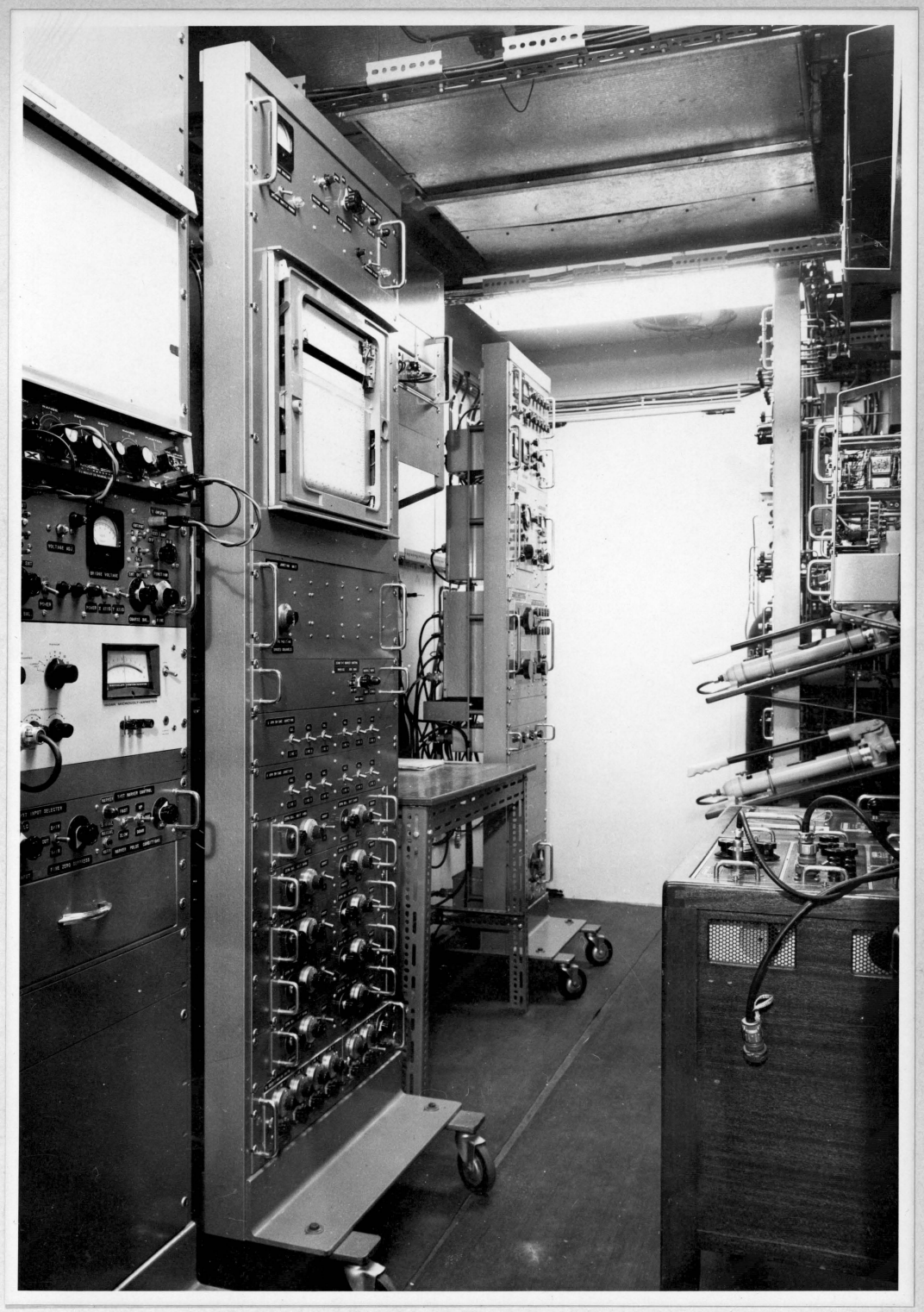


FIGURE 54 - Photograph Showing General View of Overall Measurement System.

These experiments require the recording of rapidly changing phenomena at various stages of the experiment. For example in CS experiments the Fast Y-T recorder may be employed to obtain curves of the two variables, axial strain and axial load, versus time during initial loading. Once the load is fully applied (or removed in the case of unloading) and the transient strain rate is sufficiently reduced (after approximately 20-60 minutes) the transducers associated with these two variables may be switched to the Slow Y-T recording system for display. Finally when the strain rates become very low (after perhaps 24 hours) these transducers may be switched to the manual readout system. Such an arrangement provides convenient and accurate data during all stages of the experiments.

The fourth system incorporates a single channel Y-XT recorder which will be used for direct recording of stress-strain curves during controlled stress rate (CSR) and controlled strain rate (CER) experiments planned in the near future. This system has also been used for recording strain versus time data during a series of incremental creep experiments on Wombeyan marble. Due to the high sensitivity and stability of this system it has been possible to obtain reliable transient creep curves having a magnitude of as little as 10 μs. This has made it possible to investigate the inelastic behavior of this material at stress levels very near the "elastic limit".

The purpose of the various switching units is to provide a flexible arrangement to allow the convenient connection and disconnection of the various transducers to the desired readout systems. The measurement system as a whole has developed in parts rather than being based on an original overall design and as a result the switching arrangements are perhaps more complicated than necessary. In the future it is planned to consolidate the switching operations into one unit which will greatly simplify wiring and operation. The design and construction of the various switching units, and their inter-connection will not be discussed further here.

1.5.3 Manual Readout System

This Manual Readout system has been described in detail in a previous paper, Hardy (1962), and is shown in block diagram form in Figure 55. Figure 56 shows a number of views of the completed system. It consists of five principal units: (a) A modified Baldwin strain gage indicator, to measure strain in the test specimen or load cell; (b) An adjustable power supply to operate the strain gage indicator; (c) A switching unit to select the particular specimen strain gage or load cell to be observed; (d) A constant-current unit to pass a d-c current through all strain gages (specimen and load cell) during the time between strain observations; and (e) a standard specimen unit containing a set of highly stable two-arm (2A) and four-arm (4A) dummy

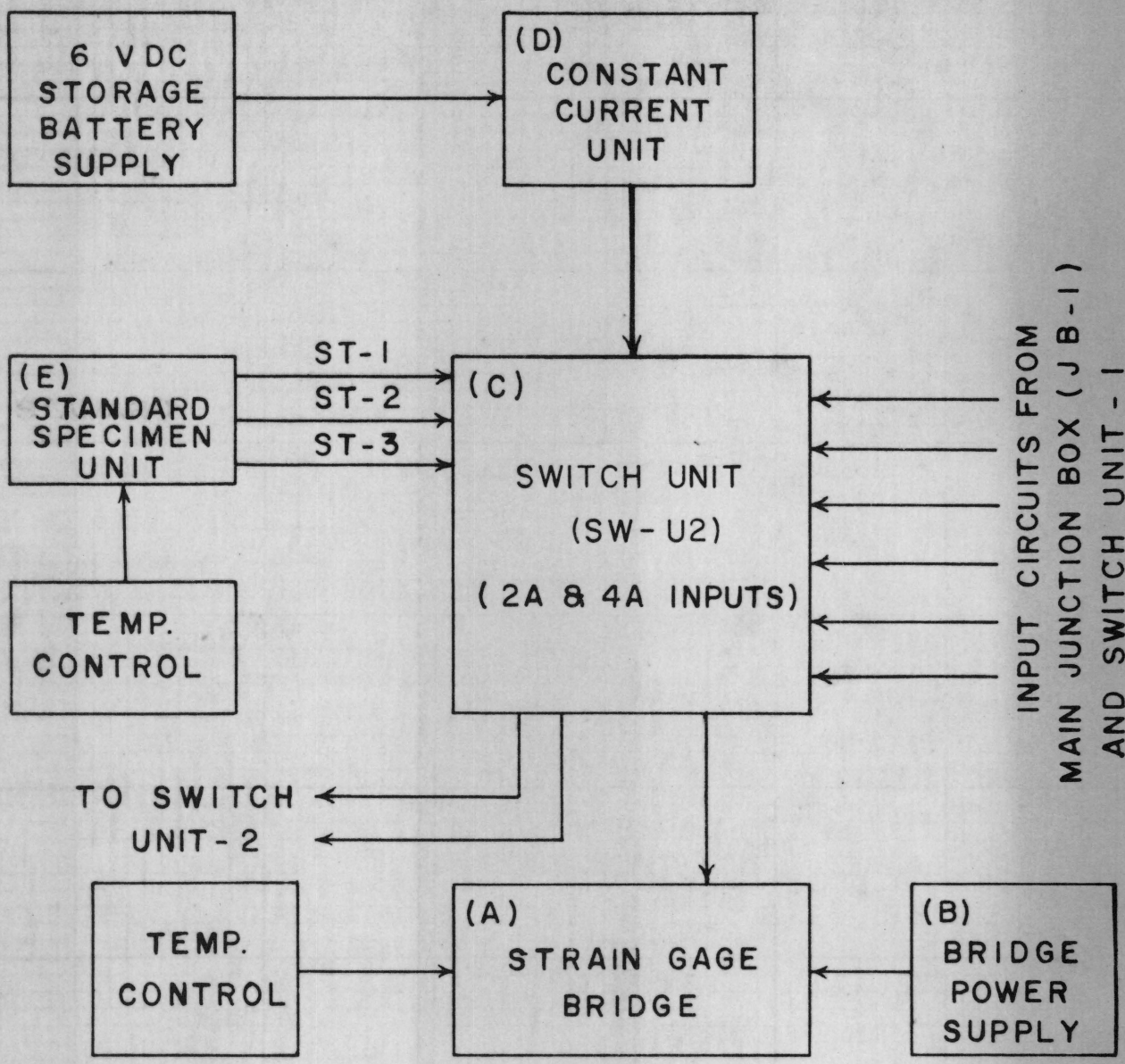
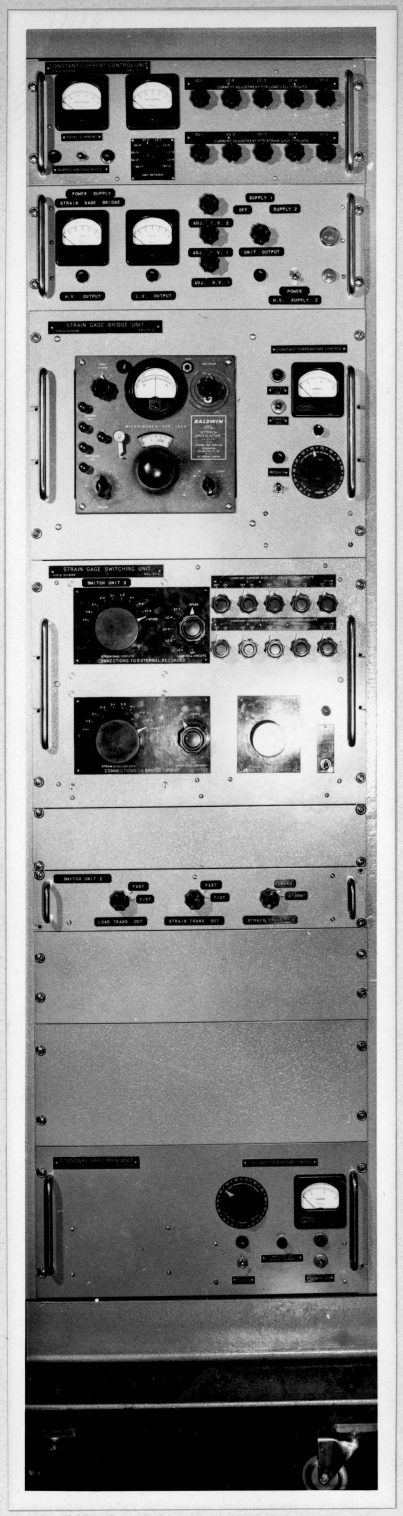
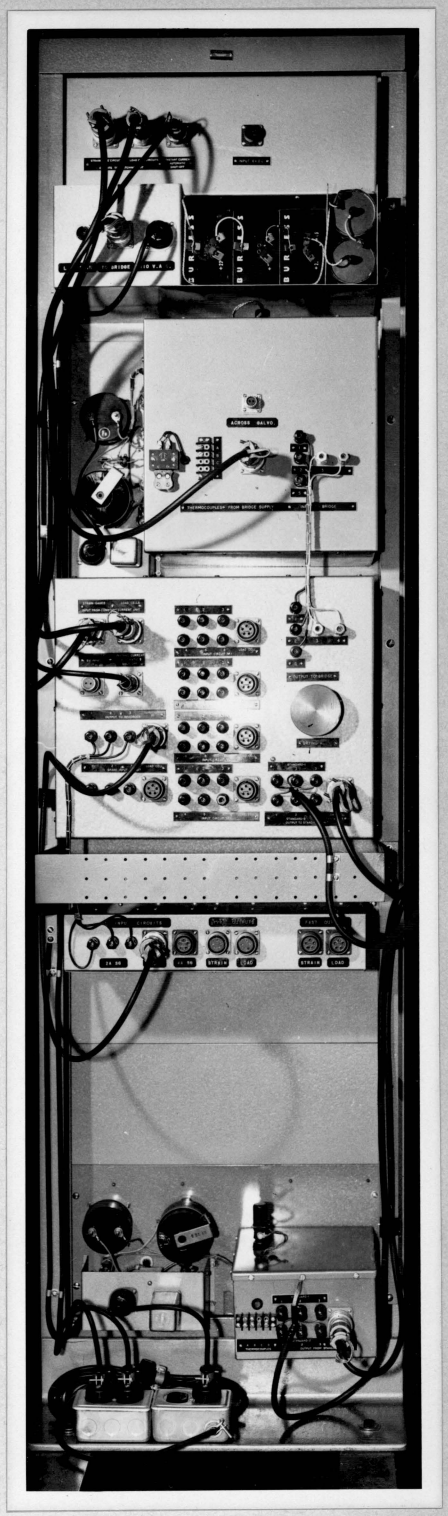


FIGURE 55 - Block Diagram of Manual Readout System.



A. Front View of System.



B. Rear View of System.

FIGURE 56 - Photographs Showing Two Views of Manual Readout System.

bridge units, to check on the stability of the complete manual readout system. Since the system has not been used extensively as yet details of its design and operation will not be described here.

A series of stability experiments have been conducted on this system over a two week period (under normal fluctuations in room temperature and humidity) using the 2A and 4A dummy bridge units as references. The standard deviation observed in the strain measurements were equivalent to $\pm$ 3.8 μs and in the load measurements were equivalent to $\pm$ 10 lbs. The variation in the observed equivalent strain and load were also plotted against room temperature and although considerable scatter was evident there appeared to be a strong dependence on temperature. Assuming a linear dependence the variation of the equivalent strain was found to be approximately 3 μs per degree celsius. This system to date has not been used for measurements over long periods of time under the strict temperature and moisture conditions of the test enclosure. However higher stability is expected under these conditions.

1.5.4 12-Channel "Slow" Y-T Recorder System

This system provides 12 channels for recording load, strain, confining pressure and temperature over periods of time from a few hours to many days. Figure 57 shows a block diagram of the system. The complete system is mounted in a standard 24 inch wide

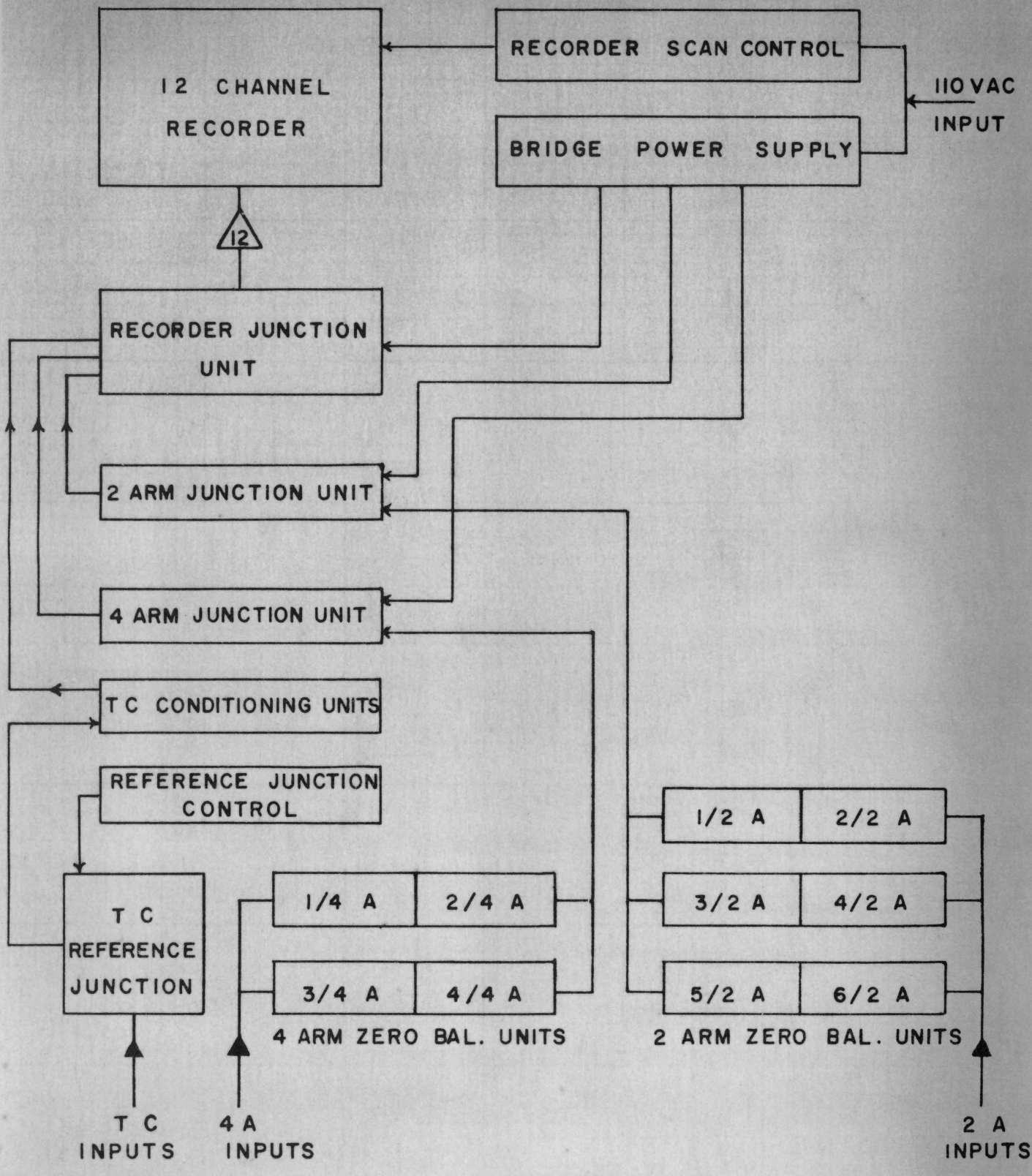


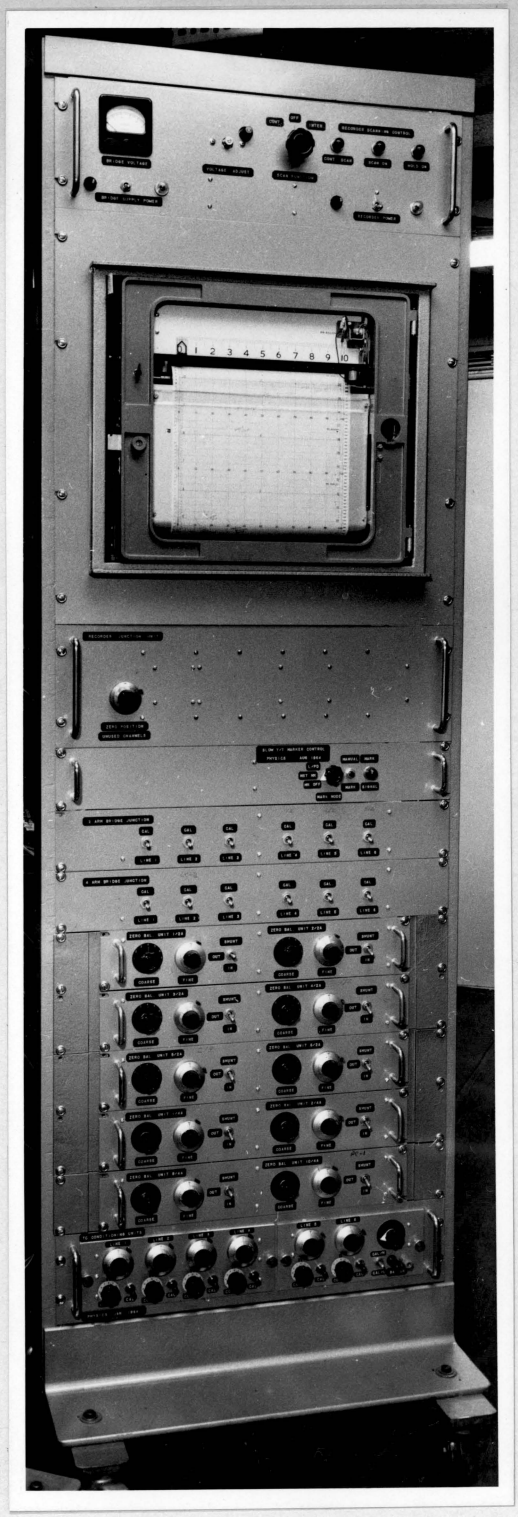
FIGURE 57 - Block Diagram of 12-Channel "Slow" Y-T Recorder System.

relay rack. Figure 58 shows a number of views of the completed system.

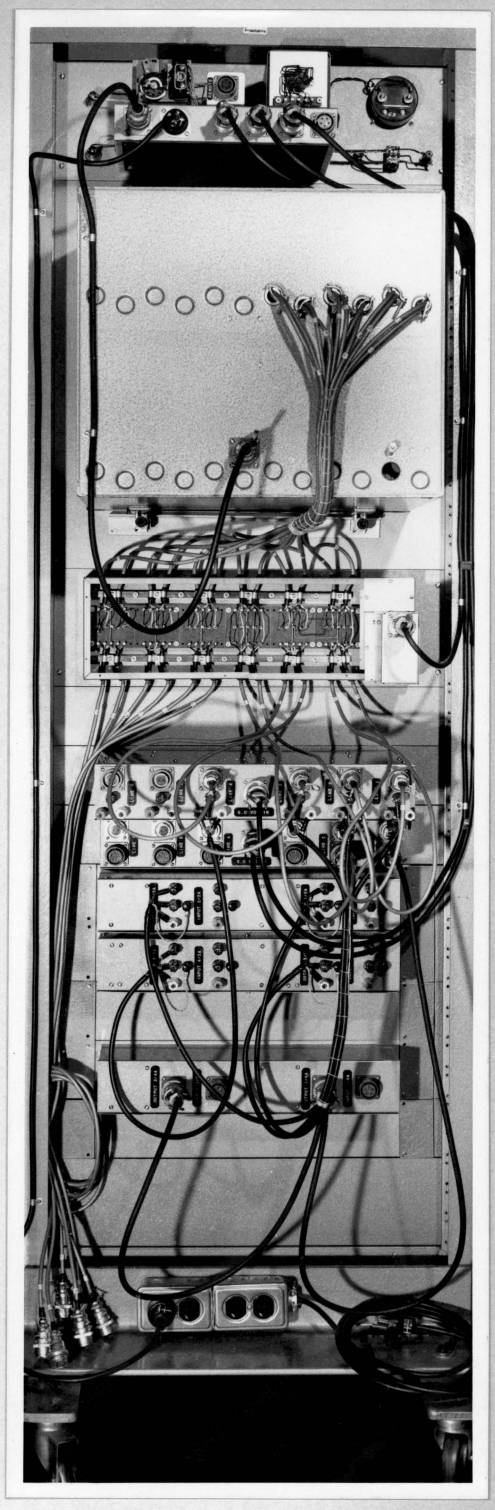
(i) Recorder and Recorder Junction Unit

The recorder itself is a Philips model PR 3210-A/100, 12 point, printing millivolt recorder with a maximum full scale sensitivity of 5 millivolts. At this sensitivity each small scale division on the recorder chart is equivalent to 50 μv, and since the chart may be read to $\pm$ 1/10 of a division it is possible to estimate the chart reading to $\pm$ 5 μv. A quick-change gear system provides chart speeds of 40, 80, 300 and 600 mm/hr. To allow the recording of very slowly changing variables the recorder chart-drive and scan-switch motor circuit has been modified to provide an adjustable scan/hold time ratio. A timer in the recorder scan control unit turns this motor on for a period of time, during which data is printed out. The motor is then shut-off for a period of time (the recorder amplifiers etc. remaining on). In this way, for example the system might be set to print out data for five minutes every four hours, giving an equivalent chart speed of approximately 1 mm/hr on the 40 mm/hr chart speed setting. The recorder scan control unit also contains a highly stable 6V d-c power supply* which powers the various transducers.

* Valor Power supply, model MB 6.3K 0.5, rated at a stability of better than 0.1 per cent.



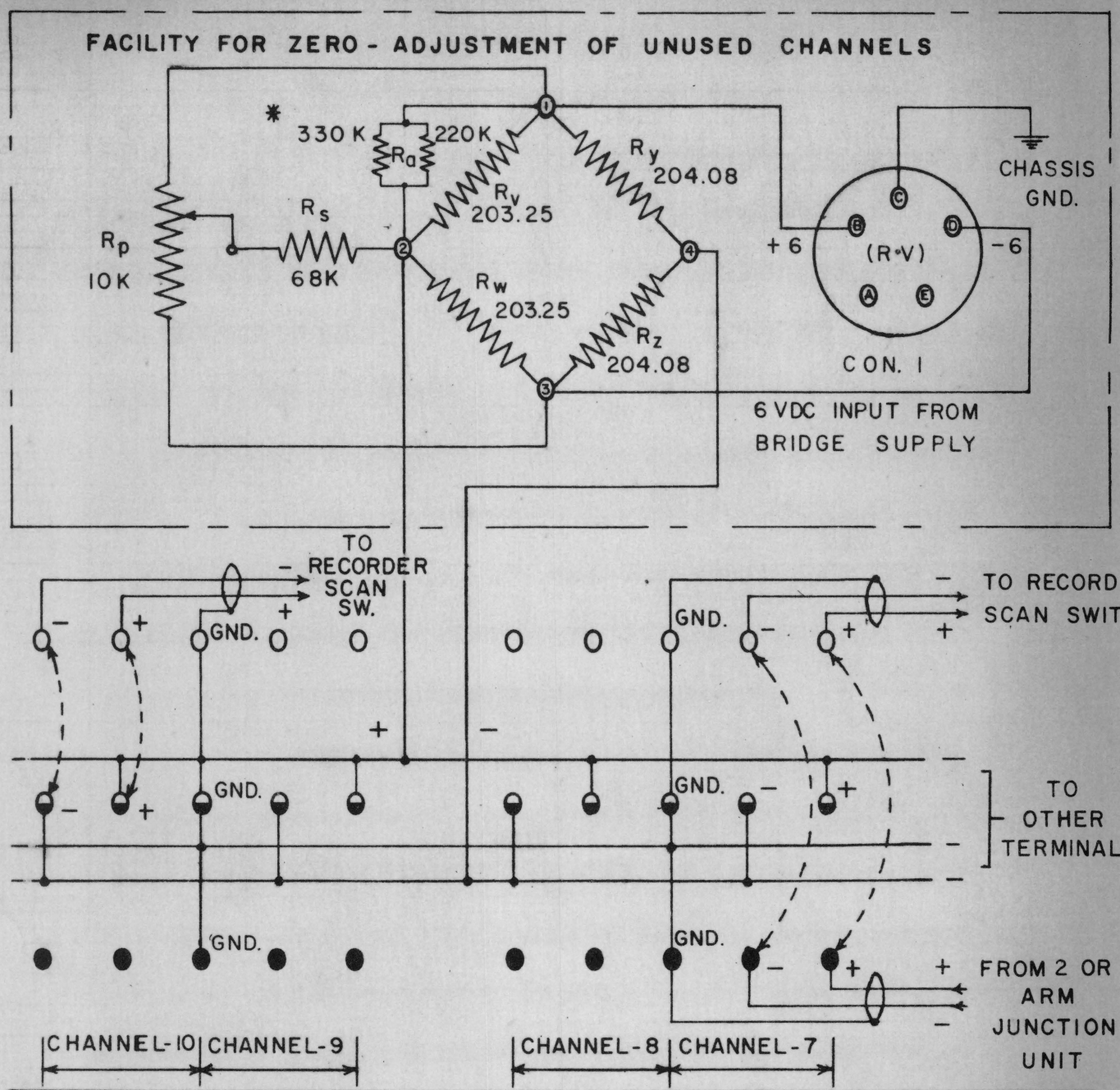
A. Front View of Recorder.



B. Rear View of Recorder.

FIGURE 58 - Photographs Showing Two Views of 12-Channel, "Slow", Y-T Recorder System.

All twelve inputs to the recorder scanning switch are brought out to a recorder junction unit. This unit includes a convenient terminal arrangement to allow individual recorder channels to be connected either to the appropriate transducers, or to a common adjustable voltage source which allows unused channels to be positioned on the recorder chart at a convenient position well away from the active channels. The circuit for the recorder junction unit is given in Figure 59. Wires carrying signals from the various transducers are connected to the unit via the lower set of soldering terminals. Connections from the various positions on the recorder scanning switch are connected to the upper set of soldering terminals. The central set of terminals are wired to the output of a highly stable bridge circuit as shown. This bridge is powered by the same 6V d-c power supply that activates the various transducers and its unbalance output voltage may be adjusted by varying resistor R_p. A particular recorder input may either be connected to a specific transducer or to the output of this adjustable bridge in which case a suitable unbalance is developed in the bridge to position the inactive channel print-out well away from those of the active channels.



Rv, Rw, Ry, Rz - Wire wound resistors, Tinsley type LF.1 (2 watt), accurate to ± 0.005 ohms

Rp - Spectrol, Model 860, Precision, 10 turn Wire wound potentiometer

Rs and Ra - 1/2 watt carbon resistors

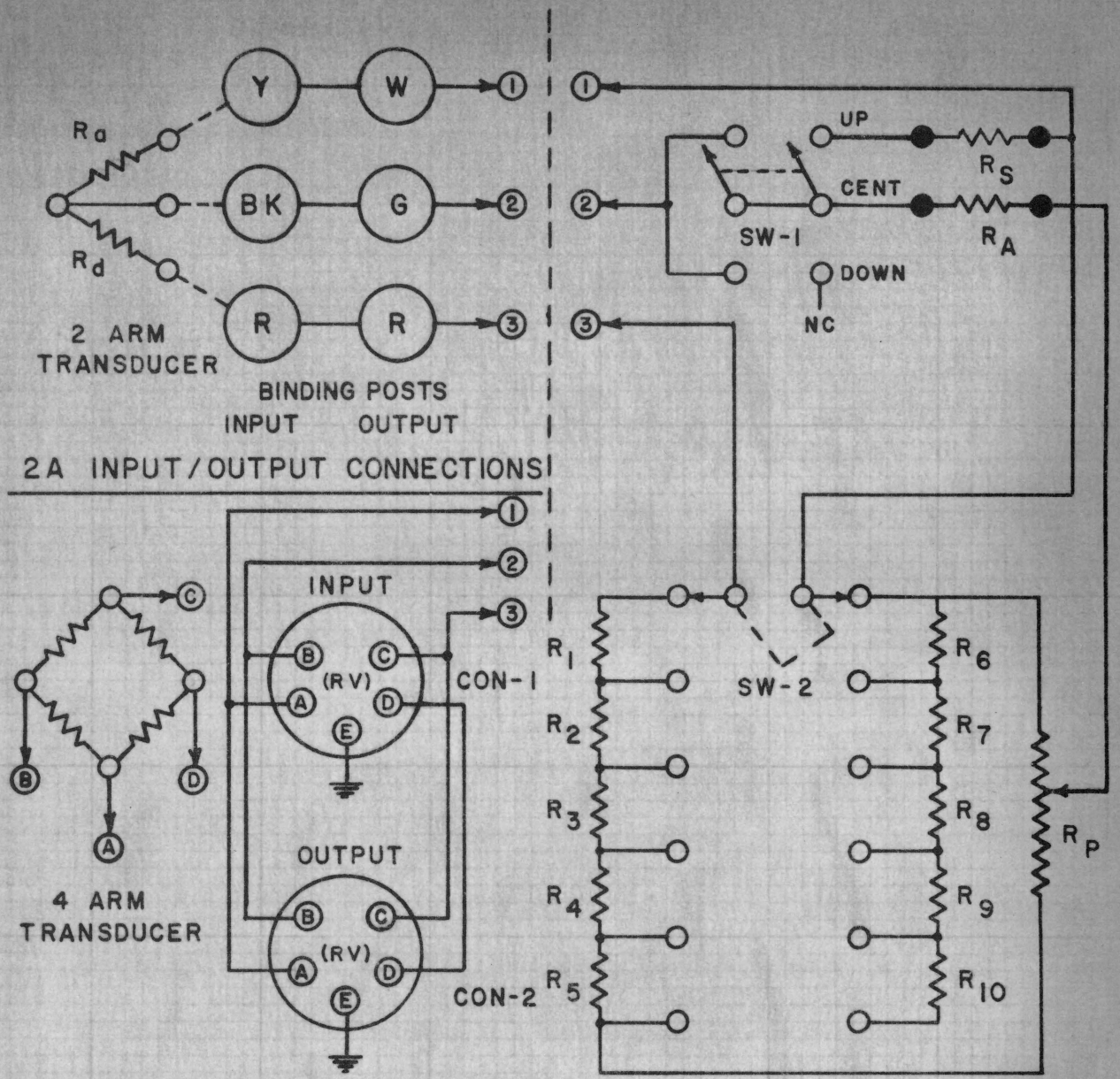
O - output term. ⬭ - zero pos. term. ● - input term.

FIGURE 59 - Circuit Diagram of Recorder Junction Unit.

(ii) Strain Gage Transducer Input Circuits

Two-arm and four-arm strain gage transducers are connected to the system via zero balancing units type-2A and -4A respectively. These provide a means for adjusting the position on the recorder chart of each separate input. The type-2A units are connected to the two-arm junction unit. This contains a series of resistors which complete the two-arm transducer inputs, forming full bridges. The type-4A units are connected to the four-arm junction unit. Power is supplied to both types of bridges at this point from the highly stable 6V d-c bridge power supply. The unbalance voltages produced in these bridges, as a result of variations in the transducer sections, are applied to the recorder via the recorder junction unit.

Figure 60 shows the circuits for the type-2A and -4A zero balance units. The two circuits only differ in the type of input and output connections and in the values of the various resistors. Switch SW-1 allows selection of three modes of operation: in the center-position the zero balance unit is out of the circuit, in the down-position the zero balance unit is in the circuit, and in the up-position the unit is in the circuit with an addition shunt (R_s) which provides an increased zero balance range. Switch SW-2 provides coarse zero adjustment in six steps, with fine zero adjustment being accomplished by a ten-turn, wire wound, potentiometer (R_p). All fixed resistors used in



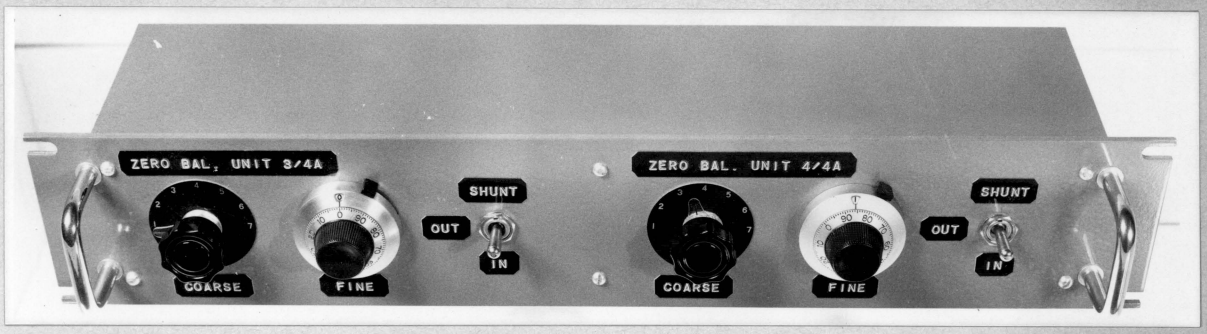
Resistors	Type	2-ARM*	4-ARM*
R_1, R_{10} R_s, R_d	1/4 Watt, precision carbon deposit resistors, 1% rating.	9760	4750
R_p	Spectrol model 860 10-turn potentiometer	10K	5K
* Resistance values in Ohms.			

FIGURE 60 - Circuit Diagram of 2-Arm and 4-Arm Zero Balance Units.

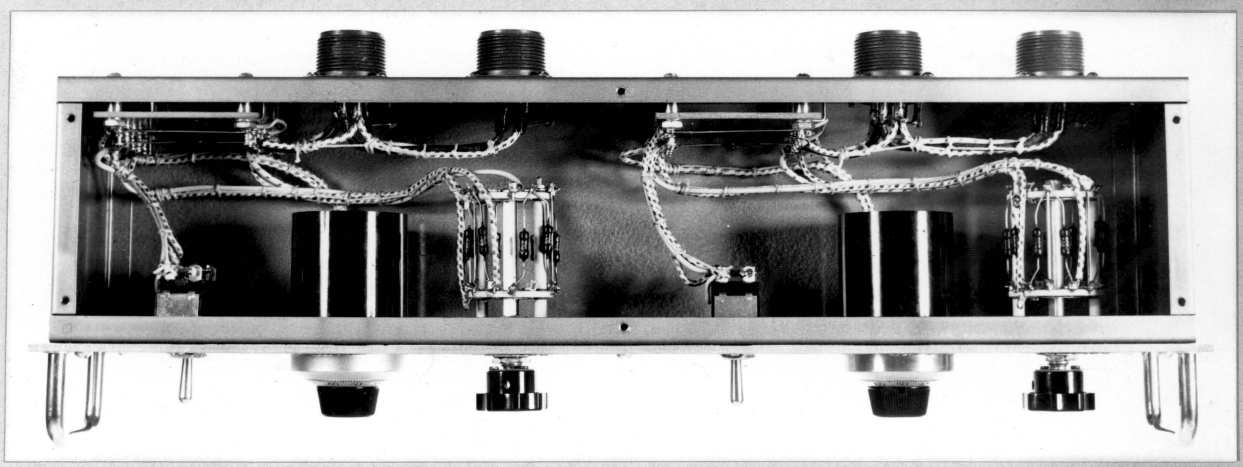
these units are 1% carbon deposit-type which have been found extremely stable in this particular application. Figure 61 shows a number of views of a completed dual type-4A unit. This unit is similar in appearance to the type-2A unit with the exception that in the latter-type binding posts rather than AN-type connectors are used on the input and output.

Figure 62 shows the wiring diagram of one of the two-arm junction circuits. A unit containing six of the circuits was constructed as shown in Figure 63. In these circuits the two external resistors R_a and R_d shown are respectively one of the strain gages attached to the test specimen and a similar unstressed dummy gage located beside the loading frame. The two internal resistors R_1 and R_2 complete the bridge circuit. Power from the bridge power supply is fed to this bridge via connector CON-2 and the unbalance voltage fed to the recorder junction unit via connector CON-1. Switch SW-1 and resistor R_c provide a means for unbalancing the bridge circuit a fixed amount to check the calibration of the recorder on that particular channel.

Figure 64 shows the wiring diagram of one of the four-arm junction circuits. A unit containing six of these circuits was constructed and Figure 65 shows a number of views of this completed unit. In these units the complete bridge circuit is outside the unit and

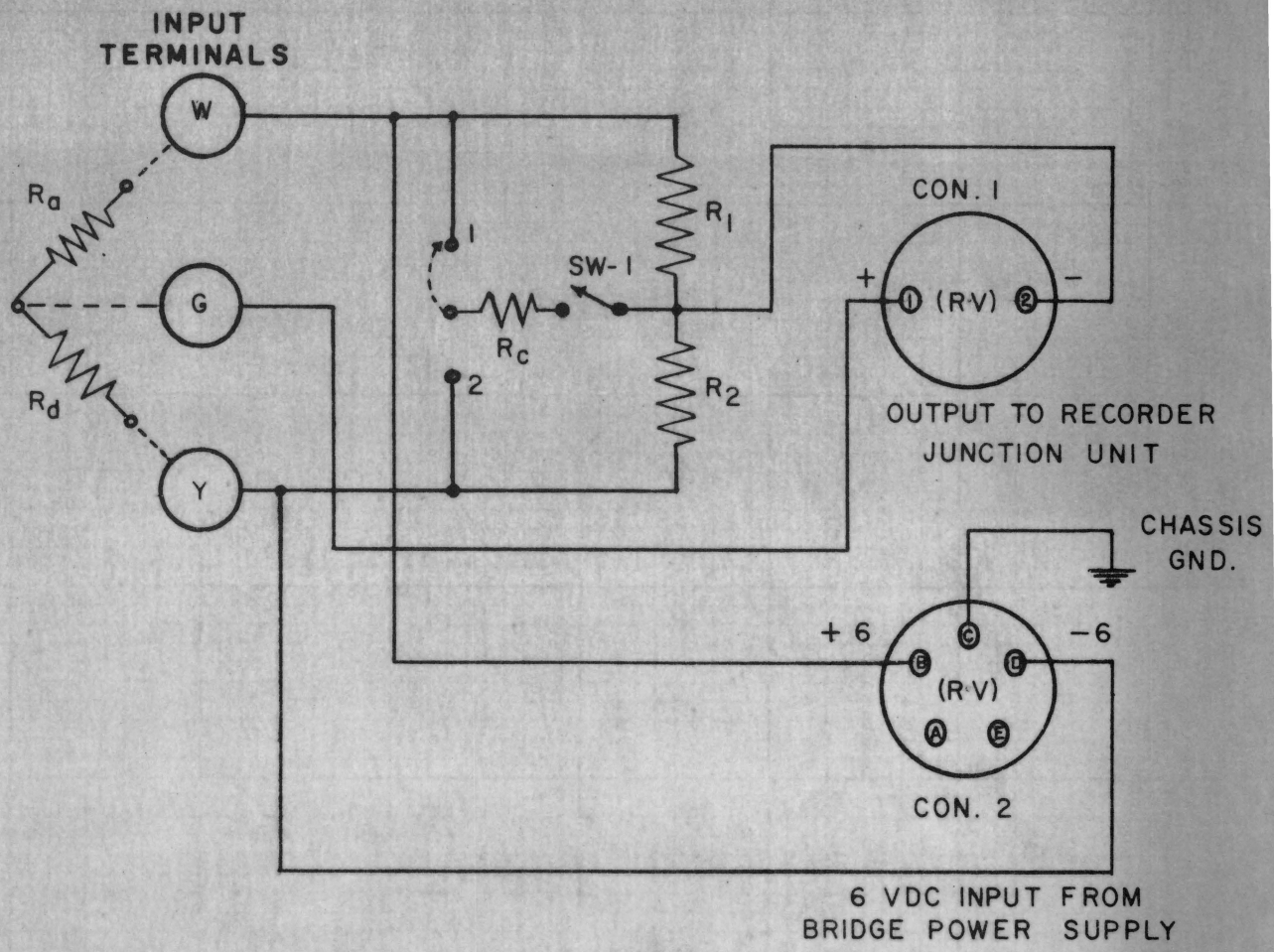


A. Front View of 4-Arm Zero Balance Unit.



B. Bottom View of 4-Arm Zero Balance Unit.

FIGURE 61 - Photographs Showing Two Views of 4-Arm Zero Balance Unit.

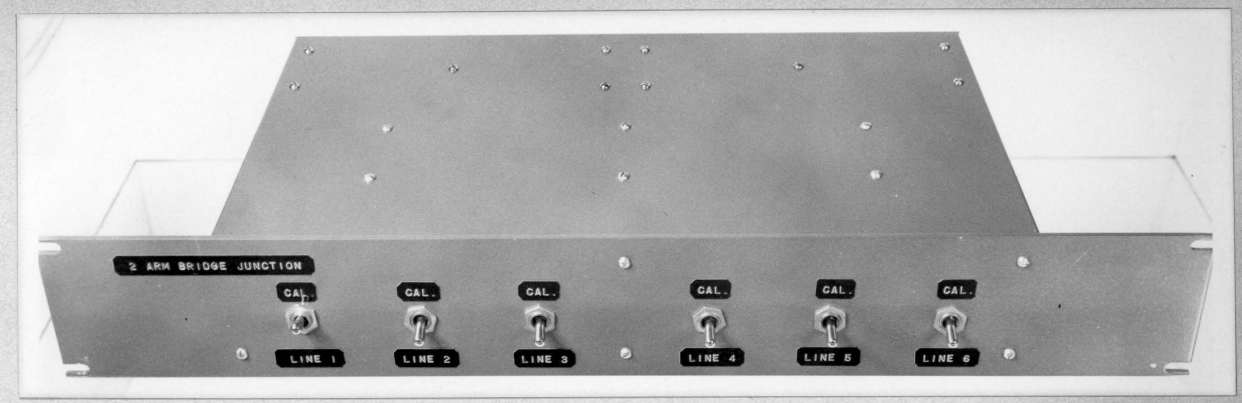


R_1 and R_2 - Wire wound resistors, Tinsley Type LF.1(2 watt)≈200 ohms, matched to ± 0.005 ohms.

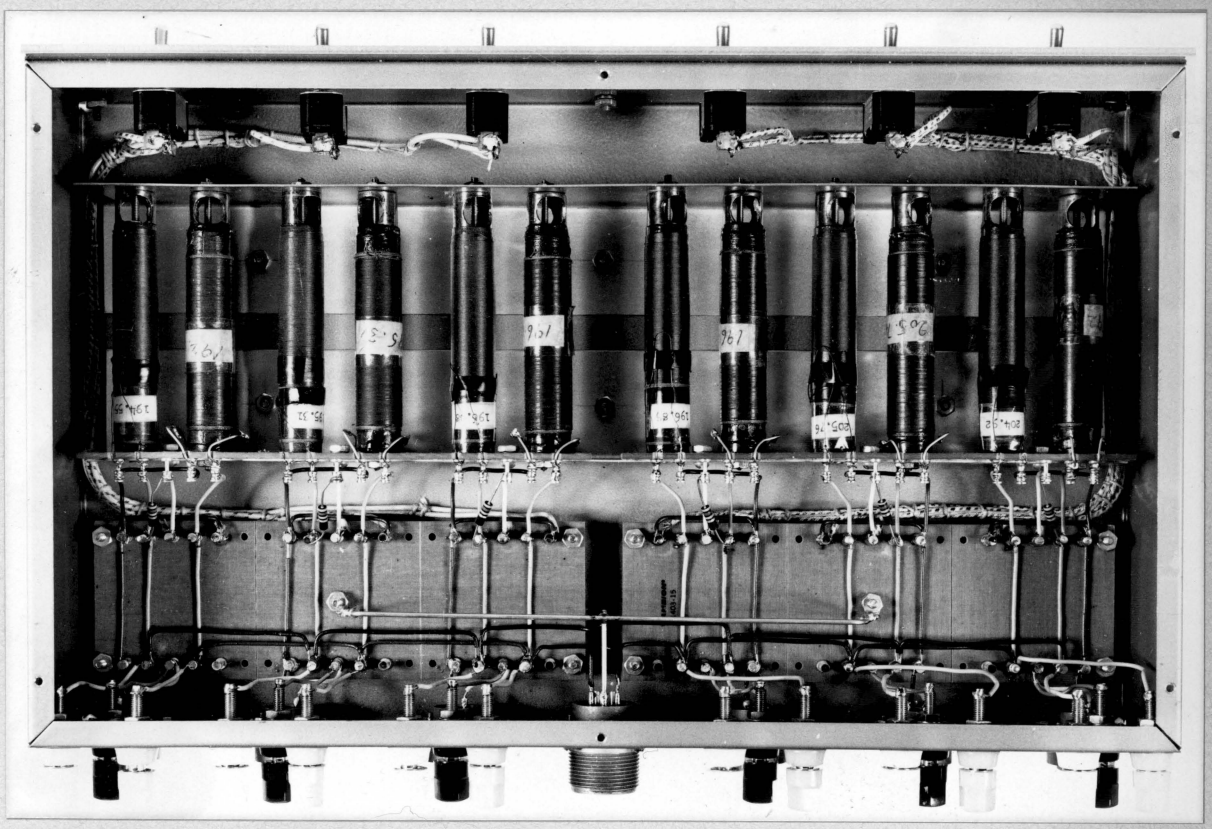
R_a and R_d - External strain gages (≈120 ohms), direct or via zero balancing units M/2A.

R_c - Calibration check resistor, 470K ohms (1/2 watt carbon type) gives approximately 20 scale divisions (1 MV) zero shift on 5 MV f.s. sensitivity

FIGURE 62 - Circuit Diagram of 2-Arm Junction Unit.

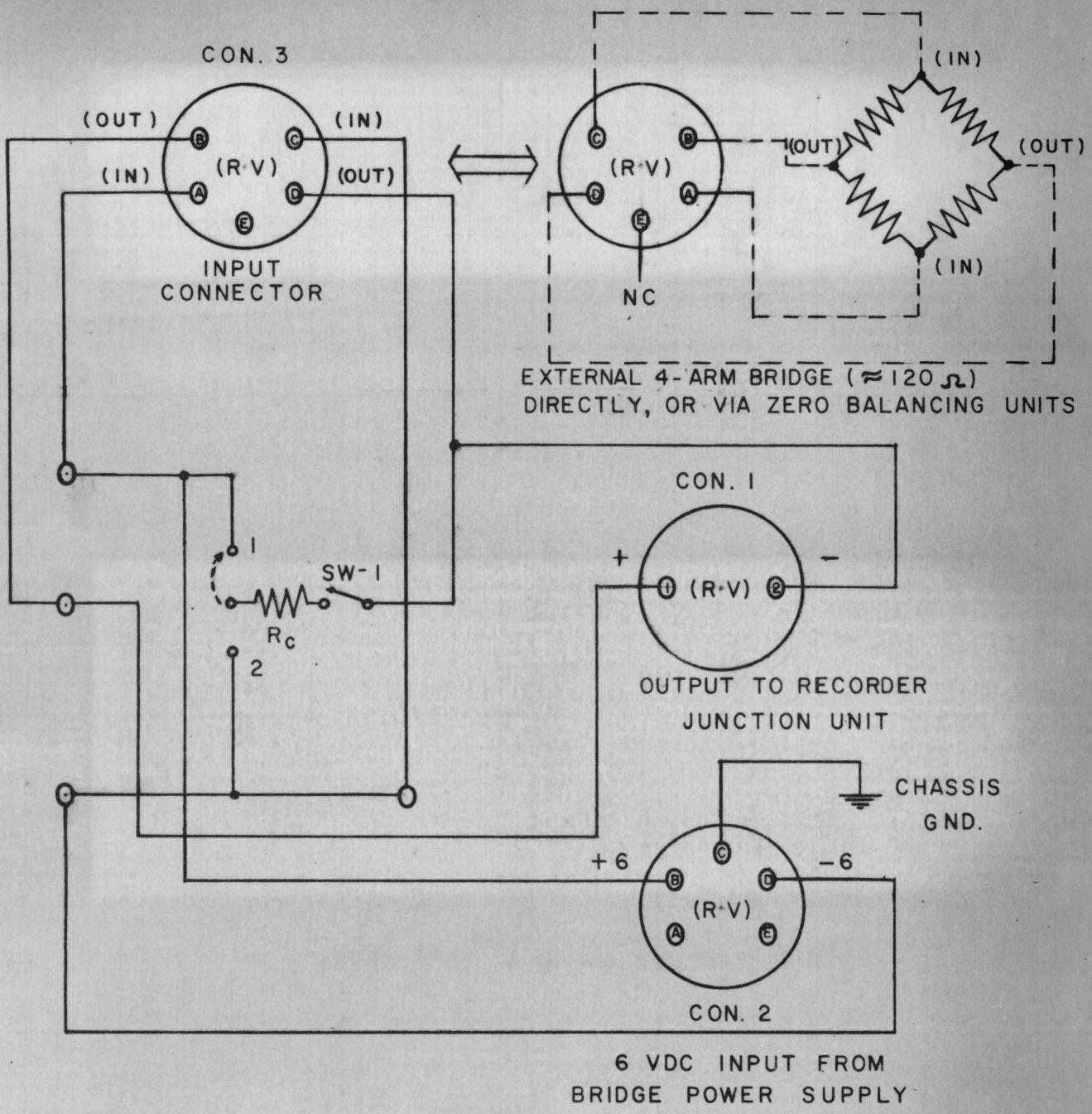


A. Front View of 2-Arm Junction Unit.



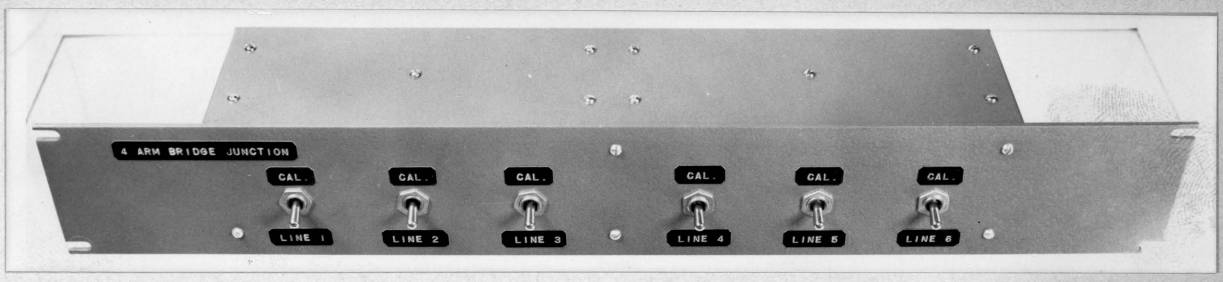
B. Bottom View of 2-Arm Junction Unit (large resistors form two arms of the completed bridge).

FIGURE 63 - Photographs Showing two Views of 2-Arm Junction Unit Containing Six Junction Circuits.

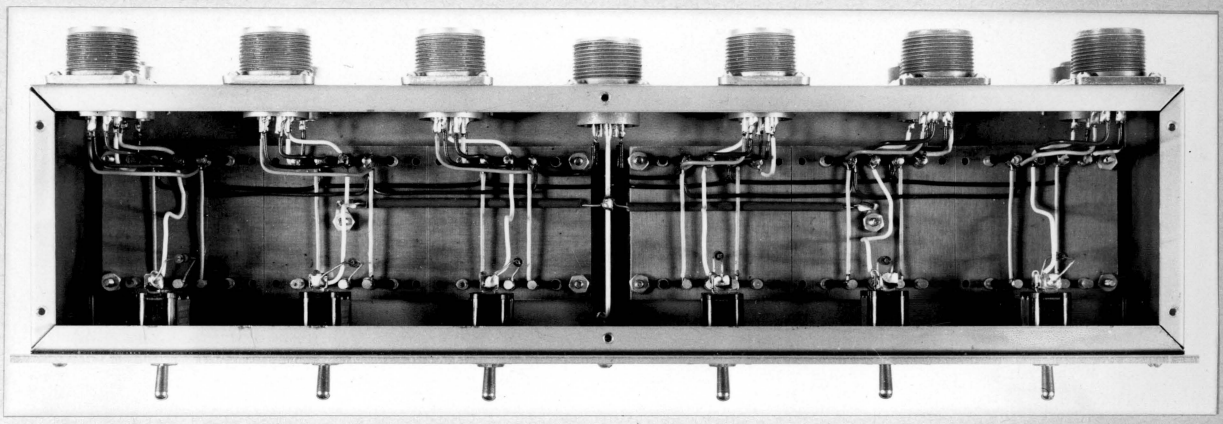


R_C - Calibration check resistor, 220K ohms (1/2 Watt carbon type gives approximately 20 scale divisions (1 MV) zero shift on 5 MV f.s. sensitivity

FIGURE 64 - Circuit Diagram of 4-Arm Junction Unit.



A. Front View of 4-Arm Junction Unit.



B. Bottom View of 4-Arm Junction Unit.

FIGURE 65 - Photographs Showing Two Views of 4-Arm Junction Unit.

is connected to it via connector CON-3. The function of the other connectors and SW-1 are the same as for the two-arm units.

(iii) Thermocouple Input Circuits

Thermocouples, which are provided to sense room and specimen temperature variation, are connected to a thermocouple reference junction unit. The voltage output of the individual thermocouple circuits are then fed via a signal conditioning unit to the appropriate connections on the recorder junction unit. Details of the reference junction and the conditioning unit are presented in a later section.

(iv) Calibration and Stability Studies*

(a) Strain Calibration

A highly stable two-arm bridge unit was constructed for strain calibration of the system. This bridge consisted of two 120 ohm strain gages attached to a steel block with a precision low resistance slide wire connected in series with one of the gages. The bridge itself was calibrated initially against a Baldwin portable strain indicator (type-N) and the slide wire calibrated in terms of strain. This unit was then attached to one of the 2-arm inputs of the recorder system and the slide wire varied over its complete range (a simulated strain of 0-700 μs), and the position of the recorder pen carriage

* Calibration and stability studies, experiments 64-1, were carried out under conditions of normal room temperature fluctuation.

was noted for a range of simulated strains. A plot of pen carriage displacement against simulated strain was found to be linear. The strain sensitivity of the system was determined from this data to be $K_e(v) = 323\,\mu s/MV$ or $K_e(d) = 16.1\,\mu s/ssd$*. A series of later checks using a "strain calibrator", developed for this purpose indicated the same sensitivity. The strain sensitivity of the system was also determined at various degrees of zero unbalance in the external bridge (necessitating various degrees of zero adjustment in the zero balance units). In all cases the same value of sensitivity was found. It was estimated that the error in the strain sensitivity factors was less than $\pm$ 2%.

(b) Load Calibration

Since no simulation method for load calibration was available it was decided to calibrate the recorder directly against a 20K load cell under actual load. The cell was connected into one of the 4-arm inputs of the recorder system and the load on the cell varied over the range 0-6630 lbs. The recorder pen carriage position was noted for various values of applied load and a plot of this data was found to be linear. The load sensitivity of the system was determined from this data and from a direct calculation based on the manufacturers

*Note that "ssd" is the abbreviation used for small scale division, which in this case represents .05MV.

quoted sensitivity for the load cell and was found to be $K_L(v) = 1633$ lbs/MV or $K_L(d) = 81.6$ lb/ssd. The experimental error in the load sensitivity factors was estimated to be less than $\pm$ 2%.

(c) Effect of Line Voltage Variations

The effect of line voltage variations on the zero point and the sensitivity of the recorder system was briefly investigated (Test 64-1). For this purpose a variac was placed in series with the 110V a-c power supplied to the recorder system. A stable 2-arm external bridge was connected to one of the 2-arm inputs and the performance of the system observed for various levels of line voltage. For line voltages in the range 105-115 volts any zero drifts or changes in sensitivity were within the reading error of the recorder itself. The overall system appeared therefore to be completely independent of the line voltage in this range.

(d) Time-Stability

The stability of the overall system over a period of time was investigated for both 2-arm and 4-arm inputs. In a 48 hour test (64-1), during which the room temperature fluctuated over the range 24.5-30°C, no long term drift was noted for either type of input. Random fluctuations in the zero point, about a relatively constant mean, were observed. These were approximately equivalent to $\pm$ 10 μs and $\pm$ 40 lbs for the strain and load channels respectively. A later test

(64-7) conducted under temperature controlled conditions of 23 ± 0.2°C also indicated no long term drift. Under these conditions the random fluctuations in the strain and load channels were reduced to the equivalent of less than ± 6 μs and ± 8.5 lbs respectively.

(e) General

Table 15 lists the general characteristics of this measurement system. It should be noted that in the stability experiments what is actually being determined is the overall stability of the measurement system and the external transducers. As a result the stability of the measurement system may be actually somewhat higher than that quoted.

TABLE 15

Characteristics of 12-Channel "Slow" Y-T Recorder System

Chart Speed (direct)	----------	40-600 mm/hr.
Basic Sensitivity	----------	5 MV full scale
Chart Readability	----------	± 0.1 ssd (± 5μv)
Strain Sensitivity	----------	(K_e(v) = 323 μs/MV (K_e(d) = 16.1 μs/ssd
Load Sensitivity (20K load cell, 6V d-c excitation)	----------	(K_L(v) = 1633 lbs/MV (K_L(d) = 81.6 lbs/ssd
Line Voltage Effect (105-115 volts)	----------	Nil
Long Term Drift (48 hour test)	----------	Nil
Zero Fluctuation (Temp 23 ± 0.2°C, 48 hour test)	----------	(Δe(d) = ± 6 μs (ΔL(d) = ± 8.5 lbs.

1.5.5 2-Channel "Fast" Y-T Recorder System

This system incorporates a Sanborn model 60-1300 dual pen recorder equipped with two strain gage amplifiers* (model 64-500B), two individual four-arm zero balancing units (which have been described in the previous section), and a marker-pen control (to allow the initiation of important operations to be indicated on the recorder chart by the action of a third recorder pen called the marker pen). This system provides facilities for plotting of axial strain and axial load versus time during the incremental loading stages of creep experiments. The behavior of the material during the actual loading period and the transient period which follows it may be investigated in detail with this arrangement. Figure 66 illustrates a block diagram of this system and a photograph of the completed system is shown in Figure 67.

The sensitivity of the recording system was measured in a manner similar to that discussed for the 12-channel system. At full gain setting of the strain gage amplifiers the strain sensitivity was found to be $K_e(d) = 3.1\ \mu s/ssd$ and the load sensitivity (using a 20K load cell) found to be $K_L(d) = 25.4$ lb/ssd. One small scale division (ssd) on the chart paper being 1.0 mm. It was found that if both

*Further details on the operation of the recorder and the strain gage amplifiers are given in the following Sanborn manuals: Instruction Manual - Sanborn Twin-Viso, recorder Unit, Model 60 and Instruction Manual - Sanborn Strain Gage Amplifier, Model 64-500B.

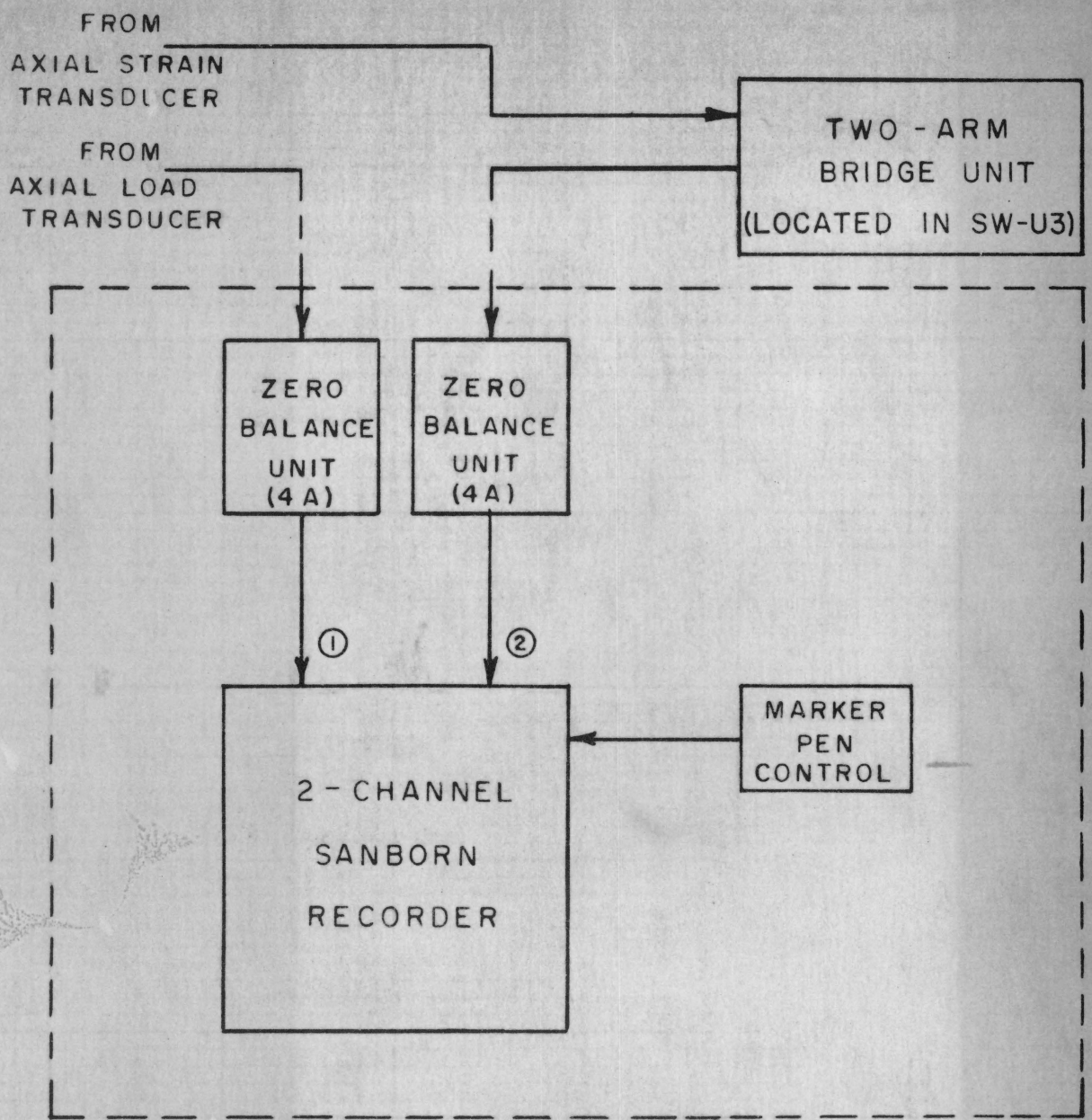


FIGURE 66 - Block Diagram of 2-Channel "Fast" Y-T Recorder System.

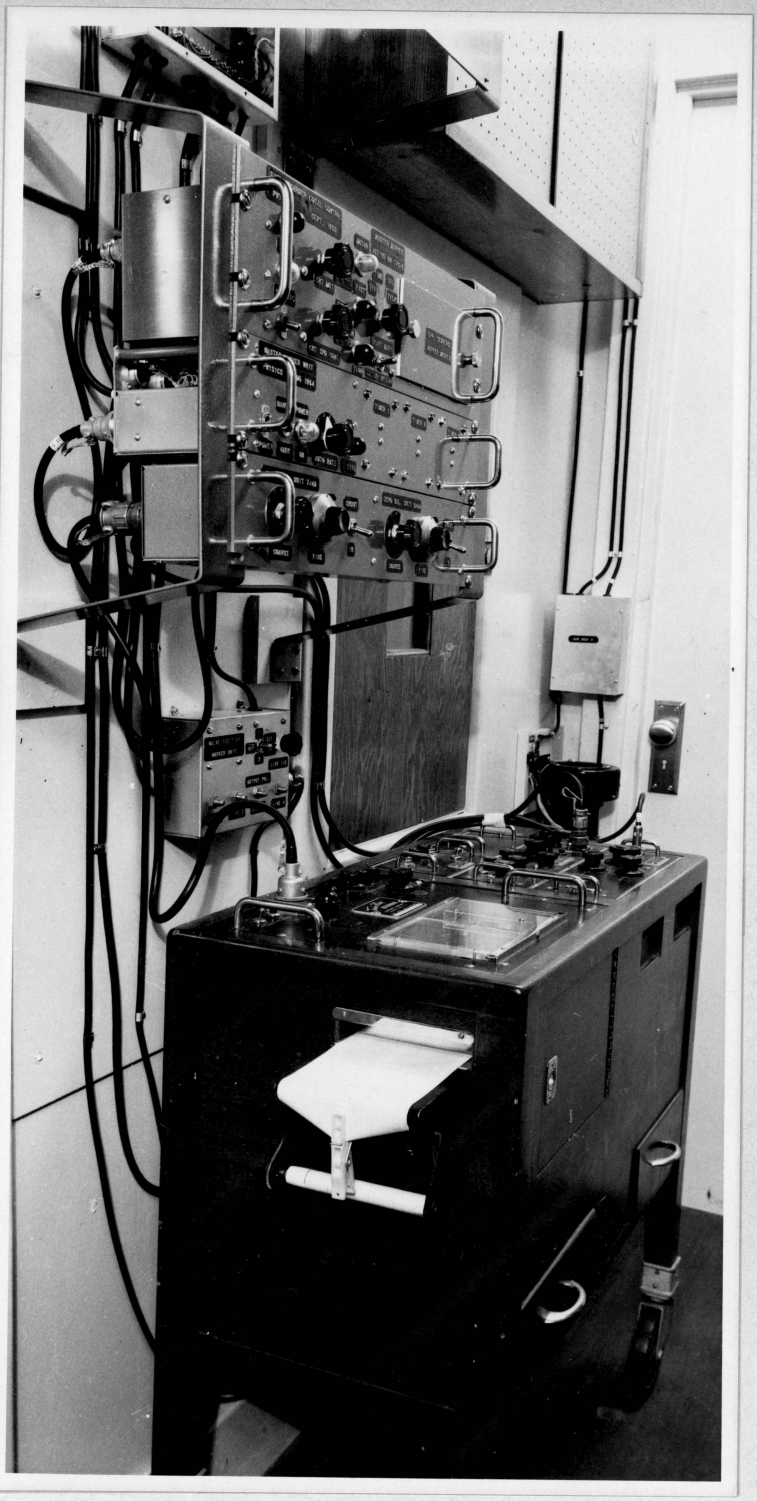


FIGURE 67 - Photograph Showing Two-Channel "Fast" Y-T Recorder System.

channels were in use at the same time the noise level on both channels increased necessitating operation at lower sensitivities. The system was found to exhibit some long term zero drift and variation in sensitivity even after a relatively long warm up period. The magnitudes of these variations were determined using the internal zero check and sensitivity check switches on the amplifiers, and it was found that over short periods of time (up to 1 hour) these effects were either not serious or could be easily corrected mathematically. Table 16 lists the general characteristics of this measurement system.

TABLE 16

Characteristics of 2-Channel
"Fast" Y-T Recorder System

Chart Speed	--------	0.5 - 100 mm/sec
Chart Readability	--------	$\pm$ 0.1 ssd
Strain Sensitivity (Maximum)	--------	$K_e(d) = 3.1\ \mu s/ssd$
Load Sensitivity (Maximum, 20K load cell)	--------	$K_L(d) = 25.4$ lb/ssd
Response Time (Full scale deflection)	--------	15 milliseconds
Marker Pulse Rate	--------	1 per second

1.5.6 Single Channel Y-XT Recorder System

Figure 68 shows a block diagram of this system and a photograph of the completed system is shown in Figure 69. The recorder section consists of a Moseley model 2DR-2 single channel Y-XT recorder*. In this system the Y-axis may be driven by a voltage proportional to strain, stress, pressure etc, and the X-axis may be driven similarly or from an internal time-based voltage. The recorder itself has a maximum sensitivity on the X- and Y-axis of 0.5 MV/inch or 50 μV/ssd. The sweep rate in the Y-T mode may be selected from 1.2 to 120 in./min.

Strain or load transducers are connected to the system via an input selector unit. Switches in this unit make it possible to display either strain or load on the Y-axis of the recorder, and either load or time on the X-axis. Thus the system may easily be set to plot load versus time, strain versus time, or strain versus load curves.

The X- and Y-axis outputs from the selector unit are fed directly to an X- and Y-axis bridge located in a dual bridge unit. Excitation voltage (6V d-c) is supplied to the transducers at this point

* Further details on the operation of the recorder itself are given in "Operating and Maintenance Manual, Model 2DR-2 Autograf X-Y Recorder", F.L. Moseley & Co., Pasadena, California.

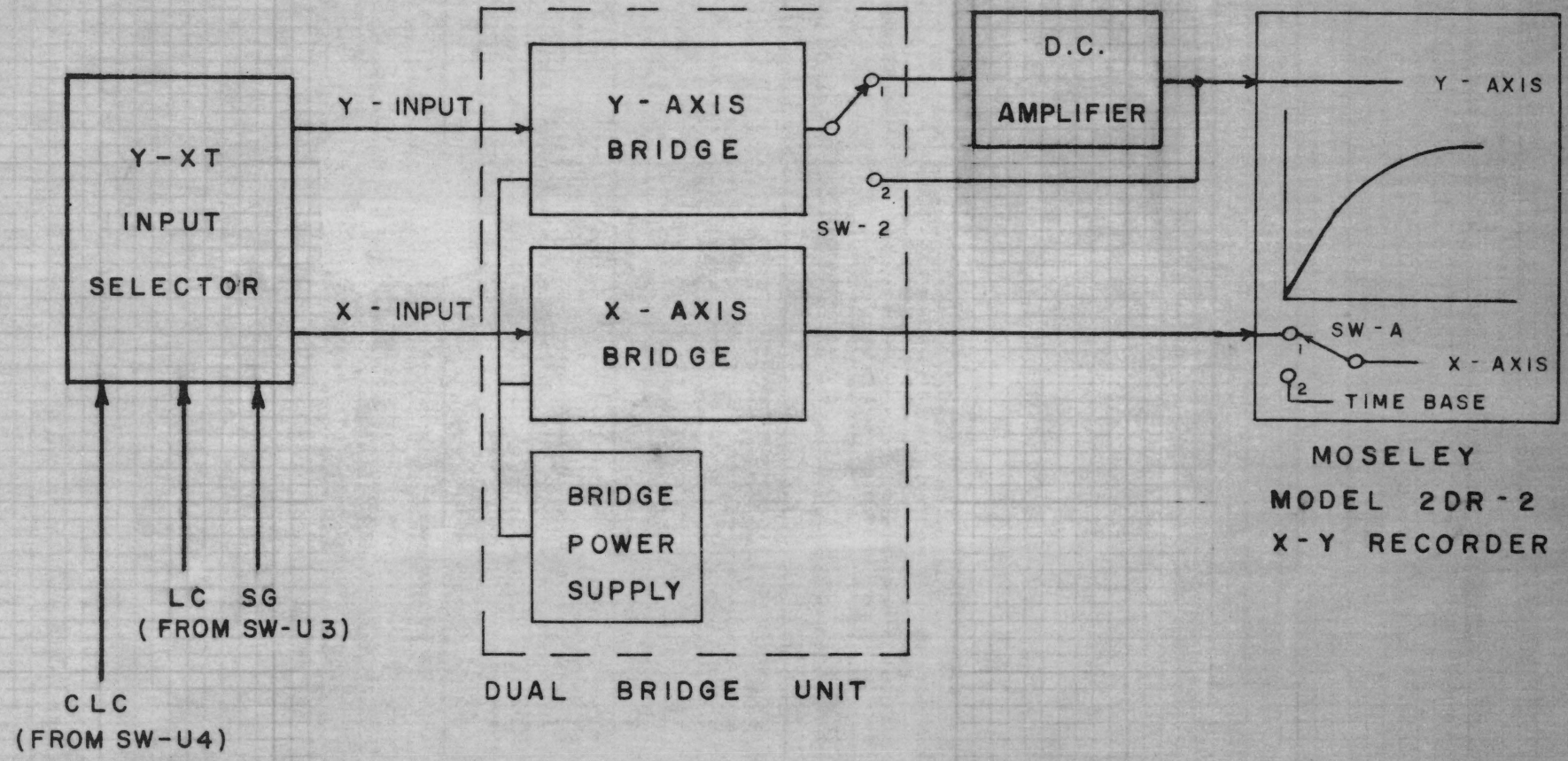


FIGURE 68 - Block Diagram of Single Channel Y-XT Recorder System.



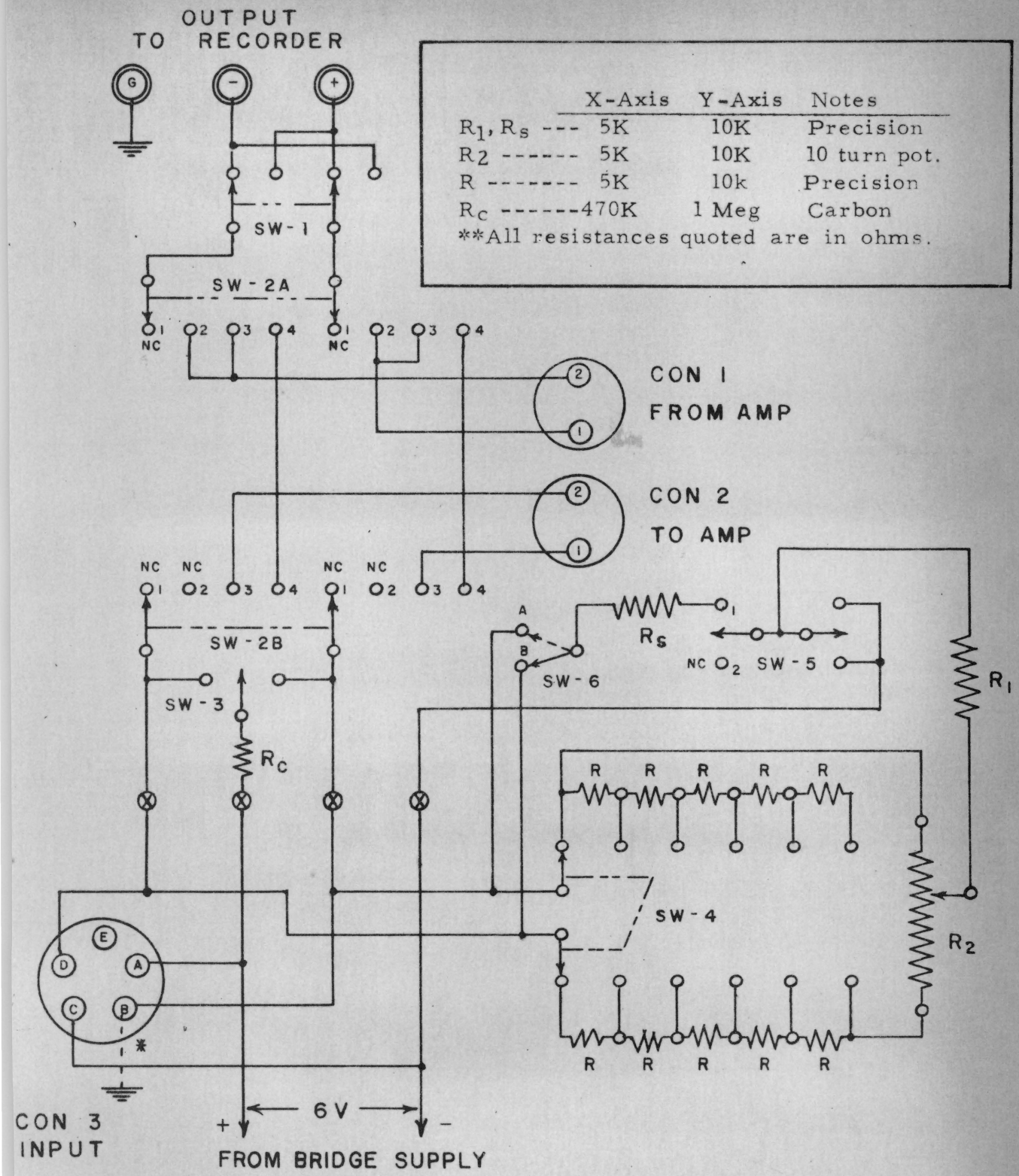
FIGURE 69 - Photograph Showing Front View of Completed Y-XT Recorder System.

by a highly stable power supply* which is also incorporated in the dual bridge unit. Figure 70 shows the circuit diagram for one of these bridge circuits. The connections from the particular transducer, as selected by the selector unit, enter the bridge via connector CON-3. The excitation voltage is applied to the transducer across pins A and C and the transducer output voltage is detected scross pins B and D. This unbalance voltage (proportional to the magnitude of the load or strain) is carried via switches SW-2 and SW-1 to the output of the unit. SW-1 allows the polarity of the output signal to be selected. Various positions of SW-2 may be selected so that the unbalance voltage either goes directly to the output terminals (switch position 4) or indirectly via a high stability D.C. amplifier** (switch position 3). The output terminals of the unit are connected directly to the input terminals of the Moseley recorder. The resistors R_1, R_2, R_s and R, and the switches SW-4, SW-5 and SW-6 are associated with a zero balance circuit contained in each bridge. The operation of this circuit has been discussed earlier when considering the 12-channel recorder system. The purpose of SW-3 and R_c is to provide an available fixed bridge unbalance to allow a periodic check to be made on the overall sensitivity of the system. A number of views

---

* Valor power supply, model MB 6.3KO.5, rated at a stability of better than 0.1 per cent.

** A Keithley model 150AR d-c amplifier has been utilized to date for this purpose. This unit provides a number of calibrated gains ranging from 10 to 10^6, and is capable of extremely low drift, low noise operation.



	X-Axis	Y-Axis	Notes
R_1, R_S ---	5K	10K	Precision
R_2 ------	5K	10K	10 turn pot.
R -------	5K	10k	Precision
R_C ------	470K	1 Meg	Carbon

**All resistances quoted are in ohms.

FIGURE 70 - Circuit Diagram of Dual Bridge Unit.

of the dual bridge unit and the selector unit are shown in Figure 71. To-date this recorder system has been utilized mainly for recording of very low level strains (2-100 μs) associated with creep experiments on Wombeyan marble. For these experiments the Y-axis of the recorder has been used on its 50 MV/inch range and the d-c amplifier has been operated at a gain of 1000. Under these conditions the relationship of recorder deflection to simulated input strain was found to be $K_e(d) = 1.65\ \mu s/ssd$. This appears to be the optimum combination of recorder and amplifier settings for low noise operation. Table 17 lists the general characteristics of this measurement system.

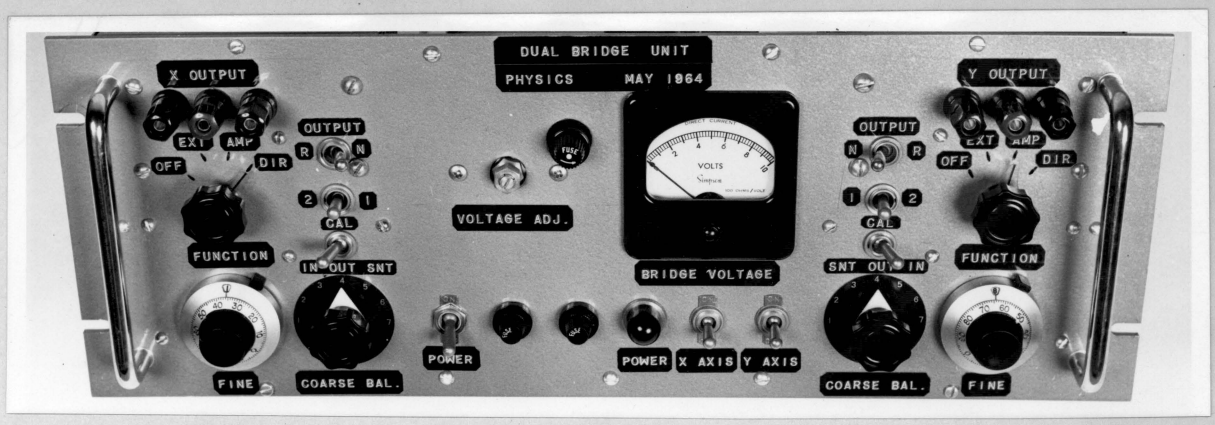
TABLE 17

Characteristics of Y-XT Recorder System

Time Base	--------	1.2 - 120 in./min
Chart Readability	--------	$\pm$ 0.1 ssd.
Strain Sensitivity	--------	$K_e(d) = 1.65\ \mu s/ssd$
Response Time (Full scale deflection)	--------	0.5 seconds

1.5.7 Development of Marker System

During some stages of certain deformation experiments strain and load data are being recorded on all three recording systems. In order to properly correlate these recordings with respect to time, it was found necessary to develop a system which would simultaneously



A. Front View of Dual Bridge Unit.



B. Front View of Selecter/Marker Unit.

FIGURE 71 - Photographs Showing Various Views of Dual Bridge and Selecter/Marker Unit.

put marker points on all three recorder charts at fixed intervals of time, throughout the deformation experiment. Figure 72 shows a block diagram of the system developed for this purpose. It consists of a master marker unit, and a remote marker unit located at each of the three recorders. The master marker unit consists of a set of three timer units each consisting of two small microswitches operated by a double-deck cam (one deck having 6 detents the other having 1 detent) driven by a small synchronous motor. The motor in each timer unit operates at a different speed and the speeds of the three motors were selected so that the unit would provide a wide range of pulse rates.

When the motor in a specific timer is activated it causes the cam arrangement to rotate switching the associated microswitch on and off at a rate dependent on the motor speed and the number of detents in the timing cam. The microswitch itself activates a relay in the master marker unit which in turn operates a relay in each of the three remote marker units which are located at the respective recorders. Figure 73 shows a number of views of the master marker unit. Only one of the timer units is shown installed. Figure 73C in particular is an enlarged view of this timer showing the double-deck cam arrangement and the two microswitches.

The actual method of obtaining a timing mark on the chart paper of the three recorders is different in each case. The

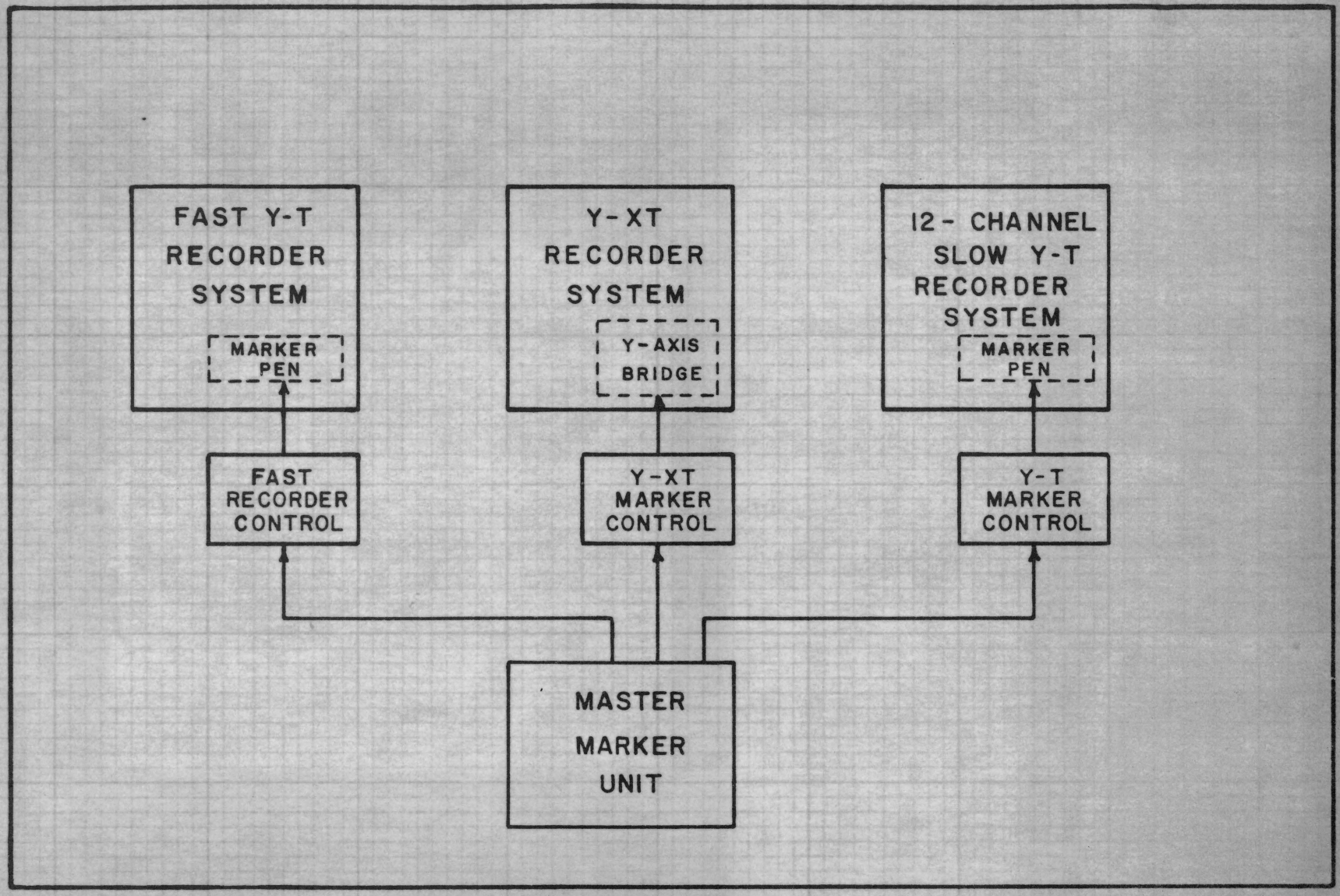
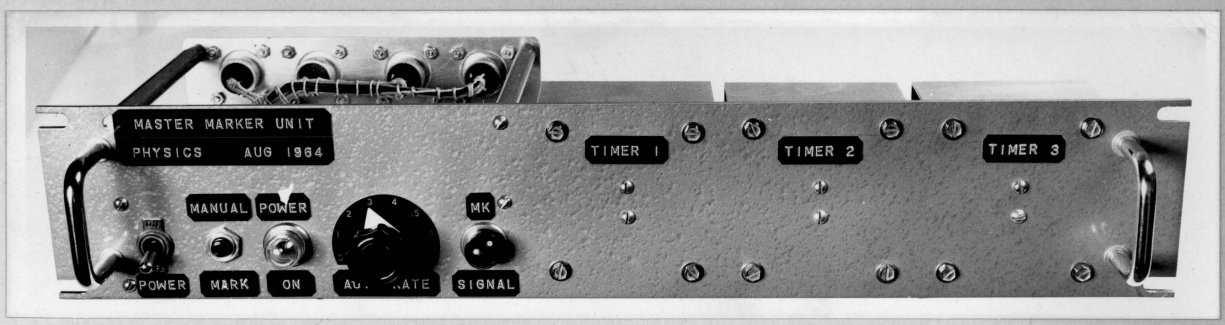
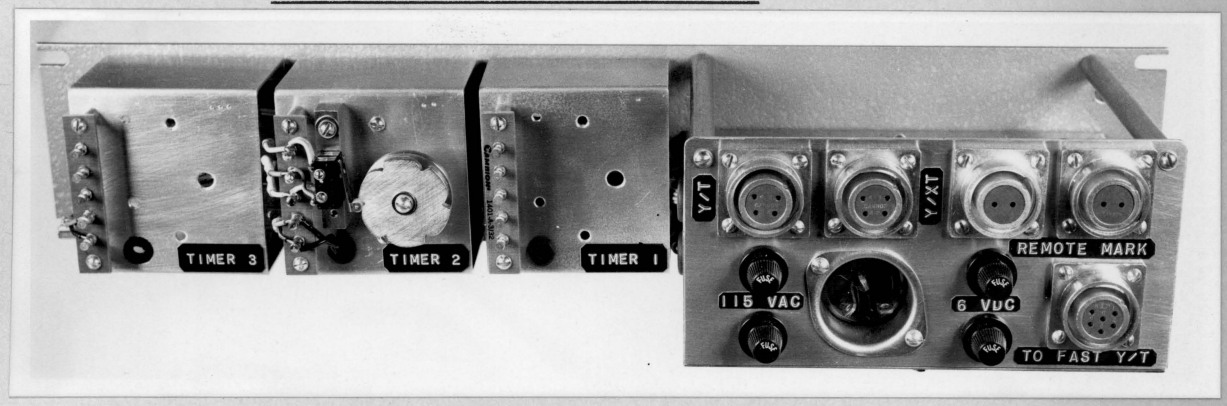


FIGURE 72 - Block Diagram of Marker System.



A. Front View of Marker Unit.



B. Rear View of Marker Unit.



C. Enlarged View of Timer.

FIGURE 73 - Photographs Showing Master Marker Unit.

2-channel "fast" Y-T recorder presents no difficulties since it is equipped with a special marker pen which is activated directly by the marker signal. It was necessary to construct a special marker pen for the 12-channel "slow" Y-T recorder. Basically this consisted of a small six volt relay modified to activate an ink-type pen from a Brush recorder. This relay and the attached pen was mounted at the top corner of the recorder frame so that the pen rested on the chart paper near its extreme right edge. The pen relay is connected to the remote marker unit associated with this recorder and is activated each time the unit receives a signal from the master unit. The method of obtaining a timing mark on the Y-XT recorder chart was more involved since in this case the paper was fixed and the time axis itself moved. The method finally decided on involved introducing a small, short period, unbalance in the bridge circuit associated with the Y-axis signal to the recorder. A high value resistance was connected in series with the contacts of a normally open relay across one arm of the Y-axis bridge circuit. This relay was triggered closed each time it received a signal from the master marker unit, which caused a sudden, short period jump in the Y-axis deflection of the recorder. This method produced well defined marker points on the curve without otherwise disturbing the recording. A number of deformation experiments on Wombeyan marble have been conducted using this marker system. For

these experiments a marker rate of one per minute was found most satisfactory.

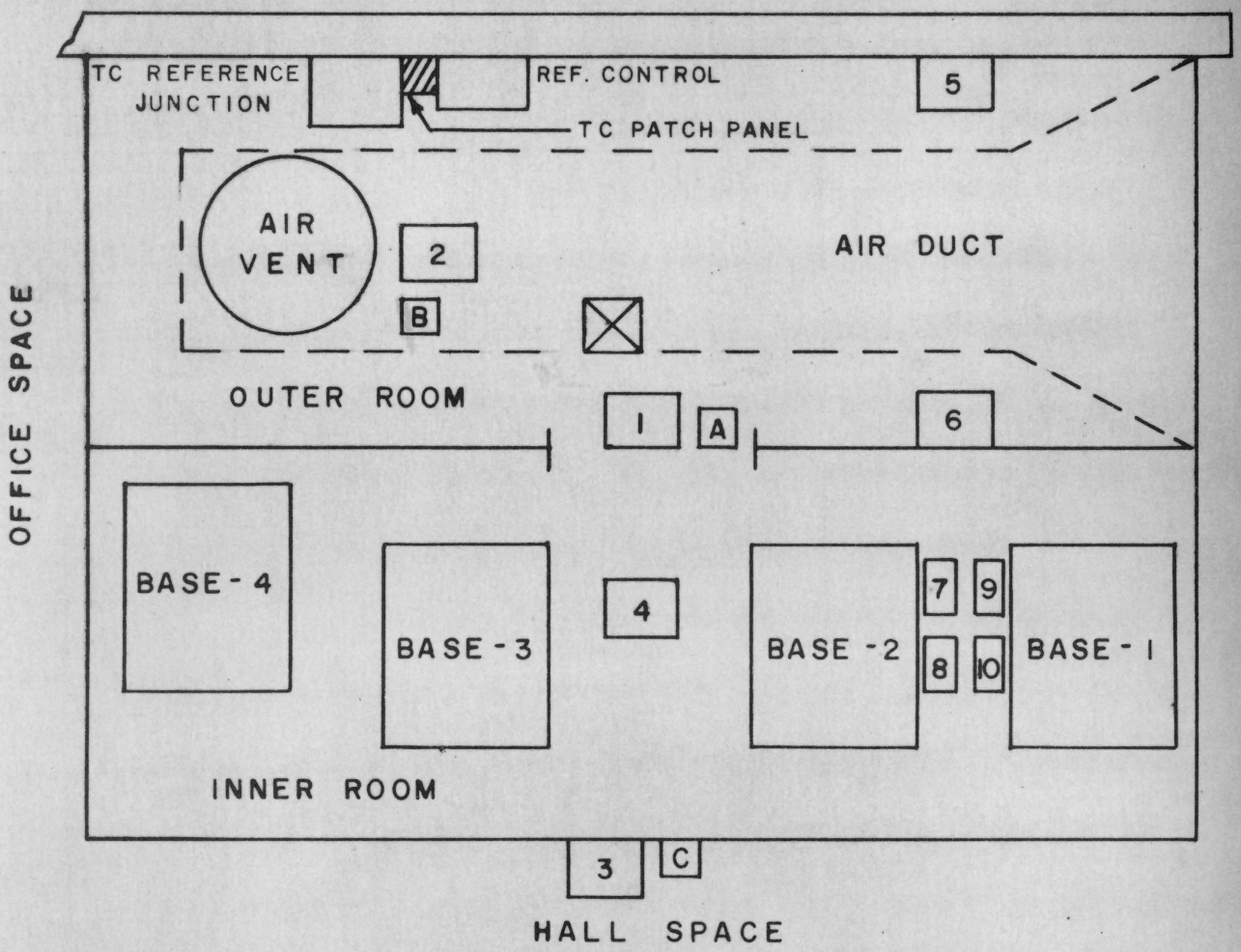
1.6 Temperature Measurement System

1.6.1 General

Since the temperature control system was designed to maintain the temperature of the test enclosure within ± 1/10°C it was considered desirable to develop a temperature measurement system capable of monitoring temperatures, at various locations within the enclosure, to at least ± 1/20°C. Since it was particularly important to be capable of sensing any long term drift of the control temperature an extremely stable system was required. With this stability requirement in mind it was decided to employ thermocouple-type temperature transducers. Lion (1959) and Cermi and Foster (1962) discuss thermocouples and the design of thermocouple signal conditioning circuits in detail. Considering the temperature range involved (15-40°C) copper-constantan thermocouples were considered to be the most satisfactory. These were manufactured by the writer from standard thermocouple wire*.

Figure 74 shows a floor plan of the test enclosure which includes the locations of the various parts of the temperature

* Type GG-18-DT, copper-constantan thermocouple wire, 18 gauge B & S, solid, fibre glass insulated. Manufactured by the Thermo Electric Company, Inc.



1.	Thermocouple Measuring Control Temperature (T_c).
2.	Thermocouple Measuring Duct Discharge Temperature (T_D)
3.	Thermocouple Measuring Hall Temperature (T_o)
4.	Thermocouple Measuring Inner Room Temperature (T_{in})
5,6	Spare Thermocouple Connections.
7-10	Specimen Thermocouple Connections.
A	Room Thermostat (TH_1)
B	Duct Discharge Thermostat (TH_2)
C	Hall Thermostat (TH_3).

FIGURE 74 - Location of Temperature Monitoring Facilities in Test Enclosure.

measurement system. The location of three thermostats (TH_1, TH_2 and TH_3) associated with the temperature control system are also indicated. Four permanent thermocouples (T-1, -2, -3 and -4) were installed for the measurement of control temperature (T_c), duct discharge temperature (T_D), hall temperature (T_o) and inner room temperature (T_{in}). Thermocouple connectors were installed at the locations marked 5 and 6 for possible use in temperature stability of various parts of the control and measurement system. A set of four similar connectors marked 7 to 10 were installed between loading frame bases 1 and 2 for measurement of specimen temperature.

Figure 75 shows a block diagram of the temperature measurement system. It consists of a thermocouple patch panel, a reference junction unit, and a signal conditioning unit. Connections from each of the various thermocouple locations are connected via thermocouple lead wire* to a dual female TC connector+ on the patch panel (marked T-1 to T-10). The thermocouple reference unit located near the patch panel contains a set of six reference junctions which are held at a fixed temperature. Patch cables connected to the junction unit allow various thermocouples to be connected into the reference unit.

---

* Type GGF-18-D, copper-constantan thermocouple lead wire, 18 gauge B & S, stranded, fibre glass insulated. Manufactured by the Thermo Electric Company, Inc.

+ TC connectors are made from thermocouple metals. Jack; type -12JB, plug; type-2PSS manufactured by Thermo Electric Company, Inc.

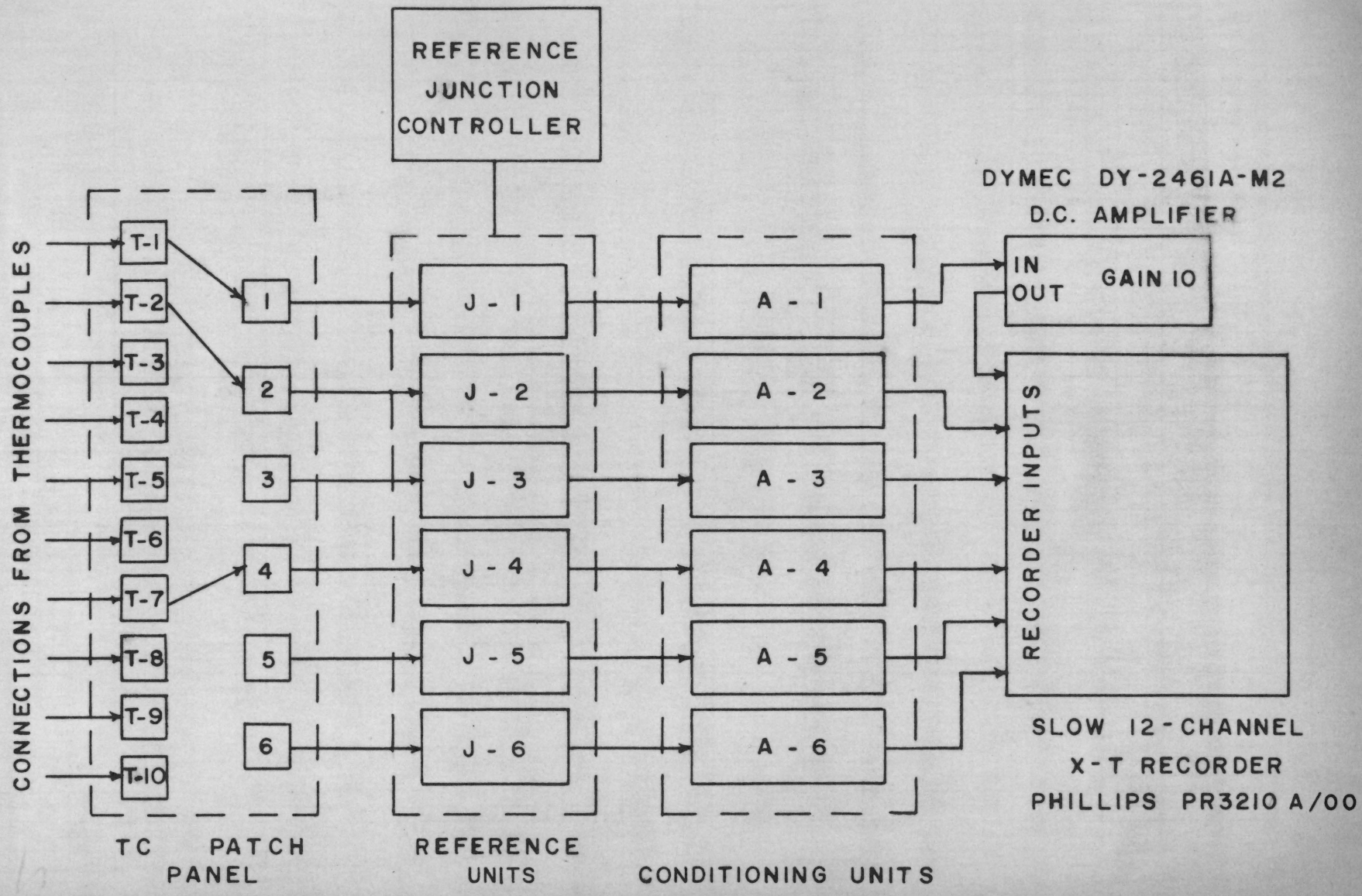


FIGURE 75 - Block Diagram of Temperature Measurement System.

The outputs from the reference junction unit are connected to a signal conditioning unit located in the 12-channel recorder system rack and the outputs from the conditioning unit are fed directly to the recorder for display. In cases where greater sensitivity is desired a high stability d-c amplifier* may be inserted in the circuit between the conditioning unit and the recorder.

Figure 76 shows a simplified circuit of the thermocouple measurement system indicating the relationship of the various sections. The voltage (V_o) observed by the recorder is given by

$$V_o = V_m - V_j \pm V_{zb} \pm V_c \qquad (32),$$

where V_m is the thermal emf produced in the junction thermocouple (dependent on junction temperature), V_{zb} is the emf induced in the conditioning circuit in order to position the recorder pen to a convenient location, and V_c is the small emf induced in the conditioning circuit for purpose of determining the overall sensitivity of the measurement system. It is important to note that if a stability of $\pm$ 1/20°C is required in temperature measurement, then an equivalent stability is required in the junction unit, the conditioning circuits, and in the d-c amplifier if it is employed.

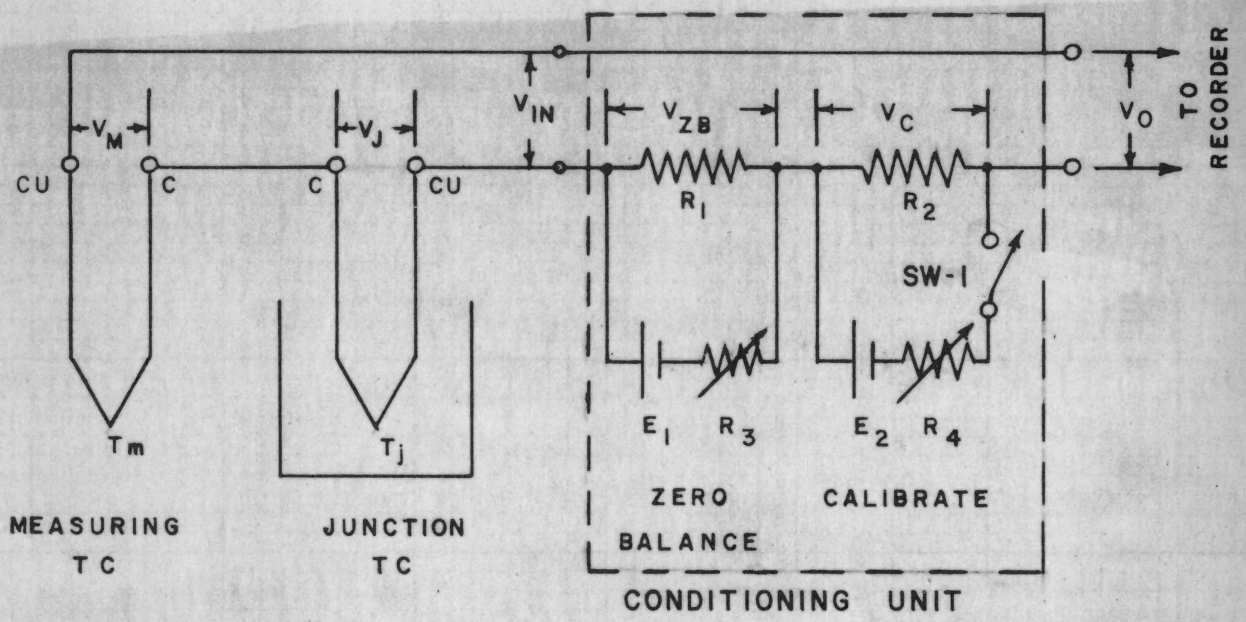
---

* Dymec model 2460A amplifier with plug-in type 2416A-M2 gain unit.

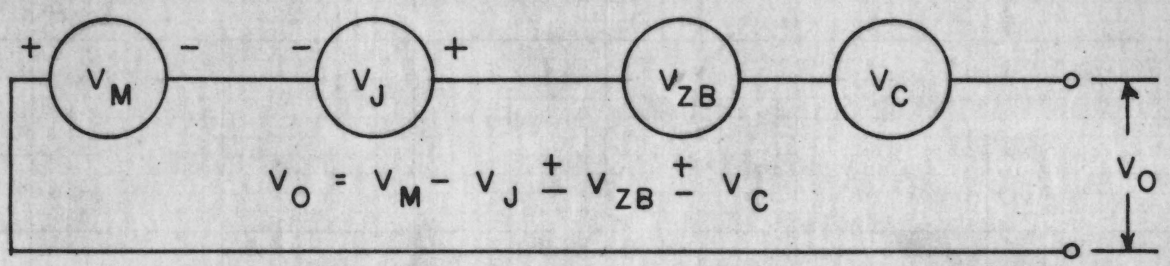
1.6.2 Reference Junction Unit

Figure 77 shows a cross-section of the reference junction unit. Basically it consists of a bundle of six copper-constantan thermocouples immersed in a vessel of oil which is held at a fixed temperature. This temperature is maintained constant to $\pm$ .05°C, at a value of approximately 42°C, by a heater immersed in the oil and controlled by a high sensitivity mercury-type thermoregulator*. A motor driven stirrer operates continuously to prevent the development of thermal gradients in the oil bath. The circuit of the junction temperature control system is shown in Figure 78. The control thermoregulator is connected to terminals (4) and (5), and the heater to terminals (F) and (G) as shown. If the junction temperature is below the control point relay RL-1 will be in the position shown (high current) and power to the heater is controlled by variac VAR-2. Once the control point is reached the thermoregulator effectively provides a short circuit across (4) and (5) which switches RL-1 into its other position (low current). Power to the heater is now supplied from another source and its magnitude is controlled by the setting of resistor R_s. The system thus provides two heating rates one (low current) to maintain the junction temperature just below the control point and the other (high current) to

* Type 4-200, Metastatic Mercury thermoregulator, manufactured by American Instrument Co. Inc.



A. ELECTRICAL CIRCUIT



B. EQUIVALENT CIRCUIT

FIGURE 76 - Simplified Circuit Of Temperature Measurement System.

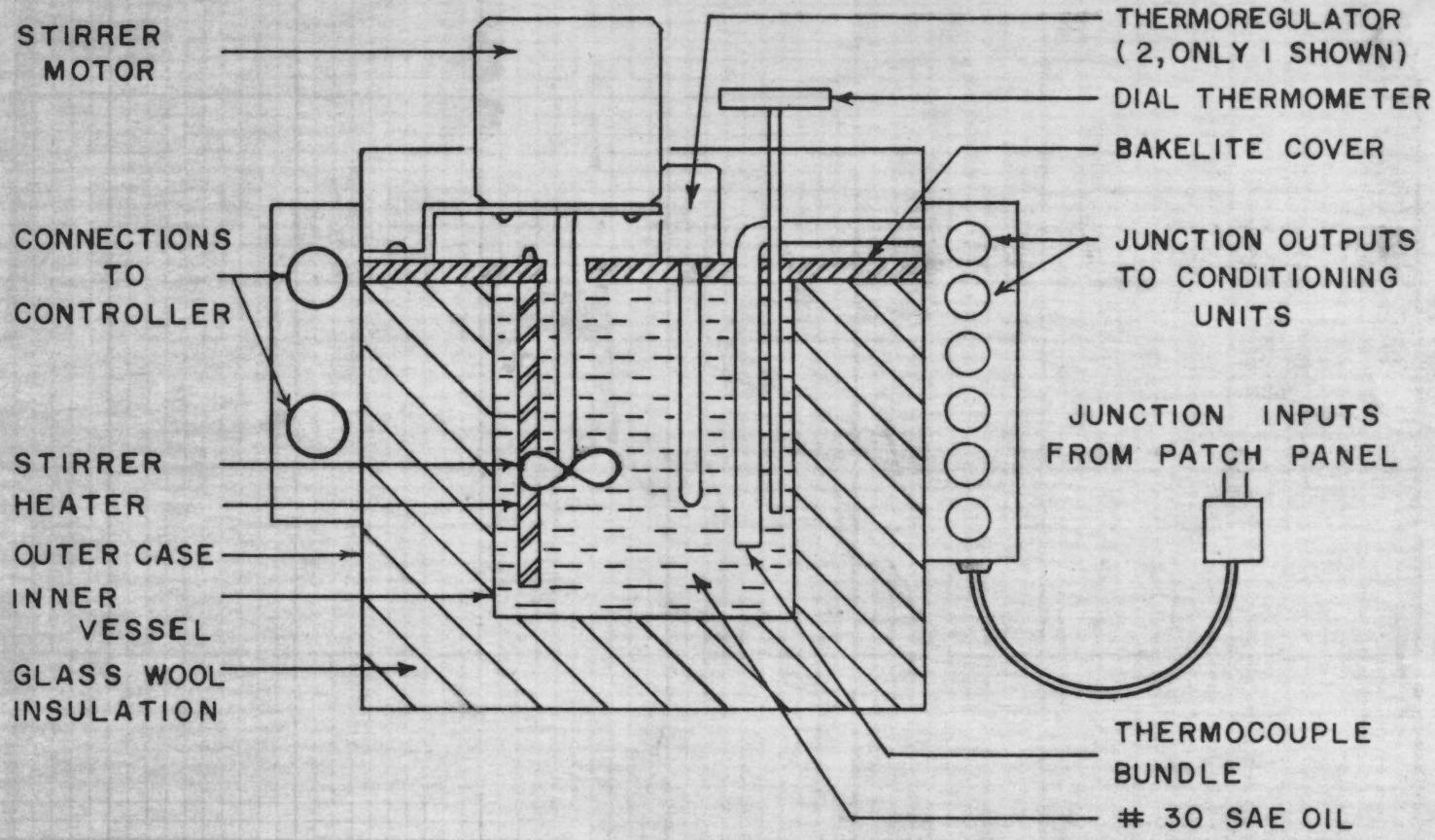
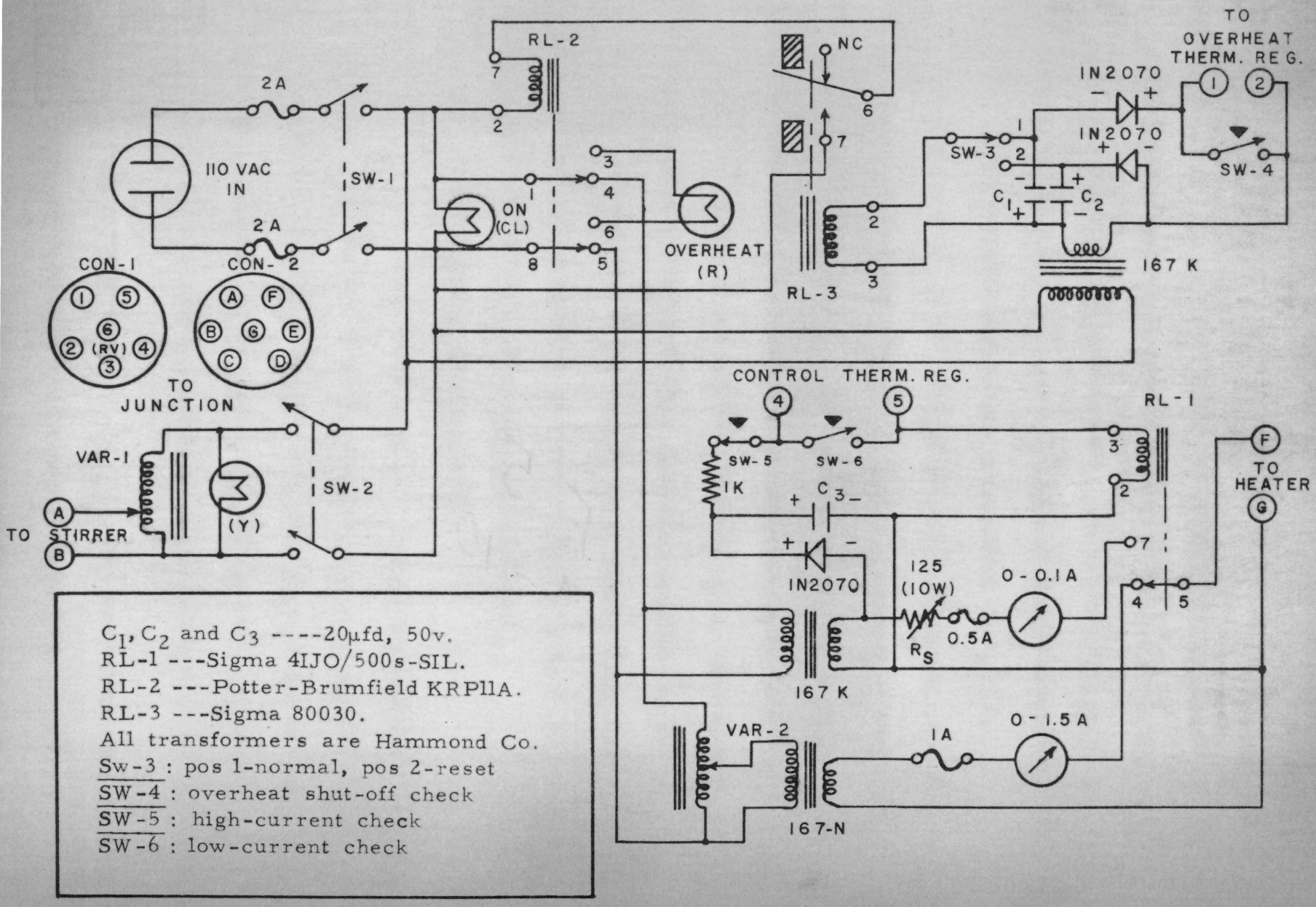


FIGURE 77 - Construction Details of Reference Junction Unit.



C_1, C_2 and C_3 ----20μfd, 50v.
RL-1 ---Sigma 4IJO/500s-SIL.
RL-2 ---Potter-Brumfield KRPllA.
RL-3 ---Sigma 80030.
All transformers are Hammond Co.
Sw-3 : pos 1-normal, pos 2-reset
SW-4 : overheat shut-off check
SW-5 : high-current check
SW-6 : low-current check

FIGURE 78 - Circuit Diagram for Reference Junction Controller.

add sufficient heat, when required, to maintain the temperature at the control point.

A second thermoregulator unit, connected across terminals (1) and (2), is also immersed in the oil bath and is set a few degrees above the control point. This unit and the associated circuit (Relay RL-3 etc.) provide overheat protection for the junction unit. If the control temperature is exceeded, due to some circuit malfunction, this circuit shuts-off all power to the heaters until the trouble is corrected. The stirrer motor is connected to the controller at terminals (A) and (B) and its speed is controlled by variac VAR-1. Figure 79 shows a top view of the reference junction unit, and Figure 80 shows a front view of the junction controller unit. An extensive series of experiments (Test 63-2) were conducted to determine the long term temperature stability of the junction unit. Over a typical ten day period the maximum fluctuation of junction temperature was ± .05°C and no long term drift of the control point was observed.

1.6.3 Signal Conditioning Unit

The conditioning unit contains six separate conditioning circuits. The purpose of these circuits are first to provide a zero adjustment for the thermocouple recording channels and secondly to provide a method for checking the overall sensitivity of the thermocouple recording system. Zero balancing is provided by the addition

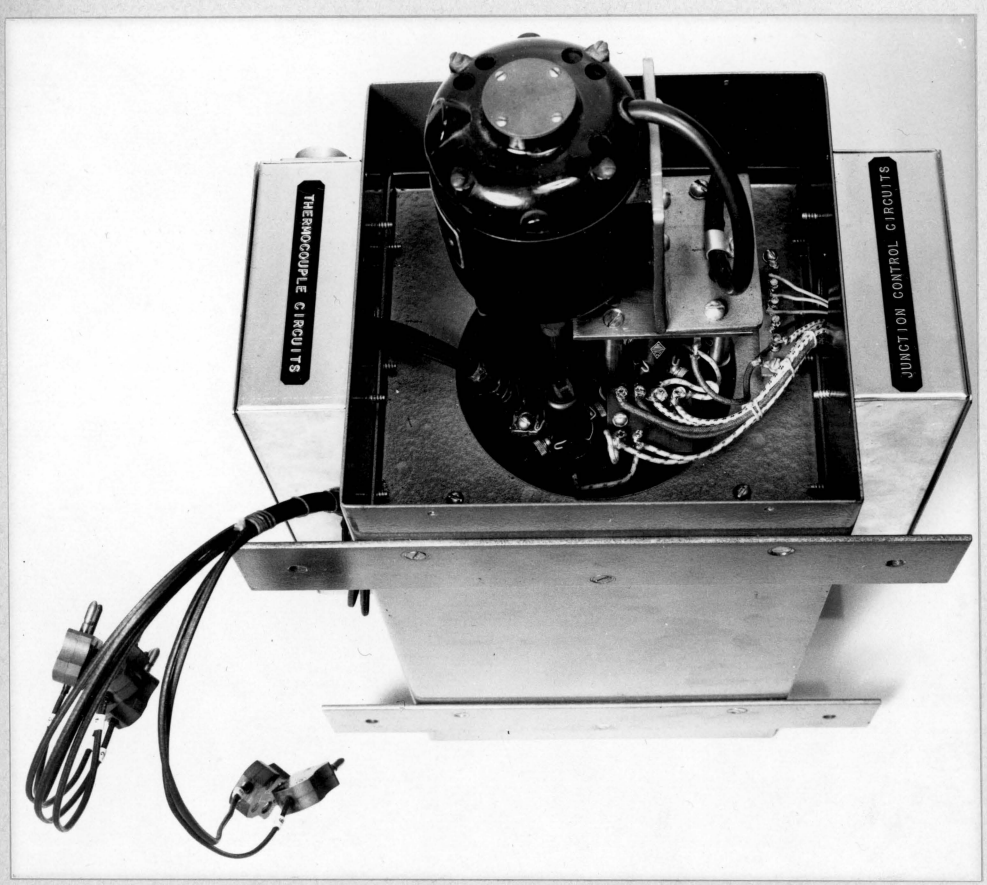


FIGURE 79 - Photograph Showing Top View of Reference Junction Unit.

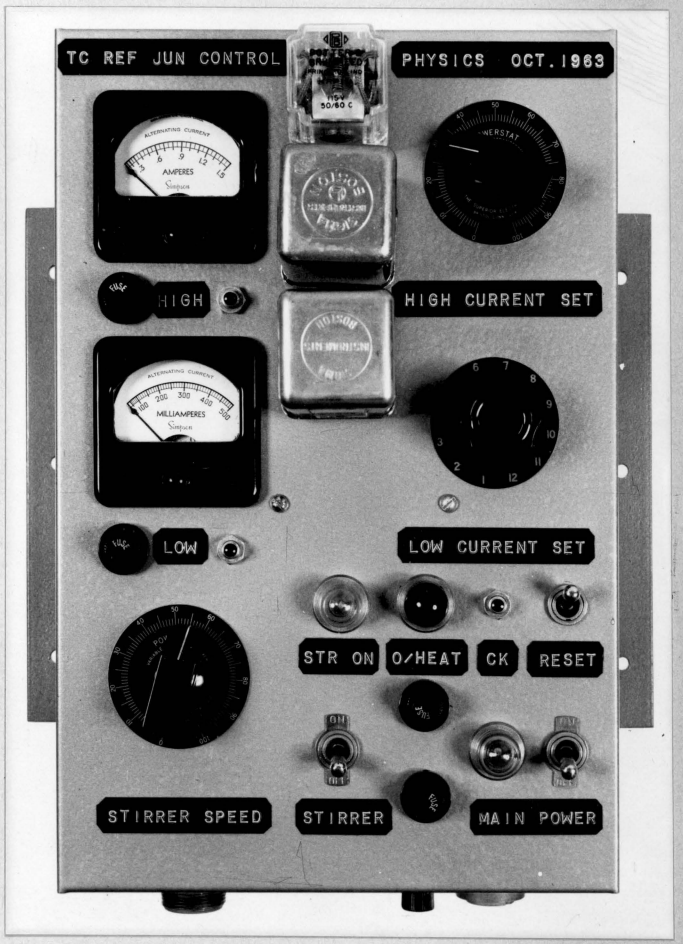


FIGURE 80 - Photograph Showing Front View of Reference Junction Control Unit.

or subtraction of a fixed (but adjustable) d-c voltage to the output of the TC junction unit (V_{in}). Figure 76A outlines how both the zero balance (V_{ZB}) and calibrate voltages (V_c) are developed. The circuit designed for this purpose is shown in Figure 81. The signal (V_{in}) from the junction unit enters the conditioning circuit via connector CON-1 and the modified signal leaves the unit via connector CON-2.

The zero balance voltage (V_{ZB}) is developed by passing a current through R_1. This current is developed by a 1.36 volt mercury cell and is adjusted to the correct value by an associated resistance network. Switch SW-1 allows the polarity of the zero adjustment voltage to be selected and provides a coarse zero adjustment. A 10 turn wire wound potentiometer (R_5) serves as a fine zero adjustment control. Switch SW-2 allows a small calibration voltage to be introduced across R_2. This voltage is developed by a 1.36 volt mercury cell in the calibration circuit. The magnitude of the calibration voltage is selected by switch SW-4 which places either a 10K or a 100K ohm resistor in series with the mercury cell.

The conditioning unit contains six zero adjusting circuits similar to that shown in section A of Figure 81. The calibration and voltage check circuits shown are common to all six zero adjusting circuits. Figure 82 shows a number of views of one section of the conditioning unit

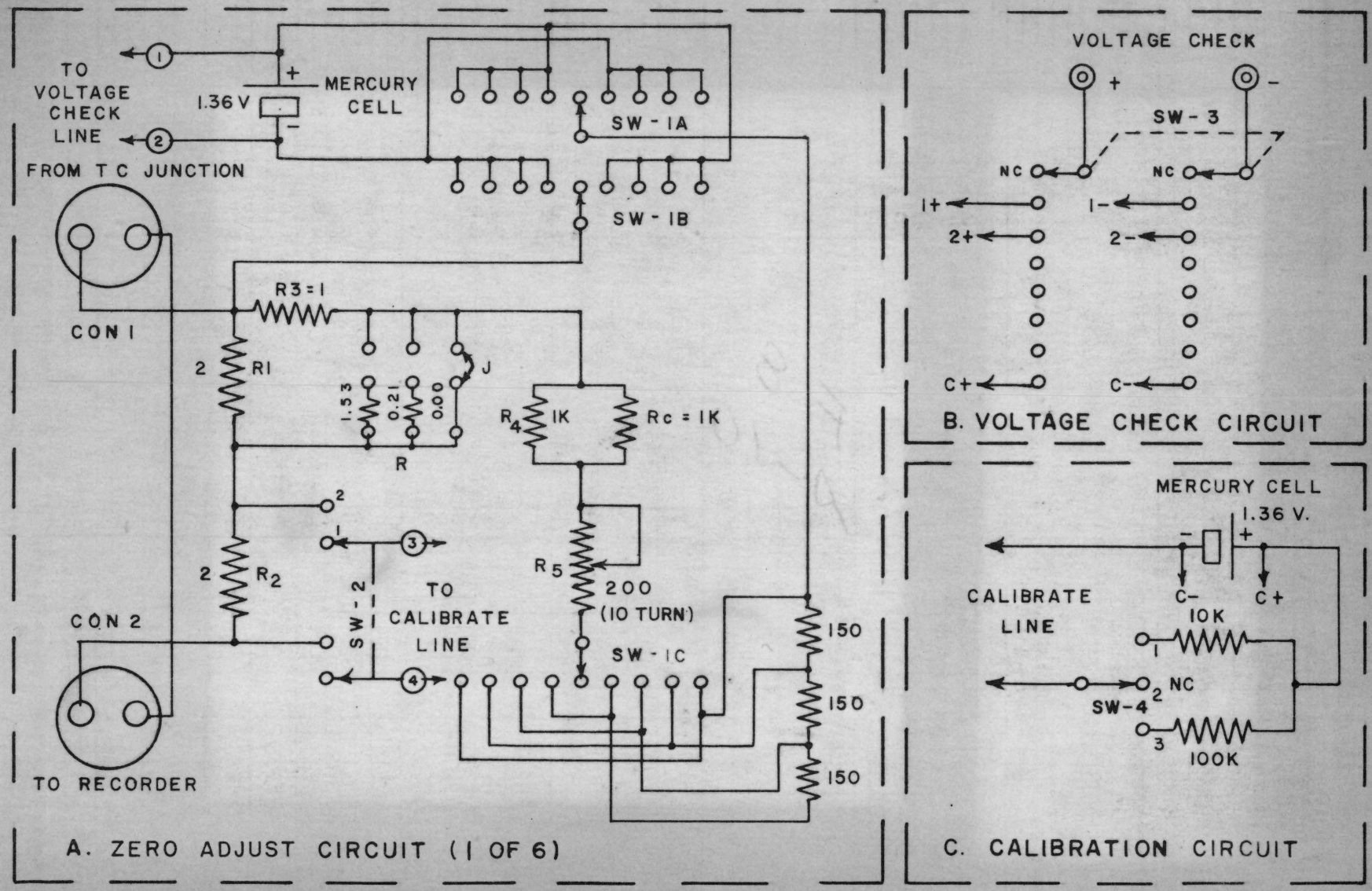
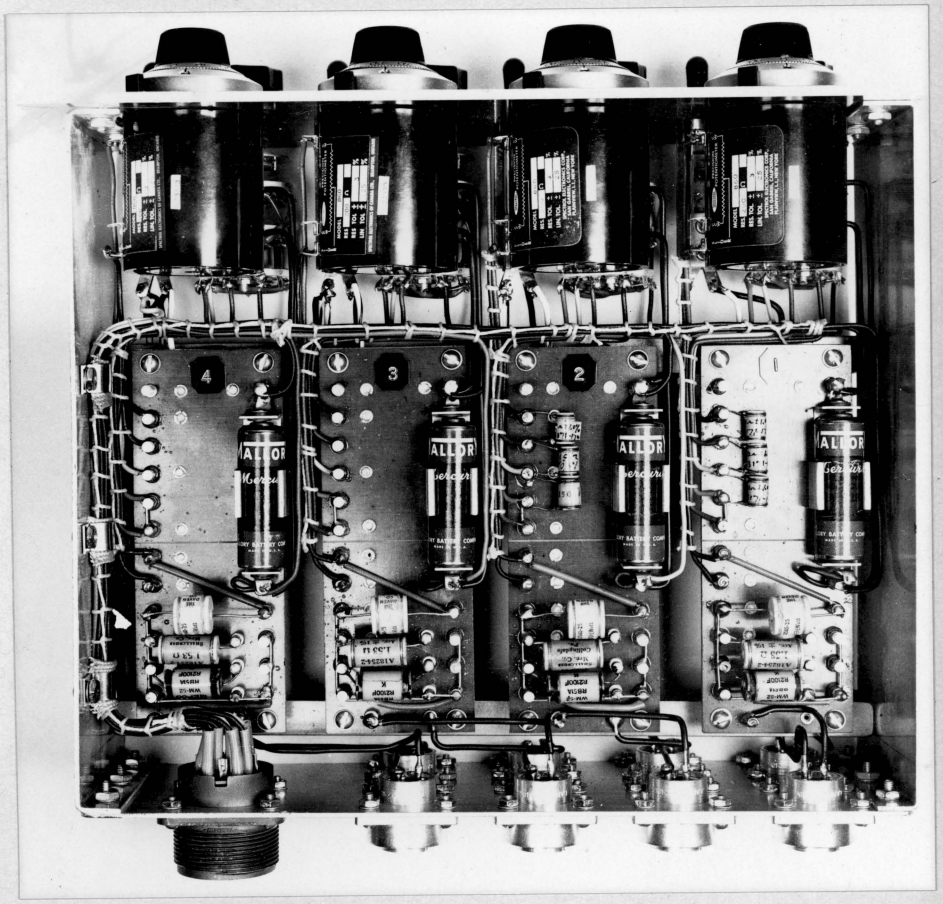


FIGURE 81 - Circuit Diagram for Thermocouple Signal Conditioning Unit.



A. Front View of Four Circuit Module.



B. Top View of Four Circuit Module.

FIGURE 82 - Photographs Showing a Number of Views of Signal Conditioning Unit.

which contains four of the zero adjusting circuits. It was estimated that at least 30 days of continuous operation could be expected for each mercury cell in the zero adjustment circuits.

The behavior of the conditioning unit was studied over a period of five days. Table 18 lists a number of important characteristics obtained from these experiments.

TABLE 18

Characteristics of Thermocouple Signal Conditioning Unit

Stability[1] -------	$\pm$ 1.0 μv
Drift[1] -------	Nil
Temperature coefficient --	0.65 μv/°C
Zero Adjustment Range ---	$\pm$ 400 to 900 μv ($\pm$ 10-22°C)[2]
Calibration Signal -------	Low - 34μv (≈ 0.81°C)[2]
	High - 340μv (≈ 8.1°C)[2]

(1) Determined over a three day test period during which the ambient temperature varied from 21 to 27°C.

(2) Equivalent temperature based on the use of a copper-constantan thermocouple which has a sensitivity of 42μv/°C.

1.7 Preparation and Strain Gaging of Test Specimens

1.7.1 Test Specimen Geometry

In the study of the mechanical properties of solids the geometry of the test specimens themselves is of the utmost importance. This is particularly true in the case of quasi-brittle solids such as geologic materials. Furthermore preparation of test specimens from such materials are considerably more difficult and time consuming than for more ductile solids like metals, and as a result the specimen geometry selected must be at best a compromise.

The majority of experiments carried out in the past have utilized solid cylindrical test specimens with a L/D ratio (length to diameter ratio) ranging from one to two. Short cylindrical specimens, $L/D < 2$, are unsatisfactory due to a distortion of the stress field along the axis of the specimen caused by forces acting at the interface of the specimen and the loading plattens. These distortions in the stress field diminish with distance from the end of the specimen and become small at distances equivalent to the specimen diameter. Long narrow specimens overcome the end-effect but they introduce problems of bending, and still leave large stress concentrations near the ends which could cause premature failure at these points. To ensure that maximum deformation and failure occur in the center region of the test specimen a reduced diameter section may be machined in this region. This

specimen shape is however, like the previous shape, susceptible to bending and as well will have stress concentrations in regions where the section diameter is abruptly changed. These stress concentrations may however be greatly reduced by necking gradually down from the end of the specimen to the reduced center section, i.e. a fillet of large radius of curvature is provided between the end section and the reduced central section. For this geometry the possibility of bending remains, but it may be greatly reduced or eliminated by very careful finishing of the specimen end-surfaces and the maintenance of a high degree of alignment both during specimen preparation and during the actual deformation experiments. The techniques involved in the design of such specimens have been treated recently by Peterson (1953). Based on these techniques Brace (1963) has developed a specimen with a reduced central section and a large radius fillet, which he has used with great success for both compression and extension experiments on a wide range of sedimentary and igneous rocks. The undesirable features of this specimen design are the time and special machines required for their preparation, and the fact that relatively large pieces of test material are required. As a result it was decided initially to utilize cylindrical specimens and to consider the use of filleted specimens only in the advent that more refined experiments were required.

Experiments by Gill and Paquin (1964) have indicated

a number of details of the strain distribution in a cylindrical rock specimen under uniaxial stress. Their work along with a complementary photoelastic study by Udd (1964) indicate that a cylindrical specimen with an L/D ratio between two and three should provide a satisfactory compromise between bending and end-effects. Recently experiments have been conducted by Larocque (1960) on a number of sedimentary and igneous rocks, under uniaxial compression, using cylindrical specimens with L/D = 1.71. The finer grained groups of igneous rocks studied gave extremely consistent results for both compressive strength and elastic modulus, standard deviations of 0.4-7.5 per cent and 4.5-8.5 per cent respectively being obtained. Since the rocks in this group were inherently macroscopically homogeneous the standard deviations obtained were mainly representative of the reproducibility of the experimental technique including any effects of specimen geometry. This does not preclude the fact that specimen dimensions themselves may be important, but rather points out that for this particular L/D ratio experimental results are reproducible.

It was finally decided to utilize cylindrical test specimens nominally 1-3/4 inches long by 3/4 inches in diameter. These dimensions allow the most economical use of the available test material, are relatively easy to prepare, and result in a L/D ratio

of approximately 2.33. Subsequent deformation experiments on an isotropic, high purity marble have indicated that extremely consistent results are obtained using this geometry.

1.7.2 Test Specimen Preparation

A great number of deformation experiments on geologic materials and most routine testing of these materials for engineering purposes have employed test specimens prepared directly from existing diamond drill core by simply cutting sections to length with a diamond saw and either lapping or grinding the ends plane-parallel (no attempt being made to first improve the quality of the circumferential surfaces). This procedure, which has been outlined by the writer, (Hardy (1959)) and by other workers (Obert et al(1946) and Fairhurst (1961)) results in specimens with ends plane-parallel to an accuracy of .005 - .00001 inches depending on the method. However in most cases, and particularly where the core was drilled in the field, the specimen axis will have a small but finite radius of curvature and will not be normal to the ends of the specimen. Such specimens when loaded in compression will strain non-uniformly and will fail prematurely due to an induced bending moment. Such specimens may be sufficiently accurate for use in determination of rough engineering parameters but are completely unsatisfactory for refined experiments.

In order to obtain reliable, reproducible data it is felt that the following conditions are required: the axis of the test specimen must be straight and normal to the end surfaces, the end surfaces must be plane-parallel to at least $\pm$ .0005 inches (over a specimen length of 1.7500 inches), the specimen cross-section must be circular to .001 inches at any position along the axis, and the diameter (0.750) must be constant to at least $\pm$ .001 over the length of the specimen. Cylindrical specimens of this quality have been prepared by Robertson (1959) using a centerless and a surface grinder and more recently at the Mines Branch using a lathe with an attached tool post grinder.

The procedure used to prepare test specimens for the current research is as follows:

(i) Sections of EX diamond drill core, nominally 0.85 inches in diameter and approximately six inches in length, free of obvious fractures or planes of weakness are selected from the available field core (or from core drilled from block samples of the test material in the laboratory using a thin walled diamond coring drill);

(ii) The rough ends of the core are cut off with a diamond saw using "Almag" oil lubrication*;

(iii) The core is gently clamped in the lathe chuck with about 1/2 inch of core exposed;

(iv) The exposed end of the core is ground perpendicular to the axis of the lathe using a three inch tool post grinder**, with the plane of the grinding wheel oriented at 15° - 30° to the plane end of the core. The rotary speed of the grinder under no load conditions is approximately 8000 RPM. Experience has shown that for this particular operation a chuck speed of 300 RPM and a cross feed of .0022 in./Rev gives satisfactory result;

---

*Almag oil is manufactured in Canada by the Texaco Oil Company. Cleaning the specimen with perchlorethylene after preparation removes all visible traces of the oil. Experience has shown that its use in specimen preparation does not appear to affect the properties of the test material.

** Two types of carborundum grinding wheels are used depending on the hardness of the materials being prepared. For soft rocks, such as marble, a fine wheel, type - C220K5V6C, 3 x 3/8 x 14 mm has been found satisfactory. For the harder rocks, such as granite, a coarser wheel, type - C150K5V6C, 3 x 3/8 x 14 mm is employed. These wheels are manufactured in Canada by the Canadian Carborundum Company Ltd., Niagara Falls, Ontario.

(v) Without disturbing the core, a 1/4 inch diameter hole, 1/4 - 3/8 inch deep is drilled into the ground-end of the core. In this operation the drill* is held fixed in the tail stock and the core is turned at a chuck speed of 300 RPM. With the softer materials it is important to use a very slow rate of drill feed, and to back the drill off after every few thousands of an inch penetration;

(vi) The core is then removed from the chuck and the other end prepared in a similar manner following steps (iii) - (v);

(vii) The core is mounted axially between the chuck and tailstock of the lathe, being supported at each end by a brass jig the diameter of which is a few thousands less than that of required finished specimen. A short 1/4 inch diameter concentric projection on these jigs fit into the end holes previously drilled in the core to insure accurate alignment of the core axis;

(viii) Initially a series of rough cuts are made to bring the core diameter down to approximately the required dimensions. For this series of cuts a chuck speed of 300 RPM, a carriage travel rate of .0043 in./Rev and a depth of cut of approximately .004 inches is used. The diameter of the core is checked at a number of points along its axis after each traverse. If the core developes high spots

---

* For the softer materials, such as marble, an ordinary high speed steel drill was used. For the harder materials, such as granite, a small diamond coring drill was employed with either oil or air coolant.

or a taper the traversing procedure is modified until these effects are removed.

(ix) When the core diameter is reduced to within .010 inches of the required finished diameter the grinding wheel is redressed using a diamond tipped tool and a series of finishing cuts are made with a chuck speed of 167 RPM, a carriage travel rate of .0021 in./Rev. and a depth of cut of approximately .001 inches. The final few thousands are removed using a depth of cut of .0005 inches or less;

(x) The core is removed from the lathe wrapped in a piece of plastic sheet to protect the finished surface and cut into lengths about 1/8 inch longer than the required specimen length, using a diamond saw with Almag lubrication. Identification such as specimen number, orientation etc. must be marked on the core at this time;

(xi) The short lengths of core are then wrapped in a single layer of plastic sheeting and gently positioned in the lathe chuck. The ends of the core are finished using the same grinding arrangement as outlined in (iv), first using a series of rough cuts with a chuck speed of 300 RPM, a cross feed of .0022 in./Rev. and a depth of cut of approximately .004 inches. Finally a series of finishing cuts are made with a chuck speed of 167 RPM, a cross feed of .0011 in./Rev.

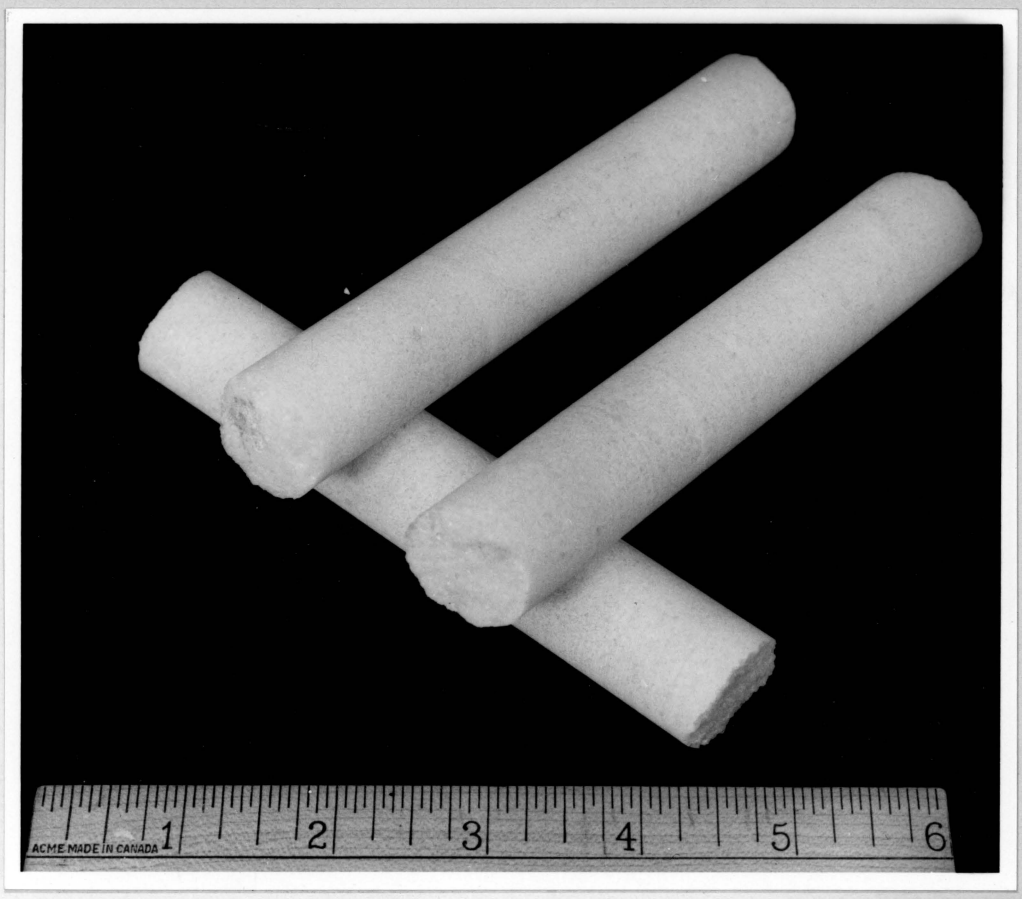
and a depth of cut of .0005 inches. One end of the specimen is first ground to the desired surface finish, the specimen is reversed in the chuck, and the other end ground to give the desired specimen length and surface finish.

(xii) The finished specimen is removed from the lathe, its dimensions at a number of locations checked, using a micrometer, to an accuracy of .0001 inches, and its weight measured to an accuracy of .0005 grams. A set of 6-8 specimens are usually prepared at one time. Total preparation time for such a set ranges from 30-40 hours.

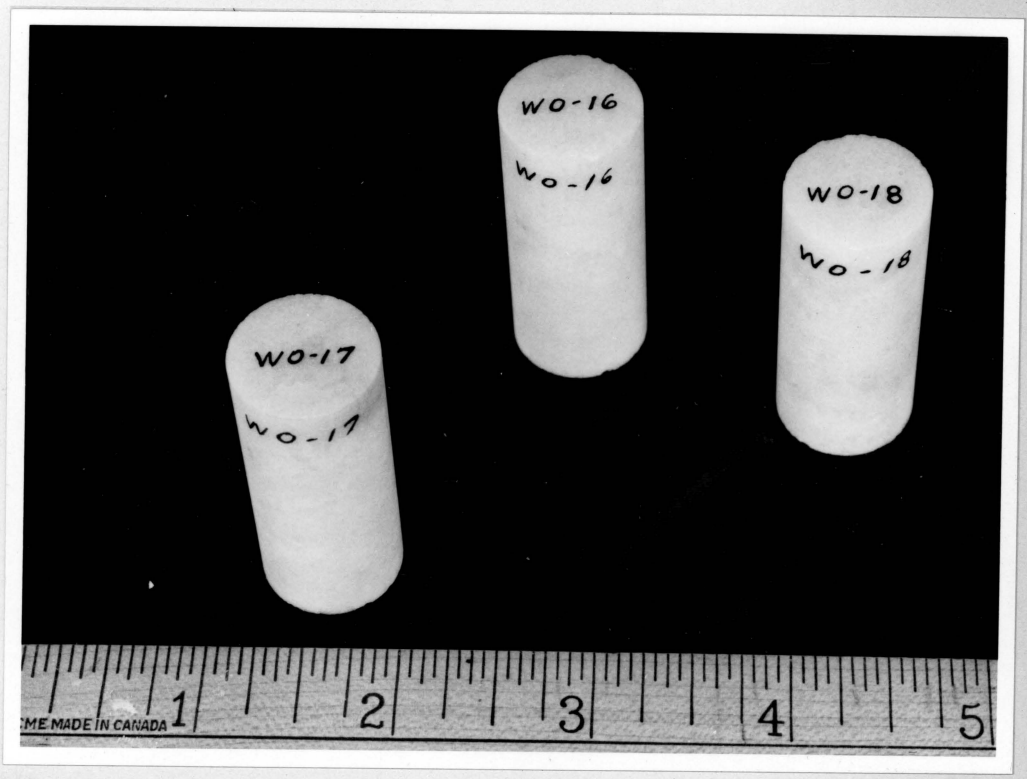
Figure 83A shows a number of lengths of Wombeyan marble core as received. Figure 83B shows a number of completed test specimens prepared from this core using the procedures just outlined.

1.7.3 Strain Gaging of Test Specimens

In the majority of experiments conducted to date only the longitudinal or axial strain (e_{zz}) has been measured. Resistance-type strain gages bonded directly to the test specimen are utilized for this purpose. Three such gages are mounted parallel to the specimen axis at 120° apart around its circumference in order to evaluate the uniformity of the axial strain. Figure 84 illustrates the gage pattern.



A. Cores of Material as Received.



B. Prepared Test Specimens Ready for Strain Gaging.

FIGURE 83 - Wombeyan Marble as Received and after Preparation.

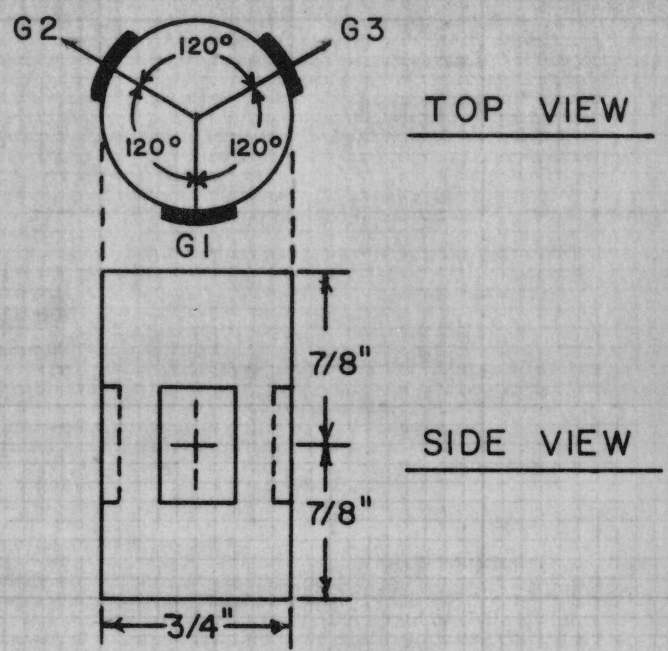


FIGURE 84 - Axial Strain Gage Pattern.

Budd* C6-131 foil-type, epoxy backed strain gages with a gage length and width of .187 inches, a gage factor of 2.05 ± 1/2%, and a gage resistance of 120.0 ± 0.2 ohms were employed. These were cemented to the test specimens using Budd B-3 epoxy-type, high stability cement. This cement is recommended by the manufacturer is for use on porous materials and has been found extremely satisfactory for this purpose at the Mines Branch. It has a setting time of about 15 minutes, and developes its full bonding characteristics after less than 24 hours curing, at room temperature. This latter point is extremely important since the majority of the high stability cements must be cured at higher temperatures, which for geologic materials might result in a modification of the properties of the test material. According to the manufacturer, after this curing period, the bond will exhibit zero creep at a strain of 1000 μs and will remain stable under static conditions for strains up to 5% and for temperatures up to 200°F.

The procedure for application of epoxy backed gages using this type of cement has been outlined by the manufacturer** however the following procedure has been found to be more satisfactory for this particular application:

---

* Budd Company, Instruments Division, P.O. Box 245, Phoenixville, Pa., U.S.A.

** See Budd Company instruction sheet BG-1203-4.

(i) The specimens are initially cleaned of all visible oil and grease using Perlux and paper tissue, followed by a final cleaning with isopropyl alcohol;

(ii) The gage locations are selected at 120° apart and if possible in regions where there are no obvious inhomogeneities in the material. Using a pencil and a small machinist's square, lines are marked parallel to the specimen axis and normal to it at the mid-point of the specimen at each of the three locations. Care must be taken not to mark the specimen in the region where the gage is to be attached. The specimen is then placed in a sponge rubber padded V-block with one of the sets of orientation axis facing upwards;

(iii) A length of masking tape (3" x 3/4") is positioned on a padded block, adhesive side up, and the strain gage pressed, rear side down, on to the tape. Using a fine pair of tweezers the temporary protective sheet is removed from the gage;

(iv) The gage backing is lightly abraded using a small square (1/8" x 1/8") of No. 1 polishing paper held with the tweezers, the gage surface is then cleaned with a cotton swab dipped in isopropyl alcohol;

(v) A small length of the masking tape, with the cleaned gage in place, is cut free and using a strong light behind the gage the location of the gage axis is marked on the back of the tape;

(vi) The B-3 cement which is supplied in a dual compartment plastic envelope, is then prepared by removing the clamp separating the cement and the hardener and kneading the package for about 60 seconds. The package is then opened by cutting one corner, and the contents poured into a watch glass where it is stirred, using a glass rod, for about another 60 seconds; at which time it is ready for use;

(vii) A thin even layer of the cement is spread on the exposed gage surface, the gage axis and orientation axis on the specimen are lined-up as carefully as possible and the gage is taped in position. A gentle pressure is applied, over the surface of the gage, to squeeze out excessive cement. The other two gages, which have also been prepared ready for mounting, are then applied following the same procedure;

(viii) Small cellophane pads, slightly larger than the gage backing are placed over the gages, and a length of teflon tape is wrapped firmly around the specimen several times and held in place by masking tape;

(ix) The gage cement is allowed to cure for 24 hours before removing the clamping tape, and gage mounting tape. The gages are then checked visually under a low power magnifier for the quality

of the gage bond and the gage orientation. The gages are then coated with waterproofing compound* and allowed to dry;

(x) The specimens are then wrapped in tissue and stored until required. Figure 85A shows a set of specimens with attached gages. The three specimens at the rear of the photograph show the typical arrangement of the gages presently used to measure axial strain (e_{zz}). The specimen in the foreground has an additional set of three gages oriented perpendicular to the specimen axis for the measurement of laterial strain ($e_{\theta\theta}$).

(xi) Just prior to testing, extension leads are soldered to the gage terminals using a quality grade of resin core solder and a fine tipped soldering iron. These leads are then firmly clamped to the specimen with masking tape. Figure 85B shows a typical specimen ready for testing.

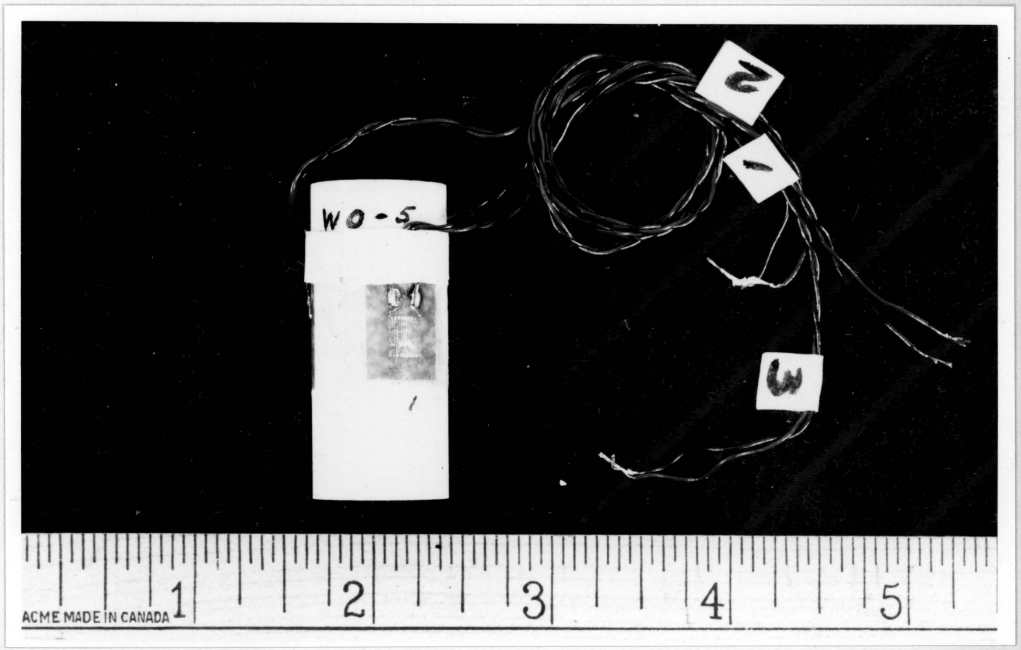
1.7.4 Errors Due to Gage Orientation

It is extremely important that the angle between the longitudinal axis of the gage and the specimen axis be kept to a minimum. If the axis of the gage and the specimen are not parallel the observed axial strains will be in error. Since it is physically extremely difficult to orient strain gages exactly parallel to the specimen axis it was considered necessary to evaluate the magnitude of the error introduced

* Budd Type GW-1 waterproofing compound has been employed on all gages to date.



A. Group of Test Specimens with Attached Strain Gages.



B. Specimen Ready for Testing with Strain Gage Leads Attached.

FIGURE 85 - Photographs Showing a Number of Views of Gaged Test Specimens.

in the observed strain as a result of imperfect orientation of the gage. A typical cylindrical test specimen having coordinate axis Z, r and θ is shown in Figure 86. Consider the test material to be elastic, isotropic and loaded uniformly in compression along the Z-axis. Since the gages are mounted on the circumferential surface of the specimen, which is a surface of r = constant, only the Z- and θ-axis need be considered. Considering the point P located at the midpoint of a line parallel to the specimen axis, let the axis of the specimen at this point be Z and θ, and of the gage be V and β and let the axis of the gage be at an angle α to those of the specimen. The relationship between strains in these two coordinates systems may be established from elastic theory using indicial notation (see for example Sokolnikoff (1956)).

Now

$$e'_{ij} = a_{im}\, a_{jn}\, e_{mn} \qquad (33).$$

where e_{mn} and e'_{ij} are the strain components associated with the axis of the specimen and the gage respectively, and a_{im} and a_{jn} are the direction cosines between the two sets of axes. In particular,

$$e'_{vv} = a_{vz}\, a_{vz}\, e_{zz} + a_{v\theta}\, a_{v\theta}\, e_{\theta\theta} + 2\, a_{v\theta}\, a_{vz}\, e_{z\theta} \qquad (34).$$

Assuming uniform compressive loading along the Z-axis of the specimen, the stresses are σ_{zz}*, and all other $\sigma_{ij} = 0$.

---

* For convenience compressive stresses and strains will be considered positive.

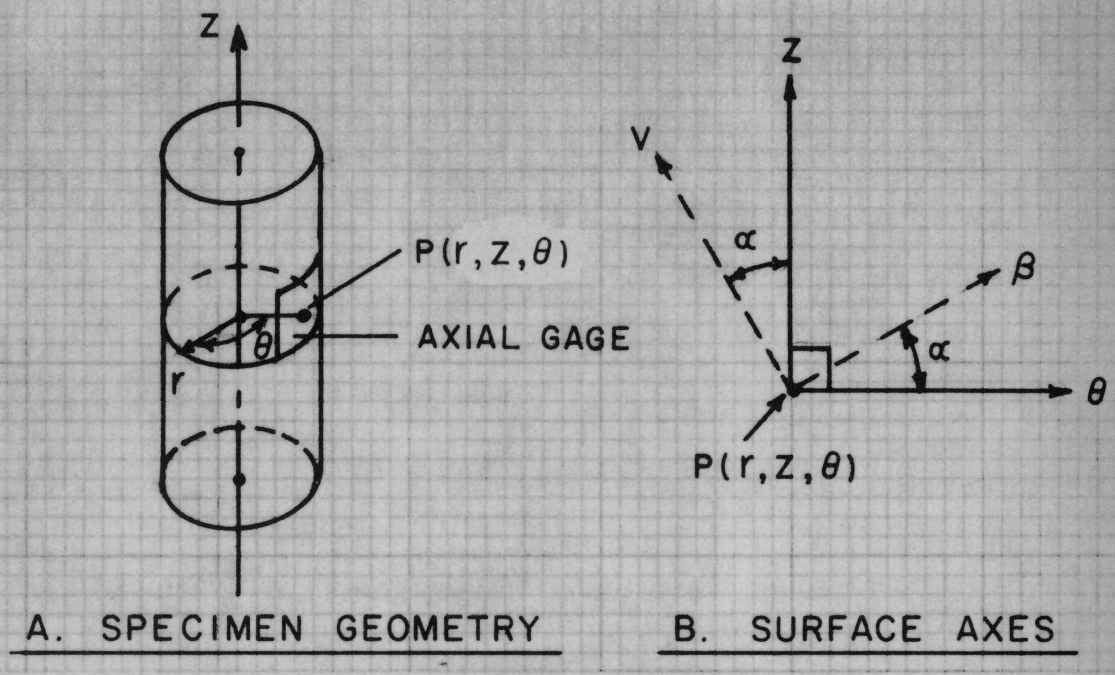


FIGURE 86 - Orientation of Gage Axes to Specimen Axes.

Hooke's law for an isotropic elastic solid may be written,

$$e_{ij} = \left(\frac{1+\mu}{E}\right)\sigma_{ij} - \left(\frac{\mu}{E}\right)\Theta\,\delta_{ij} \qquad (35).$$

where $\Theta = \sigma_{ii} = \sigma_{zz} + \sigma_{rr} + \sigma_{\theta\theta}$, and E and μ are respectively the Young's modulus and Poisson's ratio of the material. Now using (35) and the condition that $\sigma_{ij} = 0$ except for i = j = z it may be shown that

$$e_{zz} = \sigma_{zz}/E \qquad (36),$$

$$e_{z\theta} = 0 \qquad (37),$$

$$e_{\theta\theta} = -(\mu/E)\sigma_{zz} \qquad (38).$$

Substituting for σ_{zz} in (38) gives

$$e_{\theta\theta} = -\mu\, e_{zz} \qquad (39).$$

Substituting (37 and 38) into (34) gives

$$e'_{vv} = (a_{vz})^2 e_{zz} - \mu (a_{v\theta})^2 e_{zz}$$

or

$$e'_{vv} = e_{zz}\left[(a_{vz})^2 - \mu (a_{v\theta})^2\right] \qquad (40).$$

The direction cosines a_{im}, a_{jn} are the cosines of the angles between two pairs of coordinate axes. These may be obtained from Figure 86 by inspection and are as follows:

AXES	Z	θ
V	(a_{vz}) cos α	$(a_{v\theta})$ - sin α
β	$(a_{\beta z})$ sin α	$(a_{\beta\theta})$ cos α

Substituting these into (40) gives

$$e'_{vv} = e_{zz}(\cos^2\alpha - \mu \sin^2\alpha) \qquad (41),$$

or more conveniently,

$$e_{zz} = \frac{e'_{vv}}{\cos^2\alpha - \mu \sin^2\alpha} \qquad (42),$$

where e_{zz} is the true axial strain and e'_{vv} is the apparent (or measured) axial strain. The per cent error (M) due to gage orientation may be written as,

$$M = \left\{\frac{e_{zz} - e'_{vv}}{e_{zz}}\right\} \times 100\,\%$$

Substituting for e_{zz} from (42) gives

$$M = (1 - K) \qquad (43),$$

where

$$K = \cos^2\alpha - \mu \sin^2\alpha \qquad (44).$$

Measurements on a series of gages attached to typical test specimens* showed that $0 \leq \alpha \leq 3°$. Table 19 lists the calculated values of M assuming a range of values of μ, and $\alpha = 3°$.

---

* Specimens WO-6 and WO-7.

TABLE 19

Effect of Strain Gage Orientation

α	μ	K	M
degrees	---	---	per cent
3	0.25	.9965	.35
3	0.50	.9959	.41
3	2.0*	.9918	.82

*Anomalous values of μ have been reported by Evans and Wood (1937) and others for many geologic materials under creep conditions.

Under the worst possible conditions M does not exceed one per cent and hence a correction for gage orientation would not be required under normal conditions.

1.8 Uniform Loading of Test Specimens

1.8.1 Initial Investigations

Deformation of any material under compressive loading presents a number of experimental difficulties. These difficulties are further increased when geologic materials are involved. These materials are usually very weak in tension and even under moderate confining stress, normally fail as brittle materials. As a result, uniform loading is essential to insure that material does not fail prematurely. Furthermore, if meaningful strain data is to be determined from a finite number of strain gages, it is necessary that the strain

distribution requires first a suitably shaped and accurately prepared test specimen (this requirement has been discussed in detail earlier), and second a method for uniformly loading this specimen.

In previous experiments by the writer an attempt was made to obtain uniform loading by using test specimens with well prepared plane-parallel ends mounted in some form of loading jig or subpress to maintain specimen alignment during deformation. In these earlier experiments axial strain was measured by two resistance strain gages attached to the specimen and connected in series to give an output equivalent to the average strain. Such a strain measuring arrangement is convenient in some respects but provides no indication on whether bending is taking place in the specimen. The three gage arrangement presently utilized provides this additional information and makes it possible to evaluate the uniformity of loading produced by different loading arrangements.

Preliminary experiments on geologic materials indicated that extremely non-uniform loading resulted when the original type of loading jig was employed, in many cases the bending being so large that one and sometimes two of the gages indicated large tensile strains. A review of the literature dealing with geological materials indicated that many workers have recognized the existance of this problem. The majority of those in the geological field (e.g. Griggs (1936),

Handin (1953), Robertson (1955) etc.) have incorporated some form of "stress equalizer" and/or a flexible linkage in their loading arrangement. This appears to provide a satisfactory solution, at least for experiments under high confining pressure where the materials are to some extent ductile. Brace (1963) however, found this technique unsatisfactory for geological materials under conditions which favoured mainly brittle behavior and found it necessary to utilize specially shaped specimens which were loaded under forced axial alignment*. Such a loading arrangement induces a large frictional force into the loading system which is undesirable in many types of experiments. Most of those concerned with the testing of geologic materials for engineering purposes have overlooked or ignored the problem although some consideration has been given to it by Obert et al (1946) and more recently by Grosvenor (1963), Paquin (1963) and others.

In order to overcome this problem an experimental program was established to investigate various types of loading arrangements. A ground steel cylinder .75 inches in diameter and 1.50 inches in length with three attached axial strain gages (at 120° apart) replaced the test specimen in the loading jig. The strains at each gage were recorded separately and the average strain, e_a, the maximum deviation

---

*In Braces experiments the loading pistons and the enlarged head pieces of the test specimen were very accurately ground and were held concentric by the internal wall of the test vessel.

between any two gages, Δe, and the per cent deviation $(\Delta e/e_a) \times 100$ calculated at each stress level. The various jig configurations were tested in one of the loading frames, located in the deformation facility described previously. In the majority of cases load was applied to the jig via the loading button on the load cell and a spherical seat attached to the upper surface of the loading jig.

The original type of loading arrangement, Hardy (1959, 1962) was discarded almost immediately as it was found that the use of small vertical posts to align the upper and lower plattens was unsatisfactory. One modification of this type of jig was made by substituting a ball and socket (using a 1/2 inch diameter ball bearing) for the original fixed lower loading head. Figure 87A illustrates the mechanical arrangement and Figure 88A shows a typical set of experimental curves obtained using this jig*. The strain versus stress data for the three individual gages show an increasing divergence with stress, reaching a deviation of 262 μs at 17,500 psi. It is interesting to note however that the average strain curve passes through zero at zero load and remains nearly linear with increasing stress. Similar experiments

*It should be noted that this particular test, denoted as 63-0, was carried out early in 1963 at which time the hydraulic loading ram was hung from the upper platten of the loading press, rather than being threaded into it as was the case for the other experiments.

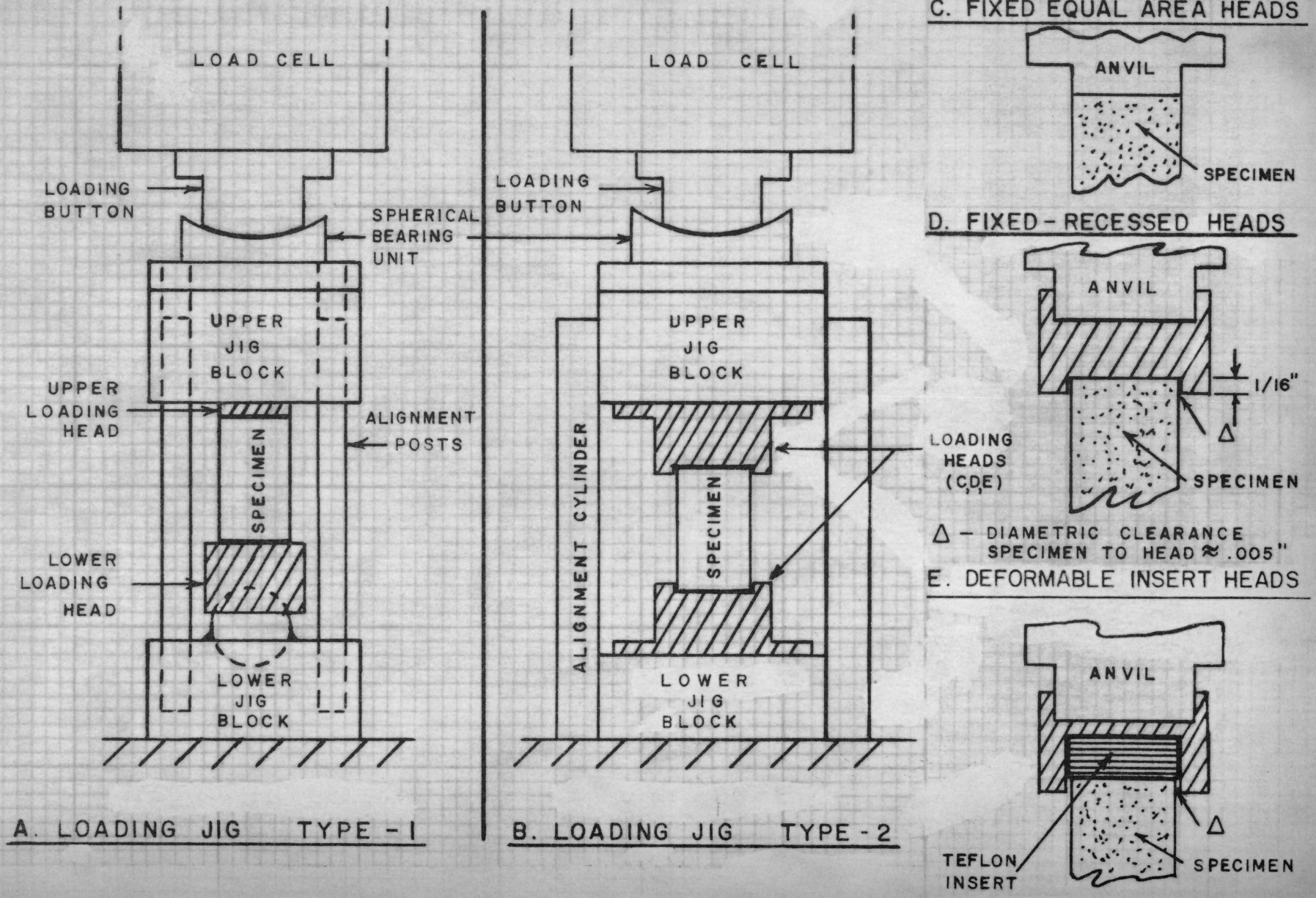


FIGURE 87 - Details of Various Types of Specimen Loading Jigs.

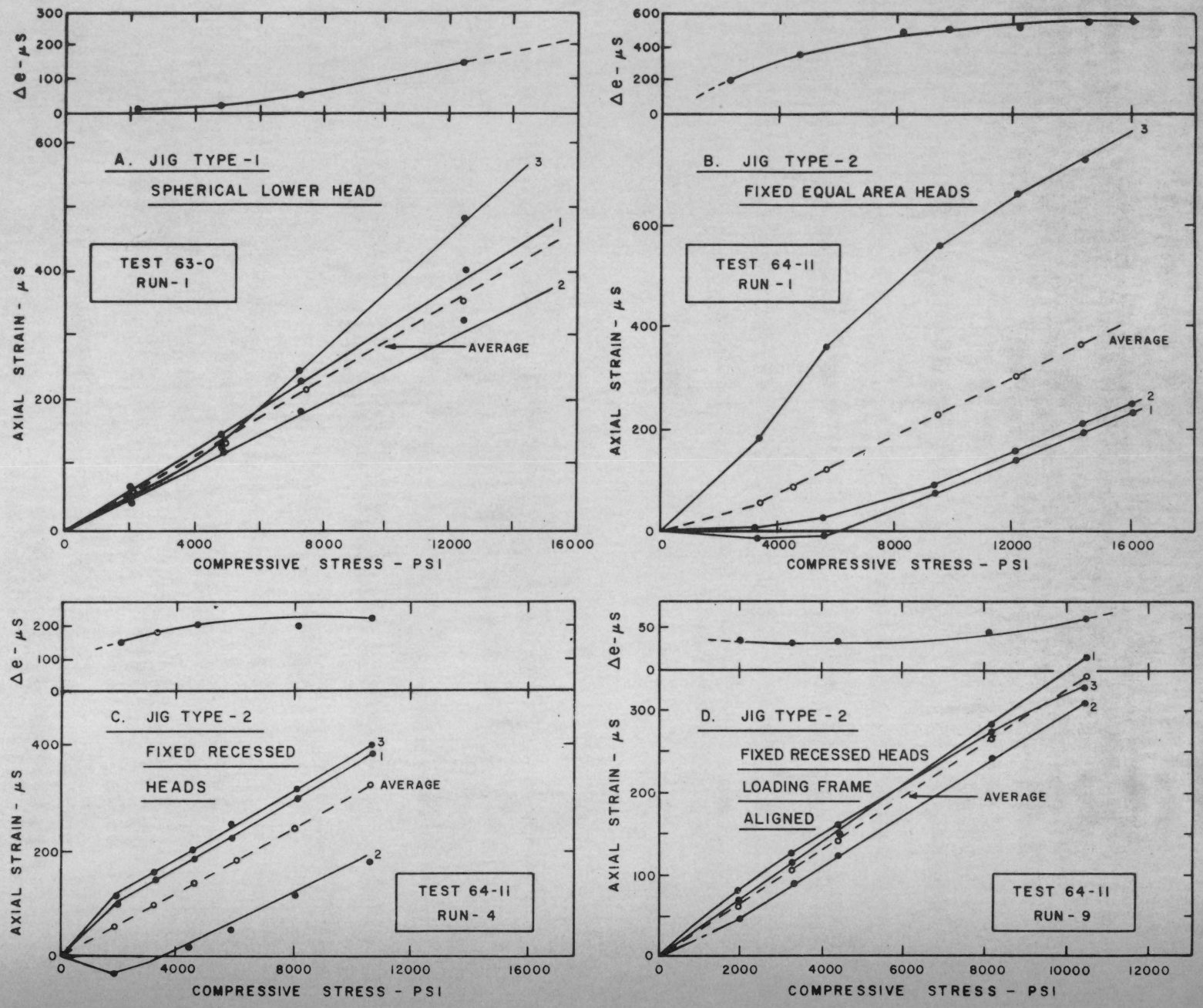


FIGURE 88 - Stress-Strain Curves Obtained Using Various Types of Specimen Loading Jigs.

by Grosvenor (1963) on rock and by Kerper et al (1958) on brittle cermets+ have indicated that the use of conventional-type swivel heads may increase rather than decrease the non-uniform loading. Grosvenor (1963) found it necessary to lock the swivel head after initial contact had been made with the specimen. Kerper et al (1958) found that, when using conventional swivel heads, considerable bending was induced in the specimen which was large enough to produce tensile strains in some areas. They found that the most satisfactory loading was obtained using a well aligned testing machine and precision finished fixed loading heads consisting of a short, hollow thick walled tool steel cylinder, shrunk-fitted onto a length of the actual test material somewhat larger in cross-section than the test specimen. Such an arrangement was not considered practical for testing of geologic materials.

1.8.2 Fixed Loading Heads

Next it was decided to carry out a number of experiments with fixed loading heads and a jig that would provide a degree of forced alignment. The jig arrangement is shown in Figure 87B and consisted of a cylindrical upper and lower jig block (3 inches in diameter) held in alignment by an outer cylinder. A centering hole and a series of threaded holes in the jig blocks allowed various loading

+ Cermets are materials formed from a mixture of ceramic and metallic powders by the process of compaction and sintering.

head arrangements to be attached. All surfaces were ground finished and the end surfaces of the jig blocks were accurately ground normal to their axis. Initially a set of anvils with a diameter equal to that of specimen were employed. This arrangement is shown in Figure 87C. A series of three experiments were conducted using this arrangement (64-11(1, 2, 3)) and Figure 88B illustrates the results for test 64-11(1) which is typical. The average strain curve appears relatively linear (although it does not pass through zero), but the curves for the individual gages are non-linear and differ greatly in magnitude. Gages 1 and 2 show a very low sensitivity, with gage 1 initially indicating a tensile strain. The deviation (Δe) between gages increases with stress but $d(\Delta e)/d\sigma$ appears to decrease up to a stress of approximately 8000 psi after which it remains nearly constant.

The results of the previous series of tests suggested that since the anvils and the test specimen were the same diameter, it was probably difficult to ensure that the specimen was in contact with the anvils over its complete end-surface. To check on this a set of precision ground, loading caps were machined as shown in Figure 87D. These were designed to be a "close sliding fit" to the anvils and to have a diametric clearance to the specimen of .005 - .006 inches, thus allowing the specimen to be aligned to within .003 of the jig axis. A series of three experiments were run using this arrangement (64-11 (4, 5, 6)), Figure 88C illustrates the results for test 64-11(4) which is

typical. The average strain curve is linear and passes through zero, however one of the gages (No. 2) goes initially into tension. As in the previous set of tests the deviation (Δe) increases with stress but $d(\Delta e)/d\sigma$ approaches a limiting value after a stress of approximately 4000 psi.

Results to this stage using modified jigs had not been very encouraging, and it was decided to check on the effect of very accurately aligning the loading frame itself. Using a micrometer dial gage, accurate to $\pm$ .0001 inches the four posts of the loading frame were adjusted so that the top and bottom plate of the loading frame were parallel to within an angle of less than 2 minutes (.0051 inches over a span of 10 inches). A series of three experiments (64-11(7, 8, 9)) similar to 64-11(4, 5, 6)) were then run. The results for test 64-11(9), which is typical of this series, are shown in Figure 88D. In these tests no gages indicated tensile strains, the deviations (Δe) at low stresses were considerably smaller (being only 35.4 μs at 3147 psi in comparison with 294 and 185 μs for tests 64-11(1) and 64-11(4)). Figure 89 illustrates the variation of the average strain (e_a) and the deviation (Δe) as a function of stress for test 64-11(1, 7, 9). It is interesting to note how closely the average strain curves agree, even in cases where Δe was large.

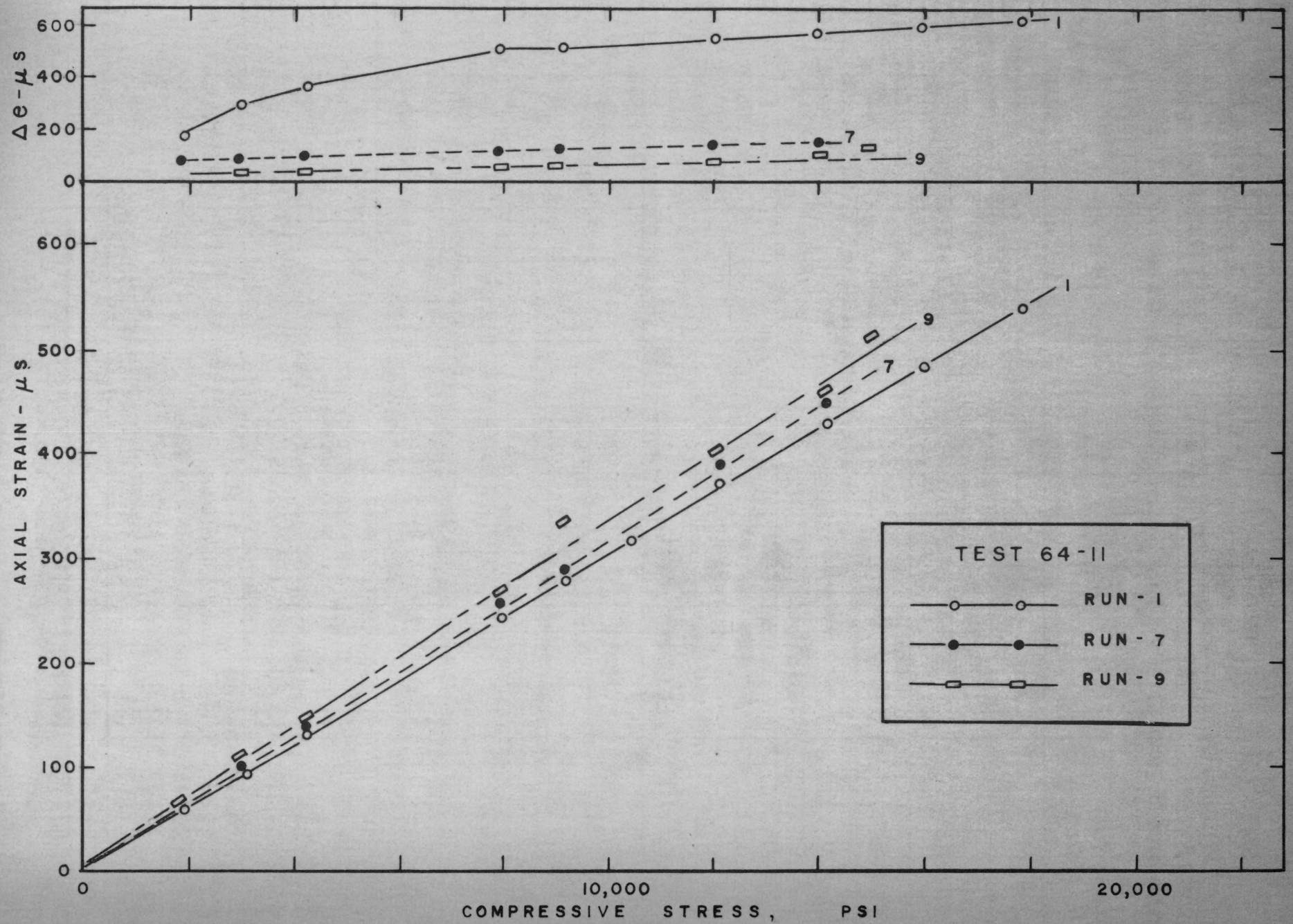


FIGURE 89 - Average Stress-Strain Curves Obtained Using Various Types of Specimen Loading Jigs.

Although the alignment of the loading frame had improved the situation considerably Δ e was still far too large, necessitating further consideration of a more effective loading jig. A number of workers in the past have utilized pads of various materials between the ends of the specimen and the loading plattens in an attempt to develop uniform loading. Obert et al (1946) found in studies of compressive strength of rocks that although such pads did tend to reduce the deviation in test results, they also reduced the apparent strength of the material. Kerper et al (1958) studying the compressive strength of cermets found that this technique did not significantly reduce the induced bending strains produced by non-uniform loading. Recently studies have been undertaken by Gill (1963), Paquin (1963), Shih (1963) and others at McGill University on the effect of various end-pads and end-lubrication but as yet no definite solution to the loading problem has been obtained. It should be noted in most cases where end-pads have been employed they were merely placed between the specimen and the loading fixture and during compression were free to extrude laterally.

In soil mechanics flat inflated rubber diaphrams filled with water or other liquid are often located between specimen and the loading plattens in an attempt to obtain uniform end loading. Harboe (1962) describes a similar arrangement using instead a thin metal diaphram. Handin has recently suggested (see Paquin (1963)) that one

solution might be obtained by loading the specimen ends using direct hydraulic pressure. Cross (1964) has used this method to obtain relatively uniform stress patterns in photostress plastic patches attached to short brass cylinders under compression. Hydraulic loading however has a number of disadvantages, first the specimen ends must be sealed against penetration by the hydraulic fluid, secondly the specimen ends must be fitted with O-rings which under pressure may cause high shear stresses to develop across the ends of the specimen, and thirdly if high axial stresses are required the end-loading attachments required to withstand the necessary fluid pressures become bulky.

As part of an experimental investigation of the yield stress of pure lead, Loizou and Sims (1953) have described an interesting method for reducing the frictional forces between the compression plattens and the test specimen. Concentric grooves 0.002 inch deep were machined on each end of the specimen and during compressive loading oil with a free fatty acid additive was entrapped in these grooves. It was found experimentally that with a spacing of 32 grooves per inch barrelling of the specimen was eliminated. Studies on specimens with D/H ratios of 1.5 and 0.75 showed that the yield stress was independent of the D/H ratio only when specimens with grooved ends were used. A similar method of end-preparation might be applied to rock specimens used in compression tests.

1.8.3 Loading Heads with Deformable Inserts

It was decided to study the effect of loading the specimen through a pad of some relatively deformable material which was contained laterally in a hollow loading head. Such an arrangement has some of the advantages of fluid-type loading but none of its disadvantages. A set of hollow loading heads were designed to fit the existing anvils on the loading jig as shown in Figure 87E. The hollow ends of these heads were machined to have a small diametric clearance (.003 inches) with the test specimen and were fitted with removable, short, cylindrical teflon inserts. Figure 90 gives further details of this loading arrangement. Two experiments (64-11(11, 12)) were carried out using this arrangement. The results for the individual gages from experiment 64-11(12) are shown in Figure 91 and the curves of average strain (e_a) and the deviation (Δe) against stress for both experiments are shown in Figure 92. The curves for the individual gages as well as the average were found to be linear and passed through zero. The maximum deviation (Δe) up to a stress level of 25,000 psi was 10 μs and appeared to be independent of stress level. It is also important to note the very close agreement between the two tests. Since the loading jig was completely disassembled after test 64-11(11) and reassembled for the following test this agreement indicates the excellent reproducibility and uniformity of the loading technique.

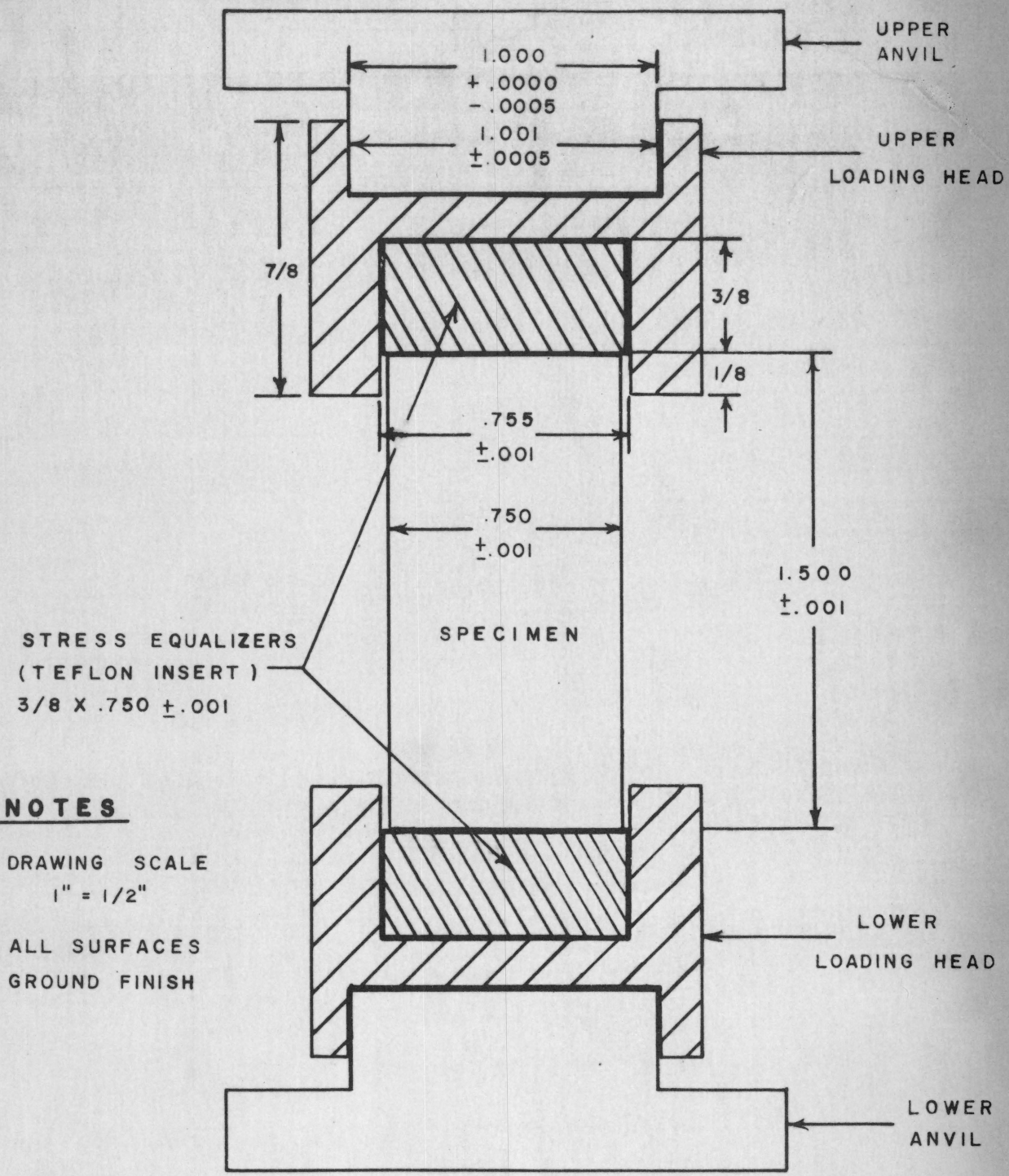


FIGURE 90 - Details of Deformable Insert Type Loading Heads.

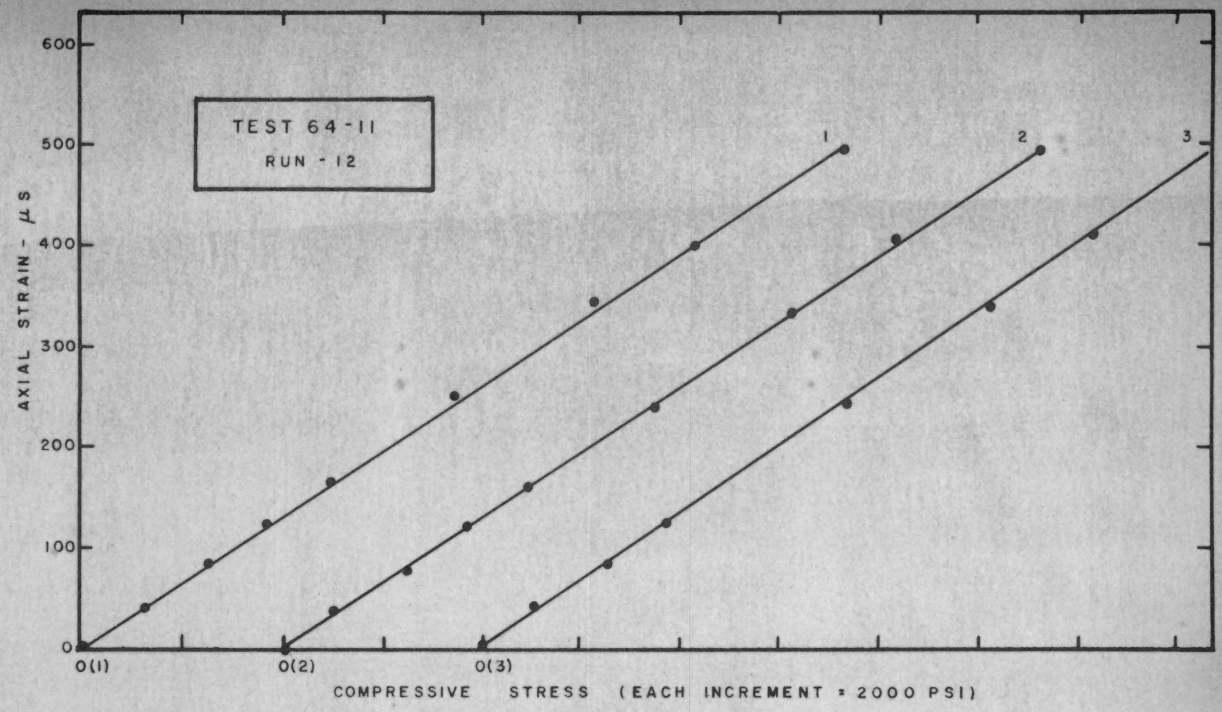


FIGURE 91 - Individual Stress-Strain Curves for Steel Specimen.

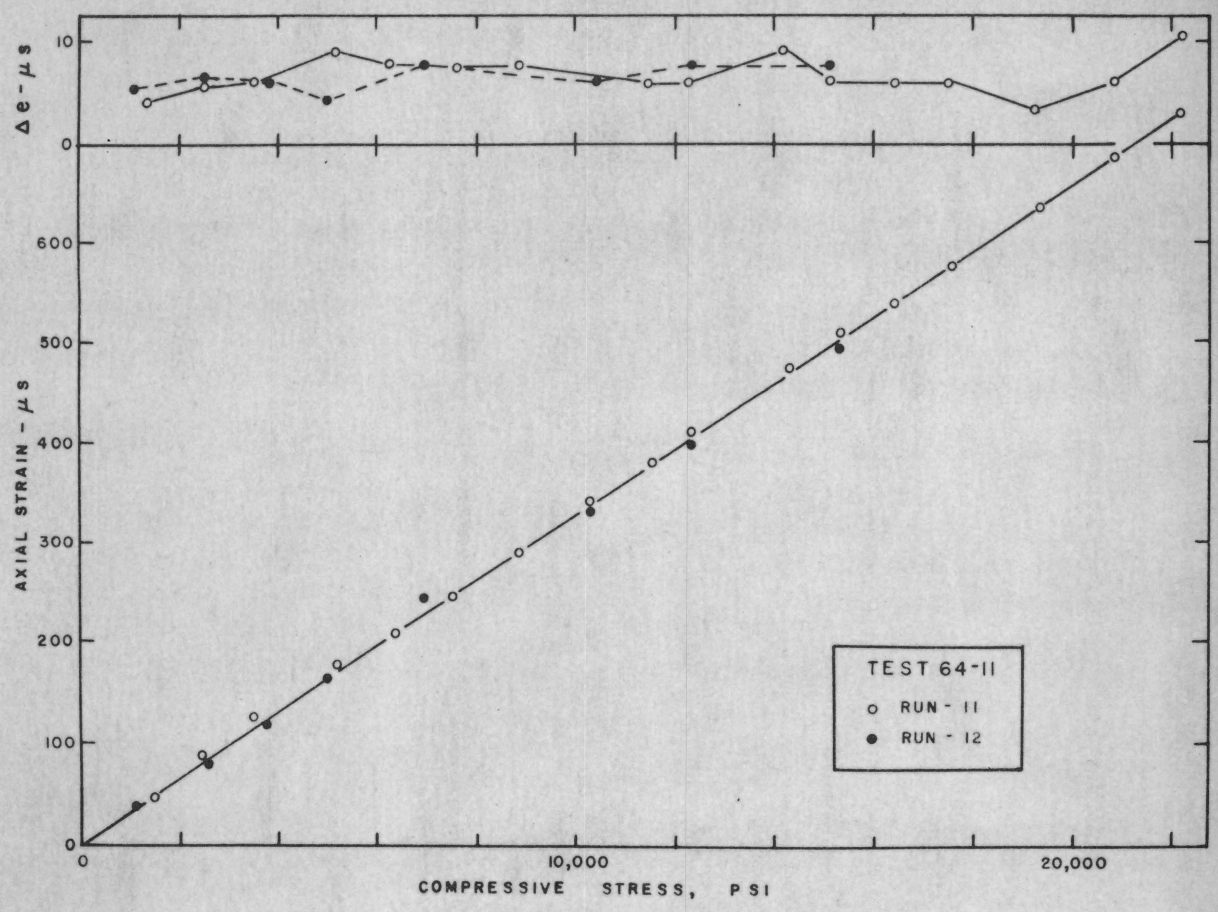


FIGURE 92 - Average Stress-Strain Curve for Steel Specimen.

Examination of the teflon insert after loading showed that a fine lip about 1/64 of an inch high had developed on the insert in the diametric clearance between the specimen and the loading head. The insert however was easily removed and appeared otherwise undamaged. It was decided however to use a new set of teflon inserts for each test to prevent any misalignment due to the presence of the lip.

A series of experiments, using this jig were later conducted on a geologic material*. It was found that although the apparent load uniformity was not as good as with the steel specimen the per cent deviation rarely exceeded 10%. This poorer uniformity is probably due in part to the fact that the material itself has a larger grain size and is not as homogeneous as the steel specimen previously studied. Figure 93 shows the individual stress-strain curves for specimen WO-3 and Figure 94 shows the average stress-strain and deviation curves for the same specimen.

This type of loading jig makes it possible to apply extremely uniform loading to the test specimen and as a result makes it possible to carry out very refined deformation experiments. Figure 95 shows a number of views of the loading jig in the form presently employed. A number of refinements to this design are planned in the future.

---

* Experiments on Wombeyan marble are described in detail earlier in the thesis.

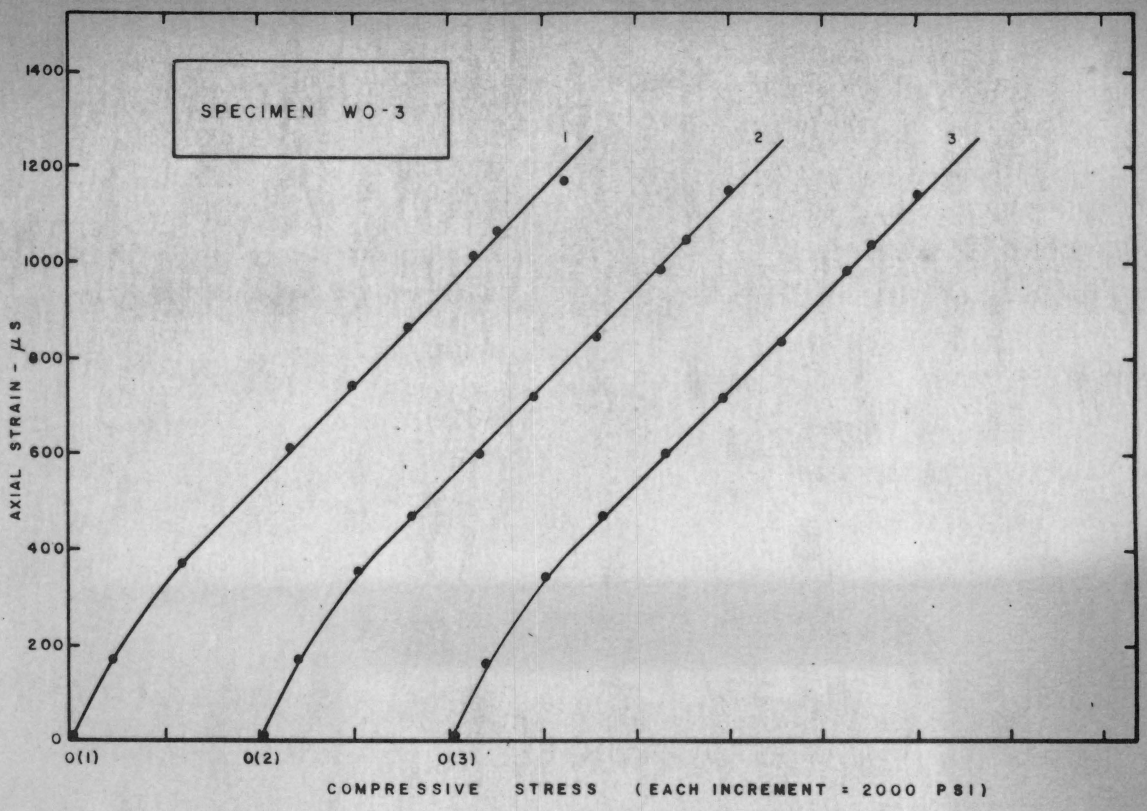


FIGURE 93 - Individual Stress-Strain Curves for Wombeyan Marble.

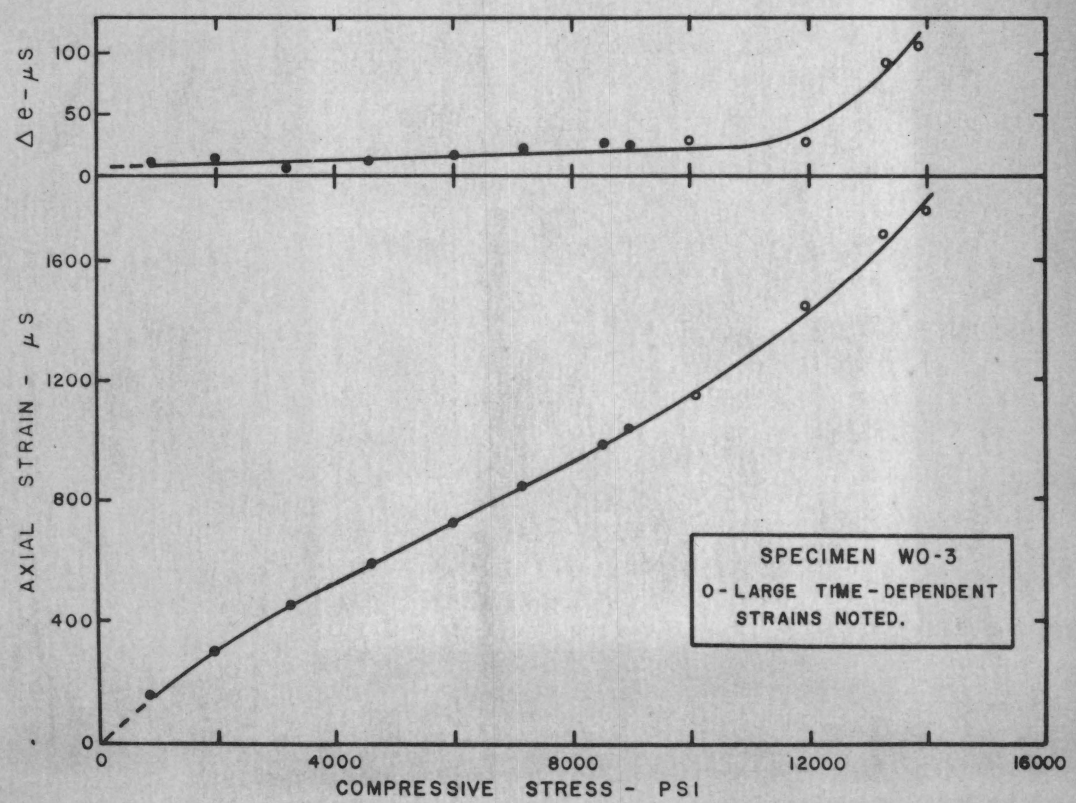
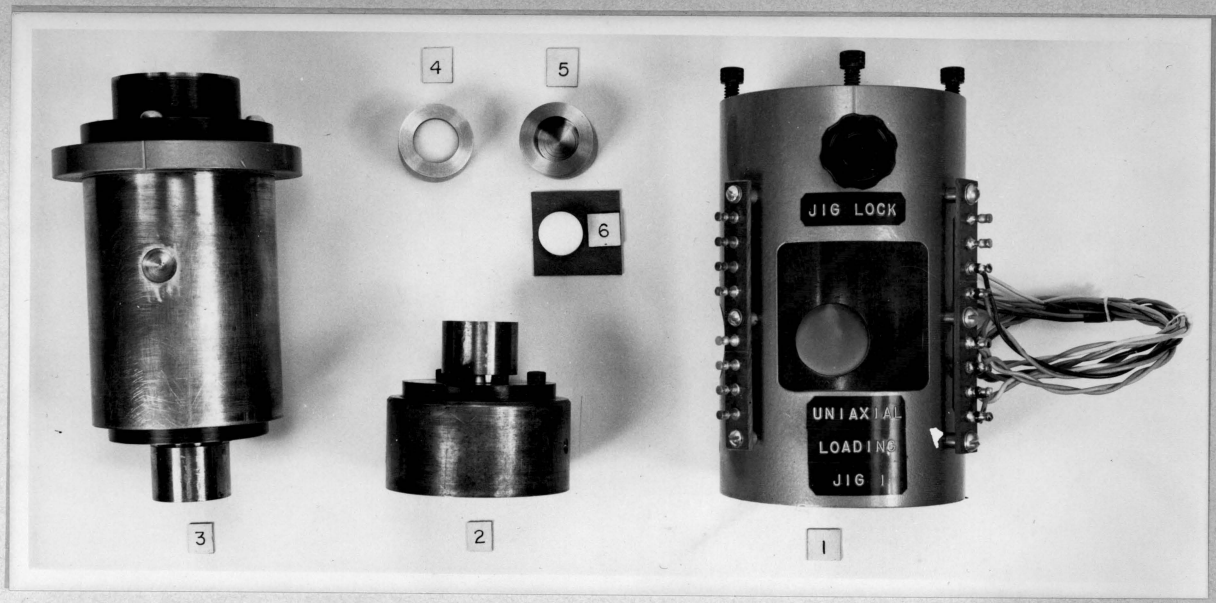


FIGURE 94 - Average Stress-Strain Curve for Wombeyan Marble.



A. Parts of Specimen Loading Jig.

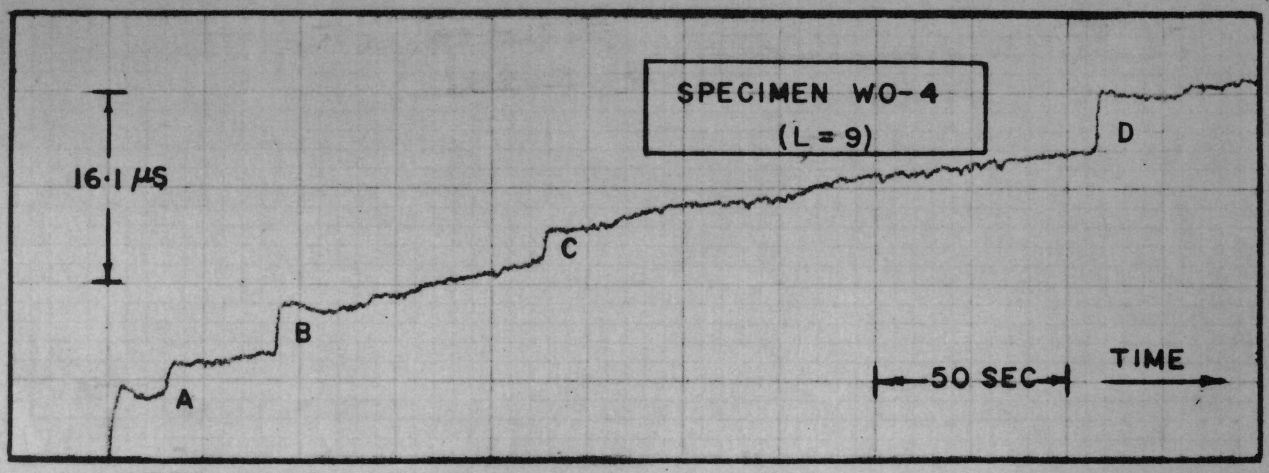


B. Loading Jig Assembled.

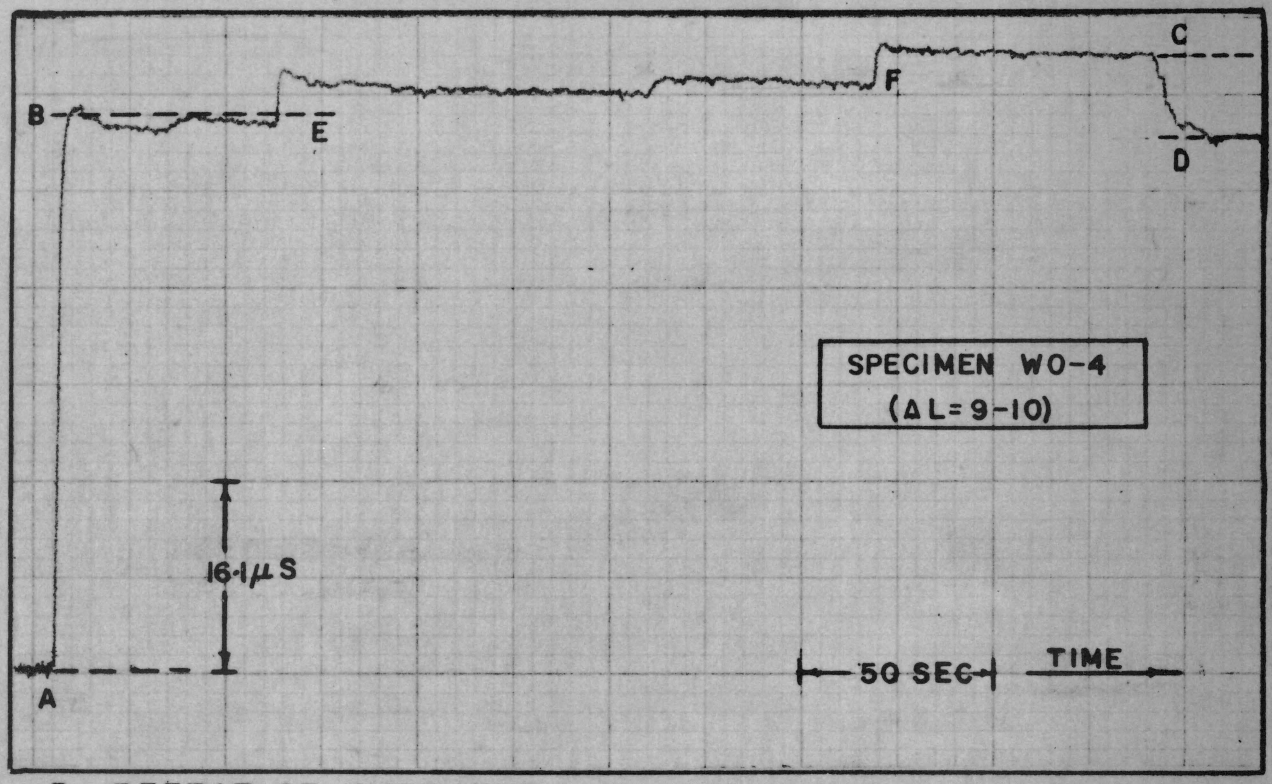
FIGURE 95 - Photographs Showing a Number of Views of Loading Jig.

1.8.4 Loading Jig Friction

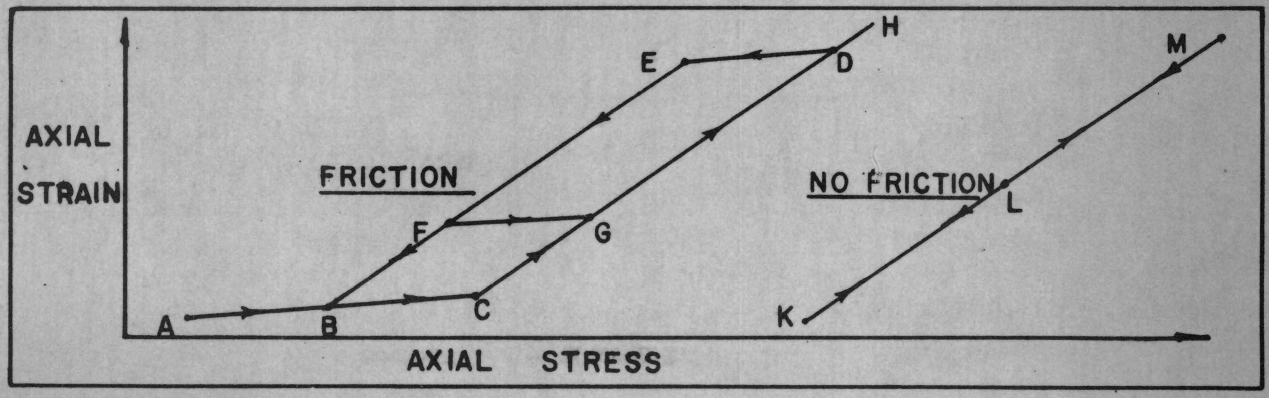
A secondary problem which arises when using a jig which introduces forced alignment is that of friction between the upper moving piston and the walls of the alignment cylinder. Originally this factor was neglected since the piston and cylinder were machined to a smooth finish and under zero load the piston could be freely rotated within the cylinder. However, during initial deformation experiments on Wombeyan marble the strain versus time curves were found to contain a series of step-like variations which appeared to develop each time the load control system brought the load up to the control point. A typical section from one of these strain versus time curves, illustrating a series of these variations at A, B, C and D is shown in Figure 96A. Originally no apparent reason could be found for their presence. Later in these experiments a series of incremental loading/unloading tests were carried out and the results indicated that only a fraction of the instantaneous elastic strain developed during loading appeared to be recoverable. Figure 96B indicates a typical example. Here the application of an incremental load (equivalent to a stress of 1030 psi) at A results in the instantaneous strain AB, however, the removal of the same load at C results in the recovery of a strain of only CD. A series of the characteristic step-like variations are also noted at E and F. At first it was thought these two phenomena were associated with the



A. STEP-LIKE VARIATIONS



B. EFFECT OF INCREMENTAL AND DECREMENTAL LOADING



C. EFFECT OF FRICTION

FIGURE 96 - Curves Showing the Effect of Friction in the Specimen Loading Jig.

material itself, but when a calibrated steel cylinder replaced the rock specimen the same phenomena was observed. To check on this anomalous behavior further, the applied load was cycled over various ranges and stress-strain curves for the steel specimen recorded directly on an X-Y plotter. In all cases an open-looped stress-strain curve was obtained similar to that shown diagrammatically in Figure 96C. As the stress increased from zero, $de/d\sigma$ was initially small up to C where it suddenly increased and remained constant with increased loading. If at some higher stress, Point D, the stress was decreased, $de/d\sigma$ became initially small again until at Point E it increased and remained constant during the remainder of the unloading. Furthermore if the stress was only partially reduced to some Point F and then increased again, the strain followed the path F-G-D-H. These observations verified the fact that the phenomena was definitely frictional, and led to the conclusion that the friction between the upper loading piston and the alignment cylinder was responsible. A rough estimate of this frictional force indicated that it was equivalent to 100 to 300 lbs ram thrust, or 260 - 790 psi specimen stress. This frictional effect easily explained the earlier anomalous behavior which had been noted.

To eliminate this effect the loading procedure was modified to the following: a) the specimen was placed in the assembled loading jig and the jig located in position in the loading frame, b) a small

preload was applied to the specimen to ensure alignment of the specimen in the loading heads, c) the set screws holding the alignment cylinder to the lower jig block were loosened and the alignment cylinder was slid upwards along the upper jig block until it eventually became free of the lower block, d) the alignment cylinder was locked to the upper block in the raised position, e) the test was then continued with the specimen effectively free of the jig. Figure 96C illustrates diagrammatically a stress-strain curve KLM for the steel specimen under these conditions. It was found to be completely closed and repeatable. Using these modified loading conditions it was found that the step-like variations in the strain versus time curves were absent and all the instantaneous strain developed during incremental loading was recovered when the load increment was removed.

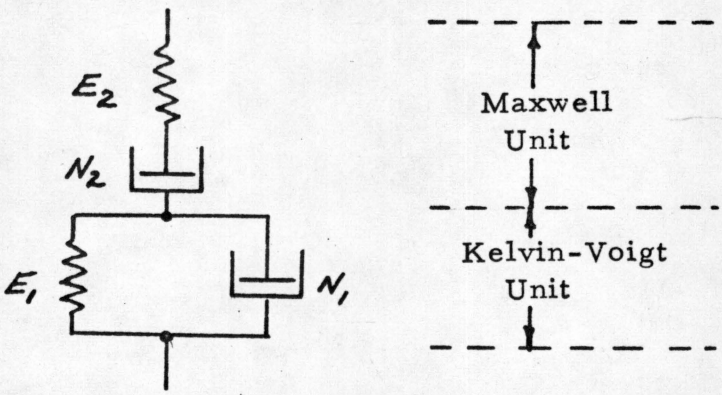
IX

APPENDIX 2

Analysis of the Burgers Mechanical Model

2.1 Governing Equation

The Burgers model consists of the series combination of two units, the Maxwell and the Kelvin-Voigt units. For convenience the governing equation of the Burgers model will be obtained by the addition of the governing equations for the Maxwell and Kelvin-Voigt units.



The combination of the basic model elements follow two sets of rules depending on whether a series or a parallel combination is being considered. In the series combination

$$\sigma_1 = \sigma_2 = \sigma_3 = \cdots = \sigma_m = \sigma \qquad (45),$$

and

$$e_1 + e_2 + e_3 + \cdots + e_m = e \qquad (46),$$

where $\sigma_1, \cdots, \sigma_m$ and $e_1, \cdots, e_m$ are the stresses and strains associated with the individual model elements, and σ and e are the overall stress and strain.

In a parallel combination

$$\sigma_1 + \sigma_2 + \sigma_3 + \cdots + \sigma_n = \sigma \qquad (47),$$

and

$$e_1 = e_2 = e_3 = \cdots = e_n = e \qquad (48).$$

The governing equations for the elastic and the viscous elements themselves are

$$\sigma = E e \qquad (49),$$

and

$$\sigma = N \dot{e} \qquad (50),$$

where E and N are the elastic modulus and the coefficient of viscosity.

For the Maxwell model $\sigma_1 = E_2 e_1$ and $\sigma_2 = N_2 \dot{e}_2$. Now using the combination rules we may write

or
$$e_M = e_1 + e_2$$

$$\dot{e}_M = \dot{e}_1 + \dot{e}_2 \qquad (51),$$

and substituting for the values of $\dot{e}_1$ and $\dot{e}_2$ we obtain

$$\dot{e}_M = \dot{\sigma}_1 / E_2 + \sigma_2 / N_2 \qquad (52),$$

and since $\sigma_M = \sigma_1 = \sigma_2$ equation 52 reduces to

$$\boxed{\dot{e}_M = \dot{\sigma}_M / E_2 + \sigma_M / N_2} \qquad (53).$$

For the Kelvin–Voigt model $\sigma_3 = E_1 e_3$ and $\sigma_4 = N_1 \dot{e}_4$.

Using the parallel combination rules

$$\sigma_K = \sigma_3 + \sigma_4$$

and substituting the values of σ_3 and σ_4 we obtain

$$\sigma_K = E_1 e_3 + N_1 \dot{e}_4 \tag{54},$$

and since $e_K = e_3 = e_4$, equation 54 reduces to

$$\boxed{\sigma_K = E_1 e_K + N_1 \dot{e}_4} \tag{55}.$$

For the Burgers model the overall strain will be given by

$$e = e_M + e_K \tag{56},$$

and the overall stress will be given by

$$\sigma = \sigma_M = \sigma_K \tag{57}.$$

Now differentiating equation 55 with respect to time we obtain

$$\dot{\sigma}_K = E_1 \dot{e}_K + N_1 \ddot{e}_K$$

and rearranging we obtain

$$E_1 \dot{e}_K = \dot{\sigma}_K - N_1 \ddot{e}_K \tag{58}.$$

Multiplying equation 53 by E_1 we obtain

$$E_1 \dot{e}_M = \dot{\sigma}_M E_1/E_2 + \sigma_M E_1/N_2 \tag{59}.$$

Adding equations 58 and 59 we obtain

$$E_1(\dot{e}_K + \dot{e}_M) = \dot{\sigma}_K - N_1 \ddot{e}_K + \dot{\sigma}_M E_1/E_2 + \sigma_M E_1/N_2 \tag{60}.$$

Using equation 57 and noting from equation 56 that

$$\dot{e} = \dot{e}_K + \dot{e}_M$$

equation 60 may be written as

$$E_1 \dot{e} = \dot{\sigma} - N_1 \ddot{e}_K + \dot{\sigma} E_1/E_2 + \sigma E_1/N_2$$

or rearranging

$$\left[1+\frac{E_1}{E_2}\right]\dot{\sigma}+\left(\frac{E_1}{N_2}\right)\sigma=E_1\dot{e}+N_1\ddot{e}_K \qquad (61).$$

Differentiating equation 53 with respect to time and multiplying by N_1 gives

$$\ddot{\sigma}_M N_1/E_2+\dot{\sigma}_M N_1/N_2=N_1\ddot{e}_M \qquad (62).$$

Adding equations 61 and 62 and noting equation 57 we obtain

$$\left(\frac{N_1}{E_2}\right)\ddot{\sigma}+\left[1+\frac{E_1}{E_2}+\frac{N_1}{N_2}\right]\dot{\sigma}+\left(\frac{E_1}{N_2}\right)\sigma=N_1\left(\ddot{e}_K+\ddot{e}_M\right)+E_1\dot{e} \qquad (63).$$

Now from equation 56

$$\ddot{e}=\ddot{e}_K+\ddot{e}_M \qquad (64).$$

Substituting equation 64 into 63 gives

$$\boxed{\left(\frac{N_1}{E_2}\right)\ddot{\sigma}+\left[1+\frac{E_1}{E_2}+\frac{N_1}{N_2}\right]\dot{\sigma}+\left(\frac{E_1}{N_2}\right)\sigma=N_1\ddot{e}+E_1\dot{e}} \qquad (65),$$

which is the governing equation for the Burgers model.

2.2 Specific Equation for $\sigma=\sigma_c$.

Considering the case where the stress is raised from zero to σ_c at $t=0$ and held constant at σ_c for time $t>0$. It is convenient to consider the effects in the Maxwell and the Kelvin-Voigt sections of the model seperately. The governing equation for the Maxwell section is given in equation 53 as

$$\dot{e}_M=\dot{\sigma}_M/E_2+\sigma_M/N_2 .$$

For $\sigma_M=\sigma_c$ this reduces to

$$\dot{e}_M=\sigma_c/N_2$$

Now $$e_M = \int (\sigma_c / N_2)\, dt$$

$$e_M = \frac{\sigma_c t}{N_2} + C_1 \qquad (66).$$

For $t=0$, $e_M = \frac{\sigma_c}{E_2}$ therefore

$$C_1 = \sigma_c / E_2$$

Equation 66 then becomes

$$\boxed{e_M = \frac{\sigma_c t}{N_2} + \frac{\sigma_c}{E_2}} \qquad (67).$$

The governing equation for the Kelvin-Voigt section is given in equation 55

$$\sigma_K = E_1 e_K + N_1 \dot{e}_K$$

For $\sigma_K = \sigma_c$ this becomes

$$N_1 \dot{e}_K + E_1 e_K = \sigma_c \qquad (68).$$

The solution to the homogeneous equation

$$N_1 \dot{e}_K + E_1 e_K = 0$$

will be $$e = \exp(-E_1 t / N_1) \qquad (69).$$

The solution to the inhomogeneous equation (68) will be of the form

$$e_K = C_2 \exp(-E_1 t / N_1) + A_1 t^2 + A_2 t + A_3 \qquad (70),$$

where the coefficients A_1, A_2, A_3 and C_2 must be determined.

Substituting equation 70 into 68 we obtain

$$N_1 \left[-C_1 \left(\frac{E_1}{N_1}\right) \exp(-E_1 t / N_1) + 2A_1 t + A_2 \right] + E_1 \left[C_1 \exp(-E_1 t / N_1) + A_1 t^2 + A_2 t + A_3 \right] = \sigma_c$$

Now the values of the coefficients A_1, A_2 and A_3 are determined by equating the coefficients of like powers of t. We obtain the following

$$E_1 A_1 = 0$$

therefore $A_1 = 0$

$$2N_1 A_1 + E_1 A_2 = 0$$

therefore $A_2 = 0$

$$N_1 A_2 + E_1 A_3 = \sigma_c$$

therefore $A_3 = \sigma_c / E_1$

Equation 70 then reduces to

$$e_K = C_2 \exp(-E_1 t / N_1) + \sigma_c / E_1 \qquad (71).$$

Now for $t = 0$, $e = 0$ equation 71 reduces to

$$0 = C_2 + \sigma_c / E_1$$

$$C_2 = -\sigma_c / E_1$$

Substituting this value of C_2 into equation 71 we obtain

$$\boxed{e_K = \frac{\sigma_c}{E_1}\left(1 - \exp(-E_1 t / N_1)\right)} \qquad (72).$$

The overall strain in the Burgers model will be given by

$$e = e_M + e_K$$

and substituting into this from equations 67 and 72 we obtain, after rearrangement

$$\boxed{e = \frac{\sigma_c}{E_2} + \frac{\sigma_c}{E_1}\left[1 - \exp(-E_1 t / N_1)\right] + \frac{\sigma_c t}{N_2}} \qquad (73).$$

2.3 Specific Equation for $\dot{\sigma}=\dot{\sigma}_c$.

Considering the case where the stress is raised from zero at a rate $\dot{\sigma}=\dot{\sigma}_c$. As previously the effects due to the Maxwell and the Kelvin-Voigt sections will be considered seperately. The governing equation for the Maxwell section is given by equation 53

$$\dot{e}_M = \dot{\sigma}_M/E_2 + \sigma_M/N_2$$

where the various parameters have been defined earlier. Now under the condition $\dot{\sigma}=\dot{\sigma}_c$ we may write

$$\sigma_M = \dot{\sigma}_c t \qquad (74),$$

and the equation for the Maxwell section becomes

$$\dot{e}_M = \dot{\sigma}_c/E_2 + \dot{\sigma}_c t/N_2 \qquad (75).$$

Now

$$e_M = \int(\dot{\sigma}_c/E_2)dt + \int(\dot{\sigma}_c t/N_2)dt$$

which after integration reduces to

$$e_M = \dot{\sigma}_c t/E_2 + \dot{\sigma}_c t^2/2N_2 + C_3 \qquad (76).$$

Now at $t=0$, $e=0$ equation 76 reduces to

$$C_3 = 0$$

Equation 76 therefore becomes

$$e_M = \dot{\sigma}_c t/E_2 + \dot{\sigma}_c t^2/2N_2$$

and substituting $t=\frac{\sigma}{\dot{\sigma}_c}$ this reduces to

$$\boxed{e_M = \sigma/E_2 + \sigma^2/2N_2\dot{\sigma}_c} \qquad (77).$$

The governing equation for the Kelvin-Voigt section is given in equation 55

$$\sigma_K = E_1 e_K + N_1 \dot{e}_K$$

Now substituting for σ_K from equation 74 we obtain

$$N_1 \dot{e}_K + E_1 e_K = \dot{\sigma}_c t \qquad (78).$$

The solution of the homogeneous equation

$$N_1 \dot{e}_K + E_1 e_K = 0$$

will be

$$e = \exp(-E_1 t/N_1)$$

The solution of the inhomogeneous equation (78) will be of the form

$$e_K = C_4 \exp(-E_1 t/N_1) + B_1 t^2 + B_2 t + B_3 \qquad (79),$$

where the coefficients B_1, B_2, B_3 and C_4 must be determined.

Substituting equation 79 into 78 we obtain

$$N_1\left\{-\frac{E_1}{N_1} C_4 \exp(-E_1 t/N_1) + 2B_1 t + B_2\right\} + E_1\left\{C_4 \exp(-E_1 t/N_1) + B_1 t^2 + B_2 t + B_3\right\} = \dot{\sigma}_c t$$

Now the values of the coefficients B_1, B_2 and B_3 are determined by equating the coefficients of terms with like powers of t . This procedure yields the following results

$$E_1 B_1 = 0$$

therefore $B_1 = 0$

$$2B_1 N_1 + E_1 B_2 = \dot{\sigma}_c$$

therefore $B_2 = \dot{\sigma}_c / E_1$

$$N_1 B_2 + E_1 B_3 = 0$$

therefore $B_3 = -N_1 \dot{\sigma}_c / E_1^2$

Equation 79 then reduces to

$$e_K = C_4 \exp(-E_1 t / N_1) + \dot{\sigma}_c t / E_1 - N_1 \dot{\sigma}_c / E_1^2 \qquad (80).$$

Now to determine C_4 we note that at $t=0$, $e=0$. Now equation 80 reduces to

$$0 = C_4 - N_1 \dot{\sigma}_c / E_1^2$$

and therefore $C_4 = N_1 \dot{\sigma}_c / E_1^2$

Substituting this value of C_4 into equation 80 we obtain

$$e_K = (N_1 \dot{\sigma}_c / E_1^2) \exp(-E_1 t / N_1) + \dot{\sigma}_c t / E_1 - N_1 \dot{\sigma}_c / E_1^2$$

Now noting that $t = \frac{\sigma}{\dot{\sigma}_c}$ and rearranging we obtain

$$e_K = \sigma / E_1 - N_1 \dot{\sigma}_c / E_1^2 \left\{ 1 - \exp(-E_1 \sigma / N_1 \dot{\sigma}_c) \right\} \qquad (81).$$

The overall strain in the Burgers model is given by

$$e = e_M + e_K$$

and substituting equations 77 and 81 into this we obtain the required specific equation, namely

$$\epsilon = \sigma\left(\frac{E_1+E_2}{E_1E_2}\right) + \frac{\sigma^2}{2N_2\dot{\sigma}_c} - \frac{N_1\dot{\sigma}_c}{E_1^2}\left\{1-\exp\left(-E_1\sigma/N_1\dot{\sigma}_c\right)\right\} \quad (82).$$

2.4 Effect of Loading Rate

The stress-strain equation for the Burgers model loaded at a constant rate $\dot{\sigma}_c$ was developed in the previous section. Rewriting this for convenience with $\mathcal{T} = \frac{N_1}{E_1}$ equation 82 becomes

$$\epsilon = \frac{\sigma}{E_1} + \frac{\sigma}{E_2} + \frac{\sigma^2}{2N_2\dot{\sigma}_c} - \frac{\dot{\sigma}_c\mathcal{T}}{E_1}\left(1-\exp\left(-\sigma/\mathcal{T}\dot{\sigma}_c\right)\right) \quad (83).$$

Now considering the effect of large rates of loading it is seen that the first two terms in equation are independent of $\dot{\sigma}_c$. The third term, which arises from the Maxwell section, will tend to zero for all but very small values of $\dot{\sigma}_c$ since N_2 for most rocks is of the order of 10^9-10^{13} psi-sec. The fourth term, which arises from the Kelvin-Voigt section, is more complex and will be considered seperately. This term is

$$T_4 = \frac{\dot{\sigma}_c\mathcal{T}}{E_1}\left\{1-\exp\left(-\sigma/\mathcal{T}\dot{\sigma}_c\right)\right\} \quad (84).$$

For most rocks investigated the values of $\mathcal{T}$ range from 10-10^5 seconds, therefore for all but very small values of $\dot{\sigma}_c$ the factor $\sigma/\mathcal{T}\dot{\sigma}_c$ will be small and the exponential may be expanded in series

form retaining only the first three terms, namely

$$T_4 = \frac{\dot{\sigma}_c \mathcal{T}}{E_1}\left\{1-\left(1-\frac{\sigma}{\mathcal{T}\dot{\sigma}_c}+\frac{1}{2}\left(\frac{\sigma}{\mathcal{T}\dot{\sigma}_c}\right)^2\right)\right\}$$

$$T_4 = \frac{\dot{\sigma}_c \mathcal{T}}{E_1}\left\{\frac{\sigma}{\mathcal{T}\dot{\sigma}_c}\left(1-\frac{\sigma}{2\mathcal{T}\dot{\sigma}_c}\right)\right\}$$

therefore

$$T_4 = \frac{\sigma}{E_1}\left(1-\frac{\sigma}{2\mathcal{T}\dot{\sigma}_c}\right) \qquad (85).$$

Now substituting equation 85 into 83 we obtain

$$e = \frac{\sigma}{E_2}+\frac{\sigma^2}{2N_2\dot{\sigma}_c}+\frac{\sigma^2}{2E_1\mathcal{T}\dot{\sigma}_c}$$

Substituting for $\mathcal{T}$ and rearranging we obtain the following

$$e = \frac{\sigma}{E_2}+\frac{\sigma^2}{2\dot{\sigma}_c}\left(\frac{N_1+N_2}{N_1N_2}\right) \qquad (86).$$

For very rapid rates of loading where $\dot{\sigma}_c \gg \frac{N_1+N_2}{N_1N_2}$ equation 86 reduces to

$$e = \sigma/E_2$$

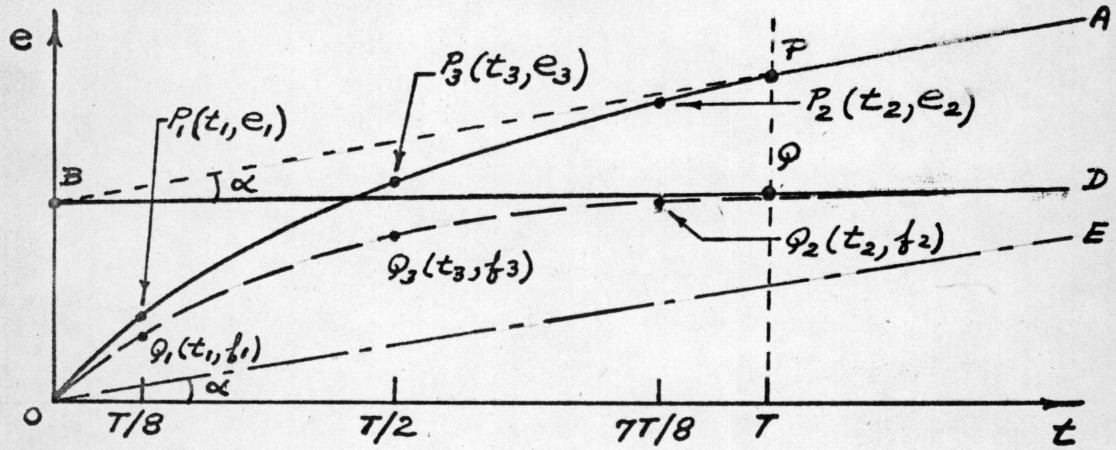
Indicating that the model behaves as a purely elastic material with modulus E_2 at very rapid rates of loading.

X

APPENDIX 3

Determination of Initial Parameters

The corrected creep curve (OPA) may be considered to consist of the superposition of two curves , the transient creep curve (OQD) and the steady state curve (OE).



The overall creep curve may be defined by

$$e(t) = A\{1 - \exp(-t/B)\} + Ct$$

where the transient creep curve is represented by

$$e_{tr} = A\{1 - \exp(-t/B)\} \qquad (87),$$

and the steady state creep curve is represented by

$$e_{ss} = Ct \qquad (88).$$

It is necessary to obtain approximate (initial) values of the parameters A, B and C , namely A_0, B_0 and C_0 from the creep curves in order to process the experimental data using the Newton-Gauss method of least squares.

The parameter C_o is the slope of the steady state creep curve. It is determined directly from the slope of the tangent (BA) to the corrected creep curve, namely

$$C_o = \tan \alpha \qquad (89).$$

The other two parameters must be determined from the transient creep curve itself. In order to eliminate actual graphical construction of this curve an analytical approach is used. To obtain suitable initial parameters it is necessary to base their calculation on a number of points on the curve. It was decided to use three such points for these calculations and for the sake of consistancy the following procedure was established for their selection: a point P was selected on the corrected creep curve at a location just outside where the line AB becomes tangent to the creep curve. The corresponding time co-ordinate T of the point was noted. Three other points P_1, P_2 and P_3 are then located on the curve with coordinates (t_1, e_1), (t_2, e_2) and (t_3, e_3), where t_1, t_2 and t_3 are defined as $T/8, 7T/8$ and $T/2$ respectively. Now the strains f_1, f_2 and f_3 at the corresponding points Q_1, Q_2 and Q_3 on the transient creep curve may be obtained by noting that

$$f_m = e_m - C_o t_m \qquad (90),$$

where $m = 1, 2, 3$. Now equation 87 may be rewritten for point on the transient curve as

$$\frac{f_m - A_0}{A_0} = -\exp\{-t_m/B_0\}$$

or

$$\ln\left(\frac{A_0 - f_m}{A_0}\right) = -t_m/B_0 \qquad (91).$$

Now the time coordinates of the points Q_1, Q_2 and Q_3 have been selected so that

$$t_3 = \frac{t_1 + t_2}{2} \qquad (92).$$

Now multiplying this equation by $1/B_0$ and rearranging we obtain

$$2t_3/B_0 = t_1/B_0 + t_2/B_0 \qquad (93).$$

Now substituting for t_1/B_0, t_2/B_0 and t_3/B_0 from equation 91 we obtain

$$2\left\{\ln\left(\frac{A_0 - f_3}{A_0}\right)\right\} = \ln\left(\frac{A_0 - f_1}{A_0}\right) + \ln\left(\frac{A_0 - f_2}{A_0}\right)$$

which reduces to

$$(A_0 - f_3)^2 = (A_0 - f_1)(A_0 - f_2) \qquad (94).$$

Expanding both sides we obtain

$$A_0^2 - 2A_0 f_3 + f_3^2 = A_0^2 - A_0 f_1 - A_0 f_2 + f_1 f_2$$

and rearranging this reduces to

$$A_0(2f_3 - f_1 - f_2) = f_3^2 - f_1 f_2$$

and finally to

$$\boxed{A_0 = \frac{f_3^2 - f_1 f_2}{2f_3 - f_1 - f_2}} \qquad (95).$$

Now equation 91 may be rewritten as

$$B_m = \frac{-t_m}{\ln\left(\frac{A_o - f_m}{A_o}\right)}$$

and rearranging we obtain

$$\boxed{B_m = \frac{t_m}{\ln\left(\frac{A_o}{A_o - f_m}\right)}} \qquad (96).$$

The value of B_o is calculated from the equation

$$\boxed{B_o = \sum_{o}^{3} B_m / 3} \qquad (97),$$

which provides an estimate of B_o which is based on the data from three points on the creep curve.

XI

APPENDIX 4

Computer Program

A copy of the Fortran program, which was written for analyzing creep data in terms of the Burgers mechanical model, is given in Table 20. The required input data is as follows:

(a) A0 , B0 , C0 , M0
FORMAT (2F 10.2 , F15.9 , I3)

(b) STRI , STRFI , STRAI
FORMAT (2F 10.1 , F 10.2)

(c) ER
FORMAT (F 5.3)

(d) M , T(I) , VX(I)
FORMAT (I3 , 2F 10.2)

where A0, B0, and C0 are the initial values of the parameters A , B and C ; M0 is the number of data points on the creep curve ; STRI and STRFI are the initial and final stress levels ; STRAI is the instantaneous elastic strain which occurs when the stress is changed from its initial to its final level ; ER is a factor which determines whether a sufficient number of iterations have been carried out (usually taken to be 0.95) ; M is the data point number ; and T(I) and VX(I) are the time and strain coordinates of the various data points* on the corrected creep curves. Tables 21 and 22 illustrates typical computer output data from the analysis on an incremental experiment.

---

* Note that the point T=0 , VX=0 is considered to be the point M=0 .

TABLE 20

Fortran Program for Analysis of Creep Data Using the Burgers Model

```
200 READ 1,A0,B0,C0,M0
  1 FORMAT(2F10.2,F15.9,I3)
    NUM=0
    IF(A0)400,401,400
400 READ 3,STRI,STRFI,STRAI
  3 FORMAT(2F10.1,F10.2)
    STRES=STRFI-STRI
    PRINT 4
  4 FORMAT(1H1,23H  BURGER MODEL ANALYSIS//8H  SAMPLE//)
    PRINT 52,STRI
 52 FORMAT(1H ,17H INITIAL STRESS =,F10.1,4H PSI)
    PRINT 53,STRFI
 53 FORMAT(1H0,15H FINAL STRESS =,F12.2,4H PSI)
    PRINT 54,STRES
 54 FORMAT (1H0,16H STRESS CHANGE =,F11.1,4H PSI/)
    L=0
    DIMENSION S(4,4),F(4),X(4),T(100),VX(100),VT(100)
    READ 33,ER
 33 FORMAT(F5.3)
100 PRINT 7,NUM,A0
  7 FORMAT(1H ,I5,10X,5H A = ,F10.2,22H  MICROINCHES PER INCH/)
    PRINT 8,B0
  8 FORMAT(1H ,15X,5H B = ,F10.2,9H  SECONDS/)
    PRINT 9,C0
  9 FORMAT(1H ,15X,5H C = ,F13.9,32H MICROINCHES PER INCH PER SECOND/)
    I=1
    B01=1./B0
    DO 5 K = 1,4
    X(K)=0
    DO 5 J= K,4
  5 S(J,K)=0
    IF(L-1)10,99,99
```

TABLE 20 (Cont'd)

Fortran Program for Analysis of Creep Data Using the Burgers Model

```
   10 READ 2,M,T(I),VX(I)
    2 FORMAT(I3,2F10.2)
   99 EXPO= EXPF(-T(I)*B01)
      F(1)= -1.+EXPO
      F(2)= A0*T(I)*EXPO*B01*B01
      F(3)=-T(I)
      F(4)=VX(I)-(A0*(1.-EXPO)+C0*T(I))
      DO 6 K= 1,4
      DO 6 J= K,4
    6 S(J,K)=S(J,K)+F(J)*F(K)
      I=I+1
      IF(L-1)97,98,98
   97 IF(I-M0)10,10,96
   96 L=1
   98 IF(I-M0)99,99,93
   93 IF(M-M0)92,20,92
   92 PRINT 91,M
   91 FORMAT(1H ,29H NUMBER OF CARDS DO NOT CHECK/4H M =,I3)
      CALL EXIT
   20 KM0 = M0 - 3
      FM0 = KM0
      RES0 = SQRTF(S(4,4)/FM0)
      PRINT 24,RES0
   24 FORMAT (1H ,25X, 17H STANDARD DEVN = ,F9.4/)
      DO 89 K = 1,4
      DO 89 J = K,4
   89 S(K,J)= S(J,K)
      DO 19 I =1,3
      IF(S(I,I))18,17,18
   18 IF(I-3)15,16,16
   15 MN=I+1
      DO 19 J = MN,3
```

TABLE 20 (Cont'd)

Fortran Program for Analysis of Creep Data Using the Burgers Model

```
      DO 19 K = MN,4
   19 S(J,K)= S(J,K)-S(J,I)*S(I,K)/S(I,I)
   17 PRINT 14
   14 FORMAT (1H ,15H S(I,I) IS ZERO)
      GO TO 200
   16 DO 13 MN= 1,3
      N= 4-MN
      X(N)= S(N,4)-S(N,2)*X(2)-S(N,3)*X(3)
   13 X(N)=X(N)/S(N,N)
      A1=A0-X(1)
      B1=B0-X(2)
      C1=C0-X(3)
      IF (C1) 201,202,202
  201  C1 = 0
  202 RES=0
      DO 12 K= 1,M0
      EXP1=EXPF(-T(K)/B1)
      DIFF=VX(K)-(A1*(1.-EXP1)+C1*T(K))
   12 RES=RES+DIFF**2
      NUM=NUM+1
      RES1=SQRTF(RES/FM0)
      IF(NUM-4)11,30,30
   11 RATIO =RES1/RES0
      IF(RATIO-ER)21,21,30
   21 A0=A1
      B0=B1
      C0=C1
      GO TO 100
   30 PRINT 7,NUM,A1
      PRINT 8,B1
      PRINT 9,C1
      PRINT 24,RES1
   38 E1= STRES/A1
```

TABLE 20 (Cont'd)

Fortran Program for Analysis of Creep Data Using the Burgers Model

```
      EN1= E1*B1/1000.
      IF (C1) 203,204,203
  203  EN2 = STRFI/C1/1000.
  204 PRINT 41,E1
   41 FORMAT(1H ,20X,5H E1= ,F20.8,22H TIMES 10 TO THE 6 PSI)
      PRINT 42,EN1
   42 FORMAT(1H0,20X,5H N1= ,F20.8,30H TIMES 10 TO THE 9 PSI SECONDS)
      IF(STRAI)37,153,37
   37 E2= STRES/STRAI
      PRINT 43,E2
   43 FORMAT(1H0,20X,5H E2= ,F20.8,22H TIMES 10 TO THE 6 PSI)
      IF (C1) 205,205,153
  205 PRINT 206
  206 FORMAT (1H0, 20X, 16H  N2 IS INFINITE/)
      GO TO 207
  153 PRINT  44,EN2
   44 FORMAT (1H0,20X,4H N2=,F21.8,30H TIMES 10 TO THE 9 PSI SECONDS)
  207 PRINT 45
   45 FORMAT (1H1,38H  DATA FOR COMPARISON OF RESULTS GRAPH//)
      PRINT 46
   46 FORMAT (1H , 10X, 2H T, 22X, 3H VX, 22X, 3H VT/)
      B02=1./B1
      DO 50 N =1,M0
      VT(N)=A1*(1.-EXPF(-T(N)*B02))+C1*T(N)
   50 PRINT 51,T(N),VX(N),VT(N)
   51 FORMAT(F15.1,2F25.3)
      GO TO 200
  401 CALL EXIT
      END
```

TABLE 21

Typical Computer Output Data : Section-1

```
 BURGER MODEL ANALYSIS
SAMPLE  WO-4

INITIAL STRESS =   11833.0 PSI
FINAL STRESS =    12338.00 PSI
STRESS CHANGE =      505.0 PSI
   0   A =      12.72  MICROINCHES PER INCH
       B =     137.00  SECONDS
       C =     .00733000 MICROINCHES PER INCH PER SECOND
                 STANDARD DEVN =     .2300
   1   A =      12.69  MICROINCHES PER INCH
       B =     134.16  SECONDS
       C =     .00715187 MICROINCHES PER INCH PER SECOND
                 STANDARD DEVN =     .1779
   2   A =      12.69  MICROINCHES PER INCH
       B =     134.00  SECONDS
       C =     .00715695 MICROINCHES PER INCH PER SECOND
                 STANDARD DEVN =     .1779

   E1=          39.78948200 TIMES 10 TO THE 6 PSI
   N1=           5.33210690 TIMES 10 TO THE 9 PSI SECONDS
   E2=           8.92226140 TIMES 10 TO THE 6 PSI
   N2=        1723.91670000 TIMES 10 TO THE 9 PSI SECONDS
```

TABLE 22

Typical Computer Output Data : Section-2

DATA FOR COMPARISON OF RESULTS GRAPH

T	VX	VT
30.0	2.720	2.760
60.0	5.120	5.010
90.0	7.360	6.851
120.0	8.480	8.367
150.0	9.760	9.621
180.0	10.720	10.667
210.0	11.360	11.546
240.0	12.160	12.292
270.0	12.480	12.931
300.0	13.280	13.485
330.0	13.760	13.972
360.0	14.240	14.403
390.0	14.720	14.791
420.0	15.040	15.145
450.0	15.680	15.470
480.0	15.840	15.774
510.0	16.160	16.059
540.0	16.320	16.330
600.0	17.120	16.841
660.0	17.440	17.323
720.0	17.920	17.785
780.0	18.400	18.236
840.0	18.560	18.679
900.0	19.200	19.117
960.0	19.520	19.552
1020.0	20.000	19.985
1080.0	20.480	20.417
1140.0	20.960	20.848
1200.0	21.280	21.278
1260.0	21.760	21.708
1320.0	22.240	22.138
1380.0	22.400	22.567
1440.0	22.720	22.997

XII

APPENDIX 5

Tabulated Data from Individual Incremental Creep Experiments

Tables 23 to 48 list the strain versus time data from the experiments conducted on specimens WO-5, WO-6 and WO-7. In each table both the corrected observed axial strain (e_c) and the corresponding theoretical axial strain (e_T) determined from the computer analysis of the overall strain versus time data are presented.

TABLE 23

Creep Strain Data - Experiment WO-5(1)

σ_f = 7,672 PSI	$\Delta\sigma$ = 646 PSI	
TIME	AXIAL STRAIN	
SECONDS	$e_c - \mu S$	$e_T - \mu S$
0.0	0.000	0.000
3.0	.100	.103
33.0	.700	.938
63.0	1.700	1.494
93.0	1.700	1.866
123.0	2.100	2.115
153.0	2.500	2.284
183.0	2.300	2.399
213.0	2.600	2.479
243.0	2.900	2.535
273.0	2.300	2.575
303.0	2.100	2.605
363.0	3.400	2.648
423.0	2.100	2.677
483.0	2.700	2.702
543.0	2.900	2.723

TABLE 24

Creep Strain Data - Experiment WO-5(2)

σ_f = 8,181 PSI	$\Delta\sigma$ = 509 PSI	
TIME	AXIAL STRAIN	
SECONDS	$e_C - \mu S$	$e_T - \mu S$
0.0	0.000	0.000
5.0	.800	.202
10.0	1.200	.393
15.0	1.000	.574
45.0	1.200	1.459
75.0	2.000	2.085
105.0	3.100	2.532
135.0	3.400	2.854
165.0	2.600	3.091
195.0	2.400	3.268
225.0	2.500	3.404
255.0	3.600	3.511
315.0	3.100	3.672
375.0	5.600	3.794
435.0	4.300	3.898
495.0	4.000	3.992
555.0	4.500	4.082
675.0	3.800	4.257
795.0	3.500	4.429
915.0	4.800	4.601
1095.0	5.100	4.859

TABLE 25

Creep Strain Data - Experiment WO-5(3)

σ_f = 8,685 PSI	$\Delta\sigma$ = 504 PSI	
TIME	AXIAL STRAIN	
SECONDS	$e_C - \mu S$	$e_T - \mu S$
0.0	0.000	0.000
3.0	1.000	.522
13.0	2.000	1.837
23.0	2.500	2.684
53.0	3.500	3.839
83.0	4.000	4.209
113.0	4.600	4.378
143.0	5.000	4.495
173.0	3.500	4.599
203.0	5.200	4.700
233.0	5.000	4.800
263.0	5.000	4.899
323.0	5.100	5.098
383.0	4.700	5.297
443.0	6.100	5.495
503.0	5.600	5.694
623.0	6.300	6.092
743.0	7.000	6.489
863.0	6.900	6.887
983.0	6.900	7.284
1103.0	7.500	7.682
1223.0	8.100	8.079

TABLE 26

Creep Strain Data - Experiment WO-5(4)

σ_f = 8,964 PSI	$\Delta\sigma$ = 279 PSI	
TIME	AXIAL STRAIN	
SECONDS	$e_c - \mu S$	$e_T - \mu S$
0.0	0.000	0.000
1.0	.200	.005
6.0	.200	.032
11.0	0.000	.058
106.0	.300	.500
136.0	.800	.618
166.0	1.000	.728
196.0	1.200	.831
226.0	.600	.927
256.0	.700	1.016
316.0	.800	1.180
376.0	2.100	1.325
436.0	1.000	1.456
496.0	1.500	1.575
616.0	2.200	1.785
736.0	2.000	1.969
856.0	2.300	2.136
976.0	1.600	2.291
1096.0	2.800	2.439
1216.0	2.600	2.582

TABLE 27

Creep Strain Data - Experiment WO-5(5)

σ_f = 9,720 PSI	$\Delta\sigma$ = 756 PSI	
TIME	AXIAL STRAIN	
SECONDS	$e_C - \mu S$	$e_T - \mu S$
0.0	0.000	0.000
5.0	1.700	1.127
10.0	3.600	2.123
15.0	4.400	3.006
45.0	5.900	6.542
75.0	8.100	8.279
105.0	8.700	9.167
135.0	8.600	9.655
165.0	9.400	9.955
195.0	10.100	10.166
225.0	9.500	10.334
255.0	9.400	10.484
285.0	10.200	10.623
315.0	10.500	10.759
345.0	11.100	10.892
375.0	10.700	11.024
435.0	11.200	11.288
495.0	12.000	11.551
555.0	13.700	11.814
615.0	13.300	12.077
735.0	13.000	12.602
855.0	14.500	13.128
975.0	14.300	13.654
1095.0	14.500	14.180
1275.0	15.800	14.968
1455.0	15.300	15.757
1635.0	16.200	16.546
1815.0	16.900	17.334
1995.0	16.900	18.123

TABLE 28

Creep Strain Data - Experiment WO-5(6)

σ_f = 10,140 PSI	$\Delta\sigma$ = 420	
TIME	AXIAL STRAIN	
SECONDS	$e_C - \mu S$	$e_T - \mu S$
0.0	0.000	0.000
5.0	.200	.138
10.0	.400	.273
15.0	.800	.405
20.0	1.100	.534
30.0	.700	.783
40.0	.900	1.020
70.0	2.500	1.668
100.0	2.500	2.232
130.0	2.900	2.724
160.0	3.200	3.154
190.0	3.600	3.532
220.0	3.200	3.866
250.0	3.400	4.161
280.0	4.200	4.423
340.0	5.100	4.869
400.0	5.400	5.232
460.0	5.300	5.535
520.0	5.900	5.795
640.0	6.300	6.228
760.0	7.100	6.592
880.0	7.100	6.919
1000.0	7.000	7.226
1120.0	7.400	7.523
1240.0	7.800	7.814
1420.0	8.500	8.246
1600.0	8.200	8.674
1780.0	9.500	9.102
1960.0	9.000	9.530
2140.0	10.700	9.957
2320.0	10.000	10.385

TABLE 29

Creep Strain Data - Experiment WO-5(7)

σ_f = 10,880 PSI	$\Delta\sigma$ = 740 PSI	
TIME	AXIAL STRAIN	
SECONDS	$e_C - \mu S$	$e_T - \mu S$
0.0	0.000	0.000
5.0	3.000	1.049
10.0	4.700	2.056
30.0	7.400	5.708
50.0	9.900	8.823
70.0	13.900	11.482
90.0	15.800	13.753
110.0	17.600	15.697
130.0	16.800	17.363
150.0	18.200	18.792
170.0	19.600	20.021
190.0	19.400	21.080
220.0	21.000	22.406
250.0	21.400	23.477
280.0	21.800	24.350
310.0	23.000	25.068
340.0	23.900	25.665
370.0	25.800	26.167
430.0	27.700	26.965
490.0	27.200	27.580
550.0	27.300	28.083
610.0	29.300	28.517
790.0	31.200	29.629
970.0	32.500	30.642
1150.0	33.300	31.631
1330.0	33.800	32.615
1510.0	34.800	33.598
1690.0	36.200	34.581
1870.0	37.000	35.564
2050.0	36.800	36.546
2230.0	38.100	37.529
2410.0	38.400	38.512
2590.0	39.700	39.494
2770.0	39.800	40.477
2950.0	40.000	41.459
3130.0	40.200	42.442

TABLE 30

Creep Strain Data - Experiment WO-5(8)

σ_f = 11,557 PSI	$\Delta\sigma$ = 677 PSI	
TIME	AXIAL STRAIN	
SECONDS	$e_c - \mu S$	$e_T - \mu S$
0.0	0.000	0.000
10.0	3.400	2.265
20.0	3.500	3.542
30.0	3.900	4.274
40.0	3.400	4.705
60.0	4.800	5.141
80.0	4.400	5.355
100.0	5.400	5.501
120.0	5.800	5.627
140.0	6.600	5.747
160.0	5.500	5.865
180.0	5.800	5.982
200.0	6.200	6.099
220.0	6.100	6.215
250.0	5.800	6.391
280.0	6.400	6.566
310.0	6.900	6.741
340.0	5.300	6.917
370.0	6.600	7.092
400.0	6.600	7.267
460.0	7.900	7.618
520.0	9.100	7.968
580.0	9.300	8.319
640.0	9.600	8.669
820.0	11.900	9.721
1000.0	12.400	10.772
1180.0	12.400	11.824
1360.0	12.700	12.875
1540.0	14.000	13.927
1720.0	14.900	14.978
1900.0	15.200	16.030
2080.0	15.700	17.081

TABLE 31

Creep Strain Data - Experiment WO-5(10)

σ_f = 12,005 PSI	$\Delta\sigma$ = 1,225 PSI	
TIME	AXIAL STRAIN	
SECONDS	$e_C - \mu S$	$e_T - \mu S$
0.0	0.000	0.000
3.0	1.400	.101
8.0	1.800	.269
13.0	1.600	.437
18.0	1.000	.604
28.0	.800	.935
38.0	.700	1.263
68.0	1.600	2.227
98.0	4.500	3.163
128.0	5.700	4.072
158.0	6.000	4.954
188.0	7.000	5.811
208.0	6.500	6.368
238.0	7.400	7.184
268.0	7.700	7.977
328.0	9.300	9.495
388.0	10.000	10.928
448.0	11.800	12.282
508.0	13.400	13.562
628.0	15.500	15.918
748.0	18.100	18.030
868.0	19.200	19.928
988.0	20.800	21.640
1108.0	23.700	23.188
1288.0	26.200	25.246
1468.0	26.700	27.040
1648.0	28.700	28.616
1828.0	30.700	30.014
2008.0	31.400	31.266
2188.0	32.400	32.398
2368.0	32.900	33.432

TABLE 32

Creep Strain Data - Experiment WO-5(11)

σ_f = 12,453 PSI	$\Delta\sigma$ = 448 PSI	
TIME	AXIAL STRAIN	
SECONDS	$e_C - \mu S$	$e_T - \mu S$
0.0	0.000	0.000
25.0	.900	4.021
40.0	3.900	6.359
55.0	5.900	8.641
70.0	10.700	10.871
100.0	16.100	15.176
130.0	20.700	19.283
160.0	24.100	23.203
190.0	27.800	26.945
220.0	32.300	30.518
250.0	35.800	33.930
280.0	39.400	37.190
310.0	41.200	40.304
340.0	43.700	43.281
370.0	47.200	46.126
430.0	51.900	51.451
490.0	56.900	56.327
550.0	61.000	60.798
610.0	64.000	64.904
730.0	70.600	72.157
850.0	76.700	78.334
970.0	81.100	83.633
1150.0	89.400	90.285
1270.0	92.100	94.040
1390.0	96.300	97.368
1630.0	100.700	103.044
1870.0	106.500	107.789
2110.0	113.500	111.915
2350.0	119.500	115.631
2590.0	122.000	119.076
2830.0	124.400	122.340
3070.0	127.400	125.485
3310.0	129.000	128.551
3550.0	131.000	131.565
3790.0	133.800	134.543
4030.0	136.000	137.499
4270.0	138.400	140.439

TABLE 33

Creep Strain Data - Experiment WO-6(1)

σ_f = 8,101 PSI	$\Delta\sigma$ = 614 PSI	
TIME	AXIAL STRAIN	
SECONDS	$e_C - \mu S$	$e_T - \mu S$
0.0	0.000	0.000
6.0	1.900	.839
21.0	4.300	2.693
36.0	4.900	4.247
51.0	5.900	5.551
81.0	7.500	7.569
111.0	8.700	9.008
141.0	9.900	10.047
171.0	10.300	10.808
201.0	9.600	11.378
231.0	11.700	11.816
261.0	11.700	12.162
291.0	12.900	12.445
351.0	13.400	12.893
411.0	13.900	13.255
471.0	12.800	13.575
531.0	14.900	13.876
591.0	14.700	14.168
711.0	14.500	14.739
831.0	15.800	15.306
951.0	16.100	15.872
1071.0	16.600	16.438
1191.0	17.400	17.004
1371.0	17.800	17.852
1551.0	17.300	18.700
2151.0	21.200	21.528
2271.0	22.100	22.094
2386.0	23.200	22.636

TABLE 34

Creep Strain Data - Experiment WO-6(2)

σ_f = 8,754 PSI	$\Delta\sigma$ = 653 PSI	
TIME	AXIAL STRAIN	
SECONDS	$e_C - \mu S$	$e_T - \mu S$
0.0	0.000	0.000
15.0	7.300	4.489
30.0	9.500	7.738
45.0	9.400	10.096
60.0	10.500	11.813
90.0	12.100	13.998
120.0	13.500	15.208
150.0	15.100	15.915
180.0	14.800	16.362
210.0	16.900	16.676
240.0	16.700	16.920
270.0	16.800	17.128
300.0	17.000	17.318
360.0	18.000	17.675
420.0	18.100	18.020
480.0	18.500	18.362
540.0	19.700	18.703
600.0	19.100	19.044
720.0	19.800	19.726
840.0	22.100	20.408
960.0	22.200	21.090
1080.0	23.800	21.772
1200.0	24.200	22.454
1380.0	25.700	23.477
1560.0	25.000	24.500
2040.0	26.700	27.228
2100.0	25.700	27.569
2190.0	25.600	28.081

TABLE 35

Creep Strain Data - Experiment WO-6(3)

σ_f = 9,380 PSI	$\Delta\sigma$ = 626 PSI	
TIME	AXIAL STRAIN	
SECONDS	$e_C - \mu S$	$e_T - \mu S$
0.0	0.000	0.000
2.0	.400	.373
4.0	1.300	.741
9.0	2.900	1.631
14.0	3.900	2.483
24.0	6.600	4.077
54.0	9.600	8.103
84.0	11.400	11.208
114.0	14.700	13.614
144.0	14.300	15.493
174.0	17.000	16.970
204.0	16.300	18.143
234.0	17.300	19.087
264.0	19.200	19.855
324.0	19.500	21.029
384.0	21.900	21.892
444.0	22.600	22.578
504.0	22.100	23.161
564.0	24.800	23.686
684.0	27.500	24.649
804.0	26.000	25.563
924.0	26.500	26.462
1044.0	27.700	27.356
1164.0	28.700	28.248
1224.0	29.300	28.694
1404.0	30.200	30.031
1464.0	30.900	30.477
1524.0	31.900	30.922
1824.0	33.000	33.150
1884.0	33.000	33.596
1944.0	35.100	34.041
2004.0	33.300	34.487
2064.0	33.300	34.933

TABLE 36

Creep Strain Data - Experiment WO-6(4)

σ_f = 10,010 PSI	$\Delta\sigma$ = 630 PSI	
TIME	AXIAL STRAIN	
SECONDS	$e_C - \mu S$	$e_T - \mu S$
0.0	0.000	0.000
5.0	0.000	1.273
10.0	4.500	2.475
25.0	9.300	5.692
40.0	13.900	8.402
70.0	14.200	12.613
100.0	14.500	15.623
130.0	15.300	17.792
160.0	17.300	19.371
190.0	18.200	20.536
220.0	20.400	21.413
280.0	20.200	22.619
340.0	23.500	23.413
400.0	23.200	24.007
460.0	24.300	24.501
520.0	25.400	24.947
640.0	26.900	25.780
760.0	27.200	26.586
880.0	28.400	27.387
1000.0	29.900	28.186
1120.0	31.000	28.984
1240.0	31.900	29.782
1360.0	32.300	30.581
1480.0	33.000	31.379
1900.0	33.200	34.173
1960.0	33.200	34.573
2020.0	34.100	34.972
2080.0	35.900	35.371
2140.0	34.700	35.770
2184.0	34.200	36.063

TABLE 37

Creep Strain Data - Experiment WO-6(5)

σ_f = 10,628 PSI	$\Delta\sigma$ = 618 PSI	
TIME	AXIAL STRAIN	
SECONDS	$e_C - \mu S$	$e_T - \mu S$
0.0	0.000	0.000
10.0	6.600	3.010
20.0	9.000	5.785
50.0	15.800	12.882
80.0	19.400	18.462
110.0	23.200	22.869
140.0	25.800	26.366
170.0	29.800	29.159
200.0	30.000	31.406
230.0	31.400	33.231
260.0	32.200	34.729
320.0	34.800	37.021
380.0	36.500	38.695
440.0	39.500	39.998
500.0	41.500	41.078
560.0	42.600	42.025
620.0	43.600	42.893
740.0	45.600	44.502
860.0	49.300	46.038
980.0	48.500	47.547
1100.0	50.900	49.046
1220.0	51.000	50.542
1340.0	52.700	52.037
1460.0	53.300	53.532
1580.0	54.800	55.026
2060.0	61.700	61.003
2120.0	61.900	61.750
2180.0	62.000	62.497
2240.0	62.000	63.244
2300.0	62.500	63.991

TABLE 38

Creep Strain Data - Experiment WO-6(6)

σ_f = 12,256 PSI	$\Delta\sigma$ = 628 PSI	
TIME	AXIAL STRAIN	
SECONDS	$e_C - \mu S$	$e_T - \mu S$
0.0	0.000	0.000
6.0	10.300	2.873
11.0	13.300	5.161
26.0	21.000	11.489
41.0	25.500	17.088
56.0	26.200	22.044
86.0	33.300	30.324
116.0	36.900	36.839
146.0	40.400	41.986
176.0	42.400	46.070
206.0	46.000	49.330
236.0	47.600	51.951
266.0	50.600	54.075
296.0	52.800	55.815
356.0	54.000	58.465
416.0	60.300	60.385
476.0	60.400	61.864
536.0	61.400	63.078
656.0	66.500	65.092
776.0	69.400	66.860
896.0	71.400	68.539
1016.0	73.100	70.185
1136.0	75.500	71.819
1256.0	77.400	73.449
1376.0	78.900	75.078
1496.0	79.100	76.706
1616.0	81.000	78.334
2036.0	83.100	84.031
2096.0	84.100	84.845
2156.0	83.900	85.658
2216.0	84.400	86.472
2276.0	83.800	87.286
2294.0	85.600	87.530

TABLE 39

Creep Strain Data - Experiment WO-6(7)

σ_f = 11,892 PSI	$\Delta\sigma$ = 636 PSI	
TIME	AXIAL STRAIN	
SECONDS	$e_C - \mu S$	$e_T - \mu S$
0.0	0.000	0.000
4.0	6.700	1.802
8.0	10.400	3.568
23.0	18.300	9.869
38.0	21.500	15.696
68.0	29.500	26.079
98.0	35.800	34.982
128.0	42.500	42.633
158.0	49.700	49.221
188.0	54.600	54.910
218.0	59.900	59.837
248.0	62.500	64.118
278.0	65.100	67.853
338.0	71.400	74.002
398.0	76.800	78.812
458.0	80.100	82.660
518.0	83.300	85.818
638.0	89.600	90.788
758.0	94.100	94.709
878.0	98.500	98.089
998.0	102.000	101.191
1118.0	106.200	104.150
1238.0	110.100	107.034
1358.0	113.500	109.881
1478.0	116.400	112.708
1598.0	119.200	115.525
1658.0	120.000	116.931
2018.0	123.900	125.356
2078.0	125.300	126.760
2138.0	126.600	128.163
2198.0	128.100	129.566
2258.0	129.300	130.969
2303.0	129.200	132.022

TABLE 40

Creep Strain Data - Experiment WO-6(8)

σ_f = 12,544 PSI	$\Delta\sigma$ = 652 PSI	
TIME	AXIAL STRAIN	
SECONDS	$e_C - \mu S$	$e_T - \mu S$
0.0	0.000	0.000
10.0	21.400	12.257
25.0	37.900	29.456
40.0	48.600	45.344
55.0	59.800	60.038
70.0	73.200	73.649
100.0	93.000	97.998
130.0	115.600	119.075
160.0	135.800	137.443
190.0	152.600	153.571
220.0	168.600	167.845
250.0	182.900	180.586
310.0	208.600	202.478
390.0	220.800	226.416
440.0	240.600	239.339

TABLE - 41

Creep Strain Data - Experiment WO-7(1)

σ_f = 8,080 PSI	$\Delta\sigma$ = 612 PSI	
TIME	AXIAL STRAIN	
SECONDS	$e_C - \mu S$	$e_T - \mu S$
0.0	0.000	0.000
10.0	5.800	2.891
25.0	7.700	6.153
40.0	8.600	8.464
70.0	10.800	11.277
100.0	11.600	12.719
130.0	12.400	13.480
160.0	12.600	13.904
190.0	13.100	14.159
220.0	13.600	14.331
250.0	14.600	14.462
280.0	13.900	14.572
310.0	14.800	14.672
340.0	14.200	14.766
400.0	15.700	14.950
460.0	15.000	15.130
520.0	16.300	15.310
640.0	16.800	15.669
760.0	17.600	16.028
880.0	18.400	16.387
1000.0	17.500	16.746
1120.0	18.000	17.106
1240.0	17.000	17.465
1360.0	17.400	17.824
1480.0	17.900	18.183
1600.0	18.200	18.542
2200.0	20.600	20.338
2260.0	18.800	20.517
2320.0	21.100	20.697
2380.0	21.100	20.876
2440.0	20.600	21.056

TABLE 42

Creep Strain Data - Experiment WO-7(2)

σ_f = 8,740 PSI	$\Delta\sigma$ = 645 PSI	
TIME	AXIAL STRAIN	
SECONDS	$e_C - \mu S$	$e_T - \mu S$
0.0	0.000	0.000
5.0	6.200	2.917
10.0	7.800	5.284
25.0	9.900	10.036
40.0	11.100	12.595
70.0	12.300	14.763
100.0	13.900	15.481
130.0	14.600	15.790
160.0	15.600	15.983
190.0	16.000	16.144
220.0	16.100	16.296
250.0	16.400	16.445
280.0	16.600	16.593
340.0	16.800	16.889
400.0	17.600	17.185
460.0	17.900	17.481
520.0	18.500	17.777
640.0	19.100	18.369
760.0	19.400	18.961
880.0	20.900	19.553
1000.0	21.200	20.145
1120.0	21.900	20.737
1240.0	22.800	21.329
1360.0	22.900	21.921
1480.0	23.100	22.513
1600.0	23.800	23.105
2140.0	24.900	25.768
2200.0	25.200	26.064
2260.0	25.100	26.360
2320.0	25.400	26.656

TABLE 43

Creep Strain Data - Experiment WO-7(3)

$\bar{\sigma}_f$ = 9,370 PSI	$\Delta\bar{\sigma}$ = 611 PSI	
TIME	AXIAL STRAIN	
SECONDS	$e_C - \mu S$	$e_T - \mu S$
0.0	0.000	0.000
4.0	2.600	.554
19.0	5.700	2.478
34.0	5.600	4.181
49.0	6.500	5.687
79.0	8.800	8.205
109.0	10.300	10.188
139.0	11.600	11.756
169.0	12.500	13.004
199.0	13.200	14.003
229.0	14.000	14.811
259.0	14.600	15.469
289.0	14.700	16.012
349.0	16.100	16.851
409.0	17.500	17.472
469.0	18.700	17.964
529.0	17.800	18.377
649.0	19.300	19.081
769.0	20.400	19.714
889.0	21.500	20.320
1009.0	21.700	20.918
1129.0	21.900	21.512
1249.0	22.700	22.105
1369.0	23.400	22.698
1489.0	23.200	23.290
1609.0	23.500	23.882
1729.0	24.400	24.475
2209.0	26.200	26.844
2269.0	27.000	27.140
2329.0	27.600	27.436
2389.0	27.300	27.732
2449.0	27.900	28.029

TABLE 44

Creep Strain Data - Experiment WO-7(4)

σ_f = 9,994 PSI	$\Delta\sigma$ = 608 PSI	
TIME	AXIAL STRAIN	
SECONDS	$e_C - \mu S$	$e_T - \mu S$
0.0	0.000	0.000
3.0	2.500	.939
18.0	8.700	5.039
33.0	11.900	8.295
63.0	12.700	12.950
93.0	15.500	15.924
123.0	16.700	17.851
153.0	17.800	19.126
183.0	17.900	19.995
213.0	19.400	20.611
243.0	20.100	21.070
273.0	20.400	21.431
333.0	21.200	21.993
393.0	22.800	22.455
453.0	23.700	22.878
513.0	23.600	23.286
633.0	24.500	24.089
753.0	26.700	24.887
873.0	26.700	25.684
993.0	27.100	26.481
1113.0	28.700	27.278
1233.0	29.900	28.075
1353.0	29.900	28.872
1473.0	29.700	29.669
1593.0	30.300	30.466
1713.0	31.200	31.263
2133.0	33.400	34.053
2193.0	34.200	34.452
2253.0	34.100	34.850
2313.0	33.800	35.249

TABLE 45

Creep Strain Data - Experiment WO-7(5)

σ_f = 10,658 PSI	$\Delta\sigma$ = 627 PSI	
TIME	AXIAL STRAIN	
SECONDS	$e_C - \mu S$	$e_T - \mu S$
0.0	0.000	0.000
6.0	1.200	1.191
21.0	7.500	3.935
36.0	10.900	6.374
51.0	12.800	8.543
81.0	14.200	12.194
111.0	16.100	15.095
141.0	17.400	17.410
171.0	18.100	19.267
201.0	18.600	20.765
231.0	20.100	21.983
261.0	21.100	22.981
291.0	21.600	23.808
351.0	22.200	25.089
411.0	24.800	26.036
471.0	26.200	26.779
531.0	26.900	27.397
651.0	28.600	28.435
771.0	29.800	29.351
891.0	31.700	30.222
1011.0	32.100	31.076
1131.0	34.200	31.923
1251.0	35.100	32.769
1371.0	36.600	33.613
1491.0	36.500	34.457
1611.0	36.500	35.300
1731.0	36.900	36.144
2211.0	38.000	39.519
2271.0	39.300	39.941
2331.0	38.400	40.363
2391.0	38.400	40.784

TABLE 46

Creep Strain Data - Experiment WO-7(6)

σ_f = 11,283 PSI	$\Delta\sigma$ = 643 PSI	
TIME	AXIAL STRAIN	
SECONDS	$e_C - \mu S$	$e_T - \mu S$
0.0	0.000	0.000
9.0	9.400	3.181
24.0	14.700	7.934
39.0	17.600	12.081
54.0	19.400	15.700
84.0	22.900	21.630
114.0	26.000	26.181
144.0	28.500	29.694
174.0	30.400	32.428
204.0	32.100	34.575
234.0	33.300	36.282
264.0	34.700	37.657
294.0	36.200	38.784
354.0	38.400	40.521
414.0	41.000	41.827
474.0	42.500	42.889
534.0	43.700	43.813
654.0	46.300	45.461
774.0	47.500	47.000
894.0	50.000	48.506
1014.0	51.700	50.000
1134.0	54.400	51.491
1254.0	56.400	52.981
1374.0	57.200	54.470
1494.0	57.800	55.959
1614.0	58.900	57.448
1734.0	60.900	58.938
2214.0	63.200	64.894
2274.0	64.200	65.639
2334.0	63.700	66.383
2394.0	64.400	67.128

TABLE 47

Creep Strain Data - Experiment WO-7(7)

σ_f = 11,851 PSI	$\Delta\sigma$ = 639 PSI	
TIME	AXIAL STRAIN	
SECONDS	$e_C - \mu S$	$e_T - \mu S$
0.0	0.000	0.000
12.0	6.400	2.571
27.0	9.600	5.619
42.0	12.200	8.494
72.0	17.400	13.764
102.0	21.900	18.458
132.0	24.100	22.645
162.0	27.500	26.385
192.0	28.800	29.730
222.0	31.500	32.727
252.0	33.600	35.419
282.0	36.500	37.840
342.0	39.800	41.996
402.0	43.400	45.410
522.0	48.700	50.635
582.0	50.100	52.674
702.0	56.200	56.002
822.0	59.700	58.666
942.0	61.500	60.928
1062.0	64.100	62.949
1182.0	66.500	64.823
1302.0	68.500	66.609
1422.0	69.900	68.342
1542.0	70.800	70.043
1662.0	72.200	71.724
1782.0	74.300	73.393
2262.0	79.000	80.024
2322.0	80.400	80.850
2382.0	79.400	81.677

TABLE 48

Creep Strain Data - Experiment WO-7(8)

$\bar{\sigma}_f$ = 12,562 PSI	$\Delta\bar{\sigma}$ = 650 PSI	
TIME	AXIAL STRAIN	
SECONDS	$e_C - \mu S$	$e_T - \mu S$
0.0	0.000	0.000
2.0	5.400	2.085
17.0	16.900	14.965
47.0	29.300	32.014
77.0	42.800	44.120
107.0	56.200	54.539
137.0	65.500	64.383
167.0	75.500	74.029
197.0	83.600	83.609
227.0	92.900	93.166
257.0	101.500	102.715
287.0	110.400	112.262
317.0	120.200	121.807
333.0	130.000	126.898

XIII

APPENDIX 6

Effect of Incremental Loading Rate

An important assumption that is made in order to simplify calculations of the instantaneous elastic modulus (E_2) and in order to determine accurately the zero level for the inelastic strain is that the instantaneous strain (Δe_ϵ) produced by an incremental rapidly applied load contains a negligible contribution from the inelastic components of the material. In this appendix an equation is derived for the strain developed in a material behaving as a Burgers model during incremental loading. Using numerical values of the model parameters determined from earlier experiments the magnitude of the elastic and the inelastic components are compared.

For simplicity the Maxwell and the Kelvin-Voigt sections of the Burgers model will be analyzed individually. The loading condition to be applied is that at the point (σ_0, e_0, t_0) an incremental load is applied at a constant rate ($\dot{\sigma}_c$) such that

$$\sigma_M = \sigma_0 + \dot{\sigma}_c (t - t_0) \qquad (98).$$

Now the governing equation of the Maxwell section is given by an earlier equation (53) as

$$\dot{e}_M = \dot{\sigma}_M / E_2 + \sigma_M / N_2$$

Substituting $\dot{\sigma}_M = \dot{\sigma}_c$ and equation 98 into this equation we obtain

$$\dot{e}_M = \dot{\sigma}_c / E_2 + \{\sigma_0 + \dot{\sigma}_c (t - t_0)\} / N_2$$

which may be integrated to give

$$e_M = \frac{\dot{\sigma}_c t}{E_2} + \frac{\sigma_0 t}{N_2} + \frac{\dot{\sigma}_c}{2N_2}(t - t_0)^2 + C \qquad (99).$$

The constant C may be determined by noting that at $t = t_0$, $e_M = e_0$ and from equation 99 we find that

$$C = e_0 - \frac{\dot{\sigma}_c t_0}{E_2} - \frac{\sigma_1 t_0}{N_2}$$

Substituting this value of C back into equation 99 we obtain, after rearrangement

$$e_M = e_0 + \frac{\dot{\sigma}_c}{E_2}(t - t_0) + \frac{\sigma_0}{N_2}(t - t_0) + \frac{\dot{\sigma}_c}{2N_2}(t - t_0)^2 \qquad (100).$$

Now let the specimen be fully loaded at $t = t_L$ and let the strain at that point be $e = e_L$. Now

$$\Delta T = (t_L - t_0) \qquad (101),$$

and at t_0

$$\Delta \sigma = \dot{\sigma}_c \Delta T \qquad (102).$$

Now equation 100 reduces to

$$\boxed{\Delta e_M = \frac{\Delta \sigma}{E_2} + \frac{\sigma_0 \Delta T}{N_2} + \frac{\Delta \sigma \Delta T}{2N_2}} \qquad (103).$$

The governing equation for the Kelvin-Voigt section is given by equation 55 as

$$\sigma_K = E_1 e_K + N_1 \dot{e}_K$$

and substituting for σ_K from equation 98 we obtain

$$E_1 e_K + N_1 \dot{e}_K = \sigma_0 + \dot{\sigma}_c (t - t_0) \qquad (104).$$

The general solution of this equation is of the form

$$e_K = D\,exp\left[(-E_1/N_1)t\right] + F_1 t^2 + F_2 t + F_3 \qquad (105).$$

Substituting equation 105 into 104 and determining the coefficients F_1, F_2 and F_3 by equating terms of like powers of t we obtain

$$e_K = D\,exp\left[(-E_1/N_1)t\right] + \frac{\sigma_0}{E_1} - \frac{N_1 \dot{\sigma}_c}{E_1^2} + \frac{\dot{\sigma}_c}{E_1}(t - t_0) \qquad (106).$$

Now at $t = t_0$, $e_K = e_0$ equation 106 gives

$$D = exp\left[(E_1/N_1)t_0\right]\left\{e_0 - \frac{\sigma_0}{E_1} + \frac{N_1 \dot{\sigma}_c}{E_1^2}\right\}$$

and substituting this back into equation 106 we obtain

$$e_K = exp\left[-(E_1/N_1)(t - t_0)\right]\left\{e_0 - \frac{\sigma_0}{E_1} - \frac{N_1 \dot{\sigma}_c}{E_1^2}\right\} + \frac{\sigma_0}{E_1} - \frac{N_1 \dot{\sigma}_c}{E_1^2} + \frac{\dot{\sigma}_c}{E_1}(t - t_0) \qquad (107).$$

Now if a long time has passed since the previous incremental load was applied then we may consider $e_0 \simeq \frac{\sigma_0}{E_1}$ and equation 105 reduces to

$$e_K = e_o + \frac{\dot{\sigma}_c}{E_1}(t-t_o) - \frac{N_1\dot{\sigma}_c}{E_1^2}\left\{1-\exp\left[-(E_1/N_1)(t-t_o)\right]\right\} \qquad (108).$$

Applying the conditions given in equation 101 and 102 , and noting that $\tau \equiv N_1/E_1$ we obtain

$$\Delta e_K = \frac{\dot{\sigma}_c}{E_1}(\Delta T) - \frac{\tau\dot{\sigma}_c}{E_1}\left[1-\exp(-\Delta T/\tau)\right] \qquad (109).$$

Now the overall strain change will be

$$\Delta e = \Delta e_M + \Delta e_K$$

and substituting from equations 103 and 109 we obtain

$$\Delta e = \frac{\Delta\sigma}{E_2} + \frac{\sigma_o \Delta T}{N_2} + \frac{\Delta\sigma\Delta T}{2N_2} + \frac{\Delta\sigma}{E_1} - \frac{\tau\dot{\sigma}_c}{E_1}\left[1-\exp(-\Delta T/\tau)\right] \qquad (110).$$

Now for rapid loading the last term in equation 110 (S) may be expanded in a power series in $\Delta T/\tau$ retaining only the first three terms giving

$$S = \frac{\Delta\sigma}{E_1}\left(1-\Delta T/2\tau\right)$$

Now substituting this into equation 110 we obtain after rearrangement

$$\Delta e = \left[\frac{\Delta\sigma}{E_2}\right] + \left[\frac{\sigma_o\Delta T}{N_2} + \frac{\Delta\sigma\Delta T}{2}\left\{\frac{N_1+N_2}{N_1N_2}\right\}\right] \qquad (111).$$

Now the R.H.S. of equation 111 may be written as

$$\Delta e = \Delta e_E + \Delta e_{IN} \qquad (112),$$

where Δe_E is the instantaneous elastic strain and Δe_{IN} is the inelastic strain which developes during the time the incremental load is being applied. The per cent error in Δe_E introduced by neglecting the inelastic strain and assuming that

$$\Delta e_E = \text{observed strain}$$

will be given approximately by R where

$$R = \left\{ \frac{\Delta e_{IN}}{\Delta e_E} \right\} \times 100\% \qquad (113).$$

Now substituting for Δe_{IN} and Δe_E from equation 111 we obtain

$$R = \frac{[\Delta\sigma/E_2]}{\left[\frac{\sigma_0 \Delta T}{N_2} + \frac{\Delta\sigma\Delta T}{2}\left(\frac{N_1+N_2}{N_1N_2}\right)\right]} \qquad (114).$$

Now the following typical experimental values were obtained from tests conducted on specimen WO-6, namely:

I. Low Stress Region

σ_0 = 7487 psi , $\Delta\sigma$ = 614 psi , $\Delta T \approx$ 4 seconds ,

$E_2 = 8.8 \times 10^6$ psi , $N_1 = 4.4 \times 10^9$ psi-sec ,

$N_2 = 1719 \times 10^9$ psi-sec .

II. High Strss Region

σ_0 = 11,256 psi , $\Delta\sigma$ = 636 psi , $\Delta T \approx$ 4 seconds ,

$E_2 = 8.8 \times 10^6$ psi , $N_1 = 1.5 \times 10^9$ psi-sec ,

$N_2 = 509 \times 10^9$ psi-sec .

Substituting the values into equation 114 we obtain

$$R(I) = 0.36\ \%$$

$$R(II) = 1.3\ \%$$

Therefore for rapid incremental loading if we neglect the inelastic strains developed during loading this will result in an error of less than 1.5 per cent in the calculated instantaneous elastic modulus (E_2) and in the zero level of the creep strain data.

ABSTRACT

THE EXPERIMENTAL INVESTIGATION OF THE INELASTIC BEHAVIOR OF GEOLOGIC MATERIALS

by

H. R. Hardy, Jr.

- - -

A knowledge of the mechanical behavior of geologic materials (rocks and minerals) has become increasingly important in mining and civil engineering, geology, geophysics and more recently in a number of defence and aerospace fields. This research describes an investigation of one particular aspect of the mechanical behavior of these materials namely the determination of their inelastic properties. The investigation consisted of two stages; first, the development of suitable test facilities and experimental techniques, and second, the detailed study of the deformation properties of a relatively simple geologic material namely, Wombeyan marble.

Deformation experiments were conducted in a test enclosure which was designed to provide controlled temperature conditions of $70 \pm 1/10°F$. Cylindrical test specimens, nominally 3/4 inches in diameter and 1 - 3/4 inches in length were machined from diamond drill core using a lathe and an attached tool post grinder. To measure

axial strain a set of three foil-type resistance strain gages were mounted to 120 degrees around the circumference of the test specimen.

During deformation experiments the specimens were mounted in a loading jig and compressed axially using a specially designed loading system. This system is basically an "on-off" pneumatic-hydraulic servo-loading system which may be operated in a variety of test modes. Experiments todate have been mainly conducted in the incremental stress mode. Here the specimen stress was increased in a number of rapidly applied, small increments. After each increment the stress was maintained constant for a period of time during which the resulting time-dependent strain was observed. At the end of this period the stress was increased to the next level. Using this system it has been possible to apply incremental stresses of up to 1000 psi in periods of less than four seconds and to maintain the stress constant to within $\pm$ 1/10 per cent at each level.

Specimen strains were monitored by the three attached strain gages and a measurement system which enabled the strains from the three gages to be recorded separately. This allowed an estimate to be made of the strain uniformity in the specimen throughout the experiment. It was found that the deviation between gages rarely exceeded eight per cent.

Experimental results were fitted, using the modified Newton-Gauss method of least squares, to the incremental form of the Burgers mechanical model, namely:

$$e_I = \frac{\Delta \sigma_n}{E_2} + \frac{\Delta \sigma_n}{E_1}\left[1 - \exp(-E_1 t/N_1)\right] + \frac{\sigma_n t}{N_2}$$

where e_I is the incremental strain, $\Delta \sigma_n$ is the stress increment, σ_n is the new stress level, t is the time from when $\Delta \sigma_n$ was applied, and E_1, E_2, N_1 and N_2 are the Burger model parameters.

A number of incremental experiments were carried out on specimens of Wombeyan marble, which was selected due to its monomineralic nature and since previous experiments had indicated that it was macroscopically homogeneous and isotropic. With few exceptions the experimental data was found to fit the incremental form of the Burgers model extremely well. Below a stress of approximately 7700 psi the material appeared to be elastic with a modulus E_2 which varied with stress level up to a maximum of approximately 9×10^6. In this region the other parameters (E_1, N_1 and N_2) were infinite. Above a stress of 7700 psi all parameters were finite. E_1, N_1 and N_2 were found to be approximately linear, decreasing functions of the stress level and E_2 was found to be approximately constant. This behavior appears to be consistent with a proposed general deformation mechanism and with the earlier experimental work of Matsushima on granite.